Title
Methodologies for the evaluation of nuclear waste management strategies and applications to advanced fuel cycles

Author
Atz, Milos Ivo

Publication Date
2019

Peer reviewed|Thesis/dissertation

Methodologies for the evaluation of nuclear waste management strategies and applications to advanced fuel cycles

by

Miloš Ivo Atz

A dissertation submitted in partial satisfaction of the

requirements for the degree of

Doctor of Philosophy

in

Engineering – Nuclear Engineering

in the

Graduate Division

of the

University of California, Berkeley

Committee in charge:

Associate Professor Massimiliano Fratoni, Chair
Professor Per Peterson
Professor Philip B. Stark
Associate Adjunct Professor Haruko Wainwright

Fall 2019

Methodologies for the evaluation of nuclear waste management strategies and applications to advanced fuel cycles

Abstract

Methodologies for the evaluation of nuclear waste management strategies and applications to advanced fuel cycles

by

Miloš Ivo Atz

Doctor of Philosophy in Engineering – Nuclear Engineering

University of California, Berkeley

Associate Professor Massimiliano Fratoni, Chair

One of the unresolved hurdles facing present and future nuclear energy systems is waste management. Recent efforts to identify promising fuel cycles have attempted to value waste management through metrics reflecting intrinsic characteristics of the wastes rather than the environmental impacts, risks, and challenges involved in their disposal. This dissertation applies three waste management models to a broad set of fuel cycle options to explore the relationship between fuel cycle characteristics and waste disposal. First, long-lived fission product inventory is used as a proxy for repository performance, avoiding the computational expense and complexity of a full performance assessment. Second, the attractiveness for diversion and recovery of fissile materials from waste streams for potential proliferation is evaluated using a figure of merit, which values the quality of the material and its retrievability. Finally, repository area and surface storage requirements are determined based on thermal constraints for waste disposal in three geologic environments.

These models are used to analyze fuel cycle options taken from the Fuel Cycle Evaluation and Screening (FCES) study. A Python package has been developed to characterize waste streams using FCES data including mass balances, discharged fuel composition(s), and details about fuel cycle technologies such as reactor type and reprocessing method. The package extends the FCES mass flow calculations to include waste package loading for spent fuels and waste loading fraction for high-level wastes. Benchmarking against FCES metric results demonstrates good agreement.

The long-lived fission product inventory is shown to be sensitive to reactor thermal efficiency — because reactors that are less efficient are required to produce more fissions — and to the extent of recycling, because the recycled fissile material generally has greater long-lived fission product yield than enriched uranium. Specific fission

product isotopes demonstrate sensitivity to fuel isotope, neutron spectrum, and residence time. Fissile material in all waste streams is shown to become attractive for recovery from waste as the self-protecting dose rate decays, but the time before that occurs is longer for high-level wastes that concentrate highly radioactive nuclides. Because high-level wastes are more dilute in fissile material, more waste packages need to be intercepted to obtain usable quantities of fissile material. The area and storage time requirements are shown to be highly sensitive to thermal properties and constraints of repository design. Fuel cycles recycling long-term heat-generating transuranic isotopes in fast reactors perform well, whereas those that utilize limited-recycling of actinides perform poorly. Parametric analysis of waste package and waste form loading with respect to these metrics demonstrates opportunities for the integration of fuel cycle operations and waste management.

Contents

List of Figures

List of Tables

Acknowledgments

I am incredibly grateful for the advice and patience of my advisor, Professor Massimiliano Fratoni. Thank you for keeping things in perspective and setting an example for balancing the demands of academic and personal life. I am deeply appreciative for the constructive feedback of my committee members, Professor Per Peterson, Associate Adjunct Professor Haruko Wainwright, and Professor Philip B. Stark. I am so thankful to have been able to study for two years with Professor Joonhong Ahn, who taught me to thoughtfully assess issues objectively from many perspectives. I hope that this achievement can be an honor to your memory.

I am fortunate to have met and worked with many wonderful people at UC Berkeley. In particular, I owe a debt of gratitude to Professor Karl van Bibber, who has been a wonderful ally. Thank you to Alan Bolind for the many favors and kind friendship. To the front office staff — Sara Harmon, Kirsten Wimple Hall, Vicky Garcia, Christina Castellanos, Lydia Liu, and Hanna Lorica — thank you for making this department a home. My research colleagues Alex Salazar, Xudong Liu, Seung Min Woo, Kyoungjin Lee, and Franziska Schmidt have been amazing mentors and collaborators. Thank you to Madison Hales for your energy and uplifting enthusiasm. To Kelly Rowland, thank you for answering all my `computer` questions. To Cathryn Carson and Khalid Kadir, thank you for challenging me to think outside of my box.

I have benefited immensely from the professional and personal mentorship of my friends, most notably Tess Smidt, Sean Lubner, Dave Frazer, and Chris Poresky. To Joey Kabel, James Kendrick, Sami Lewis, Josh Rehak, Chris Keckler, Maria Simanovskaia, Emily Vu, Ishak Johnson, Alec Christian, and all of my gym friends, thank you for distracting me from my work in ways that made my life so much better.

Of course, I am immensely grateful for the support of my family. Thank you for helping me reach so high. Above all, thank you Carolyn for your limitless patience. I love you.

This material is based upon work supported by the National Science Foundation Graduate Research Fellowship under Grant No. 1752814. I also thank the Roy G. Post Foundation for the Nuclear Waste Management Graduate Scholarship, the Nuclear Science and Security Consortium (NSSC) for travel support as an NSSC Affiliate, the United States Nuclear Regulatory Commission (NRC) for support as a graduate fellow, and the Japan Atomic Energy Agency (JAEA) for research project funding.

This research used the Savio computational cluster resource provided by the Berkeley Research Computing program at the University of California Berkeley (supported by the UC Berkeley Chancellor, Vice Chancellor for Research, and Chief Information Officer). Special thanks to Dr. Chris Paciorek and the BRC Help Staff for their endless patience and friendly counsel.

Chapter 1

Introduction

Commercial nuclear power produces carbon-free, baseload electricity, an important resource for a world increasingly concerned about the negative effects of greenhouse gases on the climate. Nuclear power is also energy-dense, enabling significant energy generation from relatively small amounts of natural resources and with small areal footprint[1]. Because of this, it can be a sustainable way to generate electricity while preserving the inhabited and wild environments. However, nuclear power faces many hurdles to increased deployment, one of which is nuclear waste management. Commercial nuclear power operation produces used nuclear fuel and high-level waste that remain radioactive for millennia. Current consensus is that final disposal of the wastes will take place in a deep geologic repository. The repository system is designed to inhibit the release of radiation to the biosphere. Although some countries have been successful in licensing and beginning construction of geologic repositories for commercial nuclear waste, many others have made little progress or have experienced significant setbacks. That no repository in the world is yet in operation illustrates the difficulty associated with repository siting, development, licensing, and operation.

The current lack of a final disposal solution for nuclear waste in most countries has been a significant driver for research and development (R&D) focused on nuclear energy systems that improve waste management and reduce long-term risks of disposal. From this view, different or advanced fuel cycles may potentially reduce risks by reducing the waste mass through improved fuel utilization. Doing so will also alter the composition and characteristics of the waste. In the United States, nuclear power is generated in light water reactors (LWRs) and current policy mandates that

[1]Burning 1 kg of coal releases about 23 MJ of thermal energy [1]. By contrast, the enrichment of 1 kg of natural uranium (0.71 wt% U-235) produces 0.096 kg of reactor-grade uranium with 5 wt% U-235; total consumption of that U-235 (200 MeV per fission) yields 397,500 MJ of thermal energy.

the used fuel be directly disposed in a geologic repository. A different fuel cycle may incorporate new reactors with very different characteristics than LWRs, as well as recycling schemes to reuse various fissile and fissionable isotopes or destroy undesirable nuclides in the waste. The processes implemented in these fuel cycles will alter the conditions of the waste in ways that affect its management and disposal.

Due to the vast range of possible combinations of nuclear technologies to achieve different fuel cycles, comparative analysis must be performed before development to improve allocation of R&D resources toward promising options. Waste management should be an aspect of that study to understand the environmental impact of wastes from different fuel cycles. Given that waste management has so far been a significant challenge for nuclear energy development, a fuel cycle system that offers improvements in waste management may be considered significantly more attractive.

Many comparative fuel cycle studies, such as the U.S. Department of Energy Fuel Cycle Evaluation and Screening and Advanced Fuel Cycle Initiative Options studies, consider waste characteristics as metrics for evaluating and ranking different fuel cycles. In these analyses, simple metrics like total mass, radioactivity, and radiotoxicity are employed. However, radioactivity and radiotoxicity are not measures of waste management strategies, risks, or impacts [2, 3, 4]. Instead, these metrics indicate the risks of exposure to or ingestion of the material itself and are intrinsic characteristics of the waste streams. They neglect the technologies and barriers involved in waste management operations and the isolation and entombment provided by deep geological disposal. Analysis of these systems can require complex, computationally expensive models. For example, the risks posed from permanent disposal of the waste in a deep geologic repository are usually evaluated probabilistically through repository performance assessment (PA) or similar comprehensive study to reflect the overall functionality of the disposal system and the behavior of radionuclides in the greater geologic environment. The results from PA are weighed against independently generated guidelines to make judgments about repository compliance. Given the complexity of the analysis, PA is not appropriate for the comparison of hypothetical fuel cycles for which many details about the reactor(s), recycling schemes, and waste forms are assumed or unknown.

This distinction divides the majority of past studies on the impact of fuel cycle on waste management and repository performance. Studies aiming to compare many fuel cycles often utilize waste radioactivity and radiotoxicity as performance metrics, avoiding the complexities of considering management operations and repository conditions. By contrast, the studies focused on more specifically on waste management or repository performance account for these complexities, but often examine only one or a few fuel cycles, including the current once-through LWR system. This divide has created a knowledge gap that has been filled by extending reactor and subsurface

transport theories to explain unstudied cases.

This chapter summarizes past research at the intersection between nuclear fuel cycles and environmental impacts of waste management and disposal. Then, that historical perspective is put into context alongside the present outlook for advanced reactor and fuel cycle development. Finally, the scope of this dissertation is introduced.

1.1 Literature review: nuclear fuel cycles and waste management

1.1.1 Historical perspective

In the early years of nuclear power development, technologists were optimistic about the future of nuclear energy and the implementation of waste management solutions [5]. Because implementation of advanced fuel cycles seemed inevitable, a significant amount of the past research into their environmental impacts has assumed that one of the primary goals would be to improve waste management. The strategy of utilizing an advanced fuel cycle with the express purpose of improving waste management is referred to as partitioning and transmutation (P&T). Partitioning is the physical or chemical treatment of nuclear wastes to separate reusable nuclides, like fissile and fissionable actinides, and elements containing isotopes unfavorable for disposal, such as long-lived and mobile fission products. One method to handle these nuclides after they are separated is transmutation. Transmutation is the process by which partitioned nuclides are converted to short-lived or stable isotopes by nuclear reaction, typically induced by neutron bombardment in nuclear reactors. Historically, investigations into the relationship between nuclear technologies, nuclear waste management, and environmental outcomes have focused on P&T. This subsection examines past work into P&T and contextualizes it with the current status of nuclear waste management and present perspective of advanced fuel cycles.

The main incentive of P&T is the potential to reduce long-term risk from nuclear waste disposal by decreasing the amount of long-lived radionuclides in the waste. A significant portion of the long-lived radioactivity in the waste comes from actinides that can be fissioned in nuclear reactors. To illustrate this point, Figure 1.1 shows the radioactivity of different species that comprise LWR spent fuel as a function of time. After a few hundred years, the radioactivity is dominated by long-lived transuranic isotopes and their decay products. Removal of these isotopes can potentially decrease the amount of waste requiring disposal and decrease the isolation time required. In addition, if fissile nuclides are removed from the waste, the attractiveness of the

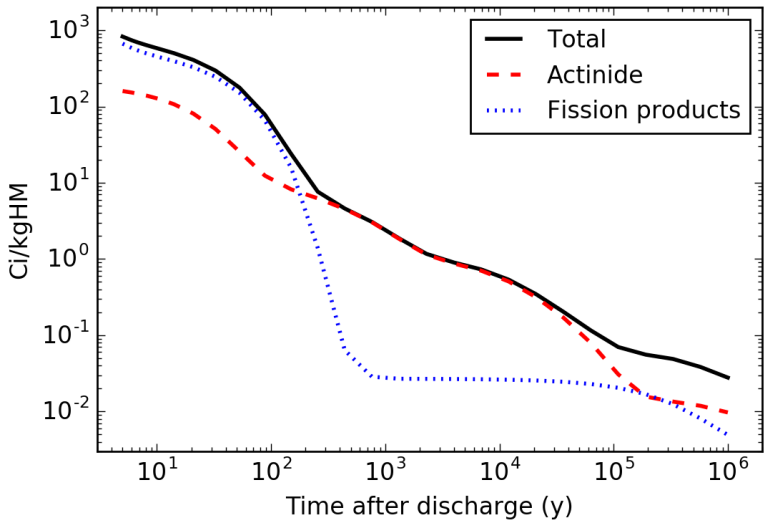

Figure 1.1: Radioactivity (Ci/kg heavy metal) of actinide and fission product species in uranium dioxide PWR used fuel over time. The fuel initial enrichment is 4.21 wt% U-235 and final burnup is 50 GWd/t, achieved over 4.1 effective full-power-years.

repository for proliferation and the risk of waste re-criticality can be reduced or eliminated [6]. Further, many argue that the separation of various nuclides from the waste can decrease the heat generation rate, potentially altering favorable the criteria by which a repository must be designed [7].

For decision-makers, the risks and costs of P&T against which the benefits must be compared are (1) the increased health risk posed by P&T in the near future due to the increase in fuel cycle activities, and (2) the increase in fuel cycle costs required to implement P&T [8]. P&T is constrained by requirements on implementation and performance. To implement P&T, reprocessing of nuclear waste is a prerequisite. The total radiological hazard arising from nuclear energy production within the P&T fuel cycle must be reduced, including the short-term hazard from P&T fuel cycle operations. Additionally, the hazards and risk from secondary wastes from P&T processes must be taken into account. If possible, the P&T system should be net energy positive, and the system should be economical.

As nuclear power technology was emerging in the 1940s and 1950s, experts recognized the need to deal with nuclear waste but felt optimistic about the implementation of disposal solutions [5]. It was commonly assumed that nuclear fuel rods from commercial power reactors would be reprocessed to recover and reuse plutonium and fissile uranium, as was done at the nuclear weapons site in Hanford. In the

1960s, studies of various selected aspects of P&T were made but none was directly concerned with the feasibility and overall incentives for implementation of the technology. All studies concerned with the long-term benefits were unrealistic in that they relied on the toxicity index of the waste, which assumes direct ingestion of the material without any change in composition [8].

In 1975, a PNL study investigated the long-term benefits of P&T while considering the leaching and transport of the waste from a repository to the biosphere. The analysis was performed under conservative assumptions that served to maximize the calculated radiation doses so as to overestimate the incentives for P&T while neglecting the risk posed by partitioned nuclides and fuel cycle activities. It was found that even under those conditions, the incentives for P&T were very small when compared with normal background radiation [9].

In 1976, the U.S. national labs and affiliates began a three-year investigation commissioned by the U.S. Energy Research and Development Administration (ERDA, now the Department of Energy) and headed by Oak Ridge National Laboratory (ORNL) to build a meaningful and defensible evaluation of the P&T concept [10]. It was found that the technology required was deemed mostly feasible; all had been verified at the laboratory level and much at the hot, production-scale. The costs and short-term risks, however, were shown to be high. The long-term benefits were small even under conservative assumptions, amounting to only about 0.001% of the effects of natural background radiation. The study concluded that no incentives exist for actinide P&T, but P&T of technetium and iodine, two long-lived and hydrologically mobile fission products, may be worthwhile under (1) very conservative long-term risk analysis assumptions, and (2) if feasible and effective P&T methods can be developed for those nuclides [8].

Though numerous studies were subsequently undertaken in Europe, they were generally similar to the ORNL study, and all found no incentives for P&T [8]. A 1982 International Atomic Energy Agency report [11] summarized that conclusion: "Since the long-term hazards are already low, there is little incentive to reduce them further by P-T. Indeed the incremental costs of introducing P-T appear to be unduly high in relation to the prospective benefits."

In the 1980s and 1990s, the U.S. Department of Energy (DOE) sponsored the Actinide-burning Liquid Metal Reactor (ALMR) program, an R&D project toward a promising advanced fuel cycle. The concept proposed reprocessing thermal LWR used fuel for use in the fast ALMR. The fuel cycle would recover and recycle all actinides (including neptunium, americium, and curium). Studies into this specific fuel cycle found little incentive for the program from a waste management perspective [2, 12]. Additionally, it was shown that implementation of the concept would result in a substantial buildup of actinides and reduction factors of 1000 could only be achieved

after 10,000 years of sustained ALMR operation [13]. Ultimately, the ALMR program was discontinued.

During this time, the focus for waste management began to shift toward direct disposal of LWR spent fuel as inventories swelled and advanced fuel cycles remained distant. A site in Nevada, Yucca Mountain, had been chosen as the sole site for research and development of a national geologic repository, and much of the work on repository performance assessment focused exclusively on the site. Significant advances were made in the understanding of subsurface radionuclide transport behavior and models for the performance of geologic repositories for direct disposal of LWR spent fuel. Nevertheless, the studies into the impact of waste transmutation continued and incorporated the knowledge gained from repository development. Numerous academic works were published on the effects of fuel cycle on generic repository performance [6, 14, 15, 16]. The goal of this research was to better characterize the impact of P&T on repository performance by improving the repository models. They found that repository performance could be improved in the very long term by reducing the inventory of long-lived actinides in the waste, but stopped short of concluding that this indicated positive waste management incentives for P&T.

1.1.2 Current context

Although the Yucca Mountain Repository (YMR) project has been stalled since 2011 and its future remains uncertain, the U.S. nuclear waste management policy remains focused on direct disposal of spent nuclear fuel. Today, it appears increasingly unlikely that any nuclear technology will alter the direct disposal pathway for most of the existing stock of LWR spent nuclear fuel due to the vast inventory and time and expense required to process it. About 2000 tons of spent fuel are produced in the U.S. each year, adding to an inventory of over 70,000 metric tons of heavy metal (tHM) [17]. In France, a country that has pursued reprocessing of spent fuel, the rate at which spent fuel is reprocessed is about 1000 tons per year [18]. Developing the capability to process fuel at a rate that outpaces the annual discharge of new fuel and can reasonably handle the existing inventory seems out of reach. Instead, it is more likely that any advanced fuel cycle implemented in the U.S. will be in addition to the development of a repository for the direct disposal of existing spent nuclear fuel.

This perspective coincides with the conclusion that the improvement in management and disposal risks from P&T on existing wastes do not warrant their adoption. Further, nuclear energy no longer seems to be an inevitable development. For the next generation of nuclear reactors, nuclear waste is a burden to be mitigated and dealt with as economically as possible, rather than a central theme to the technology.

Other incentives, such as safety, proliferation resistance, and resource sustainability have emerged as the primary technological drivers. But because waste will always require management, a fuel cycle that offers benefits should be viewed as more attractive.

This has been the perspective taken in more recent fuel cycle analyses. In the early 2000s, the U.S. DOE began the Advanced Fuel Cycle Initiative, which included research programs addressing many technical challenges associated with the implementation of advanced fuel cycles. One of those areas was an Options Study [19], which examined the issues facing nuclear power and made recommendations for future nuclear strategies. Fuel cycles were broadly categorized in groups based on the extent of recycling:

- Once-through: nuclear fuel is passed through a reactor once and then directly disposed of in a geologic repository.
- Limited-recycle: used nuclear fuel is reprocessed a finite number of times but at some point is directly disposed as spent fuel.
- Continuous-recycle: nuclear fuel is continuously reprocessed and recycled, and only high-level wastes from reprocessing operations are sent to the repository.

The Options Study identified five performance measures for nuclear waste management: repository peak dose rate, radiotoxicity of the wastes, mass and volume of the high- and low-level wastes, interim storage requirements, and decay heat load. Of these, they expected that only the continuous-recycle options could offer significant benefits over the current once-through fuel cycle. As a continuation of that work, in 2011 the U.S. DOE commissioned the Fuel Cycle Evaluation and Screening (FCES) study to generate and compare data for a wide variety of potential fuel cycles [20]. The goal of the FCES study was to help direct R&D toward promising fuel cycle options and technologies. Six evaluation criteria categorize the relative benefit of each fuel cycle over the current once-through LWR system. One of these criteria was waste management, which was assessed based on spent fuel and high-level waste mass, radioactivity at fixed times, and estimates for the accumulation of low-level radioactive byproducts (such as unused depleted or recovered uranium and low-level waste generated in fuel cycle facilities).

The DOE FCES study leaves an opportunity for further analysis on the implications of the fuel cycle on waste management and disposal. Mass, volume, radioactivity, and radiotoxicity of the waste alone are not measures of disposal risk. Although the FCES covers the measures identified in the Options Study as being most likely

affected by different fuel cycles, it produced data that enables calculations regarding other waste management considerations.

1.2 Scope of the dissertation

The goal of the study presented in this dissertation is to develop and apply models for evaluating different impacts of waste management and disposal to a comprehensive set of fuel cycles. These models are applied to the fuel cycles in the FCES to compare and contrast different aspects of their waste management. This study adds new perspective to the conclusions derived from the FCES by integrating key aspects of fuel cycle and waste disposal performance.

This study is also unique with respect to the extent of the analysis. Never before has such wide-ranging and standardized fuel cycle data been made readily available for this type of study. Whereas most previous studies in this area compared a single or a few advanced fuel cycles to the current once-through cycle, the FCES provides data for 40 fuel cycles. Additionally the uncertain political situation surrounding YMR warrants more general disposal studies encompassing a variety of possible site geologies. Together, these aspects of the project allow for broad comparison of fuel cycles in tandem with varied repository settings and concepts.

This chapter explored the past work into the relationship between nuclear energy technologies and the environmental impact of waste management. This sets the stage for the technical description of the models used to explore the impact of fuel cycle on waste management, which are introduced in Chapter 2. Chapter 3 describes the determination of nuclear waste characteristics from different fuel cycles and the data and assumptions that underlie those calculations. Results generated from applying the models introduced in Chapter 2 to the fuel cycles introduced in Chapter 3 are presented in Chapter 4. Finally, conclusions and discussions are made in Chapter 5.

Chapter 2

Methodology

Additional analysis is required to better understand the relationships between fuel cycles and the management of their wastes. Properties intrinsic to nuclear wastes, such as mass and radioactivity, do not provide comprehensive perspectives on waste management. Using waste properties as inputs to waste management models can enable further insights into waste management strategy, risk, geological repository design, and environmental impact that can improve the basis for fuel cycle comparison. Unlike detailed performance assessments, these models should be relatively inexpensive to run, allowing for broad parametric and sensitivity studies. These can indicate promising fuel cycle options and identify important parameters that require more study to reduce uncertainty.

In this chapter I introduce and discuss management models that can be used to compare different fuel cycles. In the first section, I describe the characterization of the materials in fuel cycle waste streams, which can yield data for input in subsequent models or which can be useful on its own given sufficient context. The second section describes a model for evaluating the areal footprint of generic, close-contact geologic repositories based on thermal constraints. I discuss the adoption of the thermal constraints, the heat transfer model used to evaluate them, and conceptual repository designs and material properties used in the analysis. In the third section, I present a neutronics model that can be used to screen the possibility of criticality in the far field of geologic repositories. If under conservative conditions the minimum critical mass of fissile material in wastes from a given fuel cycle is greater than the repository inventory, criticality need not be considered as a potential hazard for that fuel cycle.

2.1 Characterization of fuel cycle waste streams

Waste management analyses requires detailed data characterizing the waste. The properties of the waste are the link between the fuel cycle that generates it and the strategies and risks involved in managing it. In this section, I describe different values of interest that characterize waste streams. The data generated by characterizing fuel cycles — mass, volume, heat, radioactivity, radiotoxicity — may not be sufficient on its own, but it can be used as input to subsequent waste management models. The first subsection covers relevant intrinsic properties of the waste streams that are important inputs for waste management models.

To be useful on its own, intrinsic or bulk material property data requires context. In the second and third subsections, I discuss that context for two applications of material data. First, waste stream composition can be used to assess long-lived fission product (LLFP) inventory, which I apply as a proxy for repository performance. Second, intrinsic material properties can be used to calculate a figure of merit for material attractiveness that describes the desirability of material for weapons proliferation.

2.1.1 Determination of waste characteristics

The characteristics of nuclear waste are governed by the fuel cycle that generates it. The primary waste characteristic is the waste composition. Secondary characteristics arise from composition, including decay heat, radioactivity, radiotoxicity, and fissile enrichment. Together, these characteristics are required inputs for waste management models. As an example, in repository performance assessments, time-dependent radionuclide inventories are required to determine the source term and release rates. For another, to calculate radiation dose rates emitted from waste packages, the source spectra and strength, which in turn depend on the radionuclide inventory, must be known.

For this work, the most important characteristics of the waste streams produced by nuclear fuel cycles are the mass, composition, and decay heat of each stream, which are required for the models described later in this chapter. Changes in nuclear material composition — and therefore its characteristics — after material is removed from a nuclear reactor are dominated by radioactive decay, which can be described with a set of coupled equations called the Bateman equations, shown in Equation 2.1.

$$\frac{dX_i(t)}{dt} = \sum_{\substack{j=1 \\ j \neq i}}^{N} \left(l_{ji} \lambda_j X_j(t) \right) - \lambda_i X_i(t). \tag{2.1}$$

In Equation 2.1, X_i is the amount of nuclide i. The first term describes the generation of nuclide i from all other nuclides j, of which there are N total. l_{ji} is the branching ratio, or the fraction of decays of nuclide j that result in the formation of nuclide i and λ_j is the decay constant for nuclide j. The second term describes the decay of nuclide i.

Solving Equation 2.1 yields the time-dependent nuclide composition of material undergoing radioactivity decay, such as nuclear waste. The composition can be transformed into other values, such as decay heat or neutron and gamma emission spectra using conversion factors associated with each nuclide in the material. Because N is large for nuclear waste (usually greater than 1000), Equation 2.1 is solved using software. In this work, the decay calculations are performed using ORIGEN-S and unit conversions are performed using OPUS, both of which are modules in the SCALE-6.2 software suite [21].

Solution of Equation 2.1 yields important values for this work, including the inventory of problematic radionuclides and the fissile enrichment of the actinides that remain in the waste, the analysis of which are described more in Subsections 2.1.2 and 2.1.3. Additionally, the solution provides data required for determining the waste package inventory generated by the fuel cycle and the total decay heat generated by each package, values required for the repository footprint analysis presented in Section 2.2.

2.1.2 Long-lived fission product inventory

Radiological impact, measured by dose to the biosphere, is used in the U.S. and elsewhere as the standard risk-metric against which repository acceptability is judged. Estimation of nuclear waste disposal risks is generally done for one of two purposes: (1) licensing of a geologic repository, for which the site and proposed waste inventory are known, and (2) evaluating the favorability of fuel cycle options. The former is expensive, complex, and requires significant data about the site, making it unreasonable for comparison of hypothetical fuel cycle options. Simple metrics are preferable for this purpose, but in practice, risk is often reduced to easily obtained waste characteristics such as mass or radiotoxicity, which do not reflect many important aspects of geologic disposal [3, 4].

In reality, the repository relies on multiple barriers to delay and dilute the radionuclides that contribute to dose. By delaying release with engineered barriers, the repository allows many shorter-lived radionuclides to decay. Processes that take place in the natural barrier can physically hinder radionuclide transport or can separate radionuclides based on chemical behavior in the geologic environment. The result of these considerations is that the radionuclides that are most important to repository performance are not necessarily those that contribute to overall waste mass or radiotoxicity.

Previous work [4] studied these simple metrics for risk and proposed a new metric: long-lived fission product inventories. In a review of performance assessments performed for repositories located below the water table in different geologic environments, the authors found that five of the seven main contributors to dose out to one million years were long-lived fission products: Se-79, Tc-99, Sn-126, I-129, and Cs-135. Their half-lives and maximum permissible concentrations (MPC) for ingestion in water [22] are tabulated in Table 2.1.

Table 2.1: Long-lived fission product characteristics

Isotope	$t_{1/2}$ (y)	MPC (μCi/mL)
Se-79	1.13e+06	8e−06
Tc-99	2.11e+05	6e−05
Sn-126	2.30e+05	4e−06
I-129	1.57e+07	2e−07
Cs-135	2.30e+06	1e−05

The generation of LLFP in nuclear reactors is governed by fission yield, which in turn depends on the isotope undergoing fission and the energy at which fission takes place. LLFP and their precursors are also consumed in reactors by reactions with neutrons. In theory, then, it should be possible to use these relationships to trace LLFP generation to fuel cycle options. Although additional complexities exist, qualitative fuel cycle characteristics such as neutron spectrum (e.g. fast versus thermal) and primary fuel isotopes can be categorized.

The LLFP inventory in nuclear wastes is based wholly on the waste composition. Because they are long-lived, time-dependent analysis is not required. Further context can be gained if the waste form is specified and its loading fraction is known. These details are elaborated upon in Chapter 3.

2.1.3 Material attractiveness figure of merit

Much of the focus on advanced fuel cycles centers on proliferation and theft resistance. Fuel cycles that separate fissile materials for recycle in reactors pose nuclear security risks by both state and non-state actors. However, using the attractiveness of materials within the fuel cycle as a basis for fuel cycle comparison has been deemed insignificant because attractive materials in most fuel cycle options can be be replaced with unattractive materials by adjusting fuel cycle operating parameters such as the reactor refueling time and the discharge burnup [23].

Although less desirable than relatively pure fissile product separated and recycled within a fuel cycle, waste streams containing fissile materials require physical security and International Atomic Energy Agency (IAEA) safeguards throughout operational handling and past the point of geologic repository closure. As they are moved and stored between points of origin and a repository, wastes may become more vulnerable for diversion. For wastes emplaced in a repository, the IAEA has noted that safeguards for geologic repositories may be required for thousands of years [24]. Over time, radioactivity and heat-generation levels drop sufficiently to allow for direct-contact handling of spent fuels [25] and it has been shown the plutonium from aged spent fuel in a repository can be used to make a nuclear weapon [26]. Indefinite surveillance and maintenance is neither sustainable nor does it agree with the fundamental ethic of the geologic repository, which is to avoid imposing burdens on future generations. Therefore, evaluating the attractiveness of waste materials as potential sources of fissile material for proliferation is an important perspective for comparison.

2.1.3.1 Material attractiveness

The attractiveness of waste streams relates directly to fundamental fuel cycle choices such as species recovered in reprocessing. The source of fissile materials in nuclear waste streams depends on the type of waste. Used nuclear fuels have residual fissile material left over from irradiation. The quality of this material is generally low, given that one factor governing the removal of fuel from a reactor is a drop in reactivity as fissile isotopes are consumed by fission. By contrast, high-level wastes usually contain some amount of unrecovered material due to imperfect separations. Fissile materials may also be left wholly unrecovered by separations processes, such as TRU in a process that recovers only uranium and plutonium for recycling. Complete analysis of fuel cycle waste streams should include analysis of discharged used fuels even for fuel cycles that utilize reprocessing because if nuclear power is ever discontinued, the fuels in the reactors and those awaiting reprocessing may require direct disposal.

The characterization of material attractiveness depends on the threat and diversion scenario. The capabilities of the actor — the person or entity seeking to divert or steal nuclear material — affect the conservatism with which the material attractiveness must be evaluated. Actors with significant capabilities (such as state actors) may possess reprocessing technologies and shielded facilities, enabling them to more easily transform dilute, self-protecting waste materials into more attractive products. As an example, although the initial material target may be used fuel from light water reactors, actors with significant capabilities may be able to recover pure plutonium. In this case, the attractiveness must be evaluated for the pure plutonium. By contrast, actors with relatively few capabilities are more limited in the ways that they can transform materials after diversion. Non-state actors such as terrorists may not have shielded facilities or the ability to reprocess used fuels. Therefore, the attractiveness should be evaluated for the material that is stolen (for example, the used fuel itself).

Attractiveness of nuclear materials can be evaluated in numerous ways depending on the application. For example, in evaluating recycled plutonium streams, metrics such as fissile Pu fraction and Pu-238/Pu ratio can be illustrative of the value of the material for creating weapons and the ease with which the material can be handled, respectively. Similarly, some potential indicators of attractiveness for material streams containing actinide mixtures include overall fissile fraction, specific decay heat, and specific spontaneous neutron emission rate.

Recent work introduced methods for evaluating a figure of merit (FOM) for the attractiveness of nuclear materials [27] that consolidates three important material characteristics: (1) the critical mass, (2) the heat content, and (3) the dose rate. Materials with low critical masses can more easily be fabricated into weapons, making them more attractive. The heat content and dose rate serve to protect the material, so lower values for these quantities improve the material recovery and handling, increasing attractiveness. In the past, the FOM was applied to materials within the fuel cycle rather than the wastes produced by it. The following subsections review the scenario development and methodology for the calculation of the FOM with the intent of applying it to fuel cycle waste streams.

2.1.3.2 Scenario development

As described in the previous subsection, it is important to know from whose perspective is the material attractive and what that actor's capabilities are to handle and process it. Due to the wide range of possibilities and outcomes for the diversion of waste materials, specific scenarios can be developed to cover different degrees of conservatism.

For most waste materials, the bulk material itself is not attractive. The fissile material is too dilute to achieve a critical mass. For spent light-water reactor spent fuel, initially enriched to 4.73% and burned to 60 GWd/t, a critical mass is not possible. Additionally the material will likely have a large dose rate and decay heat content due to the high concentrations of fission products (FPs). These factors make the waste material unattractive on its own.

However, wastes are also more vulnerable for diversion. During transportation they will be beyond the boundaries of controlled facilities, and after emplacement in a repository, they will not be directly monitored. Over time, monitoring capabilities and institutional memory of the repository may be lost. Meanwhile, as controls over the waste fade, the waste self-protection will decrease as well, as the dose rate and decay heat content fall exponentially. This creates opportunities for state or non-state actors to divert or retrieve wastes and apply rudimentary separations to concentrate fissile material.

In this analysis, it is assumed that material in waste packages is diverted or stolen. This may occur by theft during transit or repository operation, or by the location and interception of buried packages in the repository after closure. After diversion, the materials are chemically treated to recovery one of two possible products, Pu or TRU. Recovery of Pu alone yields in material that is likely more attractive, but for many waste streams it may be present only in relatively dilute quantities (for example, in HLW if Pu is recovered and recycled in the fuel cycle). By contrast, TRU may be present in greater quantities and may require simpler separation chemistry but is likely less attractive due to potentially larger dose rates and decay heat and lower reactivity.

2.1.3.3 Figures of merit for material attractiveness

Two variations for the figure of merit are shown in Equations 2.2 and 2.3. In both equations, M is the bare sphere critical mass (kg), h is the heat content (W/kg), and D is the dose rate (rad/hr) from a bare sphere of the material. The equations differ in the way in which the values are calculated.

$$\mathrm{FOM}_1 := 1 - \log_{10}\left(\frac{M}{800} + \frac{Mh}{4500} + \frac{M}{50}\left[\frac{D}{500}\right]^{1/\log_{10}(2)}\right). \tag{2.2}$$

$$\mathrm{FOM}_2 := 1 - \log_{10}\left(\frac{M}{800} + \frac{Mh}{4500} + \frac{N}{10}\left[\frac{D}{500}\right]^{1/\log_{10}(2)}\right). \tag{2.3}$$

If material is recovered after it is reprocessed, or by a proliferator with significant capabilities, the negative effects of the dose and heat will be incurred when handling

the product (e.g. pure Pu) during the fabrication of a weapon. In that case, M, h, and D are calculated for the product material. The equation for FOM_1 describes this scenario. In particular, the dose rate is evaluated for a sphere with mass equal to 20% of M. The maximum amount of material is limited by criticality constraints to be M, which is used as the penalty for the dose rate in Equation 2.2.

If material is recovered before reprocessing by an actor without access to shielded facilities, the dose rate will be incurred during material recovery. Equation 2.3 describes this scenario. The dose penalty is based on the mass of material in the diverted unit (fuel rod, assembly, or waste package), N, and the dose rate D is evaluated for a sphere of the diverted material with mass equal to N. Depending on the scenario and the capabilities of the actor, M and h can be evaluated for the bulk or separated material.

When the value of the FOM is greater, the material is considered to be more attractive. Decreasing M, h, and D act to increase the FOM, making material more attractive. If the value of the figure of merit is less than 0.0, the material in question is considered unattractive for weapons. If the value is between 0.0 and 1.0, the material is considered unattractive but theoretically usable for weapons. If the value is between 1.0 and 2.0, the material is attractive, and if the value is greater than 2.0, the material is considered highly attractive for weapons.

For the scenario described above, the critical mass and the heat content are evaluated for the recovered product. The dose rate is evaluated for the diverted material with mass equal to the package loading, with the expectation that the most significant dose will be received during recovery. This roughly corresponds to a situation in which enough time has passed such that (1) the material in the packages can be handled directly without incurring a lethal dose and (2) reprocessing can be performed without a shielded facility. The evaluation of the FOM is performed for the material at time points between the discharge and 1 million years to assess the evolution of attractiveness over the lifetime of a repository.

The following subsections describe the calculation of the component values of the FOM, M, h, and D for materials of arbitrary composition. The results generated from the methodologies presented here have been checked against those presented in [27], where values are tabulated for different individual actinide isotopes.

2.1.3.4 Critical mass

To calculate the bare sphere critical mass, MCNP6 [28, 29] is run iteratively to determine the critical radius. Cross sections at 293.6 K are used for all isotopes in the stream that have nuclear data in MCNP. For each nuclide, libraries are searched starting with the most recent data, the ENDF/B-VIII library (.80c). After that,

the ENDF/B-VII (.70c), ENDF/B-VI.6 (.66c), Recommended Monte Carlo Cross Section (RMCCS; .55c), ENDL92 (.42c), and LA150N (.24c) are searched. If data for an isotope cannot be found, that isotope is excluded from the calculation.

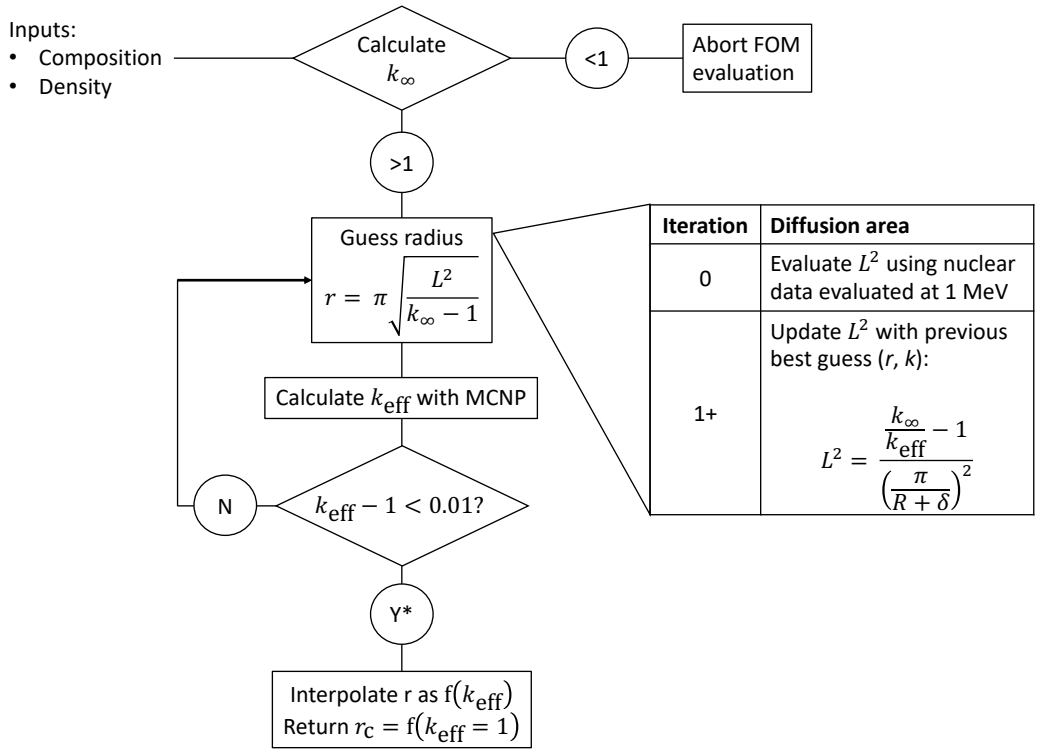

Figure 2.1: Algorithm to calculate the bare sphere critical mass of fissile material streams.

The calculation requires the composition and density of the stream. The algorithm for the calculation is presented in Figure 2.1. First, a rapid, low-fidelity kcode calculation (250 particles per cycle, 50 cycles, skip 20 before generating data) is performed to determine whether the material can achieve a critical mass. If it cannot be critical, then its attractiveness is infinitely negative. If a critical mass can be achieved, then further iterations are performed in order to determine the critical radius, from which the critical mass can be calculated.

Rather than guessing randomly, the radius is estimated using diffusion theory. The intention is not to bypass iterations in MCNP but to use physics to steer the iterations closer to the anticipated solution. From one-group diffusion theory, the

effective multiplication factor is the product of the infinite multiplication factor and the non-leakage probability.

$$k_{\text{eff}} = k_{\infty} P_{\text{NL}}. \tag{2.4}$$

For homogeneous, critical bare sphere, the non-leakage probability P_{NL} from Equation 2.4 can be represented in terms of the diffusion area L^2 and the geometrical buckling for a sphere B_g^2, a function of the sphere radius.

$$P_{\text{NL}} = \frac{1}{B_g^2 L^2 + 1}. \tag{2.5}$$

$$B_g^2 = \left(\frac{\pi}{R + \delta}\right)^2. \tag{2.6}$$

In Equation 2.6, δ is the extrapolation distance. Setting $k_{\text{eff}} = 1$ and rearranging yields an expression for the critical radius.

$$R_c = \pi \sqrt{\frac{L^2}{k_{\infty} - 1}} - \delta. \tag{2.7}$$

The value of k_{∞} is known from the initial MCNP calculation that screened for criticality. Therefore, the main unknown in Equation 2.7 is L^2. For the 0th iteration, L^2 can be approximated based on one-group cross-sections using Equations 2.8.

$$L_f^2 = \frac{D}{\Sigma_a} = \frac{1}{3\Sigma_{tr}\Sigma_a}. \tag{2.8}$$

In Equation 2.8, D is the diffusion coefficient. For fast neutrons, D is the inverse of three times the macroscopic transport cross section, which is shown in Equation 2.9 as a function of the total cross section, Σ_t, the scattering cross section Σ_s, and the scattering angle, μ, which can be approximated as $2/3A$.

$$\Sigma_{tr} = \Sigma_t - \mu\Sigma_s = \Sigma_t - \frac{2}{3A}\Sigma_s. \tag{2.9}$$

The critical radius can be then be approximated for a multi-component material stream by accounting for the major actinide species. Microscopic cross sections and neutrons per fission for different actinide isotopes at 1 MeV are shown in Table 2.2. Microscopic absorption cross sections can be approximated as the sum of the fission and capture cross sections. Given the density of the material, the macroscopic quantities for the stream can be calculated based on this data and the stream composition.

Table 2.2: Nuclear data at 1 MeV for major actinide isotopes

Isotope	σ_t (b)	σ_s (b)	σ_c (b)	σ_f (b)
Th-232	6.927	4.382	0.136	0.00142
U-333	6.791	3.784	0.077	1.85980
U-234	6.905	4.156	0.122	1.09046
U-235	6.906	3.874	0.107	1.20407
U-236	6.945	4.213	0.175	0.35799
U-238	7.091	4.259	0.128	0.01460
Np-237	6.789	3.582	0.173	1.45682
Pu-238	7.061	3.779	0.212	1.99919
Pu-239	6.973	3.650	0.042	1.7354
Pu-240	7.070	3.841	0.086	1.51822
Pu-241	7.013	3.495	0.111	1.55729
Pu-242	7.331	3.945	0.116	1.48999
Pu-244	7.439	4.183	0.074	1.36999
Am-241	7.036	4.109	0.310	1.26150
Am-243	7.164	3.896	0.215	0.98000
Cm-244	7.369	3.750	0.163	2.21099
Cm-245	7.389	3.808	0.072	1.65781

The 0th iteration produces a pair of values (R_0, k_0). To determine the radius for the next iteration, these values are input into Equation 2.4 to find the value of L^2. With this value for L^2, k_{eff} can be set to unity and the equation solved for the critical radius. This procedure is continued using the best previous result (R, k) with small perturbations. The iterations continue until either (1) a value of k_{eff} is obtained within some tolerance, by default set at 0.01; or (2) a maximum number of iterations is reached (by default set at 10). The (k_{eff}, R) parameter space is interpolated to find R when $k_{\text{eff}} = 1$. The critical mass can then be calculated based on the material density.

2.1.3.5 Decay heat

If a critical mass of the material in question is achievable, then the other parameters in the FOM must be calculated. The decay heat load, h (W/kg) is calculated based on the stream composition using ORIGEN-S and OPUS, modules included in the SCALE-6.2 software suite [21]. ORIGEN-S runs depletion and decay calculations and OPUS organizes ORIGEN-S outputs and converts between units. For this problem,

a zero-time decay calculation is performed in ORIGEN-S, after which the results are plotted in OPUS.

2.1.3.6 Dose rate

The dose rate from photons and neutrons at one meter away from a sphere of material is calculated using ORIGEN-S and MCNP6. First, the neutron and photon source spectra (particles per second) are calculated by a zero-time decay calculation in ORIGEN-S using the endf7dec library and tabulated as a function of energy by OPUS. For the neutron calculation, neutrons from (α,n) reactions and spontaneous fission are included. For the photon calculation, the bremsstrahlung medium is set to "none". Because photons are expected to be the dominant contributor to dose, a very fine bin structure is requested, as this improves the result and does not add computational expense. For both particles, the overall source strength is calculated as the sum of the spectra. Then, the neutron and photon spectra are used as the source energy distributions in separate MCNP calculations employing a surface flux tally 1-meter from the surface of the sphere.

A tally multiplier is used to convert from neutron and photon flux (n/cm^2/s, p/cm^2/s) to dose (rad/hr) based on ICRP-21 conversion factors [30], shown in Table 2.4. The neutron dose conversions account for energy-dependent quality factors, whereas the photon dose conversions assume the quality factor for all photons is 1.0. Because MCNP tallies results normalized to a single particle, the tally multiplier result is multiplied by the source strength. The neutron and photon doses are added to yield the final dose rate.

Whereas the critical mass and heat content are evaluated for the target metal, the dose rate is evaluated for the waste material itself. This requires accounting for not only the other nuclides in the waste but also the matrix in which the waste is embedded. The waste form matrix affects the material density and dilutes the concentration of waste nuclides. Although it may provide some shielding from radiation, the primary form of radiation that contributes to the dose will be gamma rays, which are unlikely to be significantly attenuated by the material.

Spent fuels and high-level wastes are treated in different ways. It is assumed that the spent fuel can be either metallic or oxide, depending on the reactor that produced it. If the spent fuel is an oxide, oxygen is added to composition based on the stoichiometric ratios of the heavy metal oxides. Then, the spent fuel density is calculated by taking a mass-average of the major heavy metal oxides. If the spent fuel is metallic, the density is calculated by taking the mass-average of the heavy metals. The densities of actinide metals and oxides are shown in Table 2.3.

Table 2.3: Heavy metal oxides and densities

Element	Density (g/cc)	Oxide form	Oxide density (g/cc)
Th	11.72	ThO_2	10.00
U	18.95	UO_2	10.97
Np	20.25	NpO_2	11.10
Pu	19.94	PuO_2	11.50
Am	13.69	AmO_2	11.65

Table 2.4: ICRP-21 dose conversion factors for neutrons and photons (from [30])

Neutron		Photon	
Energy (MeV)	Dose conversion (rad/hr)/(n/cm^2/s)	Energy (Mev)	Dose conversion (rad/hr)/(p/cm^2/s)
2.50e−08	1.67224e−06	1.00e−02	2.77778e−06
1.00e−07	2.08333e−06	1.50e−02	1.11111e−06
1.00e−06	2.27273e−06	2.00e−02	5.88235e−07
1.00e−05	2.17391e−06	3.00e−02	2.56410e−07
1.00e−04	2.08333e−06	4.00e−02	1.56250e−07
1.00e−03	1.85185e−06	5.00e−02	1.20482e−07
1.00e−02	1.78571e−06	6.00e−02	1.11111e−07
1.00e−01	2.81532e−06	8.00e−02	1.20482e−07
5.00e−01	6.49351e−06	1.00e−01	1.47059e−07
1.00e+00	1.10988e−05	1.50e−01	2.38095e−07
2.00e+00	1.53610e−05	2.00e−01	3.44828e−07
5.00e+00	1.88537e−05	3.00e−01	5.55556e−07
1.00e+01	2.16263e−05	4.00e−01	7.69231e−07
2.00e+01	2.56410e−05	5.00e−01	9.09091e−07
5.00e+01	3.27869e−05	6.00e−01	1.13636e−06
1.00e+02	4.05844e−05	8.00e−01	1.47059e−06
2.00e+02	5.15996e−05	1.00e+00	1.78571e−06
5.00e+02	8.68056e−05	1.50e+00	2.43902e−06
1.00e+03	1.62338e−04	2.00e+00	3.03030e−06
2.00e+03	2.40385e−04	3.00e+00	4.00000e−06
3.00e+03	2.85714e−04	4.00e+00	4.76190e−06
		5.00e+00	5.55556e−06
		6.00e+00	6.25000e−06

Table 2.4: ICRP-21 dose conversion factors for neutrons and photons

Neutron		Photon	
Energy (MeV)	Dose conversion (rad/hr)/(n/cm^2/s)	Energy (Mev)	Dose conversion (rad/hr)/(p/cm^2/s)
		8.00e+00	7.69231e−06
		1.00e+01	9.09091e−06
		2.00e+01	1.56250e−05
		3.00e+01	2.27273e−05
		4.00e+01	2.94118e−05
		5.00e+01	3.57143e−05
		6.00e+01	4.34783e−05
		8.00e+01	5.88235e−05
		1.00e+02	7.14286e−05
		2.00e+02	1.08696e−04
		5.00e+02	1.72414e−04
		1.00e+03	2.04082e−04
		2.00e+03	2.32558e−04
		5.20e+03	2.70270e−04
		1.00e+04	2.94118e−04
		2.00e+04	3.12500e−04

For high-level wastes, the waste form matrix material and waste form density are given based on the material. Only waste forms that contain fissile materials are considered, which for the fuel cycles described in Chapter 3 Section 3.1 are: borosilicate glass made after aqueous reprocessing and after oxidation of the crucible skull formed during melt-refining, with composition from [31]; glass-bonded sodalite ceramic ($Na_8Al_6Si_6O_{24}Cl_2$) made after electrochemical reprocessing [32]; and fluorapatite ceramic ($Ca_5P_3O_{12}F$) made after reprocessing molten salt reactor fuel [33]. These matrix materials are mixed with the nuclides in the high-level waste according to a specified mass loading fraction to produce the final waste form composition. As a simplification, the waste form density is assumed to be the bulk density of the barren matrix material. Additional details about these waste forms and the fuel cycles that produce them can be found in Chapter 3.

2.2 Repository footprint

The primary factor governing the utilization of space in a geological repository for the disposal of nuclear waste is decay heat generation. Compliance with thermal limits throughout the repository can minimize negative effects of heat on engineered and natural barriers and prevent the occurrence of thermally driven processes that affect repository performance. Thermal limits are determined based on aspects of the repository geology and design, such as the properties of the host rock and engineered barrier system (EBS) materials and the identified features, events, and processes (FEPs) of the repository system that could be negatively affected by heat.

The adoption of an advanced nuclear fuel cycle may result in changes to the amount and decay heat characteristics of the waste requiring disposal in a repository. An advanced fuel cycle may employ one or more strategies to improve natural resource utilization, such as increasing burnup in reactors or recycling and transmuting actinides. Both of these options could result in fewer waste packages requiring disposal. However, such a fuel cycle may produce multiple waste streams in which short-lived fission products are concentrated. As a result, these wastes have a higher heat load in the near term.

Previous work demonstrated an opportunity to reduce the areal footprint of repositories in multiple geological environments relative to by transitioning from the once-through light water reactor (LWR) fuel cycle to one in which transuranic (TRU) elements are partitioned from the waste and transmuted. A National Academy report quantifying the benefits of waste partitioning and transmutation estimated that removal and destruction of TRU isotopes could allow for increased repository loading of 4-5 times that of simply directly disposing of light water reactor (LWR) used fuel [34].

Later work quantified the effect of different fuel cycles on the size of repositories in various geologies. Reviews in 2006 and 2011 by the OECD Nuclear Energy Agency [35, 36] included independent and varied analyses of the relationship of fuel cycle and repository utilization in granite (Spain), clay (Belgium) [37, 38], crystalline hard rock (Japan) [39], salt (Germany) [40], volcanic tuff (USA) [41, 42, 43]. Among the studies, the reviews concluded that reduction of disposal drift length by factor of 3-6 (depending on the considered cooling time) can be foreseen by TRU transmutation in comparison with direct disposal. Further partitioning of Cs and Sr (with storage for 100-300 years) or long intermediate storage of vitrified high-level waste (VHLW) without separation could yield further gains.

In contrast with most previous work, this work focuses on the evaluation of repository footprint for wastes produced in fuel cycles rather than wastes created by partitioning and transmutation. This perspective acknowledges that waste management

is a burden on nuclear power generation and the development of new nuclear fuel cycles may not necessarily be accompanied with the means or desire to improve the condition of the waste beyond what is inherently produced in the fuel cycle. Rather than evaluating partitioning and transmutation as a waste management strategy to improve repository footprint, this work enables the evaluation of waste management strategies available to any fuel cycle in order to comply with repository thermal limits: (1) reduce the amount of waste loaded in a waste package; (2) increase the spacing in between waste packages; (3) increase the surface storage time. The relative advantage of implementing one of these strategies over another can depend on the characteristics of the waste and repository because trade-offs exist among these options. Comparative analysis of required repository footprint among fuel cycles and repository designs and geologies and makes possible the evaluation of waste management strategies from the perspective of repository footprint.

2.2.1 Repository thermal limits

The size, design, and layout of a repository for nuclear waste will be limited in part by thermal constraints. Of the many thermal constraints that can be imposed on a repository system, those applying to the near-field (such as peak temperature limits for engineered barrier materials) are of greater consequence than those applying to the far-field (such as limits for the extent of thermally-driven processes) for two reasons: (1) because the near-field temperatures are higher, and (2) far-field temperatures can be effectively limited by limiting near-field temperatures.

Two types of temperature limits can be applied: (1) peak temperatures, or (2) time-temperature exposure. Peak temperatures are useful to prevent phenomena that exhibit threshold-like behavior, whereas time-temperature exposure can be applied to engineered materials whose performance will degrade over time. Some examples of thermal constraints for the near-field and engineered barrier system are shown in Table 2.5 for repositories in different geologic settings [7].

Not all constraints are limiting. For example, a constraint may be applied to limit the waste package surface temperature, but engineered materials are likely more resilient to high temperatures than natural materials such as clay buffer and host rock, which may be in direct contact with the package. In this analysis, the limiting temperature constraint is taken as the peak waste package surface temperature because it is the highest temperature to which sensitive engineered barriers or natural materials are exposed.

Table 2.5: Thermal limits for the repository near-field

Material	Constraint	Explanation
Clay buffers	100°C	Limit thermally-driven alteration (e.g. illitization, cementation)
Crystalline rock	200°C	Limit thermally-induced micro-cracking, especially in less-ductile rocks
Salt (host rock)	200°C	Control uncertainty in performance models induced by thermal perturbation
Clay (host rock)	100°C	Avoid mineralogical changes (cementation) and thermally-driven processes
UNF Cladding	350°C	Limit degradation of cladding integrity due to thermal creep-rupture [44]
Borosilicate glass	500°C	Limit the centerline temperature to avoid devitrification or crystallization

2.2.2 Model development

In a repository with direct-contact emplacement, there is no gap between the waste packages, the EBS, and the host rock. Then, in low permeability media, heat transfer will occur by conduction. The temperature constraint is evaluated for a waste package at the center of a square, symmetrical waste package array, where the contribution of heat from adjacent packages is greatest. The temperature constraints in repositories using vertical borehole, horizontal drift, or alcove emplacement can be calculated using the same heat transfer model because it is independent of emplacement orientation.

This section describes two models used in series to evaluate the thermal constraint for an array of heat-generating waste forms. First, the contribution of heat from adjacent waste packages represented by time-varying heat sources is calculated. This yields the temperature history at the interface of the host rock and EBS for the package at the center of the array. This temperature history is then used as the outer boundary condition for the second step, a steady-state conduction calculations across the EBS layers. These steps are described in detail in the following subsections.

2.2.2.1 Calculating the heat contribution from nearby sources

Previous work [7, 44, 45, 46, 47, 48, 49] applied the superposition of analytic solutions for heat conduction with time-varying heat sources in infinite, homogeneous media to evaluate the temperature at the center of an array of heat sources. Such analytic solutions are collected in the renowned text by Carslaw and Jaeger [50]. The model described here is most closely related to that presented in [7]. The assumptions associated with this model are outlined below.

The conduction of heat from each source to the center of the array occurs through the host rock, which is assumed to be infinite. Waste packages (heat sources) are modeled as finite lines or points, depending on their proximity to the center of the array. The thermal properties of the EBS and waste packages are neglected such that the source is modeled as being surrounded by continuous rock. This homogeneity permits the superposition of analytic solutions for point and finite line sources. The decay heat for all sources of a given type is assumed to be the same (as if all packages were emplaced at exactly the same time). Although careful repository operation such as staggered loading can result in further reduction of the footprint [34], this was not considered in this work.

The thermal properties (thermal conductivity k, thermal diffusivity α) of the host rock are assumed to be time- and temperature-invariant, isotropic, and uniform in space. Although in most materials increasing temperature results in decreasing thermal conductivity, this complexity is avoided by evaluating rock properties at the value of the waste package surface temperature constraint. This is conservative, because this temperature is the maximum allowable temperature that may be experienced by the host rock. This, in turn, results in the host rock presenting the greatest allowable thermal resistance, resulting in higher waste package temperatures.

The ambient temperature is assumed to be 27.5°C in all cases. For a repository located 500 m below the surface, this corresponds to an average ground surface temperature of 15°C and a natural geothermal gradient of 25°C/km.

The package at the center of an $N \times N$ array of waste packages is modeled as a finite line source with length L_{wp}, as shown in Equation 2.10 as Q_{L} (W/m). The remaining $N-1$ packages in the central drift and the N packages in each of the $N-1$ adjacent drifts are represented as point sources Q_{P} (W), given by Equation 2.11. For both types of heat sources, the heat generation rate depends on the number of waste forms per package, n_{wf}.

$$Q_{\mathrm{L}}(t) := \frac{Q_{\mathrm{wf}}(t) n_{\mathrm{wf}}}{L}. \tag{2.10}$$

$$Q_{\mathrm{P}}(t) := Q_{\mathrm{wf}}(t) n_{\mathrm{wf}}. \tag{2.11}$$

The array dimension N is taken as odd so the number of adjacent packages on either side of the central package is equal. An example of the layout of heat sources is shown in Figure 2.2. The size of the array is determined by the center-to-center package spacing within drifts, s_p, and the center-to-center spacing between drifts, s_d.

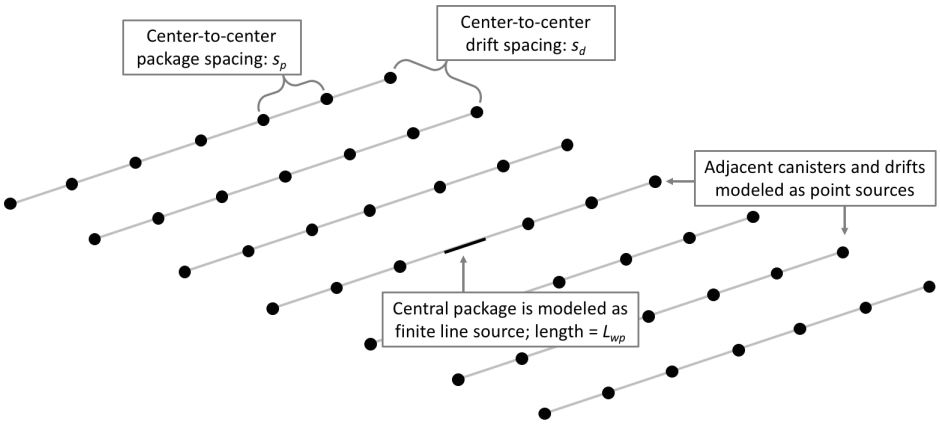

Figure 2.2: Layout ($N = 7$) of repository canister array heat sources used for footprint calculation. This layout suggests horizontal borehole emplacement, but this methodology can be used to represent vertical and alcove emplacement as well [7]. The values of s_d and s_p are used to define the area of the array.

For a given disposal concept, the change in temperature at some distance r and time t due to the heat from a finite line source of length L_{wp} is given in Equation 2.12.

$$\Delta T_{\mathrm{fl}}(r,t) = \int_0^t \frac{Q_{\mathrm{L}}(\tau)}{8\pi k(t-\tau)} \cdot \exp\left(\frac{-r^2}{4\alpha(t-\tau)}\right) \cdot \mathrm{erf}\left(\frac{L}{4\sqrt{\alpha(t-\tau)}}\right) d\tau. \tag{2.12}$$

Similarly, the temperature increase at some distance r and time t due to the heat from a point source is given in Equation 2.13.

$$\Delta T_{\mathrm{pt}}(r,t) = \int_0^t \frac{Q_{\mathrm{P}}(\tau)}{8k\alpha^{1/2}\pi^{3/2}(t-\tau)^{3/2}} \cdot \exp\left(\frac{-r^2}{4\alpha(t-\tau)}\right) d\tau. \tag{2.13}$$

For all times, the contributions from all heat sources are superposed at a point near the central package, which occupies the center of the array. That point is located just above the array plane at a distance equal to the external radius of the last EBS layer; therefore, this evaluation point marks the interface between the EBS and host rock at the central package in the array.

2.2.2.2 Calculation of temperature history in the EBS

The temperature history at the interface of the host rock and EBS is used as the boundary condition for a steady-state conduction calculation across the layers of the EBS. The EBS layers are represented as cylindrical shells, exemplified in Figure 2.3. This calculation yields the temperature history at the inner-most shell, which in a close-contact repository is the interface with the waste package surface. The magnitude of the temperature difference across each shell is affected by its thermal resistance to conduction, which in turn is dependent on its thickness and thermal conductivity. Zero contact resistance is assumed between the layers of the EBS, and the EBS thermal properties are assumed to be constant.

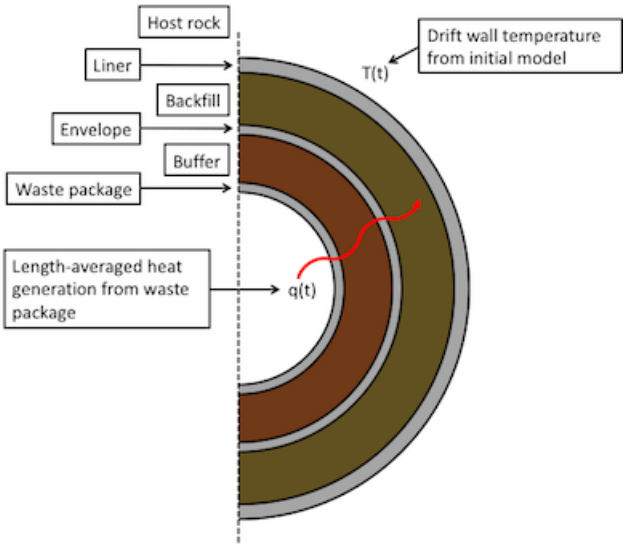

Figure 2.3: Illustration and terminology for a generic engineered barrier system.

That the conduction is steady-state indicates that the heat transferred from EBS to the host rock at all times is equal to the heat generation in the waste. This assumption is due to the fact that EBS components have a low thermal mass relative to that of the host rock, so the heat transfer in the EBS should occur quickly relative

to the heat transfer through the host rock. (The only exception is immediately after disposal when temperatures in the EBS change rapidly.) This assumption is explored in Appendix A.

Under steady-state conditions, the temperature change across the EBS shell can be calculated using Equation 2.14, a function of the inner and outer shell radii and the thermal conductivity k of the shell. In Equation 2.14, $R(r_o, r_i, k)$ is the thermal resistance of the shell. The temperature at the rock-EBS interface given as the outer boundary condition and taken as the initial value for T_o.

$$T_i(r_o, r_i, k) = T_o + \frac{q_L R(r_o, r_i, k)}{2\pi r_o}. \tag{2.14}$$

The calculation is carried out recursively across the EBS layers until reaching the waste package surface, where $r_i = r_{pkg}$. The peak temperature of the package surface is evaluated relative to the thermal limit, which along with the design of the EBS, is dependent on the disposal concept. Reference designs are introduced in a later section.

2.2.2.3 Calculation of repository footprint

The thermal model described in the previous subsections is utilized to to evaluate the temperature constraint for an array of heat-generating packages. The determination of array area requires iterative evaluation of the temperature constraint with variables in space and number.

- Space between drifts (s_d): The spacing between drifts affects the contribution of heat from adjacent drifts to the peak temperature at the calculation point.
- Space between packages (s_p): The spacing between packages affects the contribution of heat from adjacent packages to the peak temperature at the calculation point.
- Size of array (N): The number of adjacent drifts and packages in the unit cell must be large enough that the contribution of heat to the evaluation of the temperature constraint from sources outside that unit cell is negligible.

The values for drift radius r_d and the package length L_{wp} are determined based on repository design and package loading. Given these values, the repository area is defined by the drift (s_d) and package spacing (s_p), as shown in Figure 2.2. The minimum value for s_d is $2r_d$, as if two drifts were located immediately next to each other. The minimum value of s_p is L_{wp}, as if two packages were placed end-to-end.

The area of the $N \times N$ array is calculated as the product of the array length and width, shown in Equations 2.15 and 2.16, respectively.

$$L(s_p) := (n_p - 1)s_p + 2\left(\frac{1}{2}L_{wp}\right). \tag{2.15}$$

$$W(s_d) := (n_d - 1)s_d + 2r_d. \tag{2.16}$$

The minimization of package array area is carried out by the 'scipy.optimize.minimize' function [51] in Python, which minimizes a scalar function of one or more variables. For this application, the 'COBYLA' (Constrained Optimization BY Linear Approximation) algorithm is utilized [52]. The objective function is the array area, and the constraints on the minimization are the peak temperature constraint (expensive) and the minimum spacing requirements. The tolerance on constraint violation is 1%.

The $N \times N$ array represents a subset of a larger, repository-sized array. In reality, additional packages would exist beyond the $N \times N$ array. This becomes significant when the spacing between the packages becomes small and the array boundary is closer to the center. To account for the existence of packages outside the $N \times N$ array considered, the calculation for footprint is repeated with increasing N until the sensitivity of the peak temperature to the inclusion of heat from packages immediately outside the array (in the $N + 1$) row and column of the array) is less than 5.0%. The algorithm used to control this calculation is shown in Figure 2.4.

In practice, the calculation of the required package spacing yields a value for the area required per package (A/N^2), which is then multiplied by the number of packages requiring disposal to determine the repository footprint for a given waste type. For fuel cycles that produce multiple wastes, these areas are summed to find the total repository area.

2.2.3 Generic repositories and thermal properties

This section describes the generic repository designs and required parameters for calculation. This study uses generic close-contact repository designs reported in [7], which were based on comprehensive literature review. Two designs, corresponding to disposal of used nuclear fuel (UNF) or high-level waste (HLW) are proposed for repositories in three geologies—granite, clay, and salt. The EBS design for each generic repository is described by Table 2.6 and illustrated by Figure 2.5. Thermal properties of the rock and EBS materials are evaluated at the value of the peak temperature constraint. Each EBS layer is described by its thickness in order to allow for the emplacement of variably sized waste packages with different waste loading.

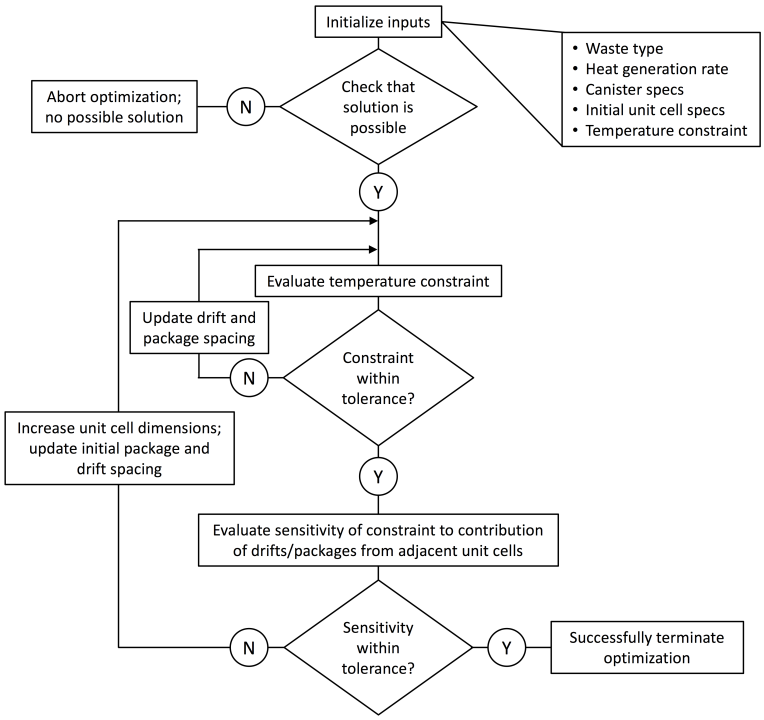

Figure 2.4: Algorithm employed to determine the required repository footprint for different combinations of waste type and disposal concept.

The generic clay design is a horizontal emplacement repository, conforming in practice to the organization of packages in parallel drifts. In the UNF design, bentonite is used as a buffer material. The envelope holds together a prefabricated assembly including the package and solid packed buffer which is slid into the drift tunnel. The HLW design omits the bentonite buffer. In both designs, the packages are separated by spacers, and a liner ensures the stability of the horizontal borehole into clay. The waste package surface temperature constraint is 100 °C to prevent illitization and cementation of the bentonite and/or the host rock clay.

The generic granite design is a vertical emplacement repository that utilizes bentonite as buffer for both UNF and HLW. In this design, the drifts are analogous to the access tunnels used for waste emplacement, and packages are inserted into boreholes in the floor. After emplacement, the access tunnels would be backfilled. The waste package surface temperature constraint is 100 °C to prevent illitization and cementation of the bentonite.

Table 2.6: Generic repository dimensions and thermal properties

Rock (Constraint) Thermal properties	Waste	EBS Layer	Material	Thickness r_o (m)	Thermal cond. k (W/m-K)
Clay $k = 1.75$ W/m-K $\alpha = 6.45\text{e}{-7}$ m^2/s	UNF	Buffer	Bentonite (dry)	0.800	0.60
		Envelope	Carbon steel	0.006	53.0
		Liner	Steel	0.025	46.0
	HLW	Liner	Steel	0.100	46.0
Granite $k = 2.50$ W/m-K $\alpha = 1.13\text{e}{-6}$ m^2/s	UNF	Buffer	Bentonite (dry)	0.350	0.60
	HLW	Buffer	Bentonite (dry)	0.345	0.60
Salt $k = 3.25$ W/m-K $\alpha = 1.60\text{e}{-6}$ m^2/s	UNF	Backfill	75 % intact salt	3.590	2.44
	HLW	Backfill	75 % intact salt	3.695	2.44

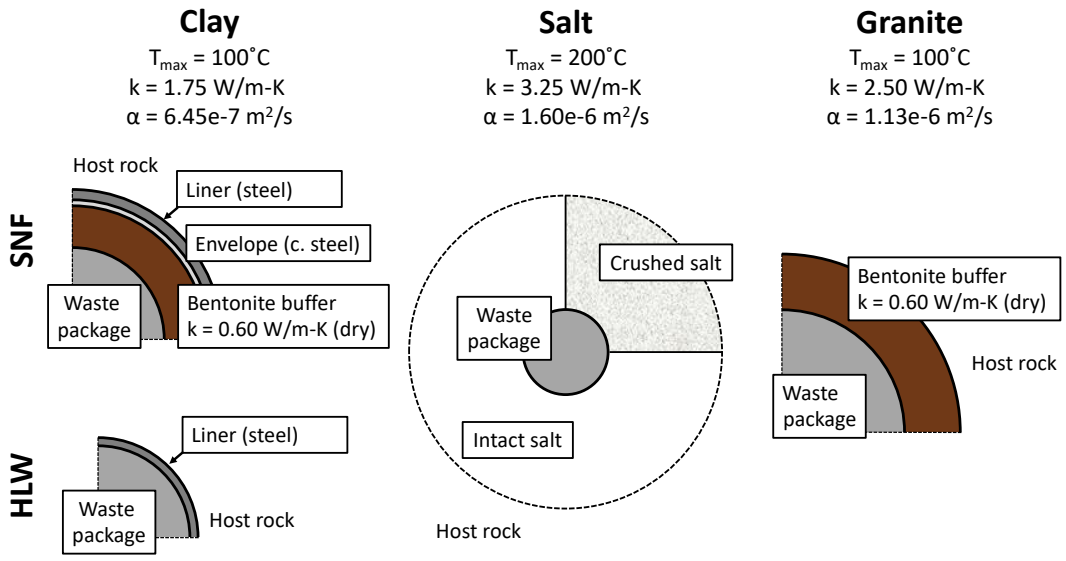

Figure 2.5: EBS concepts for SNF and HLW disposal for close-contact generic repositories in clay, salt, and granite.

In the generic salt design, UNF or HLW packages are emplaced into alcoves excavated into the sides of an access tunnel and backfilled with crushed salt. Although borehole emplacement is possible in salt, experience at the Waste Isolation Pilot Plant (WIPP) indicates that alcove emplacement is preferable [53].

The heat transfer properties of crushed salt are much more resistive than those for intact salt. During the period of peak waste package temperature, the crushed salt will reconsolidate under high temperature into intact salt, resulting in an increase in its thermal conductivity. Because the timing of this evolution is uncertain, only heat transfer through intact salt is accounted for in the calculation. This is assumed to be conservative because it should result in higher waste package temperatures due to the loss of a pathway for heat dissipation. To increase the contact area between the package and the intact salt, the design considers that the wall and floor in the back of the alcoves will be milled away to form a cylindrical resting place for the waste package. It is assumed that 75% of the package surface area is in contact with the intact salt. In previous works, this was considered to be an intermediate case between considering heat conduction through fully intact or fully crushed salt [7].

Chapter 3

Nuclear Waste Analysis in Python

The models introduced in the previous chapter require various data about the nuclear wastes produced by different fuel cycles as input. To generate that data and interface with those models, an object-oriented Python package called `nwpy` (short for Nuclear Waste Analysis in Python, pronounced "nu-pie") is being developed. The package connects the calculation of waste properties with waste management models, enabling straightforward comparison among fuel cycles. A user can engage with the package with some simple scripting or interactively, for example in a Python terminal or Jupyter notebook. In this chapter, Section 3.1 describes the package, its structure, data requirements, and assumptions. A primary objective of the package is to enable comparison of the forty analysis example fuel cycles developed in the Department of Energy (DOE) Fuel Cycle Evaluation and Screening (FCES) study. Section 3.2 describes the analysis examples, their defining characteristics, and the technologies used to obtain metric data. Section 3.3 presents benchmarking results that demonstrate package execution against metric results published in the FCES study.

3.1 Methodology of waste stream characterization

The `nwpy` package performs mass flow calculations to produce values for the mass and composition of different waste streams. Because `nwpy` distinguishes between multiple waste streams from each fuel cycle and determines the loading of wastes into forms suitable for final disposal, the results can be used as input for subsequent waste management calculations, some of which require data on a per-canister basis. The models described in the previous chapter are included in `nwpy` as subpackages.

3.1.1 Code structure

The organization of `nwpy` is loosely based on that of a nuclear fuel cycle flowsheet, which can be organized as a collection of linear stages. Figure 3.1 shows a generalized example of a fuel cycle stage in which the arrows represent the transfer of material between operations. A stage consists of a nuclear reactor and the infrastructure that supports it and is the fundamental unit of a fuel cycle. Fuel cycles may have one or more stages that may be interconnected in different ways. The stage shown in Figure 3.1 shows steps for enrichment and separations, but not all stages require these operations. Within a fuel cycle, each stage produces unique, independent waste streams based on the fuel type, the reactor, and the separations required, among other variables.

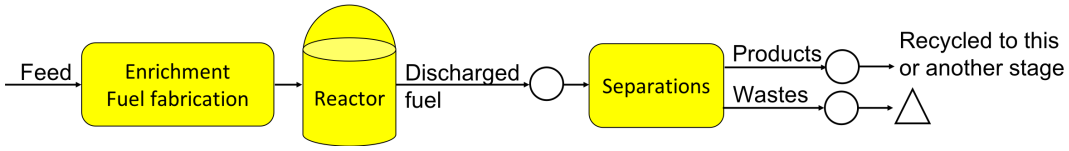

Figure 3.1: A generalized fuel cycle Stage. Different fuel cycles may be made up of one or more stages and may or may not require enrichment or separations steps.

In keeping with this structure, the main code object in `nwpy` for handling the processes that produce and act on material streams is the `Stage` object. In `nwpy`, `Stages` can be collected within `FuelCycle` objects or instantiated and studied on their own. To avoid complexity and focus on the back-end of the fuel cycle, `Stages` in `nwpy` account for only the operations occurring after fuel is discharged from a reactor, assuming that the detailed reactor physics and fuel cycle flow sheet equilibrium mass balances are carried out elsewhere. Proper determination of used fuel compositions and equilibrium mass balances is a significant task that generally requires coupled neutronic-depletion calculations. `nwpy` avoids this complexity by requiring the user to provide these data or select from pre-loaded options, which will be discussed later.

The structure of the `Stage` and the objects that comprise it is shown in Figure 3.2. The arrangement of operations is similar to that of a stage in a fuel cycle flow sheet. Each operation acts on a material `Stream` object, which contains descriptive data such as mass and composition, as well as keywords that identify the form of the stream. These material streams can be passed directly as inputs to the other waste management subpackages in `nwpy`.

Upon instantiation, the `Stage` reads essential data about the processes that comprise the stage and characteristics about the used fuels. As previously mentioned, `nwpy` was built to work with the data produced in the DOE FCES study. The fol-

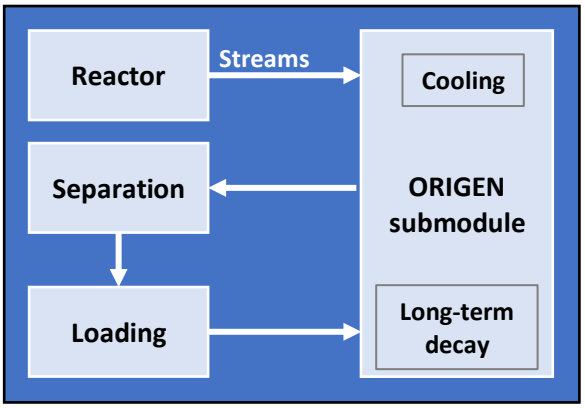

Figure 3.2: Fuel cycle stage operations abstracted in `nwpy`. Each box represents a Python module containing classes that control the indicated operation. The arrows show the flow of `Streams` within the `Stage`. Although these operations are built into methods in the Stage to run in series with a single command, the user can access them directly to examine `Streams` at various points throughout the fuel cycle.

lowing subsection describes the FCES and the data required and its manipulation into `nwpy`. Then in the following subsections, the treatment of material streams in each of the `Stage` submodules is described.

3.1.2 Underlying data and assumptions

The data underlying `nwpy` is obtained from the analysis examples generated in the production of the FCES study, which are described in Section 3.2. The data produced for each analysis example has been adapted and built into `nwpy`, allowing the user to instantiate `FuelCycles` and `Stages` by calling evaluation group identifiers and stage numbers. This subsection describes the data required from the FCES and its manipulation into `nwpy`.

Because `nwpy` handles fuel cycle processes after discharge from the reactor, two critical inputs are the mass and composition of used fuel. The mass is obtained from the mass balance tables published in Appendix B of the FCES final report [54]. The compositions are retrieved as PDFs from the Nuclear Fuel Cycle Options Catalog, hosted on Sandia Connect [55] and converted to CSVs. Each file contains the charge and discharge compositions for each stage in the fuel cycle. The simplest cases are those for which the data specifies compositions for one charged stream and one discharged stream for each stage. More complex examples required more detailed data. For the stages in which more than one discharge stream composition

is specified, multiple mass values are also given corresponding to each discharged stream.

- For some stages in which reactors utilize breeding blankets, the charge and discharge compositions of driver and blanket fuels are specified separately.
- Stages utilizing breed-and-burn operation of sodium fast reactors (SFRs) have compositions specified for initial charge and the discharge of each batch of fuel as it moves through the core
- Composition data files for molten salt reactors (MSRs) include data for charged and discharged fuel as well as well as the streams produced by online salt cleanup and/or online fuel reprocessing

Based on this data, `nwpy` creates one or more `Streams` of material discharged from the reactor. As the `Stream` is passed through the `Stage`, it is manipulated according to prescribed operations. After discharge from the reactor, used fuel must typically be cooled for some time. The FCES also specified the cooling time required for used fuel after discharge and before separations, assumed to be 5 years for all fuel cycles.

For the analysis examples employing limited- or continuous-recycling schemes, the type of separations and the recovered species were specified. For most separations, the separation efficiency (or recovery fraction) was assumed to be 99%, sending 1% of the otherwise recovered product from the feed to the waste stream. The separations processes applied in the FCES were broken into four general groups:

- Aqueous processes, which include plutonium-uranium redox extraction (PUREX), thorium extraction (THOREX), uranium extraction (UREX+; the plus refers to possible subsequent separations of TRU isotopes), co-extraction (of uranium and plutonium mixture; COEX), and new-uranium extraction (NUEX).
- Electrochemical processes (pyroprocessing)
- Melt-refining
- Online MSR separations

For all of these except MSR separations, literature review informed the separation efficiencies of any unspecified elements and the partitioning of waste species among typical waste forms produced by the process. The information for the MSR separations was obtained from the composition data. Additional details on separations are given in later in the chapter.

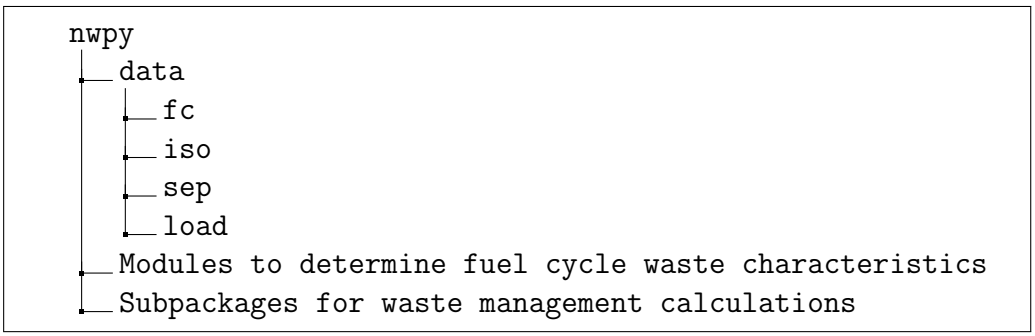

Figure 3.3: Directory structure of the `nwpy` package.

The organization of this data in `nwpy` is indicated in Figure 3.3, which shows the directory tree of the `nwpy` package. The `nwpy/data` directory contains subdirectories for different types of data that characterize aspects of each fuel cycle.

In `fc/`, data files named according to the evaluation group they represent contain data that characterize the fuel cycle. The primary data in each data file are:

1. the mass of UNF discharged from the irradiation system
2. the cooling time required for UNF after discharge
3. the method used to reprocess UNF, if applicable
4. the species recovered from the UNF, if applicable.

The `iso/` directory contains the reactor charge and discharge isotopic compositions, each saved in a CSV file named after the evaluation group to which it refers. In the `sep/` directory, data files for each separation process specified above contain the elemental partitioning fractions among characteristic waste forms for species in the waste stream after the product species have been recovered. The `load/` directory contains data describing the loading of waste streams into characteristic waste forms, described in a later section.

3.1.3 Decay calculations

To generate time-dependent data for `Streams`, `nwpy` interfaces with the ORIGEN-S and OPUS modules from the SCALE code suite [21]. The `origen` module in `nwpy` writes ORIGEN-S input using the SCALE Standard Object Notation (SON) format (in contrast to the legacy, card-based FIDO input interface). Inputs are generated based on the `Stream` mass, composition, and inputs that characterize the decay

calculation (end-time, step count, and interpolation method) and utilize the SCALE endf7dec decay library. Called from within Python, ORIGEN-S performes the decay calculations, after which the OPUS module produces the requested time-dependent results, which may include composition, decay heat, radioactivity, and radiotoxicity. These are assigned to `Streams` that are returned as output.

This capability has two important uses. First, after discharge from a reactor, used fuel must be cooled before further operations such as reprocessing or package loading. As shown in Figure 3.2, the `Reactor` object is the source of material streams in the `Stage`. To account for UNF cooling time, the `Streams` are passed to the `origen` module, which calculates composition and decay heat. These characteristics are significant because they affect the separation and partitioning of elements in reprocessing and the loading of waste streams into waste forms. The required cooling time is specified in the Stage data. For the cooling case, the number of time steps and interpolation method are specified internally.

Second, once separations and waste loading have been applied to `Streams`, the `origen` module can be used to generate time-dependent data. In contrast to the cooling case, the user specifies the end time and the number of steps for the decay calculations. The ORIGEN-S calculation produces OPUS plot files for composition, decay heat, radioactivity, and radiotoxicity, which are appended to the returned `Stream`. These data can be used to benchmark the calculations against the FCES metric data, to compare different `Streams` with the built-in plotting methods, or as input for further waste management calculations that require time-dependent data, such as those that are or will be contained in the other `nwpy` subpackages.

3.1.4 Separations

If the `Stage` requires separations to recover nuclear material for recycling, those separations are applied with the `Separation` object, which partitions the elements in the input `Stream` into multiple waste streams. The type of separation required is governed by the `Stage` data and controls the characteristics of the resulting waste streams. The separation efficiency of recovered elements can be specified by the user but is set by default at 99%. The partitioning of unrecovered elements among waste stream is governed by a data file in the `data/sep/` directory identified by the separations process.

Four different groups of separations processes have been built into `nwpy`, for which general descriptions of outlet streams are given in Table 3.1. Of these, the first three (aqueous methods, electrochemical methods, melt-refining) are separations applied to solid fuels. Although these methods may be able to accept different kinds of used

fuels as feed, in the FCES study, aqueuous processing methods are applied to oxide fuels and electrochemical separations and melt-refining are applied to metal fuels.

Table 3.1: Separations processes and characteristic high-level waste streams

Process	HLW streams	Main species	Ref.
Aqueous	Gas	H, He, C, halogens, noble gases	[56, 57]
	Iodine	I (scrubbed from gas stream)	
	Glass	Unrecovered actinides, decay products Remaining FP	
Electrochemical	Gas	H, noble gases	[58, 59]
	Metal	Most transition metal FP	
	Ceramic	Alkali metal, alkaline earth elements Halogens Rare earth elements Unrecovered actinides, decay products	
Melt-refining	Gas	H, He, halogens, noble gases Other volatile FP (Cd, alkali metals)	[60]
	Skull	Unrecovered actinides, decay products 95% Sr, Y, Te, Ba, lanthanides 1% most transition metal FP (e.g. Ga-Se, Zr-Ag, In, Sn, Sb)	
Online MSR separations	Ceramic	Unrecovered actinides, decay products 60% Y, La, Ce, Pr, Nd, Pm, Sm, Gd 6% Eu 0.1% Rb, Sr	[61, 62]

3.1.4.1 Aqueous separations

Aqueous separations include processes such as PUREX, COEX, NUEX, UREX (and the associated processes referred to as UREX+), and THOREX. Typically, these processes are applied to solid, oxide fuels and produce off-gas and liquid raffinate waste streams. In general, these processes are highly dynamic in that they can be coupled in sequence with additional separations to partition various species in the used fuel, allowing for recovery of virtually any combination of actinides.

In `nwpy`, the waste streams from these processes are assumed to be the same. Gaseous fission products and C-14 are captured during chopping and dissolution by the off-gas system. It is assumed that iodine is scrubbed from the off-gas stream for improved stability in long-term disposal. Throughout the separations steps, various products may be recovered, leaving behind a barren liquid raffinate that includes all remaining fission products as well as any unrecovered actinides remaining due to separations losses. This stream contains that vast majority of the activity and is ultimately converted to glass for long-term disposal.

3.1.4.2 Electrochemical separations

Electrochemical separations, such as pyroprocessing, involve an electrorefining operation that separates actinides and fission products. The process has been demonstrated during the U.S. fast reactor program and is being applied at the Fuel Conditioning Facility in INL for treatment of the EBR-II used fuel. In the electrorefiner, an electrical current is passed through a chloride salt bath in which uranium and other species are already present. Used fuel is chopped and lowered into the salt bath in a metal basket, which acts as the anode. Elements are partitioned between salt and metal phases in the electrorefiner based on their stability in a chloride salt. Multiple types of cathodes can be used to recover different elements that are electrotransported through the salt. A solid steel cathode collects pure uranium, while uranium, transuranics, and rare-earth elements may be recovered in a liquid cadmium cathode [63].

The elements in the used fuel can be partitioned into four groups. The first group is gaseous fission products, such as the noble gases and carbon-14. These are collected during chopping and electrorefining in the off gas system and stored in canisters. Of the remaining three groups that do not form gases, two are relatively easy to classify into one of two waste streams based on the free energy of formation of their chlorides.

Rather than reacting with the salt, noble-metal fission products exist as metals in the electrorefiner. They may remain in the anode basket with cladding hulls or in the salt as metal particulates, which can be filtered. The free energies of formation for chlorides, $\Delta G_f^0(500\ ^\circ\text{C})$ (kcal/mol) of these elements are shown on the right pair of columns of Table 3.2 [59, 64, 65]. Reactive fission products, such as alkali-metal, alkaline-earth, some rare-earth, and halide fission products are anodically dissolved and form stable chloride compounds in the salt. These elements are shown in the left pair of columns in Table 3.2.

The third group includes any remaining rare-earth (typically lanthanide) fission products, Zr, and all actinides. These elements exist in equilibrium between the metal

Table 3.2: Free energies of formation (kcal/mol) of relevant chlorides

Element	ΔG_f^0	Element	ΔG_f^0	Element	ΔG_f^0
$MnCl_2$	-90.6	$CmCl_3$	-64.0	TlCl	-37.4
$BaCl_2$	-87.9	$PuCl_3$	-62.4	InCl	-34.9
CsCl	-87.8	$AmCl_3$	-62.1	$CdCl_2$	-32.3
RbCl	-87.0	$NpCl_3$	-58.1	$FeCl_2$	-29.9
KCl	-86.7	$PbCl_2$	-58.1	CuCl	-27.9
$SrCl_2$	-84.7	UCl_3	-55.2	$NbCl_5$	-26.7
LiCl	-82.5	$CoCl_2$	-49.3	$CuCl_2$	-25.7
NaCl	-81.2	$ZrCl_4$	-46.6	$MoCl_4$	-16.8
$CaCl_2$	-80.7	$NiCl_2$	-45.1	$TcCl_4$	-11.0
$ZnCl_2$	-74.7			$RhCl_3$	-10.0
$CrCl_2$	-71.2			$PdCl_2$	-9.0
$LaCl_2$	-70.2			$RuCl_4$	-6.0
$PrCl_2$	-69.0				
$CeCl_2$	-68.6				
$NdCl_2$	-67.9				
YCl_3	-65.1				

and salt phases in the electrorefiner. These elements are shown in the middle two columns of Table 3.2. In reality, due to the similarity in behavior of some actinides and rare-earth fission products, electrorefining may not result in total fission product decontamination of the actinide product. This may be viewed as an improvement in proliferation resistance. In `nwpy`, the separation is considered in a more simplistic way in conjunction with the FCES study assumption about separation efficiencies. To that end, it is assumed that no rare-earth fission products are recovered.

With all fission products and unrecovered actinides destined for disposal, the partitioning of these elements between the waste forms characteristic of the electrochemical separations process must be determined. The primary waste forms are: (1) a metal waste form that contains the metals that do not form chlorides in the salt, and (2) a ceramic waste form that contains the waste elements that form chlorides in the salt, which are recovered and concentrated during a salt-cleanup step. Where waste species end up in the electrorefiner determines the waste form into which they are partitioned.

Of the three groups presented in Table 3.2, the partitioning of elements in the middle columns is the most complex. This is addressed with simplifying assumptions.

For this analysis, it is assumed that all actinides not recovered as product remain in the salt phase [66]. Additionally, the remaining rare-earth elements are assumed to remain in the salt as well.

The selective recovery of actinides by electrochemical separations (for example, the separation Pu from Am in fuel cycles in which transuranic elements are treated as wastes) may require extra steps or special operation of the electrorefiner. The specific determination of electrorefiner operation is well outside the scope of this work. However, it is expected that electrorefiner operation can be tailored to result in recovered product with any composition. The composition of the product mixture extracted at the cathodes depends on the amounts of U, Pu, rare-earth metals, and cadmium in the electrorefiner anode, salt, and cathode. Because there exists a salt composition that can result in recovered product of any composition, and the composition of the salt is controlled by the addition or removal of species during electrorefiner operation [67], the product mixture can be controlled by the operator.

Table 3.3: Partitioning of elements in electrorefiner wastes in `nwpy`

Salt (ceramic waste form)	Metal (metal waste form)
Alkali metals (Li, Na, K, Rb, Cs, Fr)	Noble metal FP (Y, Nb, Mo, Tc, Ru, Rh, Pd, Ag, Cd, Sn, Te, Zr, etc.)
Alkaline metal FP, decay products (Be, Mg, Ca, Sr, Ba, Ra)	Cladding materials (Fe, Cr, Ni, Zr)
Lanthanides with stable chlorides (La, Ce, Pr, Nd, Sm, Eu)	
FP with soluble anions (Br, I, Se, Te, As, Sb)	

It should be noted that a similar technology, requiring an additional head-end processing step, can be applied with equal success to fuel types other than metallic fuel, such as LWR oxide fuel (PYROX). However, this process produces somewhat different waste streams due to the volatilization of some semi-volatile fission products during the required head-end process. Because the FCES study generally applied electrochemical separations to metal fuels, this separation is not considered in `nwpy`.

3.1.4.3 Melt-refining

Melt-refining was initially proposed as the method for reconditioning the fuel for EBR-II and the Integral Fast Reactor. In the melt-refining process, metal fuel is melted in a crucible within a vacuum chamber, prompting the removal of gaseous, volatile, and reactive fission products from the melt and providing straightforward addition of makeup materials. The process is physical, not chemical, and this simplicity enables use for fuels with short cooling times. However, a side effect of this simplicity is that fission product decontamination of the process product is relatively low.

In melt-refining, gaseous and volatile fission products are released as gases. There are four main groups of volatile fission products: alkali metals (Rb, Cs), halogens (I, Br), noble gases (Kr, Xe), and cadmium. Of these, Rb and Cs make up the vast majority of the activity. The temperature of the melt is between 1300-1400 °C. For reference, the non-reactive elements with boiling points at or below that range are listed in Table 3.4; all values except for At and Fr come from [68].

Table 3.4: Boiling point ranges of non-reactive gaseous and volatile elements

Element	Boiling point (°C)
H, N, F, O, Cl Noble gases	< 0.0
Br, I, P, At, Hg, S	0 - 500
As, Cs, Fr, Se, Rb, K, Cd, Na, Zn, Po	500 - 1000
Li	1000 - 1400

Meanwhile, reactive species, such as alkaline-earth and rare-earth fission products as well as some actinides, react with the zirconia crucible via oxidation. Some uranium in the fuel is also oxidized. These species, along with about 5-10% of the fuel, remain as a solid layer (or "skull") adhered to the crucible after the molten fuel is poured out. Noble fission products and actinides will remain in the melt, which is recast into fuel. Although the new fuel still includes some noble fission products, many fission product poisons are removed. Additionally, because the new fuel is recast and recladded, melt-refining negates accumulated burnup damage.

After the skull is removed from the crucible, it can be further processed to recover uranium and purify it from the fission products in the skull. This additional processing is required if melt-refining is to be used in a continuous recycle process in order to maximize recovery of U and Pu, thereby minimizing makeup requirements, and to achieve an equilibrium concentration for noble fission products, which would otherwise build up to levels that could affect reactivity [60].

The assumptions employed for melt-refining recoveries vary between the two analysis examples in the FCES study that utilized the process. In one case, it was assumed that 50% of all fission products, regardless of expected behavior, would remain in the fuel. However, as previously discussed, fission products behave differently in the melt depending on their properties, as described above. Table 3.5 summarizes the treatment of species in melt-refining from the other analysis example (EG09) [55]. This recovery behavior was adopted largely as-is for use in `nwpy`, as shown in Table 3.1 and is supported by descriptions in [60]. The main difference is that `nwpy` assumes that that actinides not targeted for recovery are sent to the waste.

Table 3.5: Recovery fractions of species in melt-refining process

Species	Recovery fraction
Th, Am	$< 5\%$
All other actinides	99%
Br, Kr, Rb, Cd, I, Xe, Cs	$< 0.1\%$
Sr, Y, Te, Ba and lanthanides	$< 5\%$
All other FP	99%

3.1.4.4 MSR separations

The online separation was created to address MSR fuel cycles. In online fuel salt reprocessing, some fuel salt is diverted away from the main loop to undergo fission product removal after a brief holdup to allow for decay of the shortest-lived fission products. The online separation is considered separately from the online salt cleanup in which noble gas and metal fission products are removed from the fuel salt within the primary loop.

One promising separation method is the fluoride volatility process to remove uranium as fluoride gas, which is purified with sorption and desorption steps [62]. Keeping with the assumptions set forth in the FCES study, the online separation assumes a default 99% target actinide recovery. After the products are removed, the barren salt is recovered by vacuum distillation, leaving rare-earth fission products

in the still bottoms. Good separation between salt components LiF and BeF and rare-earth fluorides is expected based on their volatilities [61].

The two FCES analysis examples with MSRs utilized different fractions for rare-earth separation. One case assumed that 6% of most rare-earths (La, Ce, Pr, Nd, Pm, Sm, Gd) and Y and 0.6 % of Eu would be separated from the circulating salt. The other assumed that ten times more material (60% of most rare-earths and Y and 6% of Eu) would be separated. Both cases are accessible to the user in `nwpy`.

3.1.5 Waste form preparation and package loading

After spent fuels are discharged and separations are applied, if applicable, waste streams are loaded into waste forms and/or waste canisters for disposal in the `Loading` object, which returns a special type of `Stream` called a `WasteForm`. In addition to those that define a `Stream`, the `WasteForm` has two mandatory attributes: the dimensions of the waste package and the number of waste packages of its kind produced in the stage. Other attributes are returned on a per-package basis.

The numerical determination of waste form preparation for high-level wastes and package loading for spent nuclear fuels is based on literature review and assumptions. The following subsections describe the waste form and package loading for different types of spent nuclear fuels and high level wastes.

3.1.5.1 Spent fuel and high-level waste packages

This section describes the waste packages into which spent fuels and high-level wastes are emplaced for disposal. A waste package consists of an inner canister that is loaded with waste and an overpack that provides corrosion resistance. For spent fuels, the canisters generally contain metal inserts that hold the fuel assemblies. High-level wastes are generally poured into directly into canisters as liquids.

In reality, waste packages materials and designs are selected in concert with a repository site and as a part of an overall repository performance assessment. The material and required thickness of the overpack depend in part on the geochemical environment in which it will reside. For this work, generic waste canister and overpack designs and dimensions are assumed for disposal of spent fuels and high-level wastes. No materials are specified, and dimensions, including thicknesses, could be modified if relevant to future studies.

The spent fuel package sizes depend on the type of fuel and the number of fuel assemblies they hold and will be described in a later section along with descriptions of the spent fuels from different reactors. All SNF packages have an overpack thickness of 5 cm and most have an inner canister thickness of 7.5 cm.

Most high-level wastes described in the preceding discussions utilize a standard HLW package design. In reality, different wastes may be emplaced in different packages depending on waste loading and waste form properties, but for this analysis, the waste package design is largely standardized to facilitate comparison. The standard package has external (overpack) length of 4.7 m and diameter 0.82 m, based on a design proposed in [49]. With an overpack thickness of 5 cm and canister thickness of 7.5 cm, this yields about 1.52 m^3 of internal volume to be filled with waste. The mass limit for this canister is 2900 kg. In a following section describing the waste loading for different HLW streams, cases for which the standard package is not applied will be clarified and stream-specific designs will be introduced.

For all HLW streams, fixing the package design also fixes the amount of waste material that can be loaded into the package. This is in contrast to the SNF packages, for which discrete package designs are specified for varying waste loading. To vary HLW loading, `nwpy` provides keyword arguments through which the user can arbitrarily specify the waste fraction loaded into the waste form. In this way, although the available volume is fixed, the amount of waste occupying that volume can be manipulated.

3.1.5.2 Spent nuclear fuels

For spent nuclear fuels (SNF), the mass of initial heavy metal in each assembly is assumed. Because the waste stream mass is known, this yields the number of assemblies requiring disposal. The number of assemblies loaded into each package can be chosen by the user based on options available in the data file. Varying the number of assemblies per package affects the package dimensions.

Pressurized-water reactor (PWR)

PWR spent fuels are assumed to have 460.0 kg of heavy metal per assembly [69, 70]. Package designs are shown in Figure 3.4 based on designs specified in [49]. The 4-assembly package can be utilized with spacers in unfilled sections to achieve 2- and 3-assembly loading.

Heavy-water reactor (HWR)

For HWR spent fuels, the assembly loading refers to the number of 108-bundle baskets stacked on top of one another within the package. Each bundle has 37 elements, in total containing 18.8 kg uranium [71]. The reference data is for 324-bundle

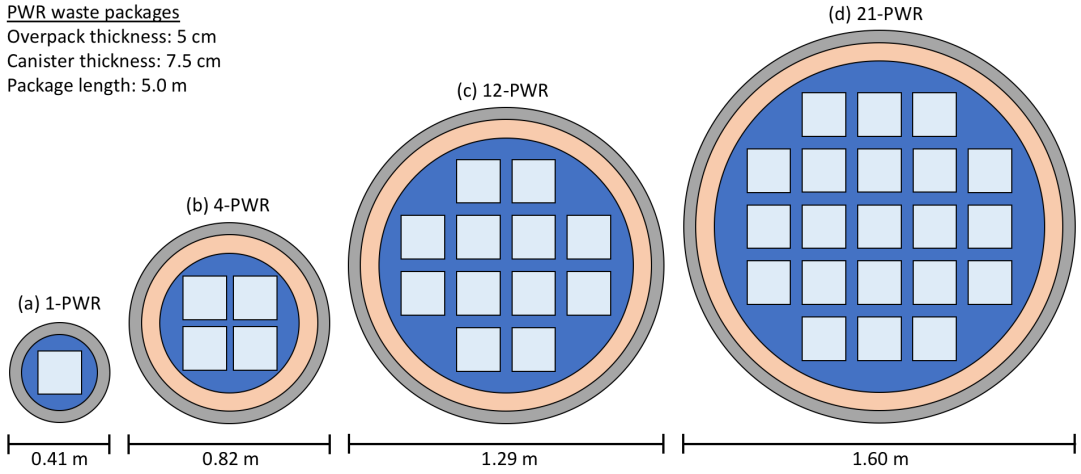

Figure 3.4: PWR spent fuel package dimensions and layouts; each light blue square represents the position of a fuel assembly in the package.

package (three 108-bundle baskets) [72], based on which additional hypothetical dimensions are proposed assuming more or fewer baskets are stacked in the package. Each basket contains two layers of 54 bundles. The bundles are 495 mm in length and the basket is 1035.4 mm in length [73]. In the 3-basket package, there is 760.8 mm of extra non-fuel material added to the package length; assuming all thicknesses stay the same, this value is added to the height of the stacked baskets to determine the height for the hypothetical packages shown in Figure 3.5.

High-temperature gas reactor (HTGR)

For the other spent fuel cases, additional inputs and assumptions may be required. The fuel for the HTGR is assumed to be in the form of prismatic graphite blocks in which vertical channels are loaded with fuel compacts made up of spherical tristructural isotropic (TRISO) particles. The prismatic block geometry and is based on the fuel utilized at Fort St. Vrain [74]. Each block has 7.2 kg of heavy metal [75]. In `nwpy`, the default is that full blocks are emplaced into waste packages, but the user may indicate whether the fuel is consolidated before loading into packages by removing the compacts from the graphite blocks. This would increase waste package heavy metal loading as compared to the direct disposal of the entire graphite block. That value is determined by approximating the volume and density of the compacts to determine the mass of fuel that can be emplaced in a canister of specified volume.

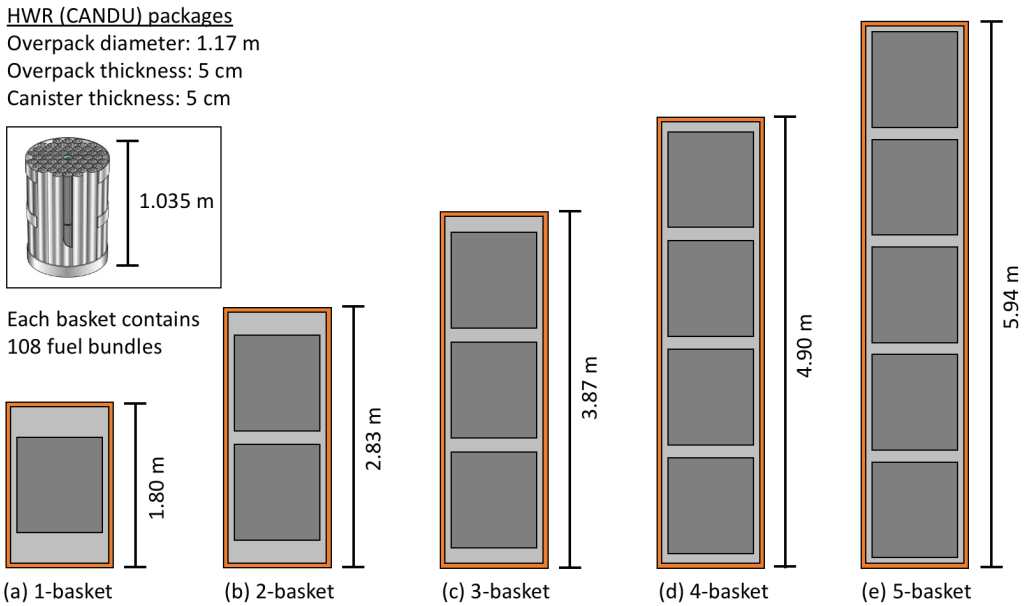

Figure 3.5: HWR spent fuel package dimensions and layouts; each dark gray square represents a basket of 108 HWR fuel bundles.

The HTGR default packages are shown in Figure 3.6, which comes from [74].

Fast reactors

Because there are few fast reactors in operation and most fuel cycle concepts involving them promote extensive breeding and recycling, the literature regarding the direct disposal of spent fuels from fast reactors is sparse. For this reason, the waste package dimensions for spent fuels from fast reactors are proposed based on approximate assembly dimensions. Two fast reactor assemblies are considered: accelerator-driven systems (ADS) and sodium fast reactors (SFR). Both use hexagonal assemblies and have similar dimensions, so one package design is assumed for both types of spent fuels.

ADS assemblies have similar dimensions and heavy metal loading to the assemblies used in the Accelerator Transmutation of Nuclear Waste (ATW) concept [76, 77]. SFR assemblies have dimensions similar to those used for the ABR-1000 reference design fuel assemblies [78] with heavy metal loading taken from [7]. The dimensions of the assemblies are shown in Table 3.6, with packages shown in Figure

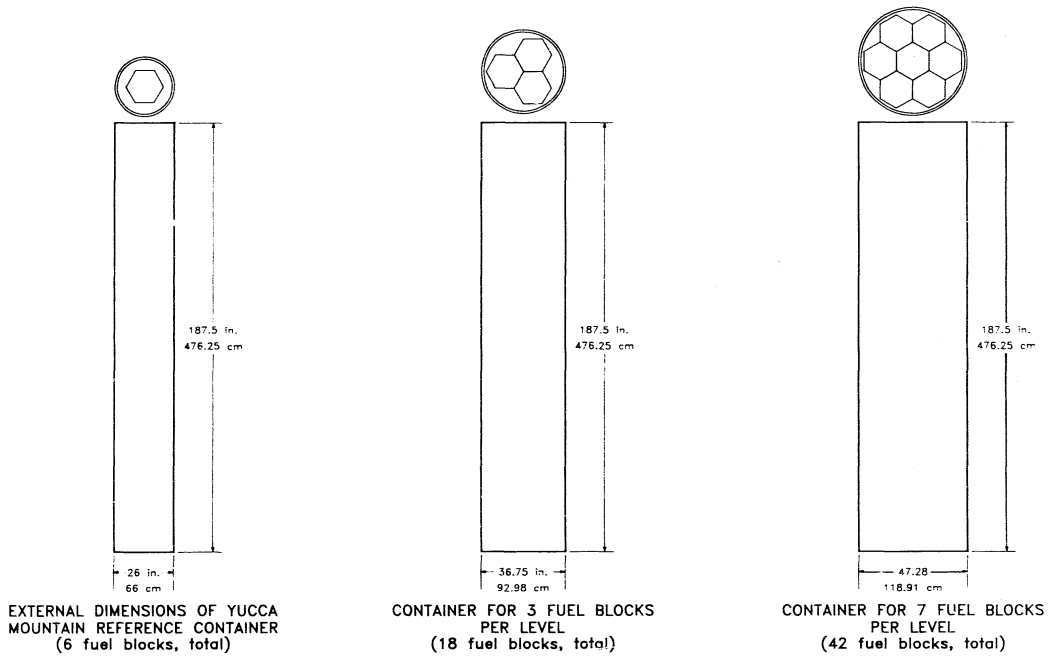

Figure 3.6: HTGR spent fuel package dimensions and layouts (from [74]).

3.7.

Table 3.6: Fast reactor representative assembly dimensions

Reactor	ADS	SFR
Heavy metal loading (kg)	11.6	97.7
Long diagonal (cm)	18.6	18.1
Short diagonal (cm)	15.6	15.7
Length (cm)	—	477.5

Molten salt reactor

Molten salt reactors utilize liquid fuel that circulates into and out of the reactor core. Fission products that are not stable in the salt, such as gases and noble metals, are removed within the primary loop. Although many molten salt reactors will utilize fuel processing to recover fuel species and remove fission products from the salt, some proposed designs involve the direct discharge and disposal of fuel salt.

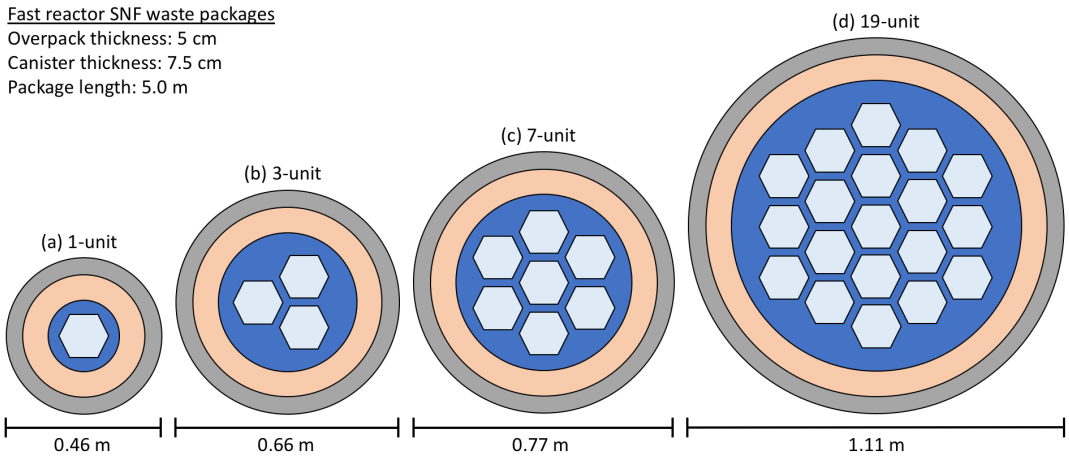

Figure 3.7: Fast reactor spent fuel package dimensions and layouts; each hexagon is a position in which to place a fast reactor assembly.

There are no proposed technologies for the direct disposal of molten salt. For most spent fuels, any chemical processing is a burden on waste management and generally defeats the purpose of planning for direct disposal. However, molten salt reactor discharged fuel is liquid. Even the cooled, solidified salt is unlikely to be an attractive candidate waste form. For this reason, it is assumed that the discharged salt is distilled to remove the carrier salt and concentrate the fission products and actinides, which are then loaded into a waste form (e.g. fluorapatite) with a loading fraction of 10%. This is similar to the way the MSR reprocessing wastes are treated, which is described in the next subsubsection. The waste package is the standard HLW waste package introduced in the previous subsubsection.

Fusion-fission hybrids

A fusion-fission hybrid (FFH) is a subcritical reactor in which the neutrons that go on to generate power in a fission blanket are generated by D-T fusion. Two types of FFH reactors are considered. One is a molten-salt reactor (MSR) blanket in which U-233 is bred from thorium and burned. The spent fuel, discharged molten salt, is treated like directly discharged MSR salt.

The second FFH fission blanket utilizes TRISO particles embedded within graphite pebbles, analogous to the Laser Inertial Fusion Energy concept developed at Lawrence Livermore National Laboratory. After discharged, the pebbles are directly disposed

in packages with the same canister and overpack dimensions as the 1-, 4-, 12-, and 21-assembly PWR packages, as shown in Figure 3.4, without the assembly-dividing inserts. The characteristics of the pebbles are shown in Table 3.7 [79].

Table 3.7: FFH fuel pebble package loading

Parameter	Value
Pebble diameter	2.0 cm
TRISO particle diameter	0.105 cm
Fuel kernel diameter	0.060 cm
Fuel kernel density	10.0 g/cc
Volume fraction of TRISO particles in pebbles	0.15
Heavy metal (HM) per pebble	1.17 g
Void fraction of pebbles in package	0.40

Using the volume of the fuel pebbles, the inner volume of the PWR packages, and a void fraction of 0.4 [80], the fuel pebble loading into each type of package can be calculated. The number of pebbles loaded into the smallest package is 2.58e5; into the largest package, 1.16e6 pebbles.

3.1.5.3 High-level wastes

For HLW streams produced by reprocessing, waste form loading is equivalent to a dilution due to the addition of matrix material to stabilize the waste for long-term disposal. A value for waste form loading fraction can be specified by the user using a keyword argument. Although the separations processes above generally produce more than one waste stream, loading is implemented only for waste streams containing the bulk of the decay heat and radioactivity. The method and constraints used to determine waste loading depends on the form of the waste streams. Support for others may be developed in the future.

Borosilicate glass (aqueous separations)

After product elements are removed from the waste stream by aqueous separations, the raffinate is loaded into a borosilicate glass waste form by mixing in a melter with glass frit. The elements in the waste stream are accounted for as oxides. The loading is determined by applying a linear programming model [81] with the following constraints [7]:

1. total glass mass limit < 2900.0 kg
2. maximum waste loading fraction < 0.45 (previous works [81] used 0.30 as the maximum)
3. heat limit < 14 kW
4. MoO_3 loading fraction < 0.025
5. Noble metal (Ag, Pd, Rh, Ru) fraction < 0.03

Notably, this methodology does not include calculation of the density of the glass waste form and the compliance with a volume constraint. This would require specifying the composition of the borosilicate glass.

Metal and ceramic waste forms (electrochemical separations)

The two waste forms produced by the electrochemical separations – one metal, one ceramic — are prepared differently. The metal waste form, which contains cladding hulls and noble metal fission products, is fabricated using the same linear programming model as applied to the glass HLW with different constraints.

1. Total waste mass < 3600.0 kg [7]
2. Target waste form composition is SS-15Zr [82, 83]

The Zr is both a fission product as well as a component of the fresh fuel, assuming fresh SFR metal fuel contains 10 wt% Zr [7]. The stainless steel comes primarily from the cladding hulls (55 kg clad/assembly [7]). Assembly hardware not sent through the electrorefiner is assumed to make up any difference between the cladding and the requirement. It is assumed that there is sufficient assembly hardware available to meet this demand, and any leftover can be treated as ILW or LLW.

The ceramic waste form is made when the electrorefiner salt is drawn down for cleanup. The loaded salt is be immobilized in zeolite (typically dehydrated zeolite-4A), which is then blended with glass frit at high-temperatures to make glass-bonded sodalite, the final waste form [57]. Waste form loading is based on assumptions for key component fractions. The maximum allowable fission product concentration in the salt is expected to be between 5-20 wt% and salt content in the sodalite waste form will be around 7.5 wt%, assuming no salt recovery [84]. In the electrometallurgical processing of the EBR-II fuels, the weight fraction of salt in the zeolite is about 10 wt% and the fraction of glass in the glass-zeolite mixture is 25 wt% [32]. Given these

example parameters, the loading of the ceramic waste form is performed assuming the following values:

1. If no salt recovery, weight fraction of fission products in the salt at drawdown: 10 wt%
2. If salt is recovered, weight fraction of fission products in the remainder: 95 wt%
3. Weight fraction of salt in salt-loaded zeolite: 10 wt%
4. Weight fraction of zeolite in glass-bonded sodalite: 75 wt%

Gas and crucible skull (melt-refining)

After melt-refining, the volatile and semi-volatile FP have been released from the molten fuel as gases. The noble gases are held in tanks to allow for decay and, ultimately, controlled release to the environment. The remaining radionuclides will be stripped from the gaseous effluent. Of these, the alkali elements (Rb, Cs) have by far the largest activity and decay heat. The primary off-gas system HLW is the molecular sieve used to capture these elements. The molecular sieve can accomodate approximately 3.14 g Cs / in^3 [85]. Assuming the sieves themselves are an acceptable waste form for disposal, they can be crushed to reduce their volume and emplaced into canisters for disposal.

As described above, the skull adhered to the crucible after the molten fuel is poured out contains uranium, reactive fission products, and unmelted fuel. The skull is removed from the crucible by oxidation, at which point additional separations and purification steps can be applied. In keeping with the relatively simple recovery behaviors described in the previous subsection for melt-refining, it is assumed that all species not recovered or volatilized are contained in the waste stream stemming from skull treatment. This waste stream can be made into a borosilicate glass waste form similar to that produced from aqueous reprocessing. Glass loading is carried out using the same linear programming model previously introduced for the aqueous HLW.

Molten-salt reactor metal and ceramic wastes

In contrast to the treatment of other waste streams described in this chapter, there is little to no experience with fabricating waste forms for the waste streams

produced in the molten salt reactor. What exists is drawn from operational experience with the Molten Salt Reactor Experiment (MSRE) at Oak Ridge National Laboratory (ORNL), which ran from 1965-1969. Although the MSRE has been out of service for almost 50 years, decommissioning is ongoing and the fission products still reside in the cold fuel salt awaiting processing and disposal. Just as the work to stabilize the EBR-II used fuels led to great advances and experience in electrochemical separations technology, the decommissioning and stabilization of the salt may yield the same for MSRs. Although this section postulates waste stream treatment for MSRs, it does so in a very general way in an attempt to remain relevant to whatever method is accepted. The values used here for fission product loading are assumptions that should be explored via parametric study to understand their impact on waste management.

The accumulation of waste over the lifetime of the MSR occurs in a fundamentally different way than for other reactors and the separations processes associated with them. In general, other reactors continuously produce spent fuels that can be treated and disposed of in a steady state way. In contrast, many MSR designs (including MSRE) proposed that waste products from online processing of the fuel salt be accumulated in tanks over the lifetime of the plant (around 30 years). Then, waste treatment would occur as a part of decommissioning. If this design is to be adopted, a comprehensive analysis of MSR waste treatment should account for this holdup. However, it should also be possible that the waste produced by the MSR is continuously processed and loaded into waste forms for disposal. In this work, MSR wastes are treated in this way, which agrees with the treatment of wastes from other fuel cycles.

There are two primary waste streams from MSRs that require treatment. The online fuel salt cleanup removes noble gases and metal fission products from the fuel salt within the primary loop. In the FCES, this is treated as a component of the reactor, not a separations process, which is why it is not mentioned in the previous subsection. However, these waste still require stabilization for disposal. The gases are held in a tank to allow for decay (primarily of radioactive isotopes of Xenon), while the noble metal fission products are loaded into a metal waste form with 10% fission product loading.

Reprocessing of the fuel salt produces a stream of fission product halides and unrecovered actinides, which can be loaded into a fluorapatite material [86]. The base case loading is assumed to be 10%. The user can specify with keyword arguments whether fuel salt is recovered (for example, via distillation), which dramatically increases fission product loading in the waste form (the default setting is for the salt to be recovered).

3.2 Fuel cycle cases

The methods presented in Chapter 2 are applied to a broad set of fuel cycles, comprised of the technologies and characteristics described in the preceding section. This section details these fuel cycles, which originate from the Fuel Cycle Evaluation and Screening study. The FCES study aimed to assess the potentially infinite space of fuel cycle technologies by differentiating them based on fundamental characteristics. The study defined a set of 4398 potentially viable fuel cycle option groups based on permutations of fuel cycle functional characteristics. These characteristics included:

- Feed element: Th, U
- Enrichment requirement
- Irradiation system: critical or subcritical
- Neutron spectrum: thermal or fast
- Extent of recycle: None, limited, or continuous
- Recycled species: Th, U, Pu, TRU, etc.

Each fuel cycle option group represents all possible specific fuel cycle options described by these fundamental characteristics. These groups were combined into forty evaluation groups based on expected performance with respect to the criteria against which they were to be judged. For each evaluation group, an analysis example was selected for in-depth analysis and metric evaluation by specifying the irradiation environment and fuel type. More details about the grouping and analysis example selection process are available in [20] and its appendices.

The `nwpy` package interfaces with data derived for these analysis examples, which are described in detail in [54]. Because the assumptions described in Section 3.1 are technology-specific, the results generated using `nwpy` for a specific analysis example may not well-describe the entire evaluation group it represents. However, these analysis examples provide a broad set of potential fuel that can be compared and contrasted based on their fundamental characteristics and specific technologies. In the FCES study, the evaluation groups are referred to by the notation "EGxx", where "xx" is a number between 01 and 40. In keeping with this notation, both `nwpy` and this thesis refer to evaluation groups in the same way.

Table 3.8 shows the fundamental characteristics for each evaluation group and the specific technologies used in the given analysis example. Although most characteristics are mentioned explicitly, for brevity some are left implied by the specified tech-

nologies. All reactors are critical except the fission-fusion hybrids and accelerator-driven systems. Evaluation groups EG01-EG08 are once-through (OT) fuel cycles; EG09-EG18 are limited-recycle (LR); and EG19-EG40 are continuous-recycle (CR). The waste forms produced by each fuel cycle are specified to the reactor or separation process.

Beneath each entry is a identification code that identifies the evaluation group by the recycle scheme and details about the fuel cycle. For the once-through fuel cycles, the code includes feed element and the reactor type (e.g. the once-through use of uranium in PWRs would appear as "1.OT—PWR—U"). For each stage of the limited- and continuous-recycle fuel cycles, the code includes the reactor type and recovered elements from reprocessing (e.g. the continuous recycle of uranium (U) and plutonium (Pu) in PWRs and SFRs would appear as "31.CR—PWR/SFR—U/Pu"). These codes will be used to differentiate the fuel cycles in later figures because they are more immediately informative than the simple evaluation group identifiers. These codes are shown in Table 3.9, to which readers can refer to connect codes with evaluation groups and the characteristics described in Table 3.8.

Table 3.8: FCES evaluation group characteristics and analysis example technologies

Eval. group	Stage	Feed element	Enrich.	Reactor	Spectrum	Burnup (GWd/t)	Separation	Recycled element
EG01	1	U	Y	PWR	Thermal	50.0	None	None
EG02	1	U	Y	HTGR	Thermal	120	None	None
EG03	1	U	Y	HWR	Thermal	7.50	None	None
EG04	1	U	N	SFR	Fast	277	None	None
EG05	1	Th, U	Y	HTGR	Thermal	100	None	None
EG06	1	Th	N	FFH	Fast	118	None	None
EG07	1	U	N	ADS	Fast	55.0	None	None
EG08	1	Th	N	FFH	Fast	729	None	None
EG09	1	U	N	SFR	Fast	492	Melt-refining	U, TRU
EG10	1	Th	N	MSR	Thermal	101.9	MSR separations Salt cleanup	Th, U None

Table 3.8: FCES evaluation group characteristics and analysis example technologies

Eval. group	Stage	Feed element	Enrich.	Reactor	Spectrum	Burnup (GWd/t)	Separation	Recycled element
EG11	1	Th U	N Y	SFR	Fast	377 130	Melt-refining	U, Th
EG12	1 2	U RU, Pu	N N	HWR PWR	Thermal Thermal	7.50 50.0	Aqueous None	U, Pu None
EG13	1 2	U RU, Pu	Y N	PWR PWR	Thermal Thermal	50.0 50.0	Aqueous None	U, Pu None
EG14	1 2	U RU, Pu	N N	SFR PWR	Fast Thermal	100.0 50.0	E-chem None	U, Pu None
EG15	1 2	U RU, Pu	Y N	PWR SFR	Thermal Fast	50.0 127	Aqueous None	U, Pu None
EG16	1 2	U Pu	Y N	PWR ADS	Thermal Fast	50.0 390	Aqueous None	Pu None
EG17	1 2	U Th, Pu	Y N	PWR PWR	Thermal Thermal	50.0 50.0	Aqueous None	Pu None

Table 3.8: FCES evaluation group characteristics and analysis example technologies

Eval. group	Stage	Feed element	Enrich.	Reactor	Spectrum	Burnup (GWd/t)	Separation	Recycled element
EG18	1 2	Th, U RTh, RU	Y N	PWR PWR	Thermal Thermal	60.0 58.0	Aqueous None	Th, U None
EG19	1	U, Pu	N	HWR	Thermal	8.00	Aqueous	U, Pu
EG20	1	U, TRU	N	HWR	Thermal	7.60	Aqueous	U, TRU
EG21	1	U, Pu	Y	PWR	Thermal	45.0	Aqueous	U, Pu
EG22	1	U, TRU	Y	PWR	Thermal	45.0	Aqueous	U, TRU
EG23	1	RU, Pu U	N N	SFR	Fast	81.5 23.5	E-chem	U, Pu
EG24	1	U, TRU	N	SFR	Fast	73.0	E-chem	U, TRU
EG25	1	Th, RU3 U	N Y	PWR	Thermal	26.0 49.0	Aqueous	Th, U U, TRU
EG26	1	Th	N	MSR	Thermal	884.9	MSR separations Salt cleanup	Th, U, TRU None

Table 3.8: FCES evaluation group characteristics and analysis example technologies

Eval. group	Stage	Feed element	Enrich.	Reactor	Spectrum	Burnup (GWd/t)	Separation	Recycled element
EG27	1	Th	N	SFR	Fast	1.4	E-chem	Th, U
		U, RU, RU3	Y			36.8		U
		U, RU	Y			37.8		U
EG28	1	Th, U3	N	SFR	Fast	63.0	E-chem	Th, U
		Th	N			4.0		Th, U
EG29	1	RU, Pu	N	SFR	Fast	96.8	E-chem	U, Pu
		U	N			20.7		
	2	RU, Pu	N	PWR	Thermal	50.0	Aqueous	U, Pu
EG30	1	RU, TRU	N	SFR	Fast	107	E-chem	U, TRU
		U	N			23.0		
	2	RU, TRU	N	PWR	Thermal	50.0	Aqueous	U, TRU
EG31	1	U	Y	PWR	Thermal	51.0	Aqueous	U, Pu
	2	RU, Pu	N	SFR	Fast	169	Aqueous	U, Pu
EG32	1	U	Y	PWR	Thermal	50.0	Aqueous	U, TRU
	2	RU, TRU	N	SFR	Fast	132	E-chem	U, TRU

Table 3.8: FCES evaluation group characteristics and analysis example technologies

Eval. group	Stage	Feed element	Enrich.	Reactor	Spectrum	Burnup (GWd/t)	Separation	Recycled element
EG33	1	RU, Pu	N	ADS	Fast	77.3	E-chem	U, Pu
		U	N			11.3		
	2	RU, Pu	N	PWR	Thermal	50.0	Aqueous	U, Pu
EG34	1	RU, TRU	N	ADS	Fast	77.6	E-chem	U, TRU
		U	N			11.3		
	2	RU, TRU	N	PWR	Thermal	50.0	Aqueous	U, TRU
EG35	1	U	Y	PWR	Thermal	50.0	Aqueous	Pu
	2	Pu	N	ADS	Fast	303	E-chem	Pu
EG36	1	U, Pu,	Y	PWR	Thermal	45.0	Aqueous	U, Pu, MA
	2	MA	N	ADS	Fast	172	E-chem	MA
EG37	1	U	Y	PWR	Thermal	50.0	Aqueous	U, TRU
	2	RU, TRU	N	SFR	Fast	103		U, TRU
		Th	N			14.0		Th, U3
	3	U, RU, RU3	N	PWR	Thermal	55.0		RU, U3, TRU
EG38	1	Th, RU3	N	SFR	Fast	49.0	E-chem	Th, U3
		Th	N			1.30		
	2	RTh, RU3	N	PWR	Thermal	50.0	Aqueous	Th, U3

Table 3.8: FCES evaluation group characteristics and analysis example technologies

Eval. group	Stage	Feed element	Enrich.	Reactor	Spectrum	Burnup (GWd/t)	Separation	Recycled element
EG39	1	U	Y	PWR	Thermal	61.7	Aqueous	U, TRU
		Th	N					Th, U3, TRU
	2	Th, U3	N	PWR	Thermal	56.0	Aqueous	Th, U3, TRU
	3	TRU	N	ADS	Fast	194.9	E-chem	TRU
EG40	1	Th	N	ADS	Fast	138	Aqueous	Th, U3
	2	Th, U3	N	PWR	Thermal	62.5		

Table 3.9: Evaluation group fuel cycle identification codes

Recycle Strategy	Evaluation Group	Identification code
No recycle	EG01	1.OT—PWR—U
	EG02	2.OT—HTGR—U
	EG03	3.OT—HWR—U
	EG04	4.OT—SFR—U
	EG05	5.OT—HTGR—U/Th
	EG06	6.OT—FFH—Th
	EG07	7.OT—ADS—U
	EG08	8.OT—FFH—Th
Limited recycle	EG09	9.LR—SFR—U/TRU
	EG10	10.LR—MSR—Th/U3
	EG11	11.LR—SFR—U/Th/U3
	EG12	12.LR—HWR/PWR—U/Pu
	EG13	13.LR—PWR/PWR—U/Pu
	EG14	14.LR—SFR/PWR—U/Pu
	EG15	15.LR—PWR/SFR—U/Pu
	EG16	16.LR—PWR/ADS—U/Pu
	EG17	17.LR—PWR/PWR—U/Th/Pu
	EG18	18.LR—PWR/PWR—U/Th/U3
Continuous recycle	EG19	19.CR—HWR—U/Pu
	EG20	20.CR—HWR—U/TRU
	EG21	21.CR—PWR—U/Pu
	EG22	22.CR—PWR—U/TRU
	EG23	23.CR—SFR—U/Pu
	EG24	24.CR—SFR—U/TRU
	EG25	25.CR—PWR—U/TRU/Th/U3
	EG26	26.CR—MSR—Th/U3/TRU
	EG27	27.CR—SFR—U/Th/U3
	EG28	28.CR—SFR—Th/U3
	EG29	29.CR—SFR/PWR—U/Pu
	EG30	30.CR—SFR/PWR—U/TRU

Table 3.9: Evaluation group fuel cycle identification codes

Recycle Strategy	Evaluation Group	Identification code
Continuous recycle	EG31	31.CR—PWR/SFR—U/Pu
	EG32	32.CR—PWR/SFR—U/TRU
	EG33	33.CR—ADS/PWR—U/Pu
	EG34	34.CR—ADS/PWR—U/TRU
	EG35	35.CR—PWR/ADS—U/Pu
	EG36	36.CR—PWR/ADS—U/Pu/MA
	EG37	37.CR—PWR/SFR/PWR—U/TRU/Th/U3
	EG38	38.CR—SFR/PWR—Th/U3
	EG39	39.CR—PWR/PWR/ADS—U/TRU/Th/U3
	EG40	40.CR—ADS/PWR—Th/U3

3.3 Benchmarking

The Fuel Cycle Evaluation and Screening study assessed the forty evaluation groups against nine criteria used to compare their performance. Six of these criteria represent opportunities for benefit, and three represent potential challenges. Each criterion is made up of one or more metrics against which analysis example data could be binned to evaluate fuel cycle performance. The waste management criterion contains five metrics, all normalized to energy production:

1. Mass of SNF and HLW disposed (t/GWe-y)
2. Activity of SNF+HLW at 100 years after disposal (Ci/GWe-y)
3. Activity of SNF+HLW at 100,000 years after disposal (Ci/GWe-y)
4. Mass of depleted uranium (DU), recovered uranium (RU), and recovered thorium (RTh) disposed (t/GWe-y)
5. Volume of low-level waste (LLW) per energy generated (m^3/GWe-y)

Of these metrics, the first three can be evaluated using `nwpy`. The mass of spent nuclear fuel and high-level waste reflects the fuel cycle mass balance at steady state. The natural resource requirement and the extent of recycling are significant factors

affecting the mass of waste produced. The major contributors to activity at 100 years are fission products and actinides with shorter half-lives. The activity at 100,000 years reflects the long-term radioactivity of the actinides in the waste. Together, these two metrics describe the composition of the waste stream.

To generate these values in `nwpy`, only the cooling and separations steps must be applied to the material streams generated based on mass flow and discharge composition data. The benchmarking results reflect the conservation of material mass throughout the `nwpy` package up through separations, including in interactions with ORIGEN. For fuel cycles that utilize separations, the characteristics for each waste stream produced are summed to yield the total value for all HLW. The benchmarking should also indicate the quality of the assumptions regarding separation efficiencies. The waste form loading step, while important for enabling different types of waste management calculations, is not required to evaluate these metrics, which only reflect characteristics of the bulk waste stream. Comparison of the results from `nwpy` with those published in the FCES [23] is a confirmation that the data produced by the package is in line with previous work. Table 1 contains the ratio of each metric as evaluated by `nwpy` to the metric reported in the FCES study. The agreement is generally good. Values for which the ratio exceeds 5% error are shown in red.

Table 3.10: `nwpy` benchmarking; values in table are the ratio between the result generated using `nwpy` and the result reported in the FCES study

Fuel cycle ID code	SNF+HLW Mass	SNF+HLW Activity 100 y	SNF+HLW Activity 100,000 y
1.OT—PWR—U	0.9998	0.9955	0.9978
2.OT—HTGR—U	1.0037	0.9986	1.0053
3.OT—HWR—U	1.0000	0.9944	1.0019
4.OT—SFR—U	0.9989	0.9972	0.9875
5.OT—HTGR—U/Th	1.0031	0.9955	1.0014
6.OT—FFH—Th	1.0026	0.9991	1.0034
7.OT—ADS—U	1.0013	0.9990	1.0000
8.OT—FFH—Th	0.9969	0.9937	0.9831
9.LR—SFR—U/TRU	0.9976	1.0020	0.9770
10.LR—MSR—Th/U3	11.831	1.0644	12.091
11.LR—SFR—U/Th/U3	1.0203	1.2977	0.9834
12.LR—HWR/PWR—U/Pu	1.0004	0.9936	1.0001
13.LR—PWR/PWR—U/Pu	1.0033	0.9962	1.0005

Table 3.10: Benchmarking of waste management metrics in `nwpy` against FCES results

Fuel cycle ID code	SNF+HLW Mass	SNF+HLW Activity 100 y	SNF+HLW Activity 100,000 y
14.LR—SFR/PWR—U/Pu	0.9991	0.9998	0.9885
15.LR—PWR/SFR—U/Pu	0.9983	0.9926	0.9908
16.LR—PWR/ADS—U/Pu	1.0143	0.9976	0.9932
17.LR—PWR/PWR—U/Th/Pu	0.9992	0.9937	0.9960
18.LR—PWR/PWR—U/Th/U3	1.0016	0.9962	0.9987
19.CR—HWR—U/Pu	0.9880	0.9991	0.9902
20.CR—HWR—U/TRU	0.9887	1.0000	0.9890
21.CR—PWR—U/Pu	0.9904	1.0013	0.9889
22.CR—PWR—U/TRU	0.9717	1.0002	0.9856
23.CR—SFR—U/Pu	0.9977	0.9955	0.9323
24.CR—SFR—U/TRU	0.9835	0.9931	0.9748
25.CR—PWR—U/TRU/Th/U3	0.9866	0.9880	0.9564
26.CR—MSR—Th/U3/TRU	98.179	1.1709	109.74
27.CR—SFR—U/Th/U3	0.9993	0.9946	0.9953
28.CR—SFR—Th/U3	1.0021	0.9935	0.9925
29.CR—SFR/PWR—U/Pu	0.9995	1.0006	0.9868
30.CR—SFR/PWR—U/TRU	1.0105	0.9998	0.9715
31.CR—PWR/SFR—U/Pu	1.0025	0.9955	0.9848
32.CR—PWR/SFR—U/TRU	0.9996	0.9989	0.9810
33.CR—ADS/PWR—U/Pu	0.9946	0.9943	0.9742
34.CR—ADS/PWR—U/TRU	0.9955	0.9946	0.9670
35.CR—PWR/ADS—U/Pu	1.0020	1.0045	0.9471
36.CR—PWR/ADS—U/Pu/MA	0.9749	0.9939	0.9793
37.CR—PWR/SFR/PWR—U/TRU/Th/U3	1.0192	0.9964	0.9779
38.CR—SFR/PWR—Th/U3	1.0249	0.9964	0.9972
39.CR—PWR/PWR/ADS—U/TRU/Th/U3	0.9826	1.0063	0.9966
40.CR—ADS/PWR—Th/U3	0.9970	0.9893	0.9402

For the most part, the agreement is good. The differences in metric values can be explained by considering the slight differences in methodology between `nwpy` and the FCES analysis examples. The two evaluation groups that fail across all metrics are those for which the analysis examples utilize molten salt reactors. The treatment

Table 3.11: Benchmarking results for MSR fuel cycles with modified recovery fractions

Fuel cycle	Recovery fraction	SNF+HLW Mass	SNF+HLW Activity 100 y	SNF+HLW Activity 100,000 y
10.LR—MSR—Th/U3	U3: 0.9999654 Th: 0.99999882 TRU: 1.0 REE: 0.4 (Eu: 0.94)	1.0515	1.0161	1.0040
26.CR—MSR—Th/U3/TRU	U3: 0.999943458 Th: 0.999999 Pu: 0.98969 REE: 0.94 (Eu: 0.994)	1.0156	1.0414	1.0320

of molten salt reactors in the FCES is unique relative to the other analysis examples in two regards. First, the values in the mass balance tables are very high, reflecting the fact that the entire fuel salt inventory circulates through the online reprocessing system 121.67 times per year (once every three days) [54]. The high values for mass flows increase the magnitude of any disagreement between the `nwpy` and FCES results. The second difference is that the recovery for product actinides assumed for MSRs in the FCES is different than that of other fuel cycles. To remedy this, the recovery of actinides can be explicitly defined to override the default value of 99%. For both MSR fuel cycles, the recoveries can be inferred based on the analysis example mass balance table [54]. The final difference is with respect to the separation efficiency of rare-earth elements (REE); in Sub-subsection 3.1.4.4, the different options for rare-earth element recovery in MSR separations were described. For fuel cycle 26.CR—MSR—Th/U3/TRU, the option for lower rare-earth recovery is required (in other words, more rare-earth elements remain in the fuel salt). Applying these modifications manually, the results are improved to those shown below in Table 3.11. In the waste management analyses presented in Chapter 4, MSR separations will be treated in the same way as the other separations technologies, with separation efficiency of 99% for all recovered species and the lower recovery fractions for rare-earth elements. Case studies utilizing the details in Table 3.11 will be presented where possible.

The differences in metric results can be explained in a similar way for other the other fuel cycles. Excluding the MSR fuel cycles, no other fuel cycle has a difference

in metric evaluation greater than 6%, and no fuel cycles have difference in the metric for mass of SNF and HLW. In addition to the MSR fuel cycles, only one other fuel cycle, 11.LR—SFR—U/Th/U3, has errors in the activity of SNF+HLW at 100 years, pointing to differences in fission product inventory. This fuel cycle example utilizes a breed-and-burn (B&B) sodium fast reactor consuming U-233 bred from thorium and in which the fuel is reconditioned using melt-refining. The FCES analysis example assumed that in melt-refining, 50% of all fission products would be recovered in the new fuel. However, as discussed above, the behavior of fission products in the melt-refining process depends on their reactivity and volatility. Accounting for these behaviors results in more fission products being sent to the waste stream, increasing the near-term activity of the waste stream.

Three fuel cycles have benchmarking differences between `nwpy` and the FCES results for activity at 100,000 years: (1) 23.CR—SFR—U/Pu, a single-stage fuel cycle in which U and Pu are continuously recycled in SFRs; (2) 35.CR—PWR/ADS—U/Pu, a two-stage fuel cycle in which Pu from used LWR fuel in the first stage is used as makeup for an accelerator-driven system (ADS) in the second stage; (3) 40.CR—ADS/PWR—Th/U3, U-233 is bred from ADS in the first stage is used to fuel PWRs in the second stage.

For 23.CR—SFR—U/Pu, the breeding ratio of Pu from U is slightly greater than break-even. The FCES study assumes that this extra Pu is treated as HLW. The `nwpy` metric evaluation can capture this by adjusting the separation efficiency of Pu to send more to the waste. When the separation efficiency equals 0.984, the mass of Pu sent to the HLW stream is equal to 0.9 tons of Pu (per 100 GWe-y), identical to the value reported in the mass flow table [54]. The result of adjusting the separation efficiency in this way is shown in Table 3.12.

The other two fuel cycles, 35.CR—PWR/ADS—U/Pu and 40.CR—ADS/PWR—Th/U3, do not have any stated differences that should cause the evaluations of the metric to differ between `nwpy` and the FCES results. One commonality is that both utilize ADS. Other continuous-recycle fuel cycles utilizing ADS, such as 33.CR—ADS/PWR—U/Pu, 34.CR—ADS/PWR—U/TRU, and 36.CR—PWR/ADS—U/Pu/MA (but excluding 39.CR—PWR/PWR/ADS—U/TRU/Th/U3) also have somewhat lower values for the long-term activity metric, as shown in Table 3.10. One possible explanation for this pattern is material losses for fuel fabrication, which are not accounted for in `nwpy`. Reducing the recovery of the primary fuel elements, as shown in Table 3.12, shows that agreement with the FCES study can be improved in this way. However, the values for recovery fractions shown are guesses. More careful study of these fuel cycles and the underlying data could improve agreement.

With the exception of the MSR fuel cycles, the benchmarking results between `nwpy` and the FCES study increase confidence that `nwpy` is treating materials in

Table 3.12: Benchmarking results for fuel cycles with custom recovery fractions

Fuel cycle	Recovery fraction	SNF+HLW Mass	SNF+HLW Activity 100 y	100,000 y
23.CR—SFR—U/Pu	Pu: 0.984	1.0068	0.9982	0.9761
35.CR—PWR/ADS—U/Pu	Pu: 0.980	1.0064	1.0080	0.9712
40.CR—ADS/PWR—Th/U3	Th: 0.989 U: 0.989	1.0080	0.9894	0.9736

the fuel cycles in an appropriate way. With the ability to generate waste stream compositions for the different FCES fuel cycles, the metrics introduced in Chapter 2 can be applied to study the fuel cycles as well as the effects of separation efficiency and waste loading fraction.

Chapter 4

Results

This chapter presents the results generated by applying the models presented in Chapter 2 to the waste streams from the Fuel Cycle Evaluation and Screening study, characterized by the methodologies presented in Chapter 3.

Section 4.1 discusses the characteristics of the nuclear waste that are important for subsequent analysis, including the total decay heat and the waste package inventory. Section 4.2 shows the results for the inventory of long-lived fission products in the waste streams. Section 4.3 presents the figure of merit calculations characterizing material attractiveness. Section 4.4 shows the results for the area required for heat-generating waste disposal in three generic, close-contact geologic repositories.

Throughout these sections, discussions and observations are made connecting the results to the characteristics of the fuel cycles that generate the waste. In many of the figures and discussions, the reference result will be that for the once-through PWR fuel cycle (EG01: 1.OT—PWR—U. In the FCES, this fuel cycle is used as the base case against which the performance of other fuel cycles is judged.

4.1 Waste characterization

Solution of Equation 2.1 to obtain time-dependent waste characteristics is required for waste management analysis. These characteristics themselves can be assessed with context or can be used as input into waste management models. Later sections in this chapter discuss some of these characteristics, including the inventory of long-lived fission products and the fissile enrichment of actinides in the waste. This section presents the waste package inventory and waste decay heat load from each fuel cycle as examples of important information required for input into waste management models, such as the repository footprint model for which results are presented in 4.4.

4.1.1 Waste package inventory

The waste package inventory is determined for each waste stream produced by the fuel cycle cases introduced in Chapter 3. Figure 4.1 shows total number of packages produced by each fuel cycle as a function of those loading values. For SNF, the color of the bar indicates the size of the package. Warmer colors indicate larger packages with higher waste loading, resulting in fewer packages. No legend is given because each reactor type produces spent fuel for which packages offer different waste loading options; these are introduced in Chapter 3. The HLW waste forms are loaded according to the waste form type associated with the prescribed separation process. This too is described in Chapter 3. This yields only a single option for HLW waste loading.

With low waste package loading, the once-through fuel cycles produce greater package inventories than the fuel cycles that utilize recycling. However, if large packages are allowable, the differences are small. The limited-recycle fuel cycles produce only modest amount of SNF, which is due to the mass balances associated with these fuel cycles [54]. The continuous recycle fuel cycles all produce approximately the same number of packages per unit energy. In Figure 4.1, there are only a few outliers. These are: 7.OT—ADS—U, a once-through ADS system with poor thermal efficiency that utilizes relatively small fast reactor assemblies; and molten-salt reactor fuel cycles 10.LR—MSR—Th/U3 and 26.CR—MSR—Th/U3/TRU, for which the separation efficiency utilized in this work was different from that assumed in the FCES study, as discussed in Chapter 3 Section 3.3. Further detail on the effects of this are given in the discussions in Section 4.4.

With further research and development, improvements and limitations may be realized for the production of different HLW streams. In Figure 4.2, the HLW loading is parameterized based on a range of potential HLW loading fractions to highlight the impact on waste package inventory. The waste loading fraction varies from 1% to 50% — in reality, 50% may be too high for some waste forms due to limitations that govern waste chemical and thermal durability. Notably, some heat-dilute waste streams, such as the metal waste forms produced from electrochemical separations, may have values for waste loading fraction that are greater than 50%.

The MSR fuel cycles 10.LR—MSR—Th/U3 and 26.CR—MSR—Th/U3/TRU are again outliers in Figure 4.2 due to the effect of separation efficiency on waste requiring disposal. For the remaining fuel cycles that produce HLW, package inventories as low as 1 package per GWe-y may be possible with high waste loading fractions. These parametric values for SNF and HLW package inventory are utilized in the thermal model for repository footprint.

Another required input for that model is the decay heat produced by each pack-

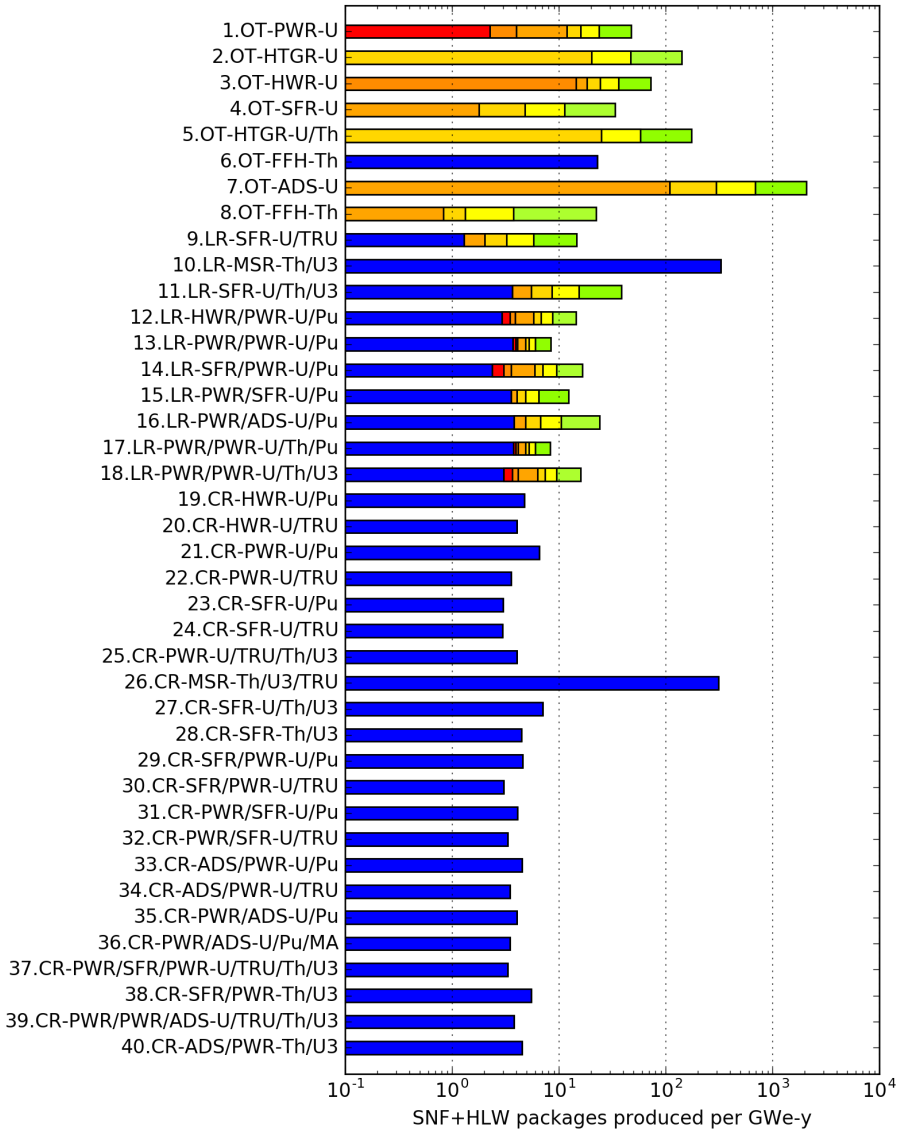

Figure 4.1: SNF + HLW waste package inventory per unit energy generated in each fuel cycle; SNF package loading is paramaterized by bar color.

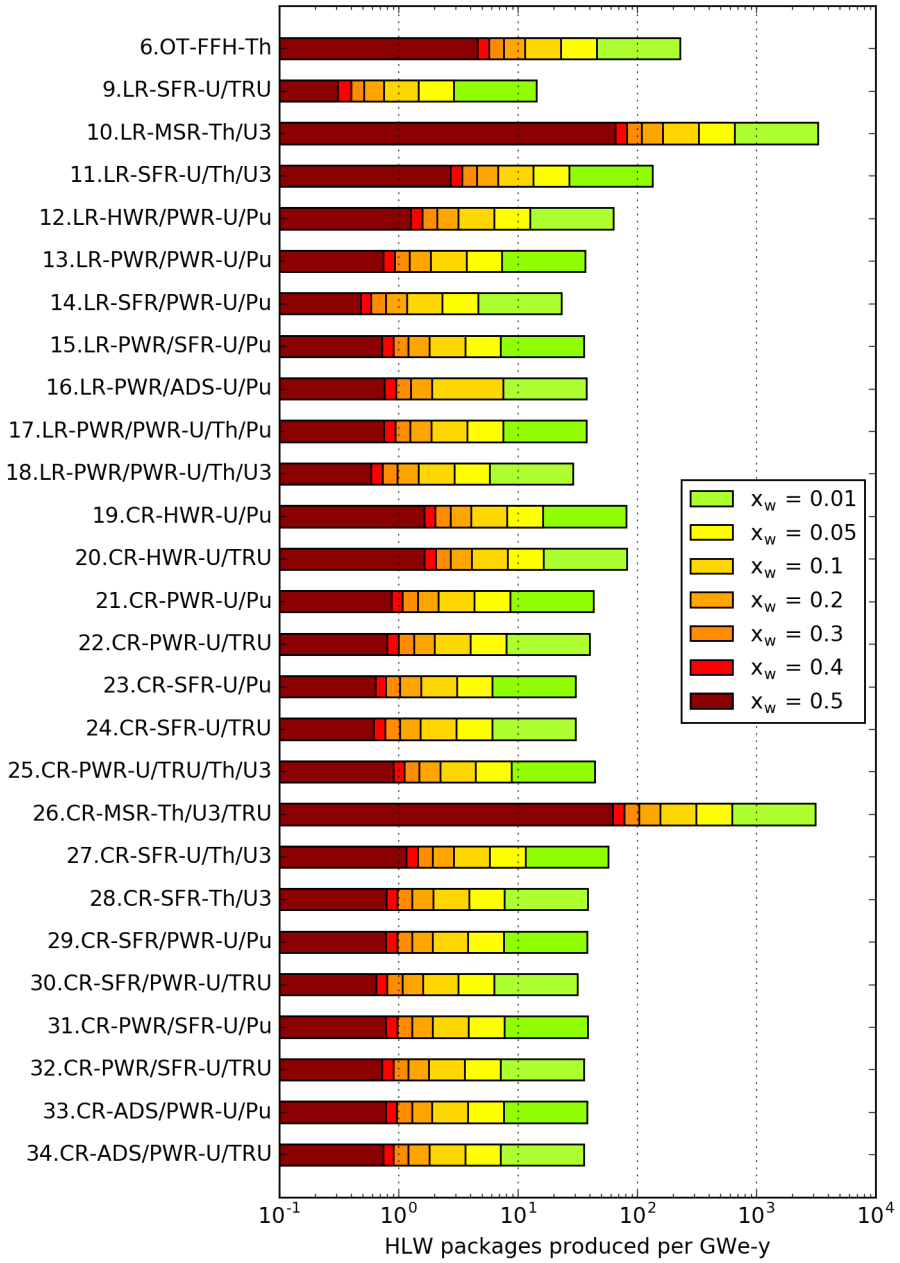

Figure 4.2: HLW waste package inventory generated for production of 1 GWe-y by each fuel cycle; hypothetical waste loading fraction is paramaterized by bar color.

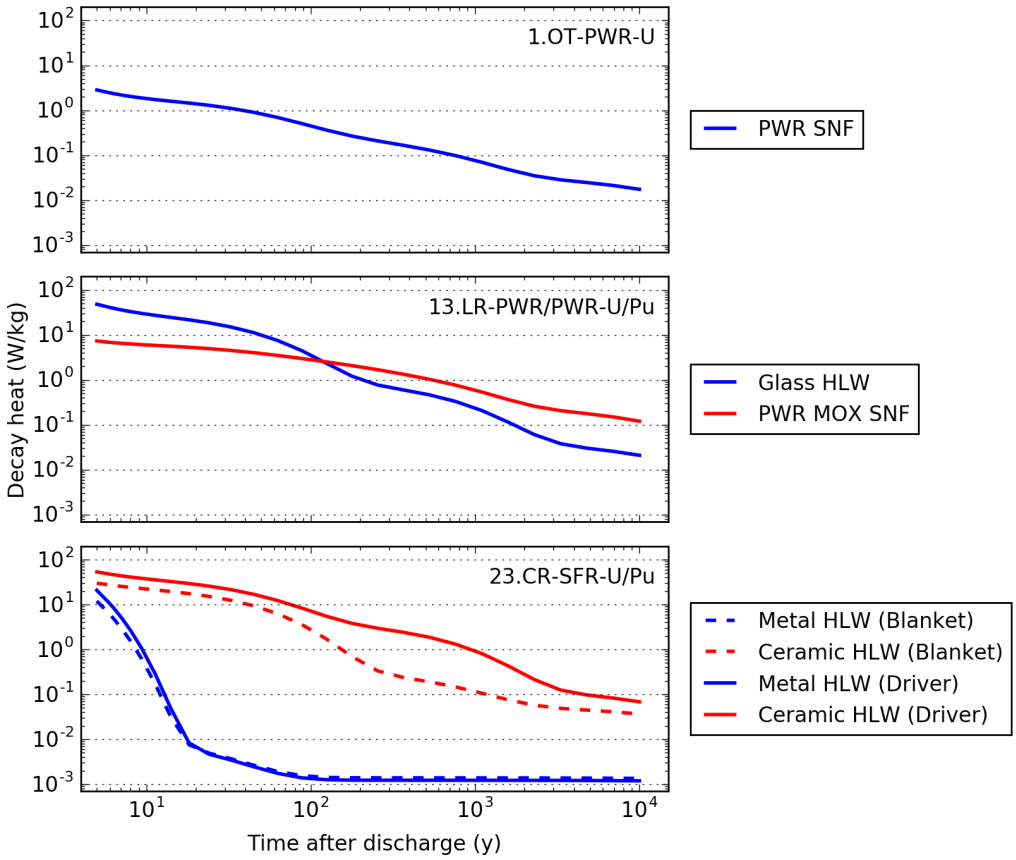

Figure 4.3: Decay heat (W/kg) produced by waste streams from 1.OT—PWR—U, 13.LR—PWR/PWR—U/Pu, and 23.CR—SFR—U/Pu. This value

age. As SNF package loading or HLW waste fraction increase, the number of packages is decreased but the per-package decay heat load increases. This trade-off is explored in along with the results for Section 4.4. Figure 4.3 shows the decay heat content for the bulk (before waste package and waste form loading) materials streams for 1.OT—PWR—U, 13.LR—PWR/PWR—U/Pu, and 23.CR—SFR—U/Pu. These fuel cycles were selected as examples because are used to illustrate other metrics in later sections. In particular, the decay heat from these fuel cycles is required for calculation of repository footprint and required surface storage time in Section 4.4.

Because the waste from 1.OT—PWR—U contains both fission products and actinides, the heat content is substantial at early times and decays away slowly due to sustained contributions from longer-lived radionuclides. However, both waste streams from 13.LR—PWR/PWR—U/Pu have initially greater decay heat content.

For the glass HLW, this is because short-lived fission products and longer-lived TRU isotopes are concentrated relative to the used fuel from which it originated. For the MOX SNF, heat-producing TRU isotopes — notably Pu-238 and Am-241 — are accumulated in large quantities due to the use of Pu-bearing fuel in a thermal spectrum. The result is that the MOX SNF from 13.LR—PWR/PWR—U/Pu remains significantly hotter than the SNF from 1.OT—PWR—U.

The waste streams from the electrochemical processing of used blanket and driver fuels from 23.CR—SFR—U/Pu show different decay heat behavior. The decay heat from the metal wastes, which contain the noble metal fission products, decreases very quickly, becoming insignificant within a few years after it is produced. The ceramic wastes, which contain the bulk of the fission products and all of the waste actinides, produce greater levels of decay heat for a longer period of time. In 23.CR—SFR—U/Pu, only Pu is recycled, so the heat from the ceramic wastes decays slowly due to the presence of TRU isotopes. The ceramic waste from the driver fuel is hotter than that from the blanket fuel because the driver fuel experiences greater fluence, resulting in accumulation of TRU isotopes.

4.2 Long-lived fission product inventory

The long-lived fission products (LLFP) that are generally mobile in groundwater and can contribute substantially to repository performance dose metrics are Cs-135, I-129, Sn-126, Tc-99, and Se-79. The total inventory of LLFPs, summed across waste streams and fuel cycle stages, is plotted in Figure 4.4 for each of the fuel cycles introduced in Chapter 3. Each bar is broken down into the contribution of each LLFP. The dotted line corresponds to the total LLFP inventory for the spent fuel from the once-through PWR fuel cycle.

Two observations can be made about the relationship between fuel cycles and LLFP inventory from Figure 4.4. The first is with respect to thermal efficiency, the underlying cause of the most significant standout cases. Thermal efficiency is related to overall fission product inventory because when the thermal energy generated from fission is used more effectively, fewer fissions are required to achieve a fixed energy goal. The fuel cycles that utilize high-temperature gas reactors ($\lambda = 0.50$) or molten-salt reactors ($\lambda = 0.44$) will produce fewer fission products overall, resulting in a smaller LLFP inventory. By contrast, fuel cycles with lower efficiency, like the once-through ADS fuel cycle (7.OT—ADS—U), produce more fission products generally — in that case, almost 100 kg/GWe-y. For this fuel cycle in particular, the plant power requirements are a significant drain on its energy production.

Outside of these extreme cases, it is difficult to attribute many of the differences

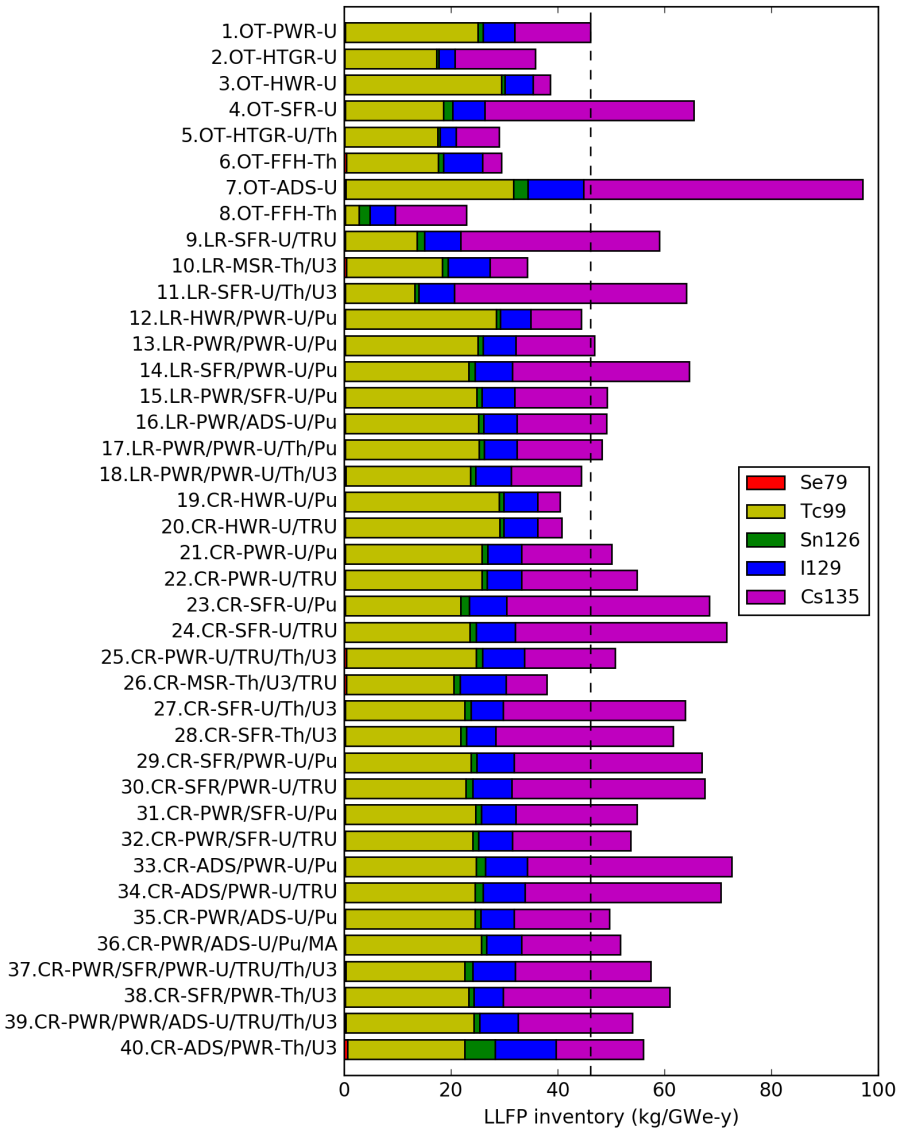

Figure 4.4: LLFP inventory generated in each fuel cycle, broken down into contributions from each LLFP isotope.

to efficiency. In particular, there is little to no correlation between the efficiency of sodium fast reactors ($\lambda = 0.40$) and pressurized water reactors ($\lambda = 0.33$). In order to have low LLFP inventory, it is helpful to have a very efficient plant. That efficiency does not fully explain total LLFP inventory indicates that other effects are significant.

The second observation that can be made from Figure 4.4 is the continuous recycle fuel cycles produce greater total LLFP inventories than the limited-recycle and once-through fuel cycles. The average LLFP inventory for the continuous-recycle fuel cycles is 45.5 kg/GWe-y, whereas that for the limited-recycles fuel cycles is 50.4 kg/GWe-y and that for the once-through fuel cycles is 57.1 kg/GWe-y. The reason for this is because these fuel cycles obtain more fissions from fuel isotopes that produce more LLFP. Tables 4.1 and 4.2 show the cumulative LLFP yields (JENDL FP Fission Yields, 2011) for different actinide isotopes at thermal and fast energies, respectively [87]. More isotopes are included in Table 4.2 because their capture-to-fission ratios are significantly lower for fast neutrons. The total LLFP yield, obtained by summing the preceding columns, is shown in the right-most column. The values for often-recycled fuel isotopes are generally greater than those for U-235, the fuel isotope utilized when uranium enrichment is required. Major examples include U-233 at thermal energies, or Pu-239 and Pu-241 at both thermal and fast energies.

Table 4.1: Thermal long-lived fission product yields (%; E = 0.0253 eV)

LLFP	Cs-135	I-129	Sn-126	Tc-99	Se-79	Total
U-233	6.256	1.573	0.224	4.911	0.143	14.818
U-235	6.552	0.540	0.056	6.142	0.045	13.335
Pu-239	7.617	1.321	0.198	6.219	0.044	15.399
Pu-241	7.165	0.804	0.082	5.983	0.015	14.049

Specific fuel cycles in Figure 4.4 can be compared in order to assess the effects of different fuel cycle characteristics on LLFP inventory. The effect of reactor spectrum can be observed by comparing fuel cycles with different reactors that utilize the same fuel elements, as shown in Table 4.3. In these examples, the fuel cycles that utilize fast reactors produce more LLFPs than those that utilize thermal reactors. The reason for this is due to the fact that LLFPs and their precursors have greater thermal cross sections, leading to greater rates of transmutation in thermal reactors than in fast reactors.

This effect, as well as the impact of other fuel cycle characteristics, can be demonstrated further by looking at the inventories of individual LLFPs. For most fuel

Table 4.2: Fast long-lived fission product yields (%; E = 500 keV)

LLFP	Cs-135	I-129	Sn-126	Tc-99	Se-79	Total
U-233	6.420	1.697	0.278	4.700	0.097	13.193
U-235	6.575	0.840	0.097	5.953	0.091	13.556
U-238	6.909	1.013	0.054	6.223	0.033	14.232
Np-237	7.264	1.617	0.164	6.138	0.057	15.240
Pu-238	6.741	1.083	0.228	6.119	0.067	14.238
Pu-239	7.551	1.406	0.263	5.990	0.061	15.272
Pu-240	7.434	1.120	0.270	5.942	0.042	14.808
Pu-241	7.055	1.142	0.222	5.548	0.036	14.003
Pu-242	6.975	1.225	0.168	5.463	0.034	13.864
Am-241	6.515	0.920	0.250	5.410	0.034	13.130
Am-243	6.778	0.893	0.228	5.417	0.019	13.336
Cm-243	6.484	1.159	0.280	4.910	0.034	12.866
Cm-244	5.684	1.006	0.279	5.115	0.025	12.108

Table 4.3: Effect of reactor spectrum on total LLFP inventory

Fuel cycle	Total LLFP inventory (kg/GWe-y)
1.OT—PWR—U	46.1
4.OT—SFR—U	65.5
19.CR—HWR—U/Pu	40.4
21.CR—PWR—U/Pu	50.1
23.CR—SFR—U/Pu	68.3
20.CR—HWR—U/TRU	40.8
22.CR—PWR—U/TRU	54.8
24.CR—SFR—U/TRU	71.6

cycles, the two major LLFPs are Cs-135 and Tc-99, whereas Se-79 and Sn-126 contribute much less to the overall inventory. This is because the cumulative fission product yields for Cs-135 and Tc-99 from fission of most actinides at fast and thermal energies are greater than those for the other LLFPs. In this analysis, the three primary LLFP — Cs-135, Tc-99, and I-129 — will be studied in detail.

Cs-135 is a major contributor to LLFP inventory. In reactors, some Cs-135 is formed directly from fission, but most is generated from the decay of precursor Xe-135. Xe-135 has a large independent fission product yield and its equilibrium concentration depends on reactor power: if the power is greater, the flux is greater, which means the concentration of Xe is greater as well. However, Xe-135 also has a large thermal absorption cross section (around 100,000 b). This means that while Xe-135 is being constantly produced in the reactor, it is also being consumed by reactions with neutrons. The cross section is only large at thermal energies and is much smaller at fast energies (around 0.1 b at 100 keV). Capture is the dominant absorption reactor for Xe-135 and Cs-135; the capture cross sections of Xe-135 and Cs-135 are shown in Figure 4.5.

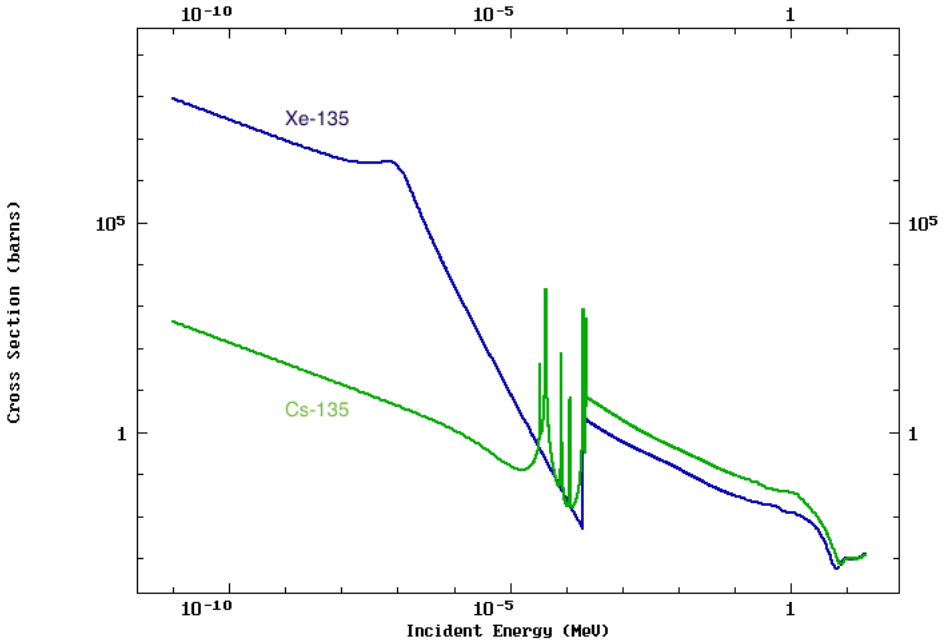

Figure 4.5: Xe-135 and Cs-135 capture cross sections (barns) as a function of energy from the ENDF/B-VIII.0 library.

Because less Xe-135 experiences neutron capture in fast reactors, more is allowed to decay to Cs-135. Figure 4.6 shows the Cs-135 inventory for all fuel cycles per

unit thermal energy, which is obtained by multiplying the value per unit electrical energy by the reactor thermal efficiency factor. The bars are sorted according to Cs-135 inventory and the color corresponds to the amount of Cs-135 generated in stages that use fast and thermal reactors. This effect dominates other factors such as the actinide isotope undergoing fission and fuel residence time. Because Cs-135 has a large cumulative fission yields for most fissioning actinides, reactors that produce more Cs-135 tend to have greater LLFP inventories as well as evidenced by Figure 4.4.

By contrast, Tc-99 exhibits more complex behavior. Although there is a difference between the fast and thermal capture cross sections of Tc-99 and its precursors, it is not nearly as significant as that for Xe-135. The capture cross section for Tc-99 and its precursors is plotted in Figure 4.7. Only two precursors are shown, because although the others (Nb-99, Zr-99, Y-99, Sr-99) have larger independent fission product yields, their half-lives are all less than 3 minutes. That the capture cross sections for Tc-99 and its precursors are slightly greater at thermal energies indicates more transmutation of Tc-99 should take place in thermal reactors.

However, other factors contribute to Tc-99 inventory. First fuels that spend more time in the reactor experience a higher fluence, giving Tc-99 and its precursors more opportunities to be transmuted by neutrons. Additionally, the Tc-99 yield from fission of U-233 is only 80% that of U-235, and the difference in yield from fission between U-233 and Pu is even greater. For this reason, reactors that rely on U-233 for fission power should produce less Tc-99.

Figure 4.8 plots the Tc-99 inventory ranked among the fuel cycles per unit thermal energy. Overall, the difference in Tc-99 inventory between the fuel cycles is very low and only the first few fuel cycles show significant variation in Tc-99 inventory. This is because Tc-99 inventory is correlated very strongly with overall fission product inventory, which is connected to thermal efficiency. Because the results in this figure are normalized to thermal energy, that effect has been removed.

The three figures show the amount of Tc-99 generated in fuel cycles with the aforementioned characteristics. None of the criteria produce particularly good distinctions because the differences in Tc-99 inventory between the fuel cycles are relatively small and each is only shows only one of multiple factors affecting the result. The left figure shows the amount of Tc-99 generated from fuels containing U-233 (or thorium, from which U-233 is bred). Although many of the fuel cycles that produce smaller amounts of Tc-99 utilize Th/U-233, there are fuel cycles that produce little Tc-99 that do not utilize Th/U-233 fuels, and there are fuel cycles that do utilize Th/U-233 fuels that produce larger amounts of Tc-99.

The color of the bars in the middle figure correspond to the amount of Tc-99 generated in reactors with thermal or fast spectra. There is a higher concentration

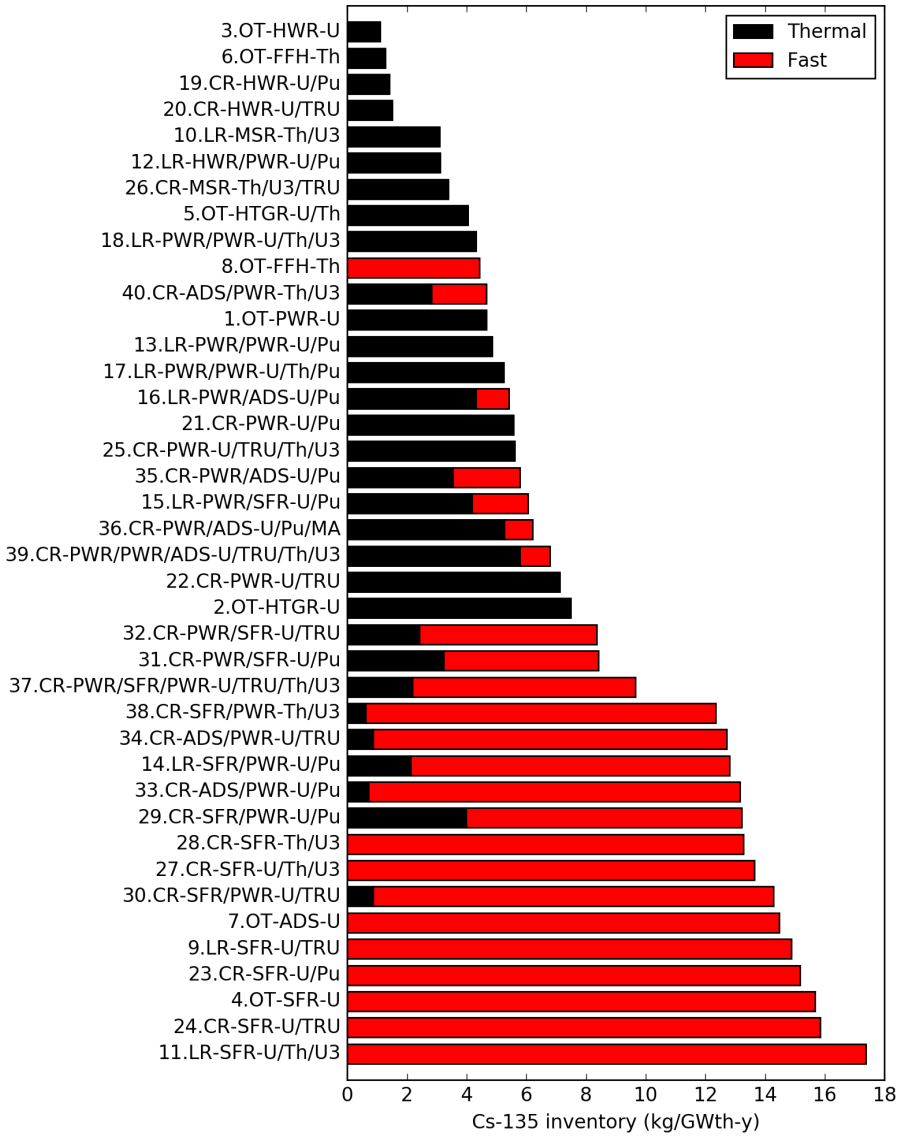

Figure 4.6: Sorted Cs-135 inventory (kg/GWth) for all fuel cycles. The color of the bars indicates the fraction of power generated in fast and thermal reactors.

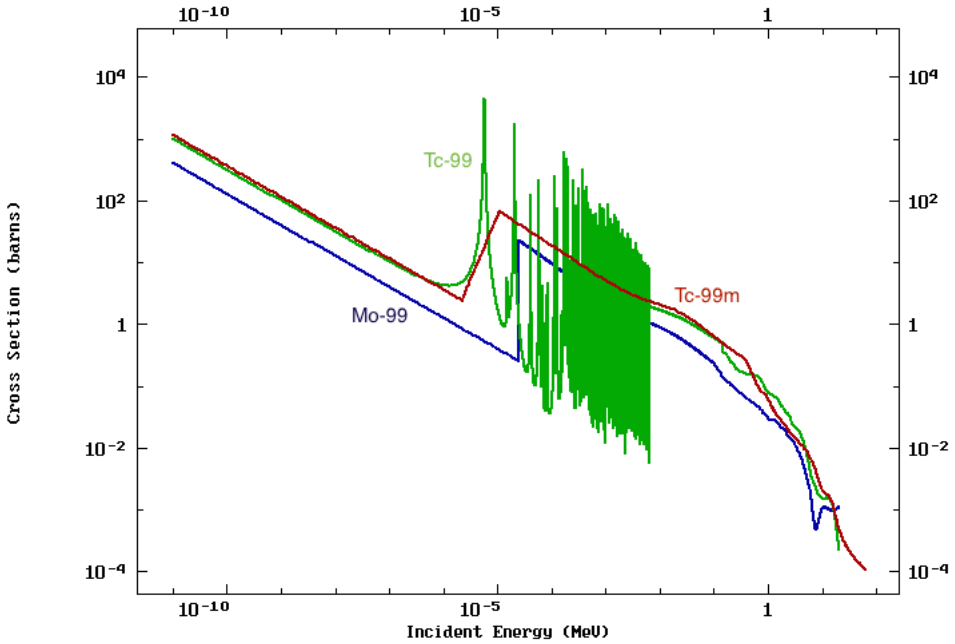

Figure 4.7: Tc-99 and precursor capture cross sections (barns) as a function of energy. The library is ENDF/B-VIII.0 for Tc-99 and Mo-99 and TENDL-2017 for Tc-99m.

of thermal reactors in the fuel cycles that produce lower inventories of Tc-99, but the distinction is not as clear as it was for Cs-135.

Finally, the Tc-99 generated in fuel cycles with residence times longer than 7 years (effective full power years) is shown in the third figure. The cutoff value of 7 years was chosen so that the breed and burn fuel cycle 11.LR—SFR—U/Th/U3 could be included among those with longer residence times, because 7.1 years is the shortest residence time among any of the fuel batches in that fuel cycle. Fuel cycles with longer residence times generally produce less Tc-99. This is exemplified by comparing breed-and-burn fuel cycles with similar fuel cycles that utilize continuous recycling. Fuels in breed-and-burn fuel cycles like 9.LR—SFR—U/TRU and 11.LR—SFR—U/Th/U3 have longer residence times and higher burnup than others, like those in 23.CR—SFR—U/Pu or 27.CR—SFR—U/Th/U3. Reactors with extremely short residence times, like HWRs, produce the most Tc-99. Although some elements in the continuous-recycle MSR (26.CR—MSR—Th/U3/TRU) may have infinite residence times, Tc-99 is actively removed during salt treatment with a cycle time (the time required to remove 100% of an element) of less than 1 year [88]. Taken together, the three figures demonstrate that fuel cycles that utilize thorium and U-233 and/or

thermal spectra and/or longer residence times will produce smaller amounts of Tc-99.

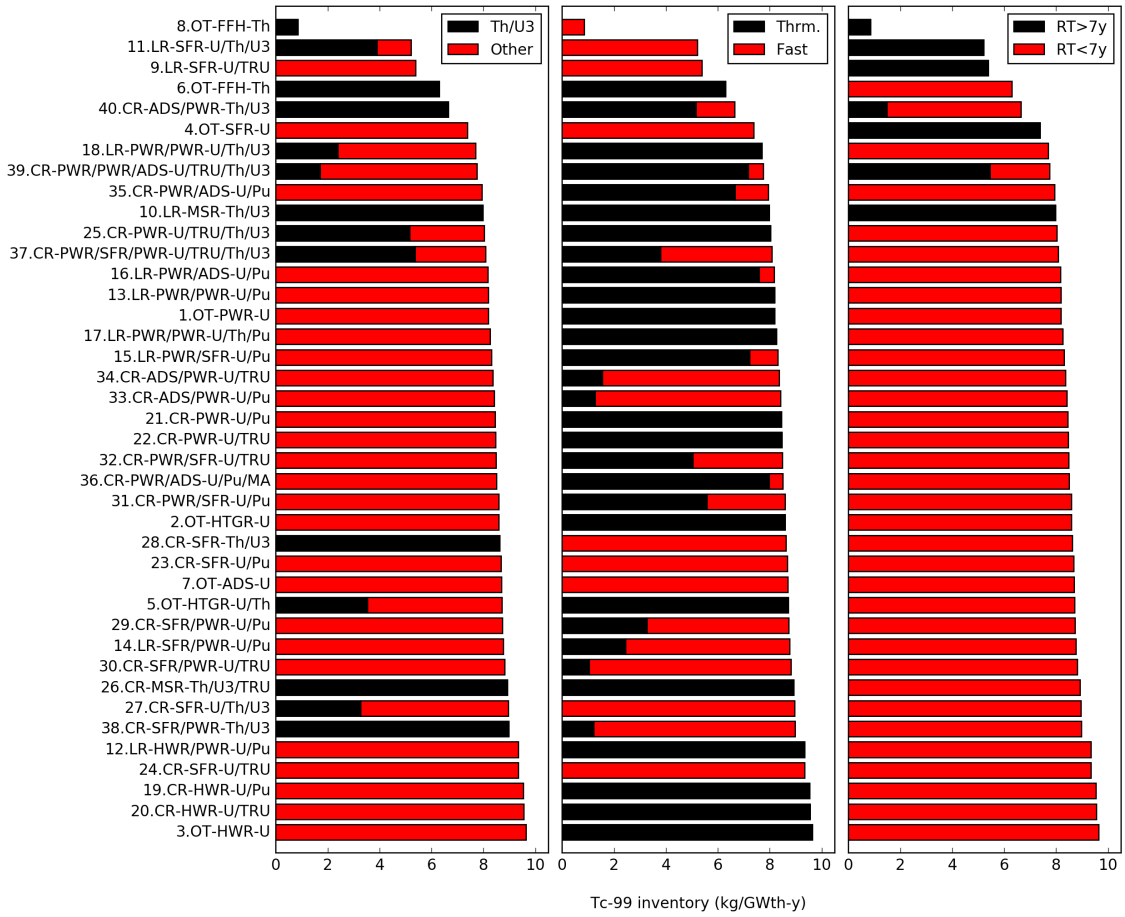

Figure 4.8: Tc-99 inventory (kg/GWth-y), sorted by inventory and marked to denote Tc-99 generated by reactors fueled with Th/U3, thermal reactors, and reactors with longer fuel residence times.

Generation of I-129 in nuclear reactors follows similar patterns as Tc-99. Like Tc-99, the thermal capture cross sections for I-129 and its precursors are greater than those at fast energies, indicating more transmutation in thermal reactors. The capture cross sections for I-129 and its precursors are plotted in Figure 4.9. Additionally, the fission product yield of I-129 is significantly lower for U-235 fission than for U-233 or Pu fission. Therefore, reactors that utilize enriched uranium fuels should be expected to produce less I-129.

Figure 4.10 shows the mass of I-129 per unit thermal power generated and sorted

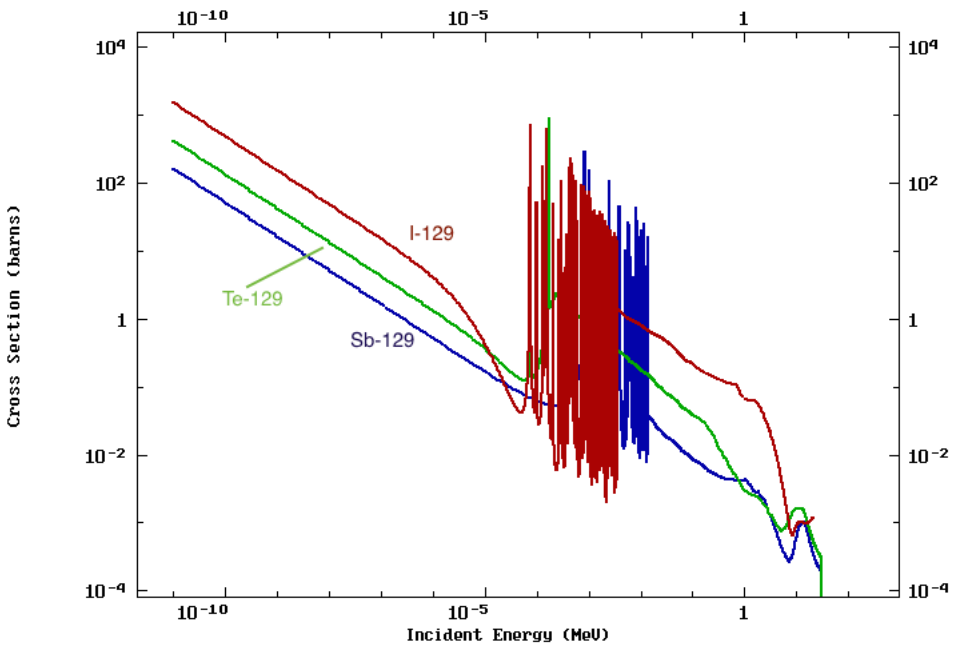

Figure 4.9: I-129 and precursor capture cross sections (barns) as a function of energy. The library is ENDF/B-VIII.0 for I-129 and TENDL-2017 for Te-129 and Sb-129.

for each fuel cycle. In the first figure, the amount of I-129 generated from thermal and fast reactors is shown by bar color. In the second figure, bar colors denote the amount of I-129 produced from reactors using either low-enriched uranium (LEU) or LEU along with another fuel material in the assembly or batch, Th/U-233 fuels, and "other", which generally comprises Pu/TRU fuels. Fuel cycles that utilize thermal reactors and enriched uranium are shown to produce less I-129, while those that utilize fast spectra and Pu or U-233 fuels produce greater amounts of I-129. The distinction drawn by these two characteristics is much clearer than that for Tc-99 due in part to the larger variability in I-129 inventory among the different fuel cycles.

4.3 Material attractiveness

The attractiveness of fissile materials in nuclear waste streams is evaluated for each of the 40 fuel cycles cases. For each actinide-bearing waste stream in each fuel cycle, the bare sphere critical mass (kg) and decay heat content (W/kg) for the fissile material and the bare sphere dose rate (rad/hr) at 1 m for the material in the waste package are calculated using the methods described in Chapter 2 Section 2.1.3. This

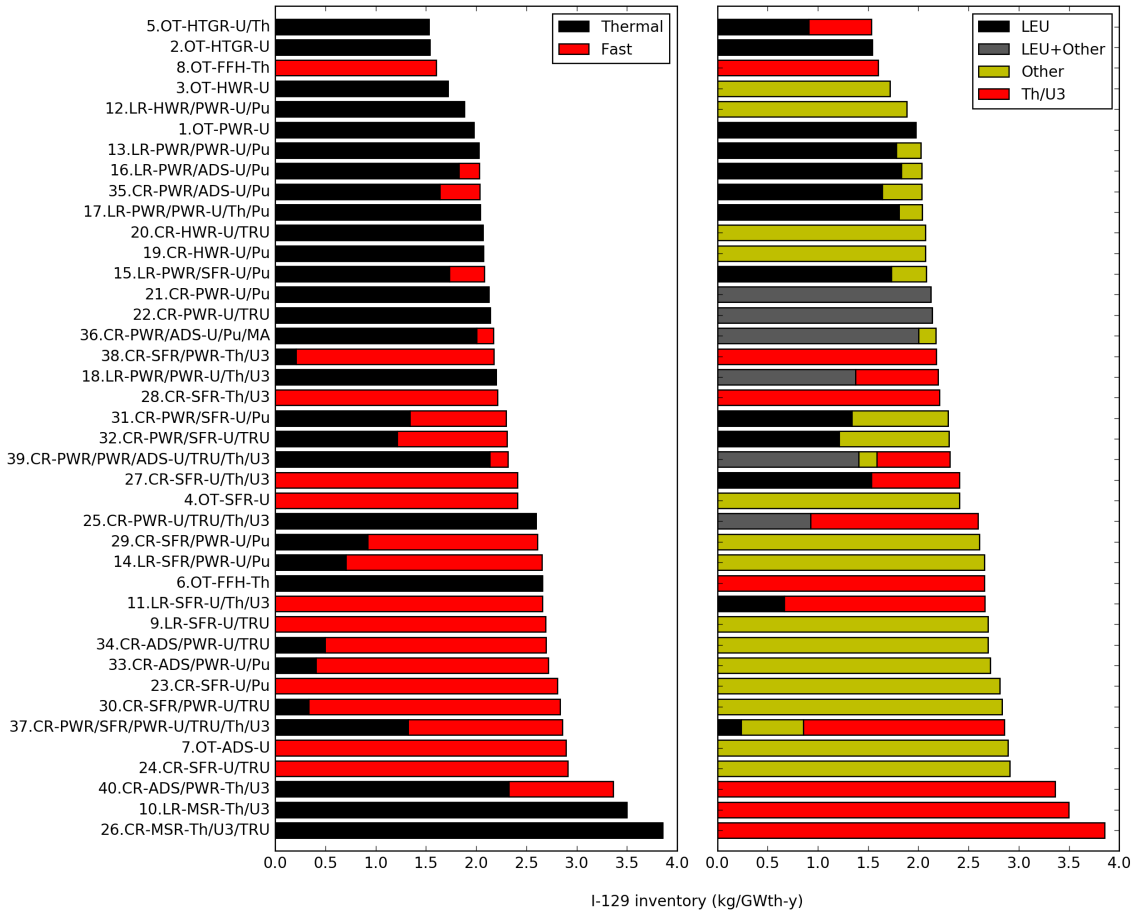

Figure 4.10: I-129 inventory (kg/GWth-y), sorted by inventory and marked to denote I-129 produced in thermal/fast reactors and by LEU, LEU-combination, Th/U-233, or other (mostly Pu/TRU) fuels.

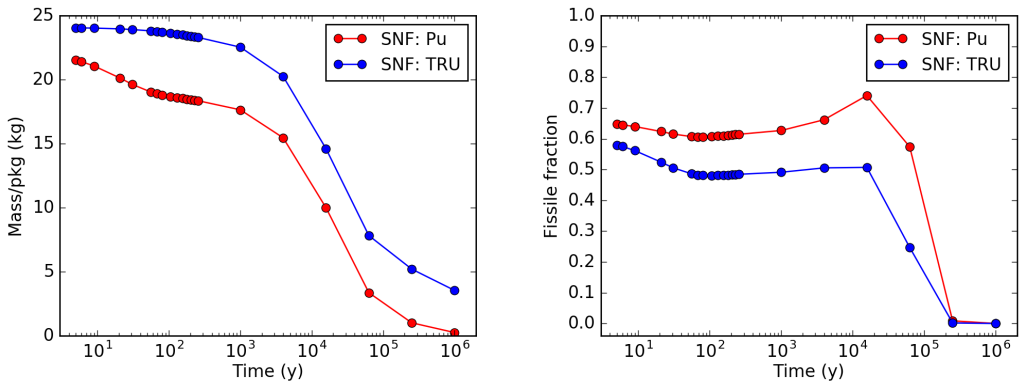

Figure 4.11: Pu and TRU package inventory and fissile fraction in 4-assembly spent fuel packages generated from 1.OT—PWR—U.

section describes the evolution of these values over time for two example fuel cycles waste streams and compares fuel cycles based on aggregate metrics using the material attractiveness figure of merit. The complete set of figures showing the time-evolution for all fuel cycles can be found in Appendix B.

Figure 4.11 characterizes the fissile materials that might be considered attractive in LWR spent fuel over time after discharge (from 1.OT—PWR—U). The inventory of Pu and TRU in each package (4 assemblies per package) is significant and the material is sufficiently fissile to warrant attention. Over time, the inventory and fissile fraction varies as radioactive decay adds to and removes different isotopes. The fissile fraction of both Pu and TRU peaks around 20,000 years after Pu-240 ($t_{1/2} = 6,560$ y) decays away, leaving fissile Pu-239 as a higher fraction of the mixture.

Figure 4.12 plots the FOM and its constituent values over time after discharge. The FOM is shown in the top left figure; in the top right, the dose rate; in the bottom left, the critical mass; in the bottom right, the decay heat. Initially, the FOM is well below zero, indicating that the fissile material in the spent fuel is wholly unattractive. However, the FOM increases quickly, and after about 100 years, the FOM for both Pu and TRU exceeds one, indicating that both species are attractive. Over this period, the critical mass and the decay heat content of the Pu and TRU experience relatively little change while the dose rate of the bulk waste material falls about two orders of magnitude. This decrease is due to the decay of shorter-lived fission products, which removes the spent fuel self-protection that would previously discourage retrieval.

Once the dose rate falls to the point that the Pu and TRU become attractive, their attractiveness dose not decrease below the attractiveness threshold before the end of the 1,000,000 year period simulated. As Pu-239 decays ($t_{1/2} = 24,000$ y), the

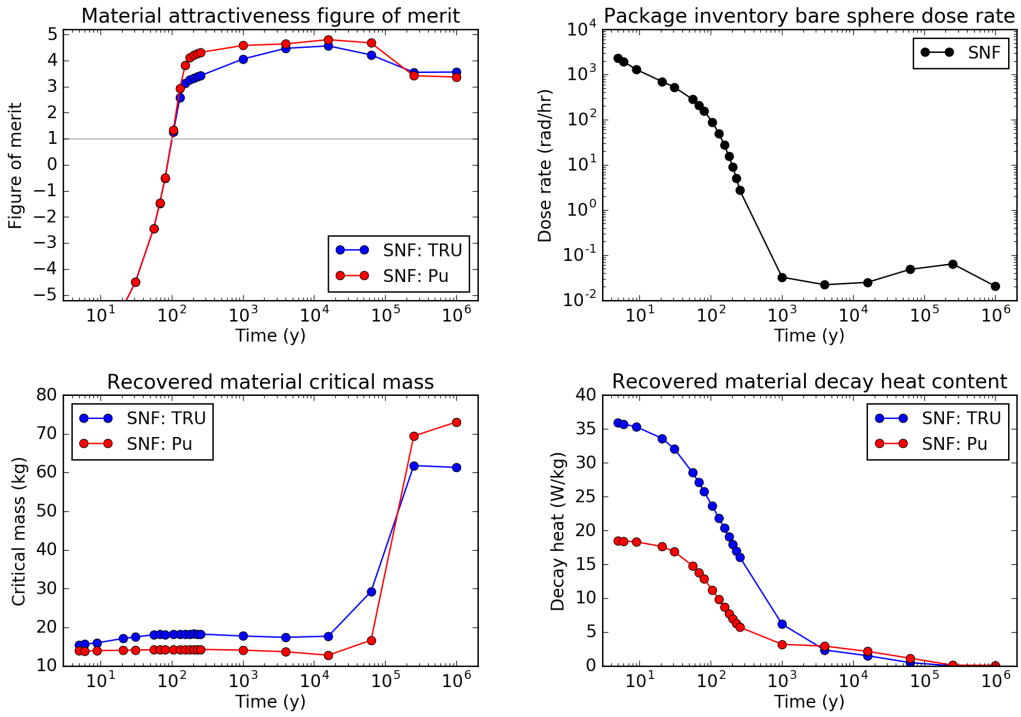

Figure 4.12: Figure of merit evaluation for Pu and TRU in 4-assembly spent fuel packages generated from 1.OT—PWR—U.

remaining Pu isotope becomes Pu-244 ($t_{1/2} = 8.08e7$ y). This corresponds to a slight decrease in the FOM as the critical mass increases due to the loss of fissile material. However, the material is still considered attractive and could be theoretically used to fabricate nuclear weapons.

In this model, the FOM is not independent of waste package loading, because the mass of material in the waste package affects the dose rate. From the perspective of long-term material attractiveness and proliferation resistance, modifying package loading is a trade-off. On one hand, increasing package loading can increase the dose rate, potentially increasing the time before the material becomes attractive. On the other hand, increasing package loading also concentrates the attractive fissile material, allowing someone to recover more material from fewer packages. Of these, only the former can be assessed using the FOM. The FOM for Pu and TRU and the spent fuel package dose rate is plotted in Figure 4.13 against time after discharge. Waste package loading is differentiated by line and marker color, and the trend in dose rate and FOM is similar for all values of package loading. Lower package loading means that the material becomes attractive earlier, but after enough time has passed,

the figure of merit is no longer significantly controlled by the dose. For this reason, the lines for all values of package loading eventually converge.

However, the trade-off can be illustrated by considering the time at which Pu becomes attractive and the amount of Pu loaded into packages. The critical mass of the Pu at 5 years after discharge is about 14 kg, and remains study until the decay of Pu-239. With that in mind, Table 4.4 shows the package inventory of Pu and the time before the material becomes attractive. A package that contains only 1 fuel assembly only supplies about 40% of the Pu required for a critical mass, its dose rate fails to be self-protecting at about 50 years after discharge. By contrast, the largest package, containing 21 fuel assemblies, does not become attractive until 155 years after discharge. However, a single package of this size contains enough Pu for 8 critical masses.

Table 4.4: Effect of package loading on Pu inventory and FOM

Package loading (assemblies)	Package count	Pu/pkg at t=5y (kg)	t (FOM > 1) (y)
1	4765	5.38	52.45
2	2383	10.8	76.43
3	1589	16.1	91.16
4	1192	21.5	101.0
12	398	64.5	137.6
21	227	113	155.1

Additional insights can be made by contrasting this result with that for an advanced fuel cycle. Figure 4.14 shows the Pu and TRU inventory and fissile fraction for 23.CR—SFR—U/Pu, a fuel cycle in which U and Pu are continuously recycled in SFRs and considered to be highly promising in the FCES study. The fuels are divided into blanket and driver fuels, denoted by marker type. Although this fuel cycle produces two waste forms, only one of them, the ceramic from electrochemical reprocessing, contains actinides. Unlike 1.OT—PWR—U, where the Pu and TRU inventories were similar because most of the TRU was Pu, this fuel cycle recycles Pu, decreasing the amount of Pu relative to TRU. However, the Pu and has a greater fissile fraction than that produced in the spent fuel from 1.OT—PWR—U.

Figure 4.15 shows the FOM and the values that comprise it against time after discharge. The behaviors of all values are similar to those in the case of 1.OT—PWR—U. The FOM, initially insignificantly low, increases rapidly as the dose rate decreases, eventually indicating high material attractiveness. The critical mass of the Pu and TRU is about constant until the decay of Pu-239, at which point it increases.

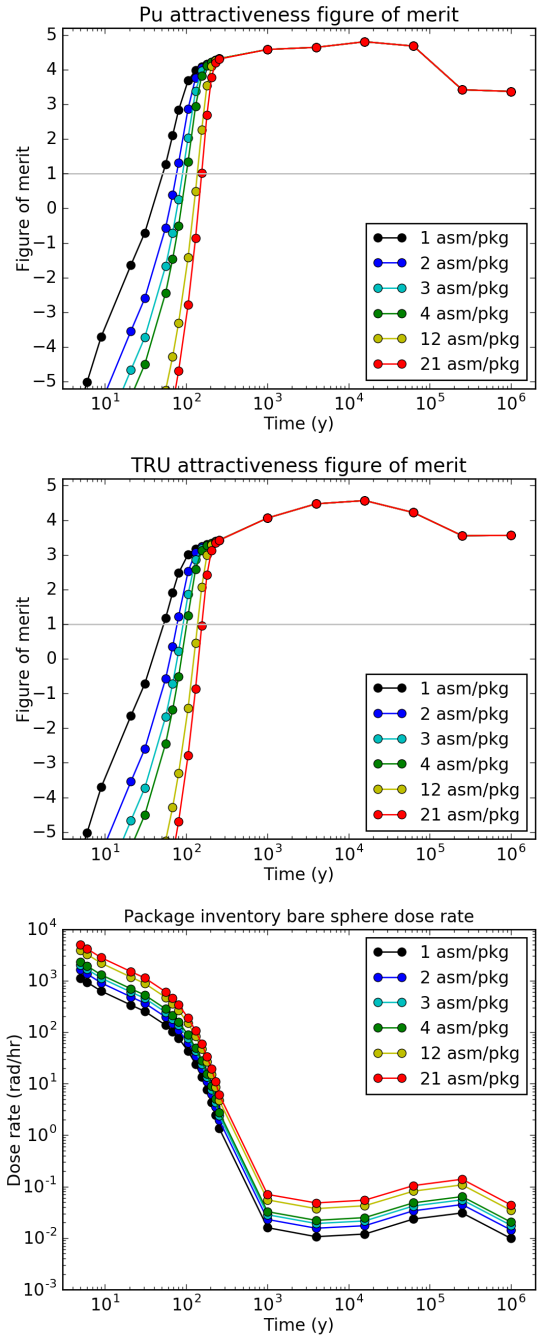

Figure 4.13: Figure of merit and dose rate evaluation for Pu and TRU in spent fuel packages with different loading generated from 1.OT—PWR—U.

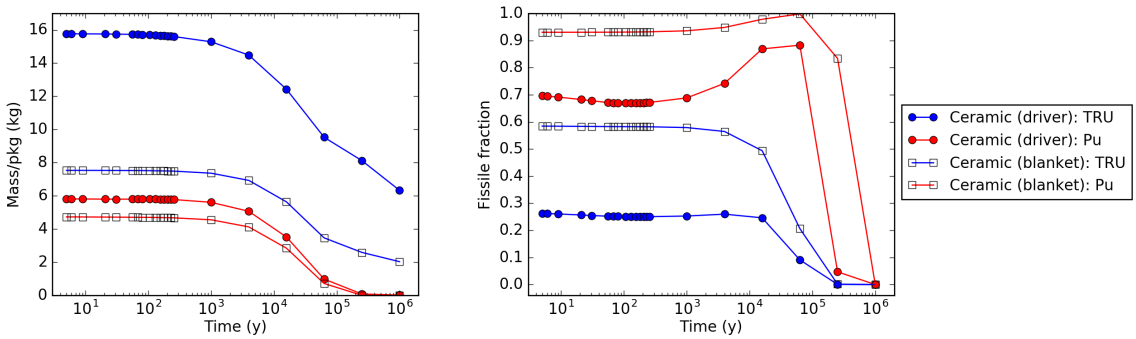

Figure 4.14: Pu and TRU package inventory and fissile fraction in ceramic HLW generated from electrochemical reprocessing in 23.CR—SFR—U/Pu.

One important difference between Figures 4.12 and 4.15 is the time at which the materials become attractive. For 1.OT—PWR—U, that time is about 101 years. For 23.CR—SFR—U/Pu, that time is 198 years for the HLW from the blanket fuels, and 220 years for the HLW from the driver fuels. The reason for the time delay before the material becomes attractive is because fission products are concentrated in the HLW, increasing the density of radioactivity and increasing the dose rate.

Another difference between the cases for 1.OT—PWR—U and 23.CR—SFR—U/Pu is the number of packages required to obtain a critical mass of Pu or TRU. Those values are reported for 1.OT—PWR—U in Table 4.4. For 23.CR—SFR—U/Pu, the Pu or TRU from three packages of HLW from driver or blanket waste is required to obtain a critical mass. Because Pu is removed from the waste stream by reprocessing, it is diluted in the HLW and therefore more packages must be recovered to acquire usable amounts of attractive material.

The package inventory of potentially attractive materials in HLW depends on both the separation efficiency of the reprocessing method and the waste loading fraction during waste form preparation. Whereas loading fraction is similar to spent fuel waste package loading in that it is a wholly waste management issue, improving separation efficiency is beneficial to many aspects of the fuel cycle because desirable resources can utilized to generate more energy. An additional benefit of increasing separation efficiency is that those the package inventory of those potentially attractive materials decreases. In the above example for 23.CR—SFR—U/Pu, the separation efficiency for the electrochemical process that produced the ceramic HLW is 99%. If that value were increased to 99.9%, the number of packages required to obtain a critical mass of Pu would increase to 23. Although not a fundamental barrier to future recovery of attractive materials from nuclear waste, diluting attractive

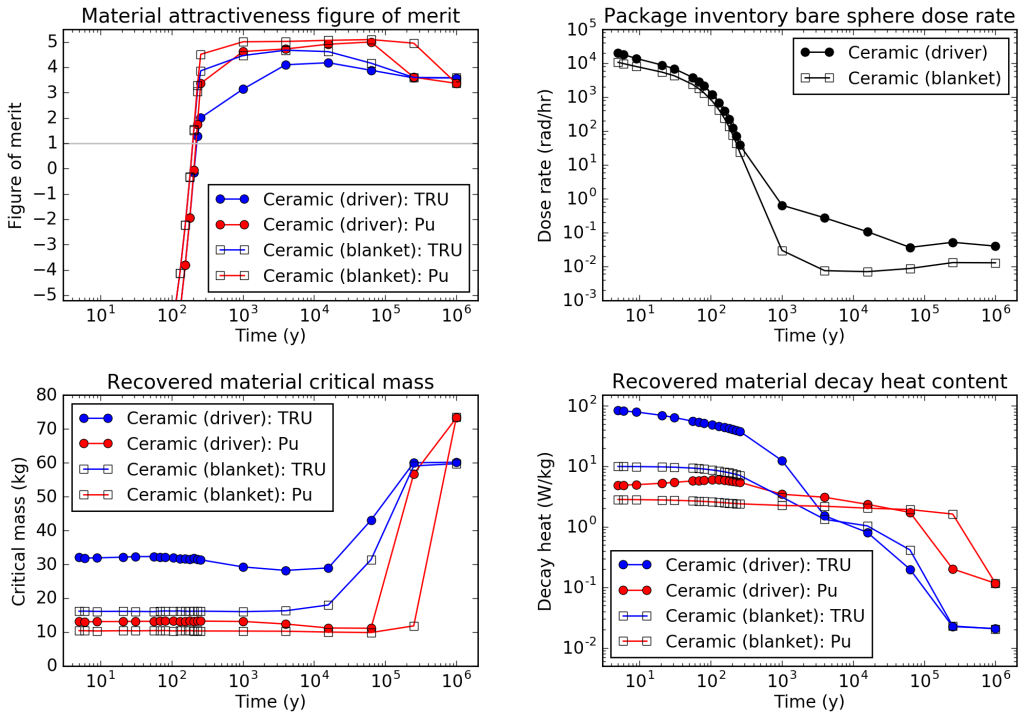

Figure 4.15: Figure of merit evaluation for Pu and TRU in ceramic HLW generated from electrochemical reprocessing in 23.CR—SFR—U/Pu.

material in the waste increases the time required to obtain weapons-usable amounts of fissile materials.

The time-to-attractiveness and the packages required for a critical mass metrics can be generalized to all fuel cycle cases. Figure 4.16 shows the minimum time-to-attractiveness for each fuel cycle case. The minimum is taken over all actinide-bearing waste forms and all potentially attractive materials in the waste. Each bar is labeled to indicate the waste form that becomes at the earliest time, and the color of the bar denotes the attractive material — U, Pu, or TRU.

The time-to-attractiveness varies from as little as zero years to over 200 years after waste fabrication and/or package loading (which is assumed to occur 5 years after discharge from the reactor). At the low-end are waste forms or waste packages with relatively low waste loading. For example, the package loading of the spent fast reactor assemblies produced by 7.OT—ADS—U is rather low (7 assemblies per package). The ceramic waste forms from the two MSR fuel cycles contain only rare-earth fission products, and the melt-refining skull from 11.LR—SFR—U/Th/U3 contains relatively few fission products because it is produced after processing the

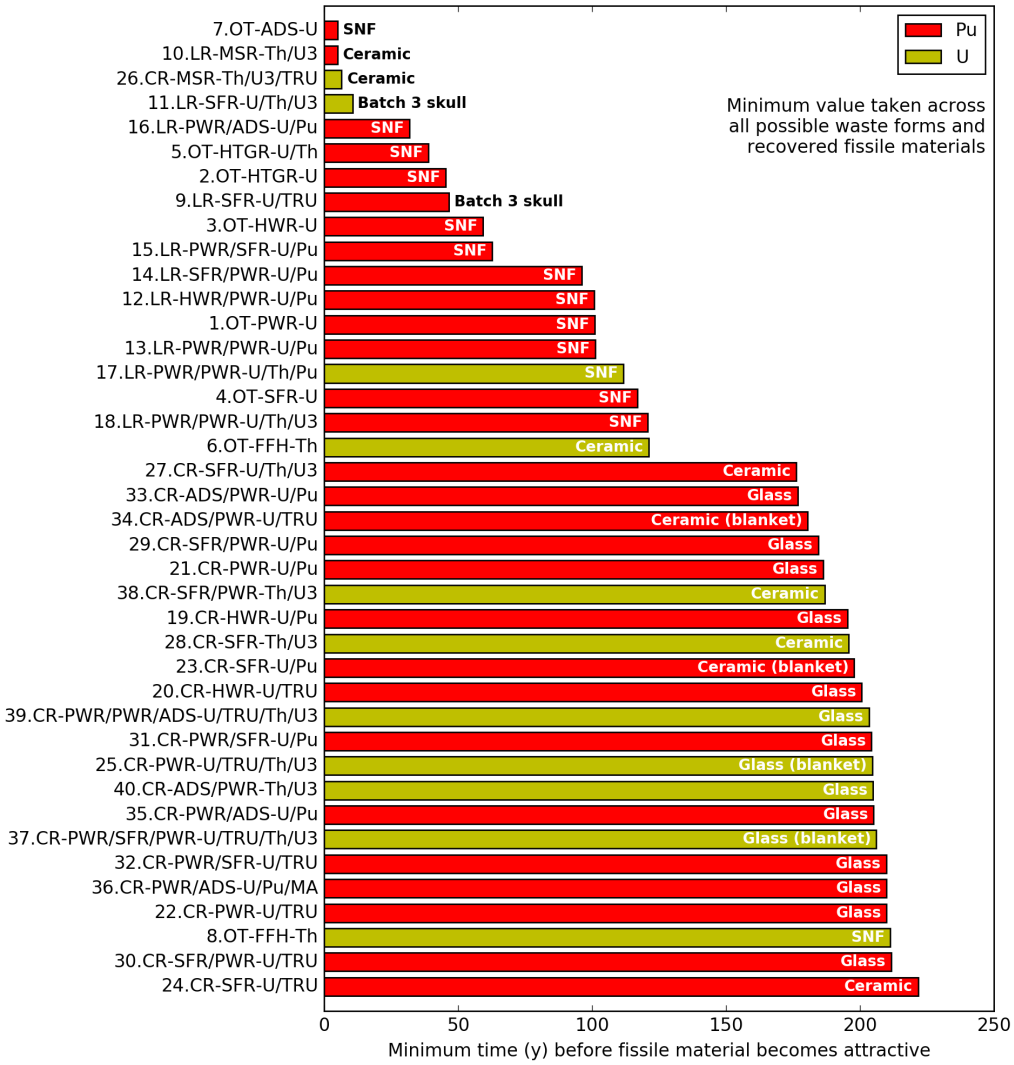

Figure 4.16: Minimum time (y) after used fuel discharge before material in waste becomes attractive. Bar color indicates the attractive material and each bar is labeled with the waste form that contains it.

breeding blanket. For these waste packages, the dose rate is low enough that the waste loses self-protection very early, potentially before it can be stored, transported, and emplaced in a geologic repository.

On the high-end, most of the waste forms are high-level wastes due to the concentration of short-lived radioactive fission products in reprocessing. For cases in which HLW is generated from processing driver and blanket fuels separately, the HLW from the blanket fuels has a lower time-to-attractiveness because the fissile enrichment of the material in the blanket fuel is much greater than that of the driver fuel. The only spent fuel case with a long time-to-attractiveness is the case of 8.OT—FFH—Th, for which the spent fuel is in the form of TRISO particle fuel embedded in graphite pebbles; the waste packages for these pebbles are very large, and the treatment of materials in the dose calculation may not be appropriate for the unique structure of the fuel pebble.

The minimum number of packages required to recover a critical mass of attractive material is shown in Figure 4.17. These values, along with those for the time before recovered material becomes attractive, are summarized in Appendix B. The number of packages required is evaluated at the time at which the material becomes attractive (shown in Figure 4.16). The bars are labeled according to the fuel cycle waste form that yields the fewest required packages, and colored according to the type of material considered attractive. The values in the plot range from 1 to 16 packages. This is dependent on the size of the package and the concentration and fissile enrichment of attractive material in the package.

Most of the waste forms for which only a single package is required to recover enough material for a critical mass are spent fuels from once-through or limited-recycle fuel cycles. These packages generally contain large amounts of potentially attractive material because it is not recovered in reprocessing. Conversely, the waste forms that require recovery of a greater number of packages are mostly high-level wastes. The exceptions are the two once-through HTGR fuel cycles 2.OT—HTGR—U and 5.OT—HTGR—U/Th, which produce waste packages with relatively low waste loading because the spent fuel is assumed to be disposed within the prismatic graphite fuel blocks in which it is loaded.

The effect of reprocessing can be assessed by comparing related fuel cycles, such at 1.OT—PWR—U, 21.CR—PWR—U/Pu, and 22.CR—PWR—U/TRU. Only a single waste package of PWR spent fuel (4 assemblies per package) is required to obtain a critical mass of Pu. Because Pu is recovered in 21.CR—PWR—U/Pu, TRU is more readily available, and five packages are required to obtain a critical mass. If both Pu and TRU are recovered, six packages are required to obtain a critical mass of Pu. The difference between 21.CR—PWR—U/Pu and 22.CR—PWR—U/TRU is small because Pu is more attractive than TRU, and therefore the

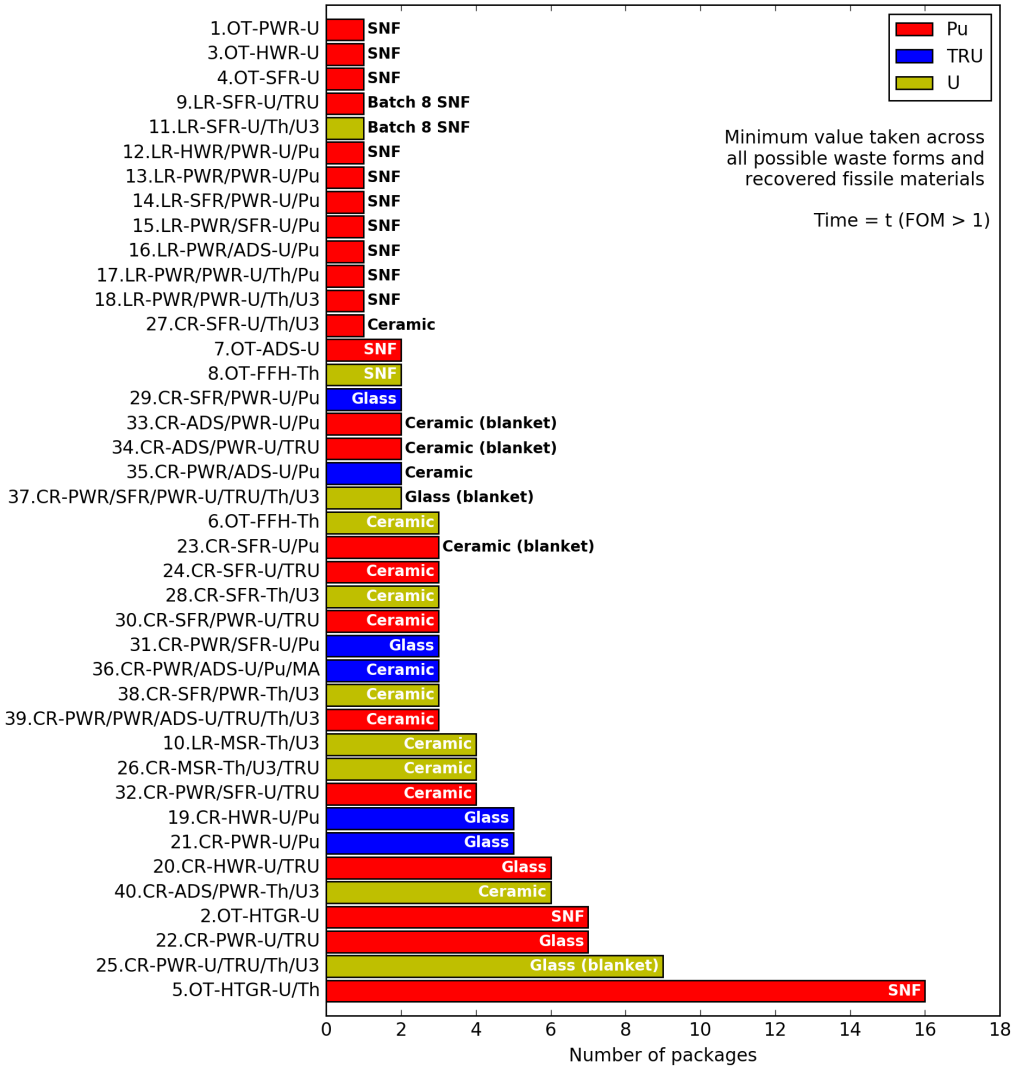

Figure 4.17: Minimum number of waste packages that must be obtained in order to acquire a critical mass of attractive material. Bar color indicates the attractive material and each bar is labeled with the waste form that contains it.

Table 4.5: Effect of MSR separation efficiency on material attractiveness metrics

Fuel cycle	Recovery fraction	t (FOM > 1) (y)	$N_{\text{pkgs}}^{\text{CM}}$
10.LR—MSR—Th/U3	Actinides: 0.99 REE: 0.4 (Eu: 0.94)	5.0	4.0
	U3: 0.9999654 Th: 0.99999882 TRU: 1.0 REE: 0.4 (Eu: 0.94)	105.0	4.0
26.CR—MSR—Th/U3/TRU	Actinides: 0.99 REE: 0.4 (Eu: 0.94)	6.5	4.0
	U3: 0.999943458 Th: 0.999999 Pu: 0.98969 REE: 0.94 (Eu: 0.994)	233.3	3.0

returns of recovering both Pu and TRU from the waste diminishes.

The MSR fuel cycles (10.LR—MSR—Th/U3 and 26.CR—MSR—Th/U3/TRU) perform poorly for the time-to-attractiveness metric due to the low separation efficiency relative to what was utilized in the FCES (and described in Chapter 3 in Table 3.11). The primary diluent material not recovered from the waste is thorium. To demonstrate the difference in waste material attractiveness for MSR fuel cycles with different separation efficiency, the time-to-attractiveness and number of packages required to recover a critical mass of material are shown in Table 4.5. When more thorium is recovered by separations processes, the dose rate of the waste increases because the highly radioactive fission products are more concentrated. This increases the time before the fissile material in the waste — U (mostly U-233) for both cases — becomes attractive. However, although some U is removed from the waste with increased separation efficiency, the vast majority of recovered material is Th, resulting in a significant change in the number of waste packages produced but relatively little change in the amount of U in each package. Therefore in these cases, even with improved separation efficiency, there is no improvement in the number of packages required to obtain a critical mass of fissile material.

One final comprehensive metric for comparing all fuel cycle cases is the maximum value of the figure of merit, taken across all waste forms, attractive materials, and times. Because the behavior of the figure of merit is similar for all fuel cycles, it is a

bounding value for the attractiveness of materials in a fuel cycle. These are plotted in Figure 4.18 for all forty fuel cycles. The values range from 4.33 to 5.10, and for all fuel cycles, the fissile material that yields that greatest FOM value is Pu. In all cases, the maximum FOM occurs after 10,000 years, after Pu-240 has decayed away but before Pu-239 can decay, meaning that the Pu has a high fissile enrichment. Because all fuel cycles produce wastes that yield such large maximum values for FOM, this metric is not effective for differentiating among the fuel cycles. Rather, it highlights that care should be taken when considering the proliferation resistance of fuel cycle waste disposal. Future work might enable technologies that can further reduce the long-term attractiveness of wastes disposed in geologic repository.

4.4 Repository footprint

This section presents the results for the geologic repository footprint required for disposal all waste streams from each of the 40 fuel cycles cases in three generic repository environments. The repository footprint is explored with respect to two important factors affecting waste decay heat: surface storage time and waste package loading (for SNF) or waste form loading (for HLW).

Figure 4.19 shows the repository area required for the disposal of LWR spent fuel from 1.OT—PWR—U in repositories in granite, clay, and salt host rocks as a function of surface storage time. Waste package loading is distinguished by line and marker color and marker shape. The legend indicates the various waste package and waste form parameters, as well as the number of waste package that are produced per unit electricity. Only a few examples of this type of figure are shown in this chapter; the figures showing all waste streams produced by each fuel cycle can be found in Appendix C.

Packages that emit more heat require greater spacing, so the required area decreases with increased surface storage time. In Figure 4.19, two limits are apparent with respect to surface storage time. First, at shorter surface storage time, many package loading options cannot be emplaced without breaching the temperature constraint. In these cases, storage is mandatory to allow cooling before emplacement. In cases where certain package loading options are not plotted at all (for example, 12-assembly packages in clay), disposal is not possible in the time period shown without breaching the temperature constraint.

Second, at sufficiently long surface storage times, the area required for disposal of a particular package may reach the minimum value defined by the drift radius and package length, as described in the previous section. From this point onward, surface storage time has no effect on the area because the package heat content is low enough

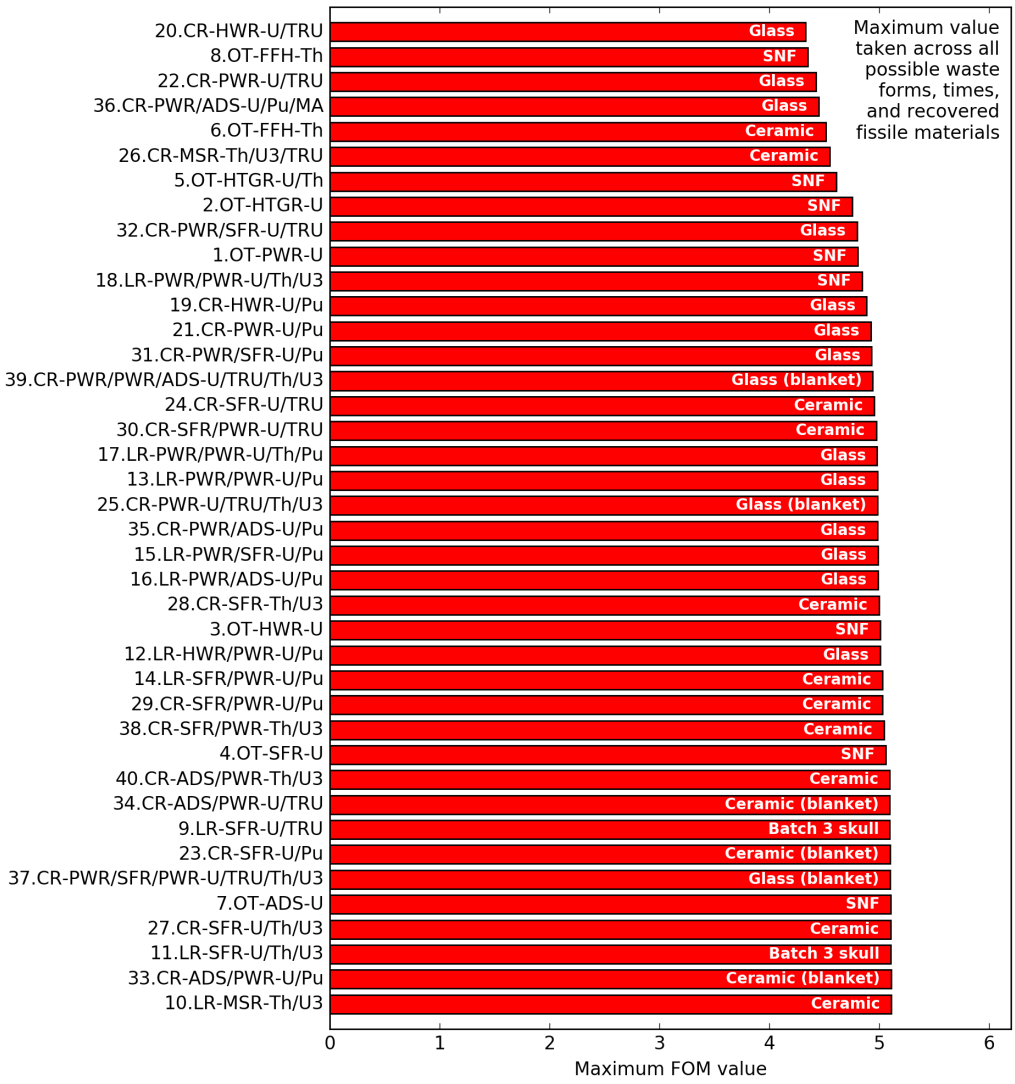

Figure 4.18: Maximum value of the material attractiveness figure of merit (FOM), taken over waste form, recovered attractive material, and time after fuel discharge. Each bar is labeled with the waste form that contains it; for all fuel cycles, the maximum value of the FOM is for recovered Pu at some time beyond 10,000 years after discharge.

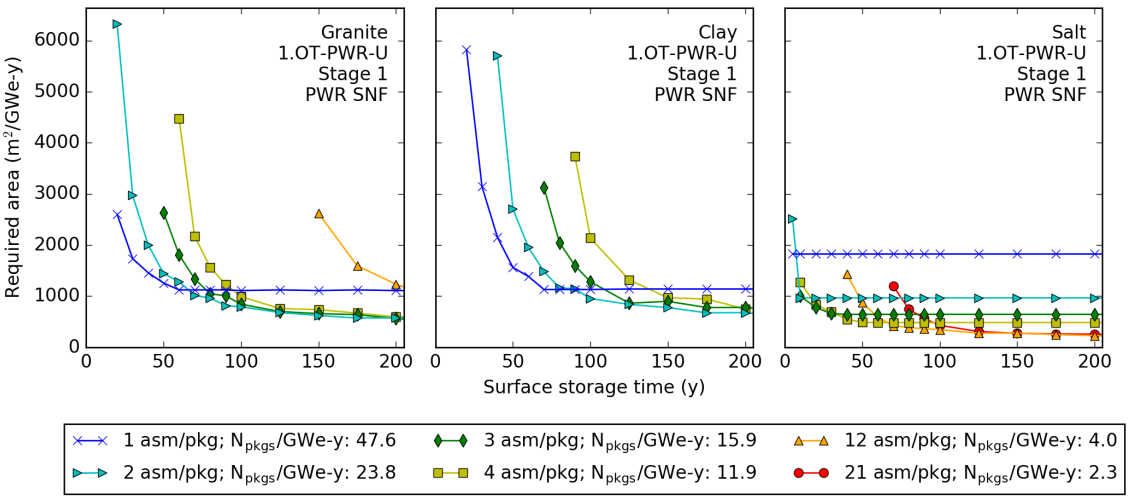

Figure 4.19: Required repository area for disposal of PWR SNF from 1.OT—PWR—U in granite, clay, and salt repository concepts. The different line colors and marker styles distinguish package loading options, for which package inventories are reported in the legend.

that they cannot be placed any closer together. This behavior is exhibited by the 1-assembly package in all host rocks, and by the 2-, 3-, and 4- assembly packages in the salt repository.

The effect of waste package loading depends on the surface storage time. When disposal of larger packages initially becomes possible, the area required may be greater than that for smaller packages because the heat content is greater. However, as the heat decays, the area decreases below that for smaller packages because fewer large package are required.

The areal requirement for emplacement of the same waste in the three repository concepts depends on the thermal conductivity of the rock and EBS materials and the magnitude of the temperature constraint. For spent fuels, the clay repository is the most thermally restrictive due to the low thermal conductivity of the host rock and the use of thermally resistive bentonite buffer in the EBS. The granite repository also utilizes bentonite buffer in the EBS but has greater host rock thermal conductivity, improving heat dissipation from the spent fuel packages. The salt repository has the greatest host rock and EBS material thermal conductivity and the most lenient temperature constraint, so hotter waste can be emplaced sooner and with smaller spacing than in the other repository concepts. For example, in the salt repository, disposal of very large SNF packages up to 21-assemblies per package is possible within

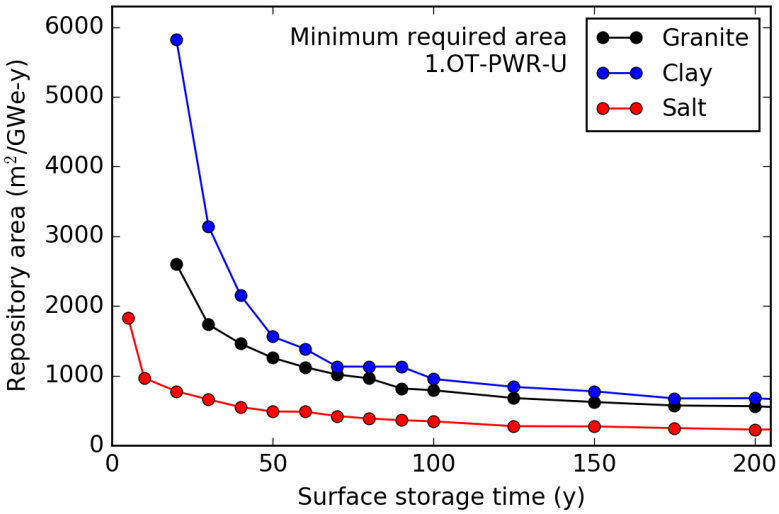

Figure 4.20: Minimum required repository area for disposal of PWR SNF from 1.OT—PWR—U in granite, clay, and salt repository concepts. The minimum is taken from the range of possible waste package loading options.

100 years of surface storage time. However, because the EBS dimensions for the salt repository are larger than those for the granite and clay repositories, the minimum required area achieved for disposal of cold wastes is greater than that for the other repositories. This is illustrated by the area required for the disposal of the 1-assembly package at 200 years of surface storage time.

Figure 4.20 plots the minimum area required for disposal of the spent fuel from 1.OT—PWR—U against surface storage time for the three repository concepts. The minimum is taken with respect to package loading. At all surface storage times, the required repository area in salt is less than that required in granite, which in turn is less than that required in clay.

It is important to note the magnitude of the y-axis, which is in units of m^2/GWe-y, and put these values into context. The order of magnitude of thousands of square meters is about the footprint of a large building. For example, Etcheverry Hall, on the University of California, Berkeley campus, has a footprint of about 2000 m^2 — enough area for disposal of 1 GWe-y spent fuel after 50 years of surface storage in any of the examined repository concepts. For reference, the UC Berkeley central campus is about 180 acres (728,434 m^2) [89], and the U.S. produced about 92 GWe-y of electricity from nuclear power in 2018 [90].

Another perspective into the thermal management of heat-generating wastes is the surface storage time required before emplacement in a repository is possible.

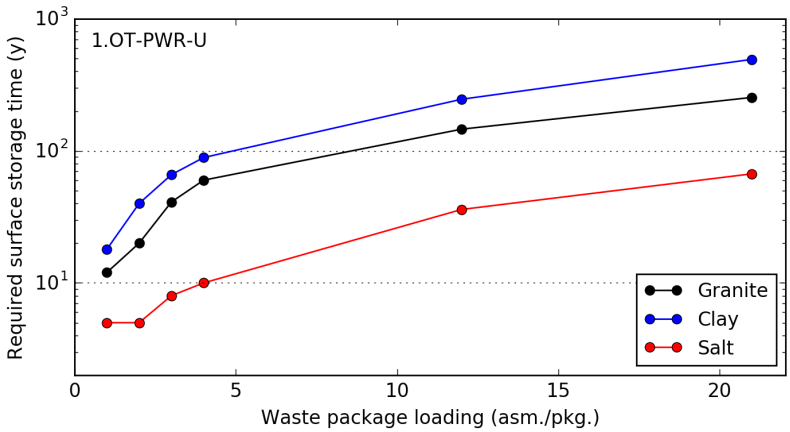

Figure 4.21: Required surface storage time as a function of waste package loading for disposal of PWR SNF from 1.OT—PWR—U in granite, clay, and salt repository concepts.

In Figure 4.19, that is illustrated by the point at which each curve appears on the figure. For further investigation, Figure 4.21 visualizes required surface storage time directly as a function of waste package loading for each of the repository host rocks.

The minimum possible value for required surface storage is five years: this is the mandatory cooling time after fuel discharge from the reactor. The 1- and 2-assembly packages can be emplaced in the salt repository immediately after this period. Even the 21-assembly packages can be emplaced in the salt repository after just 67 years of surface storage. In clay and granite, however, the required surface storage times are much longer due to the more restrictive temperature constraints and the use of thermally insulating bentonite buffer. The use of larger packages (12-assemblies per package or greater) in these disposal concepts is difficult because greater than 100 years of surface storage would be required.

The results for 1.OT—PWR—U can be compared to those from other fuel cycles to compare and contrast the effects of heat load and package inventory on repository area requirement. First, the limited-recycle of Pu in LWR (13.LR—PWR/PWR—U/Pu) represents an advanced fuel cycle reasonably attainable in the near-term. Figures 4.22 and 4.23 show the area required for disposal in each repository concept for the glass HLW produced in Stage 1 and the MOX SNF produced in Stage 2 of 13.LR—PWR/PWR—U/Pu, respectively. In Figure 4.22, the different line colors and marker styles distinguish waste loading fractions (the mass fraction of waste in the final waste form) for the glass HLW. One of the values — denoted by the blue line and "x" markers — indicates the baseline waste loading, obtained by the method

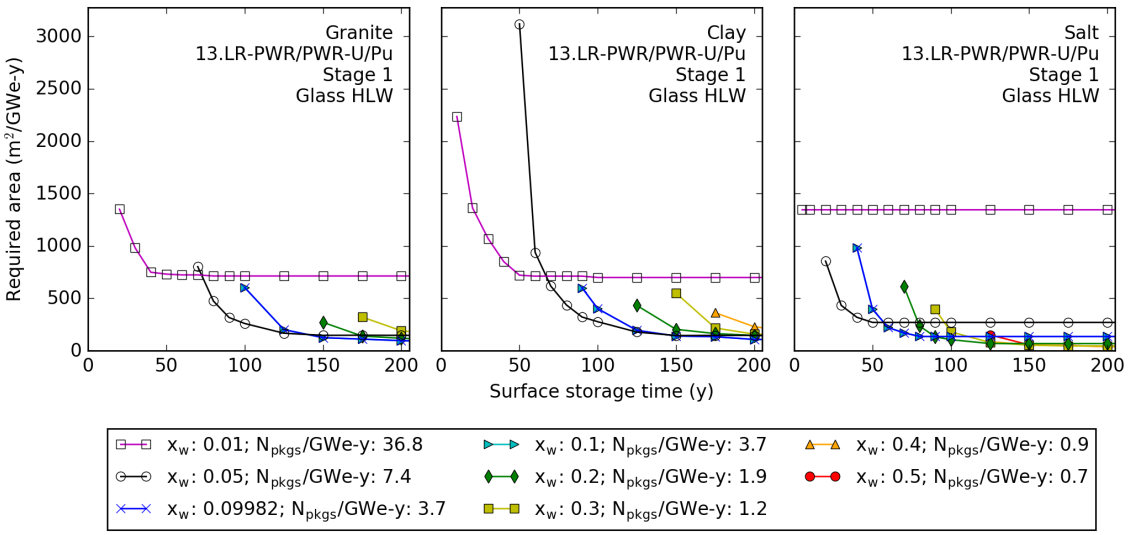

Figure 4.22: Required repository area for disposal of glass HLW produced in Stage 1 of 13.LR—PWR/PWR—U/Pu in granite, clay, and salt repository concepts. The different line colors and marker styles distinguish package loading options, for which package inventories are reported in the legend.

for glass HLW loading presented in Chapter 3. The other values are included for parametric analysis.

Heat-generating fission products are concentrated in the glass HLW, resulting in fewer packages, but each having a substantial decay heat load. For this reason, increasing the waste loading fraction results in large increases in required surface storage time. The baseline waste loading requires 100 years of surface storage before disposal in granite; 90 years for clay; and 40 years for salt. (Note that because the EBS concept for disposal of HLW in clay does not utilize bentonite, disposal of HLW in clay is slightly less restrictive than disposal in granite). However, the area required can be very small, well below 1000 m^2/GWe-y.

Disposal of the MOX SNF produced in Stage 2 presents a challenge. In thermal spectrum reactors, many actinide isotopes — starting from U-238, but including Pu-240 and Pu-242 — are more likely to capture neutrons than to fission. Over multiple cycles in the reactor, successive captures on these isotopes create larger inventories of heat-generating TRU isotopes, greatly increasing the decay heat content of the waste. The MOX SNF requires over 150 years of surface storage for the disposal of five 1-assembly packages in granite and cannot be disposed of at all in the clay repository before 200 years of surface storage. Due to the greater thermal conductivity and less

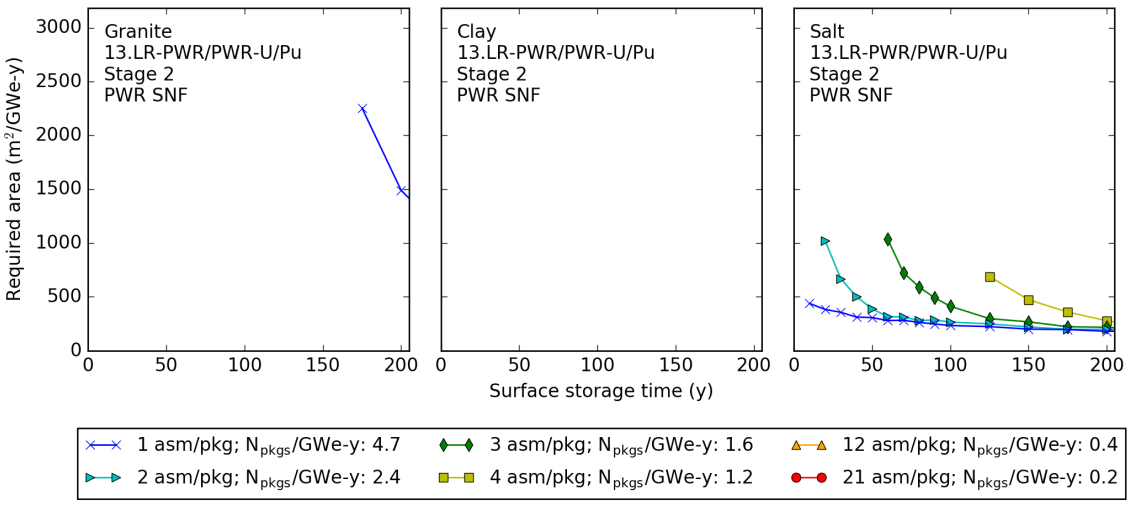

Figure 4.23: Required repository area for disposal of PWR MOX SNF from 13.LR—PWR/PWR—U/Pu in granite, clay, and salt repository concepts. The different line colors and marker styles distinguish package loading options, for which package inventories are reported in the legend.

restrictive thermal constraint, the salt repository offers greater flexibility, but waste package size is limited to 4-assemblies per package.

Figure 4.24 shows the minimum disposal area for the wastes produced by 13.LR—PWR/PWR—U/Pu as a function of surface storage time. No line is shown for disposal in clay, because the MOX SNF cannot be emplaced in clay before 200 years of surface storage. Disposal in granite is only slightly less restricted. This figure highlights the thermal flexibility of the salt disposal concept.

Figure 4.25 shows the required surface storage time as a function of waste form (HLW; left) and waste package (SNF; right) loading for the wastes produced by 13.LR—PWR/PWR—U/Pu. The estimated waste loading for the glass HLW based on the method described in Chapter 3 is 9.98 wt%. The required surface storage time before emplacement of glass HLW with this waste loading is 96 years for the granite repository, 82 years for the clay repository, and 39 years for the salt repository.

The surface storage times required for the MOX SNF produced in Stage 2 of 13.LR—PWR/PWR—U/Pu are much greater, indicating that the required storage time for MOX SNF is by far the waste stream that limits emplacement time for this fuel cycle. Over 100 years are required before the 1- assembly packages can be emplaced in the clay and granite repositories, and larger packages would require over 1000 years of surface storage.

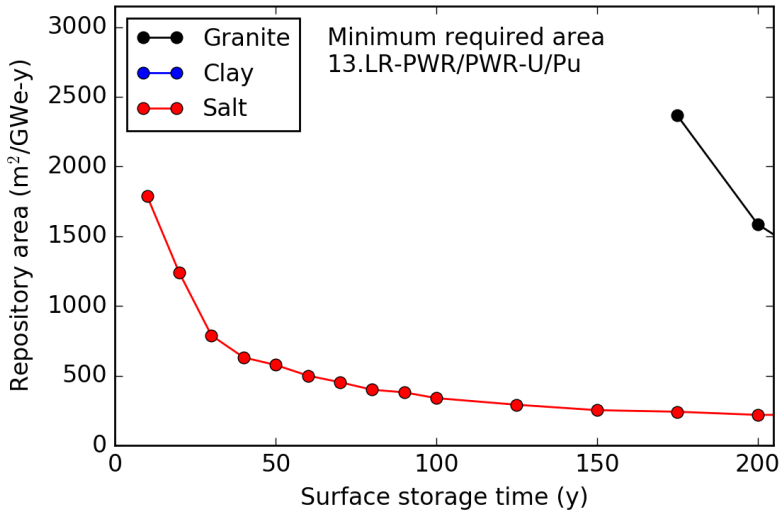

Figure 4.24: Minimum required repository area for disposal of HLW and SNF from 13.LR—PWR/PWR—U/Pu in granite, clay, and salt repository concepts. The minimum is taken from the range of possible waste package loading options. Where no values are shown (e.g. for disposal in clay), disposal is not possible.

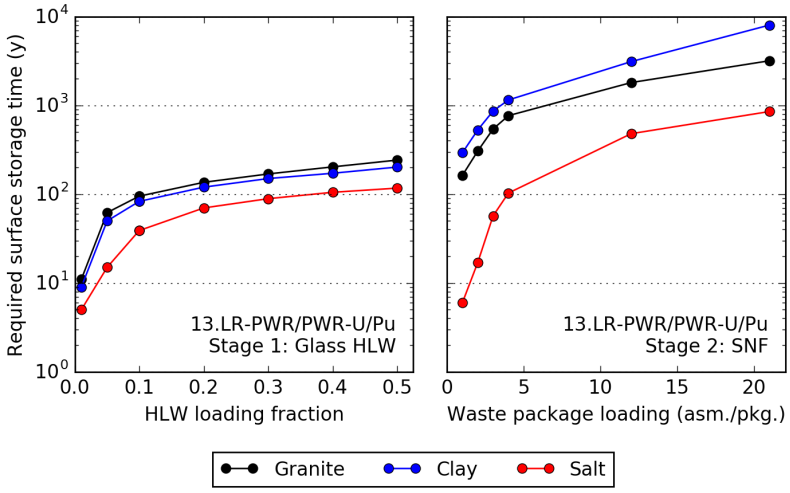

Figure 4.25: Required surface storage time as a function of waste form and package loading for disposal of glass HLW (left) and PWR MOX SNF (right) from 13.LR—PWR/PWR—U/Pu in granite, clay, and salt repository concepts.

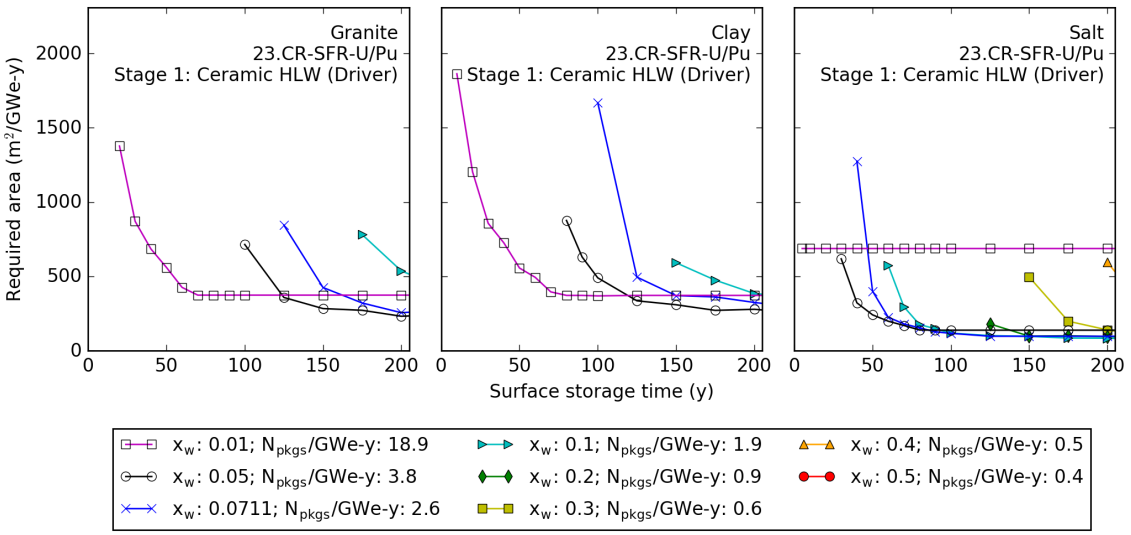

Figure 4.26: Required repository area for disposal of ceramic HLW produced from processing SFR driver fuel in 23.CR—SFR—U/Pu in granite, clay, and salt repository concepts. The different line colors and marker styles distinguish package loading options, for which package inventories are reported in the legend.

Finally, the high-level wastes produced by a continuous-recycle fuel cycle offer a contrasting third example. Selected for closer examination is 23.CR—SFR—U/Pu, which was identified as promising in the FCES study. In this fuel cycle, driver and blanket fuels are treated separately, and the mass of the driver fuels is greater than that of the blanket fuels. Reprocessing each produces metal and ceramic waste forms. Together, these wastes contain fission products and unrecovered actinides, including U and Pu from separation losses and TRU, which is not recycled in this fuel cycle. All of the actinides and reactive fission products end up in the ceramic waste form, whereas the metal contains only the noble metal fission products. Therefore, the vast majority of the waste decay heat and mass is in the ceramic HLW. The area required for disposal of the ceramic HLW from the driver and blanket fuels is shown in Figures 4.26 and 4.27. The figures showing the corresponding results for the metal HLW are included in Appendix C.

23.CR—SFR—U/Pu produces relatively few HLW packages but each one has a significant heat load, which limits the required storage time. The required storage for the baseline loading for the driver fuel ($x_w = 0.0711$) is about 125 years, and for the blanket fuel ($x_w = 0.0684$) is 70 years. For disposal in granite and clay before 50 years of surface storage, only the very dilute waste with $x_w = 1\%$ can be emplaced

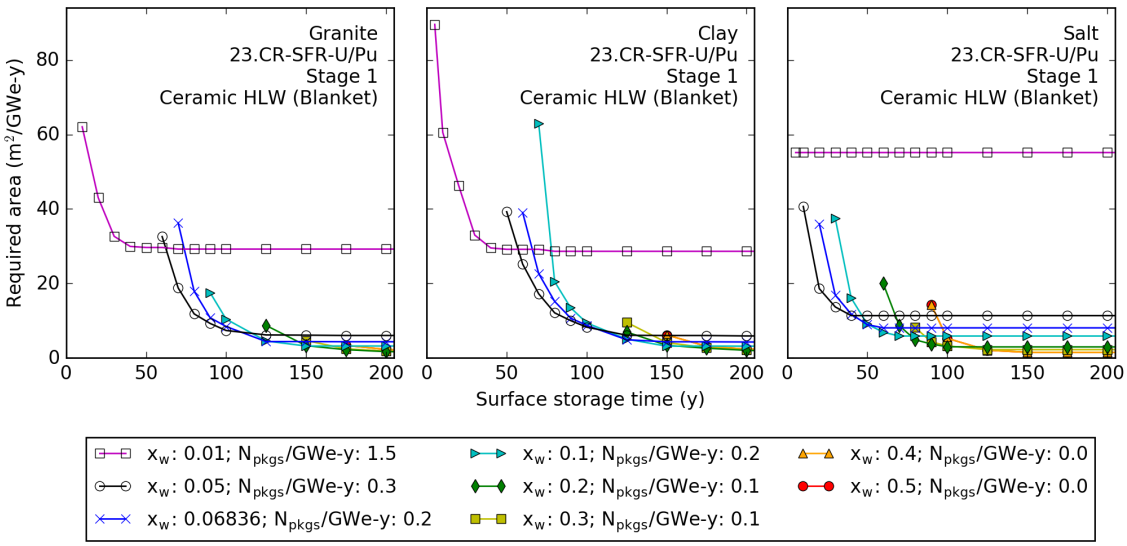

Figure 4.27: Required repository area for disposal of ceramic HLW produced from processing SFR blanket fuel in 23.CR—SFR—U/Pu in granite, clay, and salt repository concepts. The different line colors and marker styles distinguish package loading options, for which package inventories are reported in the legend.

before 50 years of surface storage. Although longer surface storage is undesirable, it allows a significant reduction in repository area. Figure 4.28 shows the minimum area required for disposal of all HLW (ceramic and metal, driver and blanket) produced by this fuel cycle in each repository concept.

Figure 4.29 shows the required surface storage time for the ceramic and metal HLW produced from electrochemical processing of driver and blanket fuels from 23.CR—SFR—U/Pu. Three subfigures show the results for each repository concept, and the result for each HLW waste stream is distinguished by line color and marker style. As mentioned previously, the metal waste is relatively dilute in waste nuclides, so high waste loading can be achieved without incurring large requirements for surface storage. That the curves for the metal HLW required surface storage are flat indicate that to not increase waste loading as much as possible would be inefficient. The model-estimated loading for the metal waste from the driver fuels is greater than 70 wt%, which would require 15 to 16 years of surface storage time in all of the repository environments. The metal waste from the blanket fuels is more dilute than that from the metal fuels, and requires only 13-15 years of surface storage.

The ceramic HLW, which contains most of the waste nuclides and decay heat content, exhibits surface storage requirement more similar to that of the glass HLW

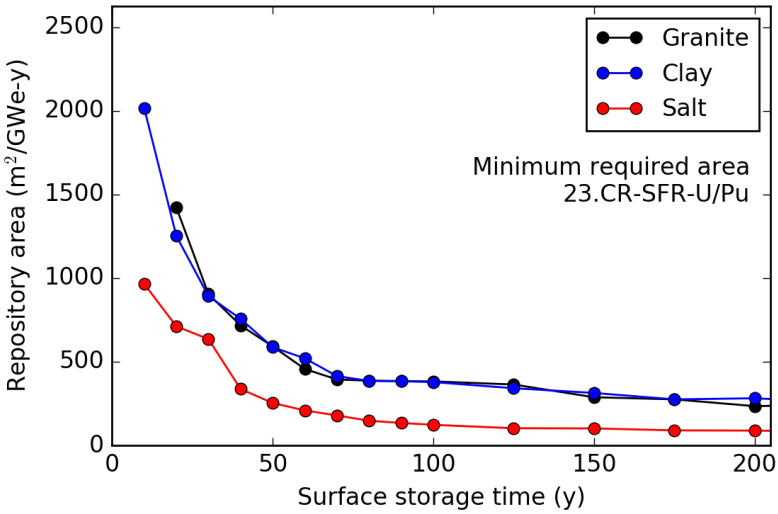

Figure 4.28: Minimum required repository area for disposal of HLW from 23.CR—SFR—U/Pu in granite, clay, and salt repository concepts. The minimum is taken from the range of possible waste package loading options.

from 13.LR—PWR/PWR—U/Pu. Although with low waste loading, the storage time requirement for the ceramic HLW from the driver fuels is less than 10 years, at the model-estimated waste loading (about 7 wt%), the requirement is 121 years in granite, 100 years in clay, and 40 years in salt.

The areal requirements for two fuel cycles can be compared by plotting the ratio between them as a function of surface storage time. In this way, the potential benefit for a smaller repository can be visualized. Figure 4.30 shows the ratio between the minimum area required for disposal of wastes from 13.LR—PWR/PWR—U/Pu and 23.CR—SFR—U/Pu against that for the waste from 1.OT—PWR—U. Due to the high decay heat load of the packages produced by 13.LR—PWR/PWR—U/Pu, no reduction in area is made over the disposal of wastes from 1.OT—PWR—U within 200 years of surface storage.

However, because the decay heat of HLW produced in 23.CR—SFR—U/Pu decreases quickly, the required area is reduced for repositories in all rock types. In previous work [91], it was observed that advanced fuel cycles generated reductions in repository area that diminished with increasing surface storage time. In these analyses, HLW loading was fixed. This meant that at longer storage times, the decay heat load was already very dilute and no further reductions in area were possible. Meanwhile, the areal requirement for wastes with larger heat loads from other fuel cycles continued decreasing. In this context, the advanced fuel cycle provided di-

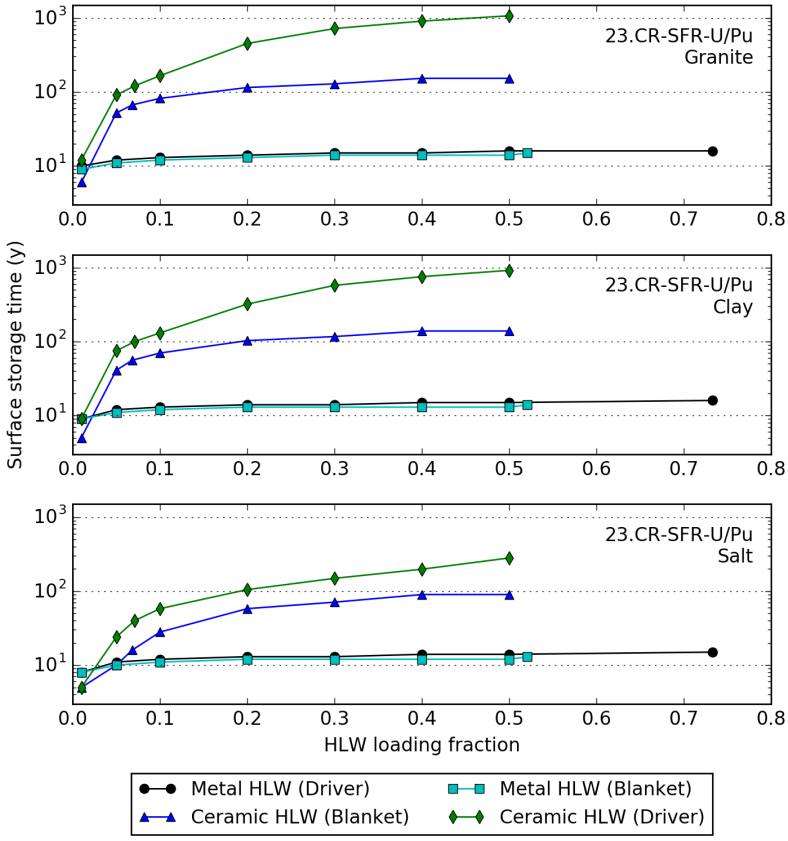

Figure 4.29: Required surface storage time as a function of waste form and package loading for disposal of metal and ceramic HLW from 23.CR—SFR—U/Pu in granite, clay, and salt repository concepts.

minishing returns. In this analysis, because the HLW loading was allowed to vary, sustained benefit can be achieved with surface storage time in all repository environments. The minimum area required for disposal of wastes from 23.CR—SFR—U/Pu is about two times less than for those from 1.OT—PWR—U.

Comparative visual analysis can be extended to the other fuel cycles by selecting a single surface storage time and plotting the minimum required area for all fuel cycles at that time. Figure 4.31 shows the minimum required area for each fuel cycle in each repository after 20 years of surface storage. The values are sorted by increasing area, and fuel cycles that produce wastes that cannot be disposed without further surface storage lack a bar in the plot but are included in the axis labels.

The bars are colored according the type of fuel used in each fuel cycle. Fuel cycles

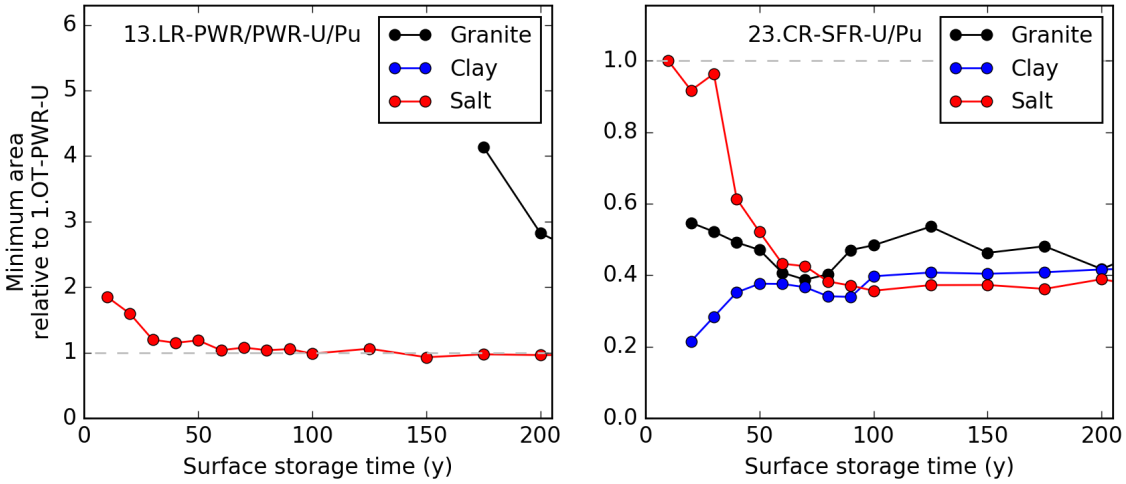

Figure 4.30: Ratio of minimum required repository area for disposal of SNF and HLW from 13.LR—PWR/PWR—U/Pu and 23.CR—SFR—U/Pu relative to that required for 1.OT—PWR—U, in each repository environment.

that recycle TRU or utilize Th send less highly radioactive transuranic isotopes to the waste. An option for "other" mainly includes fuel cycles utilizing uranium fuel. Although uranium is the starting point for TRU creation, it is different than recycling Pu in fuel in that the Pu and higher actinides must be accumulated throughout the irradiation cycle. Starting the irradiation cycle with Pu provides a shortcut to further TRU accumulation by skipping the reactions on uranium necessary to form Pu. Many of the bars that are not shown because disposal is not possible are for fuel cycles that involve recycling Pu.

After 20 years of surface storage, decay heat is still dominated by fission products. Therefore, fuel cycles also benefit from flexibility in waste package loading in order to dilute the fission product heat content at relatively short surface storage times. The fuel cycles that require the greatest area in each repository concept also produce larger package inventories with lower heat content: fuel cycles that utilize MSR (10.LR—MSR—Th/U3 and 26.CR—MSR—Th/U3/TRU), and in granite, HWR (3.OT—HWR—U, 19.CR—HWR—U/Pu, and 20.CR—HWR—U/TRU). The once-through ADS fuel cycle, 7.OT—ADS—U, also produces large amounts of heat-dilute waste and requires the greatest area for disposal in all three host rocks.

Another important point is that limited-recycling fuel cycles produce wastes that require longer storage times before emplacement in thermally restrictive repositories. The wastes from most of the limited-recycle fuel cycles is not able to be emplaced

after 20 years of surface storage and is not plotted in Figure 4.31 for the granite and clay repositories. By contrast, the salt repository can accept waste from any of the fuel cycles after only 20 years of surface storage.

The surface storage time value used in Figure 4.31 (20 years after discharge) was selected as an attractive target value for an integrated fuel cycle and waste management system. On the timescale of repository operation and waste radiotoxicity, 20 years is very short. However, on the timescale of human activity, 20 years is relatively long, approximately half of a long career. One way to potentially decrease the waste management requirements for an advanced fuel cycle would be to shorten the time for which stewardship over the waste is required.

However, as mentioned earlier, longer surface storage time offers benefits, enabling closer emplacement of cooler wastes and/or the use of larger packages. A long term management strategy might involve storage times of up to 100 years or longer. Figure 4.32 shows the minimum area required after 100 years of surface storage in each repository. Again, the bar colors indicate area required for disposal of wastes from fuel cycles stages utilizing TRU and/or U3/Th, Pu, or another fuel element. After 100 years, most of the fission products have decayed, and a significant fraction of the heat is generated by intermediate-lived isotopes like Pu-238 ($t_{1/2} = 87.7$ y) and Am-241 ($t_{1/2} = 432.2$ y). These TRU isotopes are concentrated in wastes from fuel cycles that recycle Pu, which require greater disposal area and are concentrated toward the bottom of each subfigure in Figure 4.32. The fuel cycles that produce wastes that still cannot be emplaced in granite or clay repositories after 100 years of surface storage are all limited-recycle fuel cycles that recycle Pu.

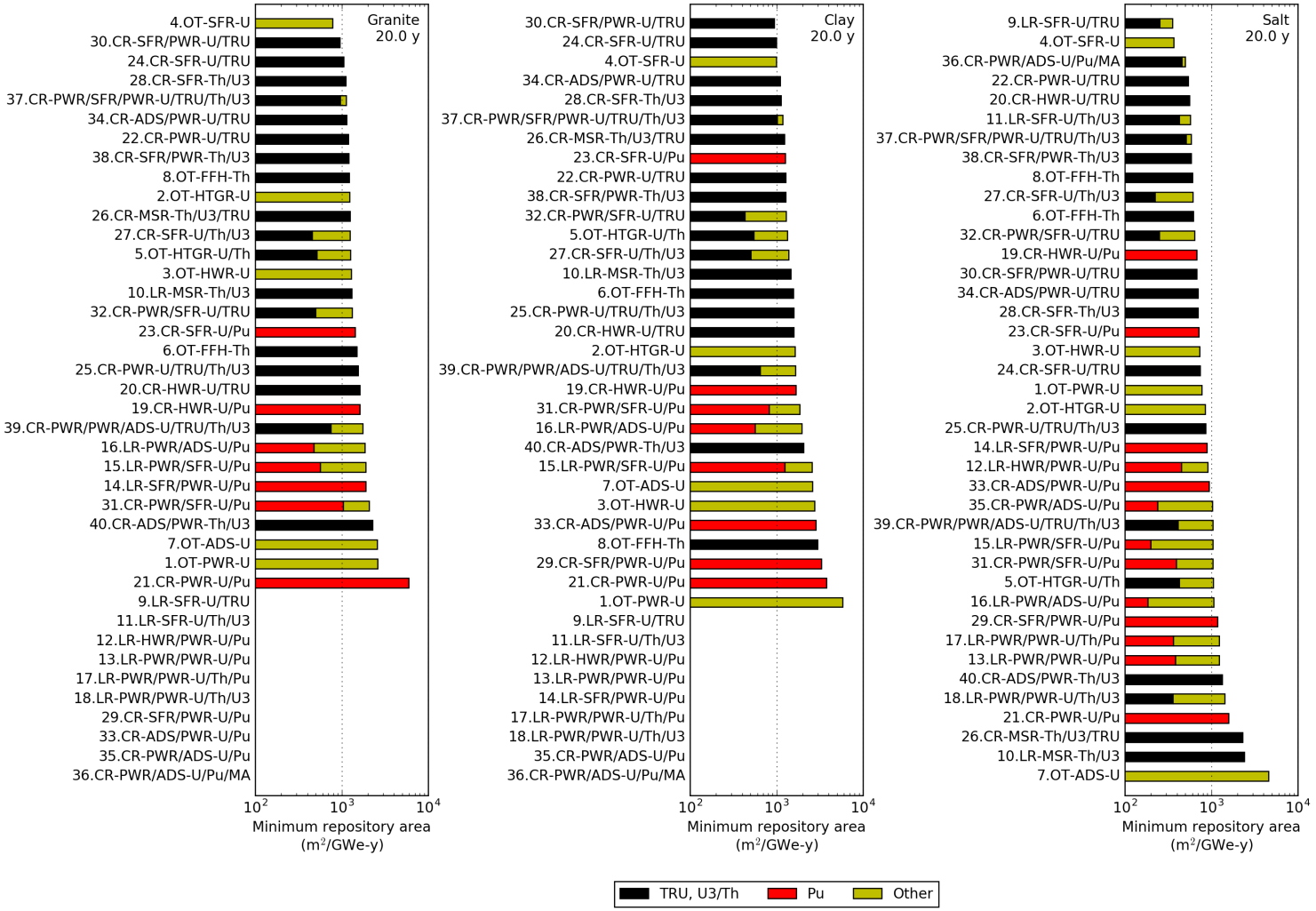

Figure 4.31: Minimum required area after 20 years of surface storage in granite, clay, and salt repositories.

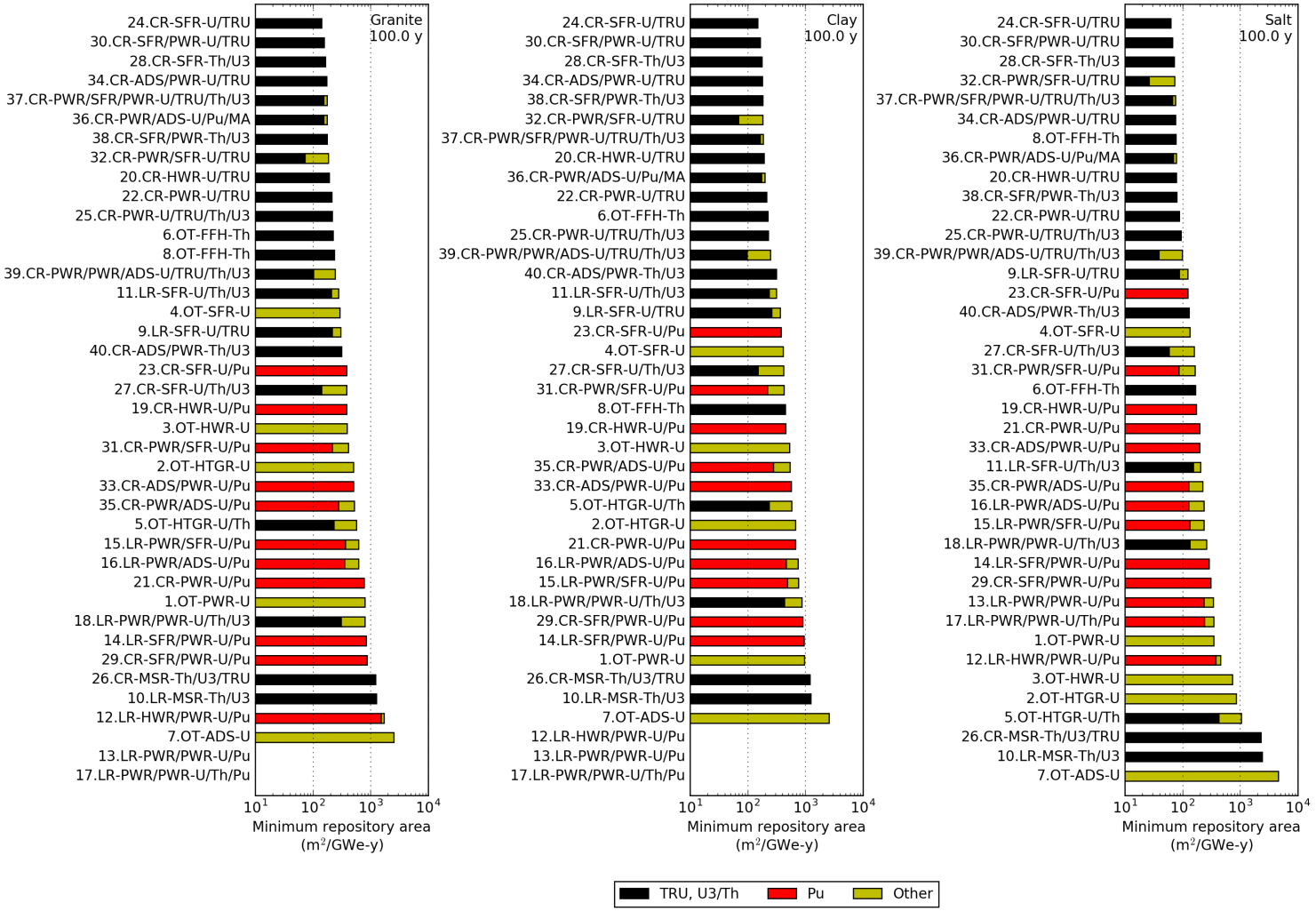

Figure 4.32: Minimum required area after 100 years of surface storage in granite, clay, and salt repositories.

A few fuel cycle examples illustrate the effect of fuel cycle characteristics on repository area. These are included in Figures 4.31 and 4.32 and tabulated in Table 4.6. First, as mentioned previously, recycling TRU offers substantial benefits relative to recycling Pu alone. In nearly every case, the fuel cycle that recycles TRU achieves a reduction in required area. The only exception is for disposal of waste from 23.CR—SFR—U/Pu, the fuel continuous-recycle of U/Pu in SFR, which produces fewer packages than its partner, 24.CR—SFR—U/TRU. In general, the reduction is more apparent at greater surface storage times when TRU contributes more to the decay heat content of the waste.

Table 4.6: Minimum required area for similar fuel cycles recycling different elements

	Granite		Clay		Salt	
Fuel cycle	20 y	100 y	20 y	100 y	20 y	100 y
19.CR—HWR—U/Pu	1607	386.1	1661	451.0	674.8	173.3
20.CR—HWR—U/TRU	1606	190.2	1580	191.7	555.8	78.05
21.CR—PWR—U/Pu	N/A	771.5	N/A	670.8	1573	198.1
22.CR—PWR—U/TRU	1190	213.1	1266	212.6	538.6	86.86
23.CR—SFR—U/Pu	N/A	382.4	1252	378.1	711.4	122.8
24.CR—SFR—U/TRU	1050	142.0	989.7	147.6	740.4	62.61

The examples in Table 4.6 also demonstrate the effect of reactor spectrum on repository footprint, with the first four rows representing thermal reactors and the last two rows representing fast reactors. The capture-to-fission ratio of TRU isotopes is generally lower for fast neutrons, leading to greater TRU transmutation. Because TRU is a significant contributor to decay heat at longer times, this impact is apparent after 100 years of surface storage time. In all three repository environments, the waste from the fast reactor (23.CR—SFR—U/Pu for U/Pu recycle; 24.CR—SFR—U/TRU for U/TRU recycle) requires smaller disposal area than that from the thermal reactors (19.CR—HWR—U/Pu and 21.CR—PWR—U/Pu for U/Pu recycle; 20.CR—HWR—U/TRU and 21.CR—PWR—U/Pu for U/TRU recycle).

In Figure 4.32, the MSR fuel cycles perform poorly in all repository environments, requiring more area than almost all of the other fuel cycles for which disposal is possible after 100 years of surface storage. This is due to the low value assumed for separation efficiency, as compared to what was apparently utilized in the FCES (described in Chapter 3 in Table 3.11). As shown, the MSR fuel cycles produce large package inventories with relatively low decay heat content. After 100 years of surface storage, the repository area is controlled entirely by package inventory.

Table 4.7: Effect of separation efficiency on required repository area and surface storage time for 10.LR—MSR—Th/U3 ceramic HLW

Fuel cycle	10.LR—MSR—Th/U3	
Recovery fraction	Actinides: 0.99 REE: 0.4 (Eu: 0.94)	U3: 0.9999654 Th: 0.99999882 TRU: 1.0 REE: 0.4 (Eu: 0.94)
N_{pkgs}/GWe-y ($x_w = 0.1$)	327	28
Granite		
Area ($t = 20$ y); (m^2)	6311.6	1724.3
Area ($t = 100$ y); (m^2)	6311.6	533.7
Storage time (y)	11.0	11.0
Clay		
Area ($t = 20$ y); (m^2)	6182.4	—
Area ($t = 100$ y); (m^2)	6182.4	547.3
Storage time (y)	11.0	21.0
Salt		
Area ($t = 20$ y); (m^2)	11928.3	997.7
Area ($t = 100$ y); (m^2)	11928.3	997.7
Storage time (y)	11.0	11.0

Tables 4.7 and 4.8 show results describing MSR fuel cycle waste repository area and surface storage time requirements for the different separation efficiency cases for cases 10.LR—MSR—Th/U3 and 26.CR—MSR—Th/U3/TRU, respectively.

As shown in Tables 4.7 and 4.8, increased separation efficiency results in an order of magnitude reduction in package inventory, concentrating the decay heat load in fewer packages. For 10.LR—MSR—Th/U3, which produces more packages, this results in a roughly proportional decrease in required area at both 20 and 100 years of surface storage in all repository environment. The required surface storage time only increases for disposal in the clay repository. By contrast, the increased separation efficiency for 26.CR—MSR—Th/U3/TRU results in substantial concentration of decay heat, and disposal is not possible in any repository environment after 20 years of surface storage. After 100 years of surface storage, disposal in salt is still the only option. This issue can be mitigated by decreasing waste package loading, yielding a proportional increase in the number of packages; relative to the package

Table 4.8: Effect of separation efficiency on required repository area and surface storage time for 26.CR—MSR—Th/U3/TRU ceramic HLW

Fuel cycle	26.CR—MSR—Th/U3/TRU	
Recovery fraction	Actinides: 0.99 REE: 0.4 (Eu: 0.94)	U3: 0.0.999943458 Th: 0.999999 Pu: 0.98969 REE: 0.94 (Eu: 0.994)
N_{pkgs}/GWe-y ($x_w = 0.1$)	312	2
Granite		
Area ($t = 20$ y); (m^2)	6034.3	—
Area ($t = 100$ y); (m^2)	6034.3	—
Storage time (y)	11.0	119.0
Clay		
Area ($t = 20$ y); (m^2)	5910.8	—
Area ($t = 100$ y); (m^2)	5910.8	—
Storage time (y)	11.0	108.0
Salt		
Area ($t = 20$ y); (m^2)	11404	—
Area ($t = 100$ y); (m^2)	11404	74.752
Storage time (y)	11.0	66.0

inventories from other fuel cycles, increasing from 2 to 20 packages per GWe-y is not an unreasonable burden.

The minimum required surface storage times for all fuel cycle cases, including the MSR fuel cycles with low separation efficiency, are shown in Figure 4.33. This value indicates the minimum time at which all wastes can be emplaced. Therefore, although a fuel cycle may produce wastes that can be emplaced earlier, the values shown in Figure 4.33 reflect the time required for the wastes with the greatest decay heat content, taken here as limiting. A dotted line at 5 years indicates the minimum possible value.

Because all waste streams were given multiple waste form or package loading options, the values shown in Figure 4.33 are generally the lowest possible waste loading, which results in the greatest number of packages requiring emplacement. The labels on the right edge of each subfigure are the total number of packages per GWe-y produced by each fuel cycle with required surface storage time less than or

equal to to the value shown in the figure. For disposal in clay and salt, the MSR fuel cycles produce the greatest number of packages; for disposal of 26.CR—MSR—Th/U3/TRU wastes in granite, that number is significantly smaller because by the time the heat content has decayed to allow for emplacement, it becomes possible to emplace wastes with greater waste loading fraction.

In clay and granite (the thermally restrictive repository concepts), only a few of the fuel cycles require surface storage of 5 years, the mandatory cooling time after discharge. These wastes can be emplaced in a repository immediately after cooling and/or reprocessing. Only a few extreme cases require exceedingly long (greater than 50 years) surface storage times. In salt, many fuel cycles produce wastes that can be emplaced after 5 years, and no fuel cycle requires surface storage time greater than 10 years.

This figure demonstrates the combinations of fuel cycle and repository environment for which an integrated waste management approach can be flexible: if the required surface storage time is short, more waste formation, packaging, and disposal options are available. For many fuel cycles, this flexibility is not possible. When decades of storage are required before the wastes with the lowest decay heat content can be emplaced in a repository, the options available for waste management are much more limited.

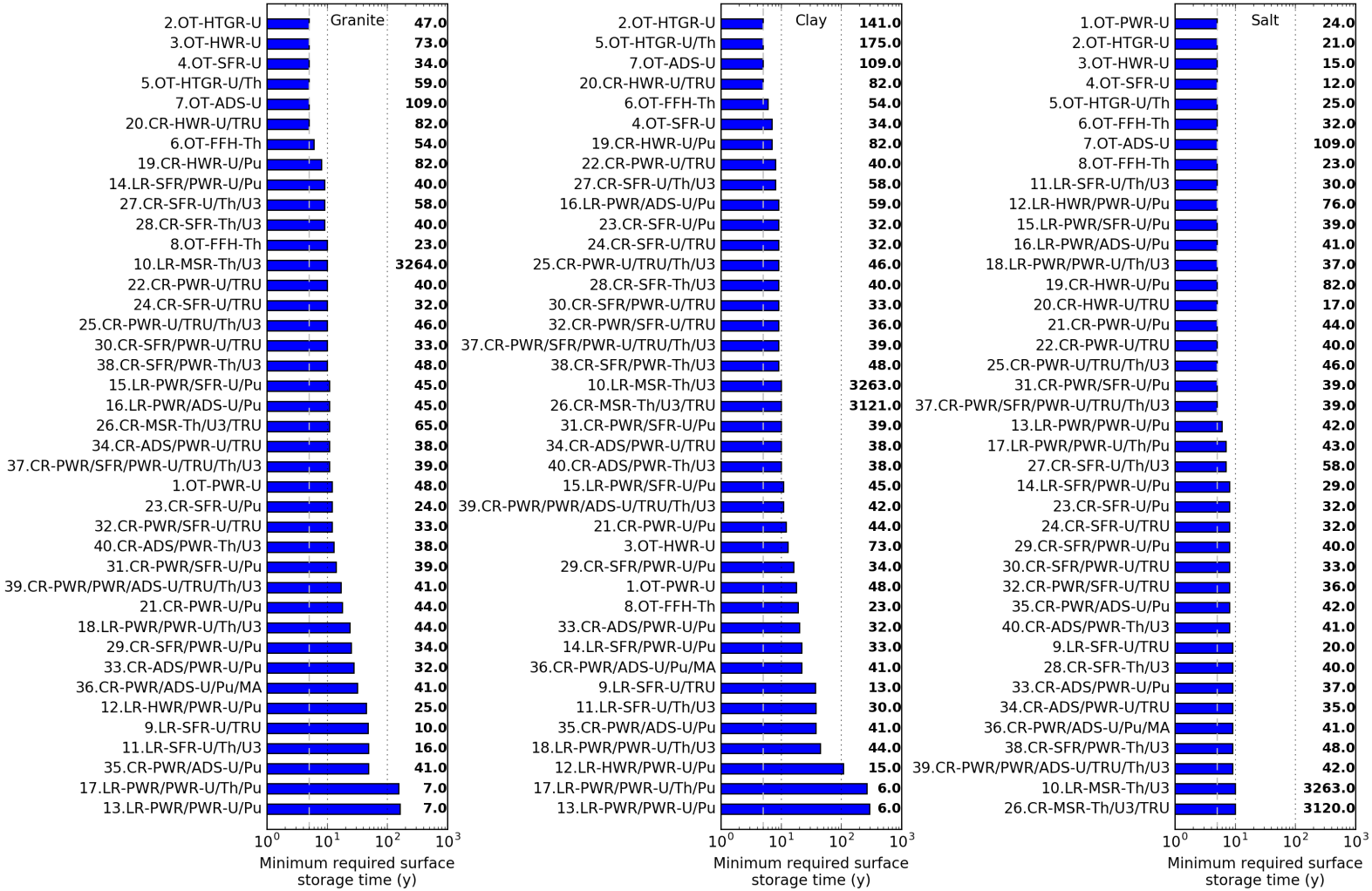

Figure 4.33: Minimum required surface storage time before disposal in granite, clay, and salt repositories.

Chapter 5

Conclusions and Future Work

In this chapter, the analysis performed in this dissertation is summarized to form the basis for discussions about waste management strategies. Opportunities for future analysis are proposed.

5.1 Summary and conclusions

In this dissertation, three management models were applied to the fuel cycles studied in the Fuel Cycle Evaluation and Screening study to explore the relationship between advanced fuel cycle options and the management of their wastes. The novelty of this analysis stems from both the waste management models themselves, as well as the large number of fuel cycles to which they were applied.

The first model evaluated the long-lived fission product inventory of the waste streams for each fuel cycle as a proxy for geologic repository performance. LLFPs are mobile in many geologic environments and therefore may be significant contributors to repository dose. In a review of repository performance assessments [4], five LLFPs were shown to contribute to repository dose: Cs-135, Tc-99, I-129, Sn-126, and Se-79. Total fission product inventory, and by extension, LLFP inventory, is shown to be related to thermal efficiency. As fuel is recycled more extensively, the fuel isotopes (such as Pu-239 and Pu-241, or U-233 at thermal energies) tend to have greater overall LLFP fission yields, resulting in greater LLFP inventories for continuous-recycle fuel cycles. Of the five LLFP identified, Cs-135, Tc-99, and I-129 are produced in the greatest quantities and therefore were considered for further analysis. All three LLFP and their precursors are transmuted at a greater rate in thermal reactors. Additionally, Tc-99 and I-129 have significantly different yields depending on the fissioning isotope. Relative to other actinide isotopes, fission on U-233 produces less

Tc-99 but more I-129; fission on U-235 produces less I-129.

The second model examined the attractiveness of waste materials for potential proliferation using a figure of merit (FOM) that assesses the quality of the fissile material in the waste and the ease of with which the waste can be recovered. The studied scenario involves the unshielded recovery of waste from a package and subsequent separation of an attractive species from the waste form — either U (mainly U-233), Pu, or TRU. The FOM incorporates the bare sphere critical mass (kg) and decay heat content (W/kg) of the recovered material, and dose rate (rad/hr) at 1-m from a sphere of the waste form mixture with mass equal to the amount of material in the waste package. For nearly all waste streams, the dose rate from the waste is self-protecting at early times, increasing the difficulty of retrieval to the point that the recovered material is very unattractive. However, over time, that self-protecting dose rate decays away and the recovered material becomes attractive.

Although all fuel cycles produce wastes that become attractive for recovering fissile materials, some fuel cycles offer advantages over others. Two barriers to fissile material recovery are: (1) the time before the waste becomes attractive, and (2) the number of packages that must be recovered in order to obtain a critical mass of material. In both respects, fuel cycles that produce high-level wastes from reprocessing perform better than those that produce spent fuels. First, because strongly radioactive fission product isotopes are more concentrated in HLW than SNF, the dose rate from HLW is greater. This increases the time before the fissile material in HLW becomes attractive. Second, because HLW is more dilute than SNF in potentially attractive fissile material, more HLW packages must be intercepted to acquire a critical mass of fissile material. In addition, reprocessing offers the possibility of improving the separation efficiency, resulting in even less fissile material sent to HLW.

The third model evaluated various strategies for waste decay heat management to comply with thermal constraints for close-contact geologic repositories based on thermal constraints: (1) waste package and/or waste form loading; (2) waste package spacing in the repository; and (3) surface storage time before emplacement. Generic repository concepts in three host rocks — granite, clay, and salt — were considered. Clay and granite repositories were shown to be more sensitive to package heat load due to the lower thermal conductivity of the EBS materials and host rock and the more restrictive thermal constraint; the salt repository was shown to be more sensitive to package inventory because of the larger EBS dimensions. Continuous recycling of TRU and utilization of fast reactors offer benefits in repository area by consuming keeping heat-generating actinide isotopes out of the waste stream. By contrast, due to the accumulation of heat-generating TRU, limited-recycle fuel cycles are shown to produce wastes that are more difficult to manage, requiring larger disposal areas and longer surface storage times.

In the Fuel Cycle Evaluation and Screening study, the most promising fuel cycles exhibited four fuel cycle characteristics: (1) continuous-recycling of actinides; (2) fast-spectrum reactors; (3) critical reactors; and (4) reactors and fuels with high conversion ratios. To visualize how these characteristics impact the waste management metrics evaluated in this dissertation, Table 5.1 offers brief summaries about the impact of each fuel cycle characteristic. For some combinations of fuel cycle characteristics and waste management model there are no conclusions to summarize. In some cases, there is a lack of a causative relationship; in others, the waste management model did not capture the impact of the fuel cycle characteristic.

Table 5.1 shows that some fuel cycle characteristics are generally positive or negative with respect to waste management outcomes. For example, greater thermal efficiency in reactors decreases the fuel requirement, resulting in lower waste generation. Therefore, systems with lower efficiency or large parasitic load (such as externally driven systems) may be viewed unfavorably. Despite producing more LLFPs due to greater reliance on fuel isotopes with greater overall LLFP yields, continuous-recycling of actinides (specifically all TRU) reduces the attractiveness for proliferation of wastes emplaced in a repository and offers benefits in repository thermal management over other recycling schemes. By contrast, limited-recycle fuel cycles: (1) perform worse than once-through fuel cycles with respect to LLFP generation; (2) offer little benefit over once-through fuel cycles with respect to waste proliferation resistance; but (3) offer significant disadvantages with respect to repository thermal management.

These general conclusions can be compared to the results presented in the FCES, which summarized fuel cycle metric performance against an index representing benefit over the current once-through LWR fuel cycle. Those results are shown in Figure 5.1 [20]. The two orange lines indicate performance improvement that might be considered significant by policymakers. Fuel cycles that offered significant improvement include 23.CR—SFR—U/Pu, 24.CR—SFR—U/TRU, and 30.CR—SFR/PWR—U/TRU, which are all are ranked approximately equally in terms of overall benefit and achieved identical performance according to the five waste management metrics utilized in the FCES [23]. However, by the models presented in this dissertation, their waste management benefit is not entirely equal. The three fuel cycles produce roughly comparable amounts of LLFP. The time before the fissile material in the wastes from 24.CR—SFR—U/TRU and 30.CR—SFR/PWR—U/TRU becomes attractive is longer than that for any of the other fuel cycles, including 23.CR—SFR—U/Pu. Disposal of waste from 24.CR—SFR—U/TRU requires less area and can occur with less storage time than required for waste from 23.CR—SFR—U/Pu and 30.CR—SFR/PWR—U/TRU. These outcomes point to benefits for 24.CR—SFR—U/TRU and 30.CR—SFR/PWR—U/TRU that are not reflected in the FCES.

Table 5.1: Summary of fuel cycle characteristics on waste management outcomes

Fuel cycle characteristic	Options	Long-lived fission product generation	Waste material attractiveness	Required repository area and storage time
Extent of recycling	Once-through	Empirically produce smaller amounts of LLFP than CR fuel cycles	TTA (SNF) < TTA (HLW); Significant quantities of fissile material in packages	Greater area and storage time requirement due to larger decay heat load
	Limited-recycle	Empirically produce smaller amounts of LLFP than CR fuel cycles	Marginally better than OT, but same applies for the SNF produced by LR	Particularly negative: limited recycling results in the disposal of waste that has accumulated heat-generating actinides
	Continuous-recycle	Appear to produce more LLFP than OT and LR fuel cycles, potentially due to the recycling of fuel elements with greater LLFP yield.	TTA (HLW) < TTA (SNF) because concentrated FP dose rate; attractive fissile material is diluted in HLW	Continuous recycling of TRU offers opportunities to remove heat-generating nuclides from the waste, reducing area and RST
Reactor spectrum	Thermal	Greater rate of LLFP transmutation: ex. Cs-135 (Xe-135), Tc-99, I-129	---	Accumulates TRU, which ends up in the waste either through disposal in SNF or in reprocessing losses.
	Fast	Lower capture cross section for LLFP and precursor, less transmutation	---	Greater rate of TRU transmutation: less long-term heat generation in the waste
Reactor self-sustainability	Critical	Reactor systems with greater thermal efficiency require fewer fissions and produce fewer FP overall	---	Greater thermal efficiency reduces fuel requirement, decreasing package inventory
	Subcritical	Lower thermal efficiency and greater parasitic load means more fissions required and greater FP generation	---	Lower thermal efficiency means more fissions (and therefore fuel) required
Fissile material breeding (high converson ratio)	Low (requires enrichment)	U-235 has low I-129 yield	---	---
	High	U-233 (low Tc-99 yield, high I-129 yield); Pu-239 (greater LLFP yield than U-235)	---	---

Abbreviations used in table:
OT: Once-through
LR: Limited-recycle
CR: Continuous-recycle
FPY: fission product yield
TRU: Transuranic
TTA: time-to-attractiveness

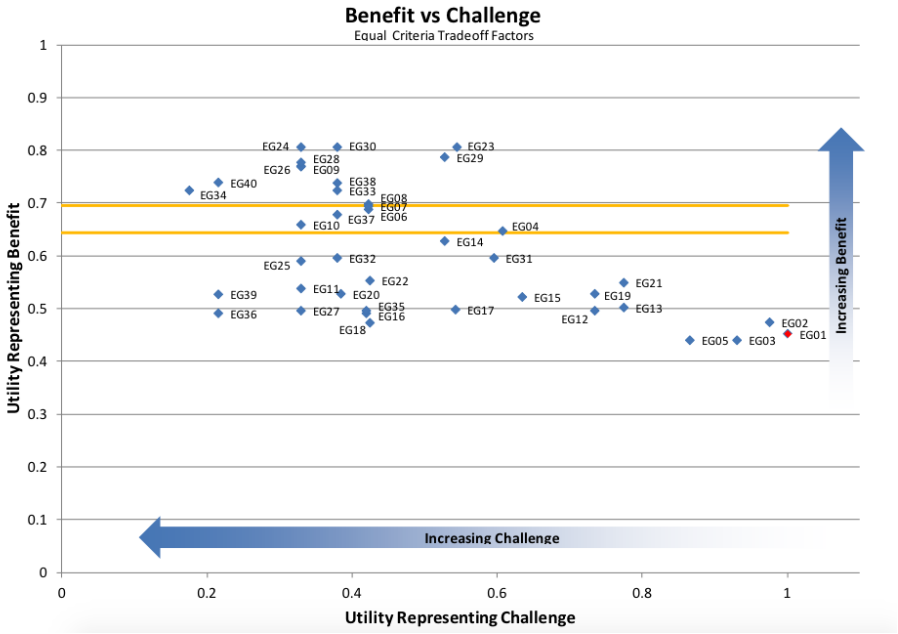

Figure 5.1: FCES aggregate results for relative benefit and challenge of different fuel cycles over the current once-through LWR fuel cycle [20].

That said, some of the results demonstrated in this dissertation agree with those in Figure 5.1. For example, only one limited-recycle fuel cycle (10.LR—MSR—Th/U3) is ranked above the lower performance improvement threshold. That the others exist below that line echoes the conclusions made about limited-recycle fuel cycles here.

The majority of fuel cycle options present waste management trade-offs: adoption of one fuel cycle characteristic may present both advantages and disadvantages in waste management. For example, thermal spectrum reactors are more effective than fast spectrum reactors at transmuting the LLFP that contribute to long term repository performance. However, they also accumulate more TRU in the waste, which can complicate compliance with repository thermal constraints.

Circumstance may be an important determinant in identifying workable strategies. Between fuel cycle and repository geology, the options available for a repository may be much more constrained because siting a repository requires suitable host rock. In countries with limited size, there may be little variety in available geologic formations in appropriate areas, such as those with low population. In this case, the repository disposal environment may be fixed. This could inform the choice of a suitable fuel cycle. For example, countries that are focusing on clay geologies for

repositories may not be able to dispose of LWR UOX used fuel in multi-assembly packages, but rather will have to employ interim storage for significantly long times or incur additional costs by decreasing waste package loading. If clay is the only repository environment available, employment of a limited-recycle fuel cycle may be impossible altogether. However, clay is highly sorbing and greatly retards the transport of many radionuclides. This may alleviate concerns about adopting a fuel cycle that breeds and continuously recycles fissile material but produces greater LLFP inventories in the process. In a clay repository, the impact of those LLFP on repository performance may be smaller than if that waste were disposed of in a different geological environment.

Alternatively, if thermally conductive rock, such as salt, is available to host a repository, disposal of once-through wastes may actually be preferential due to the small package inventory attained by utilizing large waste packages. If considered important by policy makers, these factors could dis-incentivize the adoption of an advanced fuel cycle. Even if an advanced fuel cycle is pursued, salt can remain an attractive option for a repository due to its thermal flexibility. If there is ever a decision to discontinue the use of nuclear power, the materials throughout the fuel cycle, including used fuels and stockpiled actinides, will require permanent disposal. The salt repository offers flexible thermal performance to accept disposal of these wastes, whereas disposal in granite or clay repositories may be much more challenging.

More broadly, adoption of an integrated fuel cycle and waste management strategy will require value judgments about what outcomes are most desirable. A strategy that minimizes environmental impact (for example, by minimizing repository footprint) may not be easy to maintain (for example, if long surface storage times are required to achieve that minimized repository footprint). A strategy that is simple in some aspects (for example, with a short surface storage requirement) may be complex in others (for example, if the shorter storage requirement requires preparation and management of a vastly larger package inventory). These questions are a matter of policy and practice, but the work presented in this dissertation can help foster a diversity of perspectives required to make informed choices. Unfortunately, the pace of policy and practice has been slow. This underscores an important requirement for an integrated fuel cycle and waste management strategy: flexibility. A robust strategy should be able to achieve its desired outcomes through many paths, because policy is subject to change and many technical hurdles exist in practice.

5.2 Future work

There are many opportunities to extend the work presented in this dissertation. Additional insights can be made by further analysis using the models discussed here, and new models can be developed and studied to gain more perspectives on waste management for advanced fuel cycles.

Additional parametric analysis is certainly warranted. The models utilized to obtain waste stream characteristics and the models used to study the waste management performance of those waste streams involved parameter specification. Although most of these values are determined based on literature review, in some cases the technologies being assessed are not yet sufficiently developed that reference values are available. Some parametric analysis was performed for this dissertation, such as exploring the effect of waste package loading on the dose rate evaluation for the FOM, or of waste package and waste form loading on repository footprint and surface storage time. One major opportunity for additional parametric analysis is for separation efficiencies, which can be studied to reflect expected performance of different technologies or to identify separation requirements to meet waste management outcomes. As mentioned, this has a direct impact on the attractiveness of wastes because it keeps fissile material out of the repository. Additionally, it should impact the decay heat characteristics of the waste, potentially affecting the difference in repository area and storage requirements between fuel cycles that recycle Pu and those that recycle TRU. For the repository footprint analysis, parameters associated with the repository design can be varied, including EBS dimensions, the thermal properties of the EBS materials and host rock, and the value of the thermal constraint. Ventilated repositories (in which the waste package is not in direct contact with the EBS or host rock) can be studied as well, enabling the comparison of fuel cycles with respect to disposal in a repository like Yucca Mountain. These avenues have been explored for a limited number of fuel cycles [49], but further work would provide better context for the future of advanced fuel cycles in the U.S.

In addition to further parametric analysis, there is an opportunity to further refine and understand the data produced by these models in an integrated way by applying machine learning methods. A model that can consider fuel cycle characteristics alongside waste management metrics within a large parameter space may enable new, finer conclusions about fuel cycle advantages and disadvantages. At the very least, success criteria can be identified for each of the waste management metrics considered here and the fuel cycles can be binned based on their performance. This process would be similar to that utilized in the FCES study, which sought to identify fuel cycles with respect to their relative benefit and challenge over a common basis. Even more ambitious would be a decision analysis framework that could report workable

fuel cycle and waste management strategies based on values judgments given by the user.

Finally, comparing fuel cycle performance against additional waste management models will add more perspective that may aid decision-making. Low- to intermediate-fidelity radionuclide transport models, such as those implemented in [92], could be used to validate the use of LLFPs as a proxy for repository performance, identify other potentially problematic radionuclides in waste streams, and to compare performance for different fuel cycles. Far-field criticality can be evaluated for different fuel cycles, examining the effect of removing certain species from the waste for recycling on the risk of criticality. It may be possible to screen criticality altogether for the disposal of wastes from some fuel cycles in repositories in different geologic environments [93]. In all, a more comprehensive suite of models can further expand the understanding of the advantages and trade-offs inherent in different fuel cycle and waste management strategies.

Bibliography

[1] Energy Information Administration. *Table 7.3. Average Quality of Fossil Fuel Receipts for the Electric Power Industry, 2007 through 2017*. URL: `https://www.eia.gov/electricity/annual/html/epa_07_03.html`.

[2] T. H. Pigford. "Actinide Burning and Waste Disposal". In: *MIT International Conference on the Next Generation of Nuclear Power Technology*. UCB-NE-4176. Oct. 1990.

[3] J. Kessler et al. ""Radiotoxicity Index": An Inappropriate Discriminator for Advanced Fuel Cycle Technology Selection". In: *Proceedings of the Waste Management Symposium*. 12276. 2012.

[4] A. G. Croff and S. L. Krahn. "A simple improved measure for risk from a geologic repository". In: *Proceedings of the 15th International High-Level Radioactive Waste Management Conference (IHLRWM 2015)*. American Nuclear Society. Charleston, SC, Apr. 2015, pp. 207–217.

[5] J. S. Walker. *The Road to Yucca Mountain*. University of California Press, 2009.

[6] J. Ahn. "Advanced Nuclear Fuel Cycle for Improved Safety of Geologic Disposal". In: *Proceedings of the 2nd NUCEF International Symposium*. JAERI-Conf 99-004. 1998.

[7] E. Hardin et al. *Generic Repository Design Concepts and Thermal Analysis*. Tech. rep. SAND2011-6202. Sandia National Laboratories, 2011.

[8] C. Forsberg, A. Croff, and D. Kocher. *Historical Perspective, Economic Analysis, and Regulatory Analysis of the Impacts of Waste Partitioning-Transmutation on the Disposal of Radioactive Wastes*. Tech. rep. ORNL/TM-11650. Oak Ridge National Laboratory, 1990.

[9] H. C. Burkholder et al. *Incentives for Partitioning High-Level Waste*. Tech. rep. BNWL-1927. Pacific Northwest Laboratory, 1975.

[10] A. G. Croff, J. O. Blomeke, and B. C. Finney. *Actinide Partitioning-Transmutation Program Final Report: 1. Overall Assessment*. Tech. rep. ORNL-5566. Oak Ridge National Laboratory, 1980. URL: https://www.osti.gov/servlets/purl/5417858-MUbIjs/Actinidepartitioning-transmutationprogramfinalreport.I.Overallassessment.pdf.

[11] International Atomic Energy Agency. *Evaluation of Actinide Partitioning and Transmutation*. Tech. rep. 214. International Atomic Energy Agency, 1982.

[12] L. D. Ramspott et al. *Impacts of New Developments in Partitioning and Transmutation on the Disposal of High-Level Nuclear Waste in a Mined Geologic Repository*. Tech. rep. UCRL ID-109203. Lawrence Livermore National Laboratory, 1992.

[13] T. H. Pigford and J. S. Choi. "Inventory Reduction Factors for Actinide- Burning Liquid-Metal Reactors". In: *Transactions of the American Nuclear Society* 64 (1991).

[14] J. Ahn. "Relationship between deposited nuclide inventory and HLW repository performance". In: *Progress in Nuclear Energy* 40 (3-4 2002), pp. 415–422.

[15] J. Ahn. "Integrated radionuclide transport model for a high-level waste repository in water-saturated geologic formations". In: *Nuclear Technology* 121 (1 1998), pp. 24–39.

[16] P. L. Chambre J. Ahn D. Kawasaki. "Relationship Among Performance of Geologic Repositories, Canister-Array Configuration, and Radionuclide Mass in Waste". In: *Nuclear Technology* 140 (2002), pp. 94–112.

[17] Energy Information Administration. *Nuclear Fuel Data Survey*. Dec. 2015. URL: https://www.eia.gov/nuclear/spent_fuel/.

[18] M. Schneider and Y. Marignac. *Spent Nuclear Fuel Reprocessing in France*. Tech. rep. 4. International Panel on Fissile Materials, 2008. URL: http://fissilematerials.org/library/rr04.pdf.

[19] T. Taiwo R. Wigeland et al. *AFCI Options Study*. Tech. rep. INL/EXT-10-17639. Idaho National Laboratory, 2009. DOI: 10.2172/978356.

[20] R. Wigeland et al. *Nuclear Fuel Cycle Evaluation and Screening - Final Report*. Tech. rep. INL/EXT-14-31465. Idaho National Laboratories, 2014. URL: https://fuelcycleevaluation.inl.gov/SitePages/Home.aspx.

[21] B. T. Rearden and M. A. Jessee, eds. *SCALE Code System, Version 6.2.2*. ORNL/TM-2005/39. Oak Ridge, TN: Oak Ridge National Laboratory, 2017.

[22] *Appendix B to Part 20—Annual Limits on Intake (ALIs) and Derived Air Concentrations (DACs) of Radionuclides for Occupational Exposure; Effluent Concentrations; Concentrations for Release to Sewerage, 10 CFR Part 20*. 2018. URL: https://www.nrc.gov/reading-rm/doc-collections/cfr/part020/appb/.

[23] R. Wigeland et. al. *Appendix D - Nuclear Fuel Cycle Evaluation and Screening*. Tech. rep. INL/EXT-14-31465. Idaho National Laboratory, 2014.

[24] G. Linlsey and A. Fattah. "The interface between nuclear safeguards and radioactive waste disposal: Emerging issues". In: *IAEA Bulletin* (Feb. 1994). URL: https://www.iaea.org/sites/default/files/publications/magazines/bulletin/bull36-2/36202682226.pdf.

[25] P. F. Peterson. "Long-term safeguards for plutonium in geologic repositories". In: *Science & Global Security* 6 (1996), pp. 1–29. URL: http://scienceandglobalsecurity.org/archive/sgs06peterson.pdf.

[26] J. Swahn. "The Long-term Nuclear Explosives Predicament: The Final Disposal of Militarily Usable Fissile Material in Nuclear Waste from Nuclear Power and the Elimination of Nuclear Weapons". PhD thesis. Goteberg, Sweden: Technical Peace Research Group, Institute of Physical Resource Theory, Chalmers University of Technology, 1992.

[27] C. G. Bathke et al. "The Attractiveness of Materials in Advanced Nuclear Fuel Cycles for Various Proliferation and Theft Scenarios". In: *Nuclear Technology* 179 (1 2012), pp. 5–30. DOI: 10.13182/NT10-203.

[28] X-5 Monte Carlo Team and D.B Pelowitz (editor). *MCNP6 User's Manual*. LA-CP-11-01708. Los Alamos National Laboratory. Los Alamos, NM, 2011.

[29] T. Goorley et al. "Initial MCNP6 Release Overview". In: *Nuclear Technology* 180 (2012), pp. 298–315. DOI: 10.13182/NT11-135.

[30] International Commission on Radiological Protection. *Data for Protection against Ionizing Radiation from External Sources: Supplement to ICRP Publication 15*. ICRP Publication 21. Oxford, New York, Toronto, Sydney, Braunschweig: Pergamon Press, 1973. URL: https://journals.sagepub.com/doi/pdf/10.1016/S0074-27407380002-9.

[31] Nuclear Waste Technical Review Board. *On the Calculation of HLW Loading in Borosilicate Glass*. 2010. URL: https://www.nwtrb.gov/docs/default-source/staff/bk-hlwloading.pdf?sfvrsn=6.

[32] S. Priebe and K. Bateman. "The Ceramic Waste Form Process at Idaho National Laboratory". In: *Nuclear Technology* 162.2 (2008), pp. 199–207. DOI: 10.13182/NT08-A3948.

[33] D. Lexa. "Preparation and Physical Characteristics of a Lithium- Beryllium-Substituted Fluorapatite". In: *Metallurgical and Materials Transactions A* 30A (1997), pp. 147–153. URL: https://link.springer.com/content/pdf/10.1007/s11661-999-0202-x.pdf.

[34] Committee On Separations Technology and National Research Council Transmutation Systems. *Nuclear Wastes: Technologies for Separations and Transmutation*. Washington, D.C.: National Academy Press, 1996.

[35] NEA. *Advanced Nuclear Fuel Cycles and Radioactive Waste Management*. Tech. rep. Paris: OECD/NEA, 2006.

[36] NEA. *Potential Benefits and Impacts of Advanced Nuclear Fuel Cycles with Actinide Partitioning and Trasnmutation*. Tech. rep. Paris: OECD/NEA, 2011.

[37] J. Marivoet and E. Weetjens. "Impact of Advanced Fuel Cycles on Geological Disposal in a Clay Formation". In: *Nuclear Technology* 163 (2008), pp. 74–84.

[38] J. Marivoet et. al. "Impact of Advanced Fuel Cycle Scenarios on Geological Disposal". In: *7th European Commission Conference on the Management and Disposal of Radioactive Waste (Euradwaste '08)*. EUR 24040. Luxembourg, Oct. 2009.

[39] K. Nishihara et. al. "Impact of Partitioning and Transmutation on LWR High-level Waste Disposal". In: *Journal of Nuclear Science and Technology* 45 (1 2008), pp. 84–97.

[40] H. Geckeis et. al. "Impact of Innovative Nuclear Fuel Cycles on Geological Disposal". In: *Annual Meeting of Nuclear Technology*. 2008.

[41] R. A. Wigeland et al. "Separations and Transmutation Criteria to Improve Utilization of a Geologic Repository". In: *Nuclear Technology* 154 (2006), pp. 95–106.

[42] R. A. Wigeland et. al. "Impact on Geological Repository Usage from Limited Actinide Recycle in Pressurized Light Water Reactors". In: *Nuclear Science and Technology* 44 (3 2007), pp. 415–422.

[43] R.A. Wigeland and T.H. Bauer. *Repository Benefits Of AFCI Options*. Tech. rep. ANL-AFCI-129. Argonne National Laboratory, 2005.

[44] Sandia National Laboratories. *Postclosure analysis of the range of design thermal loadings*. Tech. rep. ANL-NBS-HS-000057 REV 00. Sandia National Laboratories, 2008.

[45] Sandia National Laboratories. *In-Drift natural convection and condensation*. Tech. rep. MDL-EBS-MD-000001 REV 00 AD 01. Sandia National Laboratories, 2007.

[46] J. Roglans-Ribas and B. I. Spinrad. "A simplified thermal analysis of a nuclear waste repository". In: *Annals of Nuclear Energy* 16 (8 1989), pp. 371–382.

[47] J. Li, M.-S. Yim, and D. McNelis. "A simplified methodology for nuclear waste repository thermal analysis". In: *Annals of Nuclear Energy* 38 (2011), pp. 243–253.

[48] M. Sutton et al. *Disposal system evaluation framework (DSEF) version 1.0 - Progress report*. Tech. rep. LLNL-TR-484011. Lawrence Livermore National Laboratory, 2011.

[49] E. Hardin et. al. *Repository Reference Disposal Concepts and Thermal Load Management Analysis*. Tech. rep. FCRD-UFD-2012-000219 Rev.2. Sandia National Laboratories, 2012.

[50] H. S. Carslaw and J. C. Jaeger. *Conduction of heat in solids*. Second. Oxford: Clarendon Press, Oxford, 1959.

[51] E. Jones et al. *SciPy: Open Source Scientific Tools for Python*. http://www.scipy.org/. 2001-present.

[52] M. J. D. Powell. *A view of algorithms for optimization without derivatives*. Tech. rep. DAMTP 2007/NA03. Cambridge University, 2007.

[53] F. D. Hansen and C. D. Leigh. *Salt Disposal of Heat-Generating Nuclear Waste*. Tech. rep. SAND2011-0161. Sandia National Laboratories, 2011. URL: `https://prod.sandia.gov/techlib-noauth/access-control.cgi/2011/110161.pdf`.

[54] R. Wigeland et. al. *Appendix B - Nuclear Fuel Cycle Evaluation and Screening*. Tech. rep. INL/EXT-14-31465. Idaho National Laboratory, 2014.

[55] Sandia National Laboratory. *Nuclear Fuel Cycle Options Catalog*. 2014. URL: `https://energy.sandia.gov/energy/nuclear-energy/advanced-nuclear-energy/nuclear-fuel-cycle-options-catalog/`.

[56] International Atomic Energy Agency. *Spent Fuel Reprocessing Options*. Tech. rep. IAEA-TECDOC-1587. Vienna, Austria: International Atomic Energy Agency, 2008. URL: https://www-pub.iaea.org/MTCD/Publications/PDF/TE_1587_web.pdf.

[57] J. J. Laidler. *GNEP Spent Fuel Processing; Waste Streams and Disposition Options*. Washington, DC, 2007. URL: https://www.nwtrb.gov/docs/default-%20source/meetings/2007/may/laidler.pdf.

[58] J. P. Ackerman et al. "Treatment of Wastes in the IFR Fuel Cycle". In: *Progress in Nuclear Energy* 31.1 (1997), pp. 141–154. DOI: 10.1016/0149-1970(96)00008-X.

[59] National Research Council. *Electrometallurgical Techniques for DOE Spent Fuel Treatment*. Washington, DC: National Academies Press, 2000. DOI: 10.17226/9883.

[60] J. C. Hesson, M. J. Feldman, and L. Burris. *Description and Proposed Operation of the Fuel Cycle Facility for the Second Experimental Breeder Reactor (EBR-II)*. Tech. rep. ANL-6605. Argonne, IL: Argonne National Laboratory, 1963. URL: https://www.osti.gov/servlets/purl/4675689.

[61] W. L. Carter and M. E. Whatley. *Fuel and blanket processing development for molten salt breeder reactors*. Tech. rep. Oak Ridge, TN: Oak Ridge National Laboratory, 1967. URL: http://moltensalt.org/references/static/downloads/pdf/ORNL-TM-1852.pdf.

[62] L. E. McNeese, L. M. Ferris, and E. L. Nicholson. *Molten-salt breeder reactor fuel processing*. Tech. rep. Oak Ridge, TN: Oak Ridge National Laboratory, 1972. URL: https://www.osti.gov/servlets/purl/4628558.

[63] J. J. Laidler et al. "Development of pyroprocessing technology". In: *Progress in Nuclear Energy* 31.1 (1997), pp. 131–140.

[64] L. Pancratz. *Thermodynamic Properties of Halides*. Bulletin 674. Washington D.C.: United States Department of the Interior, Bureau of Mines, 1984.

[65] J. Fuger et al. *The Chemical Thermodynamics of Actinide Elements and Compounds, Part 8, The Actinide Halides*. Vienna, Austria: International Atomic Energy Agency, 1983.

[66] K. M. Goff et al. "Electrochemical Processing of Used Nuclear Fuel". In: *Nuclear Engineering and Technology* 43.4 (2011), pp. 335–342.

[67] J. P. Ackerman. "Chemical Basis for Pyrochemical Reprocessing of Nuclear Fuel". In: *Industrial and Engineering Chemistry Research* 30.1 (1991), pp. 141–145.

[68] "CRC Handbook of Chemistry and Physics (Internet Version 2018)". In: ed. by J. R. Rumble. 99th ed. Boca Raton, FL.: CRC Press/Taylor & Francis, 2018. Chap. Melting, Boiling, Triple, and Critical Point Temperatures of the Elements.

[69] J. W. Roddy et al. *Physical and Decay Characteristics of Commercial LWR Spent Fuel*. Tech. rep. ORNL/TM-9591/V1-R1. Oak Ridge National Laboratory, 1986. DOI: 10.2172/6105618. URL: https://www.osti.gov/biblio/6105618-physical-decay-characteristics-commercial-lwr-spent-fuel.

[70] J. Hu et al. *US Commercial Spent Nuclear Fuel Assembly Characteristics: 1968-2013*. Tech. rep. NUREG/CR-7227, ORNL/TM-2015/619. Oak Ridge National Laboratory, 2016.

[71] K.M. Wasywich. *Characteristics of Used CANDU Fuel Relevant to the Canadian Nuclear Fuel Waste Management Program*. Tech. rep. AECL-10463, COG-91-340. Table 5: Bruce 37-element bundle data. Pinawa, Manitoba, Canada: AECL Research - Whiteshell Laboratories, May 1993. URL: https://inis.iaea.org/collection/NCLCollectionStore/_Public/27/002/27002285.pdf?r=1&r=1.

[72] A. Husain and K. Choi (Kinectrics Inc.) *Background paper on the Status of Storage, Disposal and Transportation Containers for the Management of Used Nuclear Fuel*. NWMO Background Papers 6-7. Canada: Nuclear Waste Management Organization, 2003.

[73] CTECH Radioactive Materials Management. *Conceptual Design for a Deep Geologic Repository for Used Nuclear Fuel*. Tech. rep. Prepared for Ontario Power Generation, New Brunswick Power, Hydro-Quebec and Atomic Energy of Canada Limited, 2002. URL: https://www.nwmo.ca/~/media/Site/Files/PDFs/2015/11/17/23/25/993_deepgeologicrepository_mainrep.ashx?la=en.

[74] A. L. Lotts et al. *Options for Treating High-Temperature Gas-Cooled Reactor Fuel for Repository Disposal*. Tech. rep. ORNL/TM-12027. Oak Ridge, TN: Oak Ridge National Laboratory, 1992. URL: https://www.osti.gov/servlets/purl/5350512.

[75] S. J. Piet, S. E. Bays, and N. R. Soelberg. "HTGR Technology Family Assessment for a Range of Fuel Cycle Missions". In: *Proceedings of the 11th Information Exchange Meeting on Actinide and Fission Product Partitioning and Transmutation*. 2010. URL: https://inldigitallibrary.inl.gov/sites/sti/sti/4654912.pdf.

[76] W. S. Yang and H. S. Khalil. "Blanket Design Studies of a Lead- Bismuth Eutectic-Cooled Accelerator Transmutation of Waste System". In: *Nuclear Technology* 135 (2 2001), pp. 162–182. DOI: 10.13182/NT135-162.

[77] R. N. Hill and H. S. Khalil. "Physics studies for Sodium Cooled ATW Blanket". In: *Technical Coordination Meeting on Emerging Nuclear Energy Systems*. ANL/RAE/CP-105355. International Atomic Energy Agency. Argonne National Laboratory, Nov. 2001.

[78] C. Grandy and R. Seidensticker, eds. *Advanced Burner Reactor 1000MWth Reference Concept*. ANL-AFCI-202 (ANL-ABR-4). Nuclear Engineering Division, Argonne National Laboratory, Sept. 2007. URL: https://publications.anl.gov/anlpubs/2017/04/134264.pdf.

[79] J. Powers. "TRISO Fuel Performance: Modeling, Integration into Mainstream Design Studies, and Application to a Thorium-fueled Fusion-Fission Hybrid Blanket". PhD thesis. Berkeley, CA: University of California, Berkeley, 2011.

[80] P. E. Owen. "Waste Characteristics of Spent Nuclear Fuel from a Pebble Bed Reactor". MA thesis. Cambridge, MA: Massachusetts Institute of Technology, 1999.

[81] J. Ahn and M. Cheon. "Linear Programming Approach for Optimization of Radionuclide Loading in Vitrified HLW". In: *Nuclear Technology* 156 (2006), pp. 303–319.

[82] S. M. McDeavitt, D. P. Abraham, and J. Y. Park. "Evaluation of stainless steel zirconium alloys as high-level nuclear waste forms". In: *Journal of Nuclear Materials* 257 (1998), pp. 21–34. DOI: 10.1016/S0022-3115(98)00433-4.

[83] S. M. McDeavitt, J. Y. Park, and J. P. Ackerman. "Defining a metal-based waste form for IFR pyroprocessing wastes". In: *Annual meeting of the Minerals, Metals and Materials Society*. ANL/CMT/CP–80022. Argonne National Laboratory. San Francisco, CA, 1994. URL: https://inis.iaea.org/search/search.aspx?orig_q=RN:25059088.

[84] M. F. Simpson. "Projected Salt Waste Production from a Commercial Pyroprocessing Facility". In: *Science and Technology of Nuclear Installations* 2013 (2013). Article ID 945858. DOI: 10.1155/2013/945858.

[85] J. Wolkoff and A. A. Chilenskas. "The Melt Refining of Irradiated Uranium: Application to EBR-II Fast Reactor Fuel. IX. Sorption and Retention of Sodium and Cesium Vapor on Stationary Beds at Elevated Temperature". In: *Nuclear Science and Engineering* 9.1 (1961), pp. 71–77. DOI: 10.13182/NSE61-A25868.

[86] D. D. Siemer. "Molten Salt Breeder Reactor Waste Management". In: *Nuclear Technology* 185.1 (2014), pp. 100–108. DOI: 10.13182/NT12-164.

[87] Nuclear Data Center Japan Atomic Energy Agency. *Graph of Fission Product Yields*. Tokai-mura, Naka-gun, Ibaraki-ken, 319-1195, Japan, 2013. URL: https://wwwndc.jaea.go.jp/cgi-bin/FPYfig.

[88] J. C. Gehin and J. J. Powers. "Liquid Fuel Molten Salt Reactors for Thorium Utilization". In: *Nuclear Technology* 194 (2), pp. 152–161. DOI: 10.13182/NT15-124. URL: https://doi.org/10.13182/NT15-124.

[89] Daft Logic. *Google Maps Area Calculator Tool*. URL: https://www.daftlogic.com/projects-google-maps-area-calculator-tool.htm.

[90] World Nuclear Association. *Nuclear Power in the USA*. Aug. 2019. URL: https://www.world-nuclear.org/information-library/country-profiles/countries-t-z/usa-nuclear-power.aspx.

[91] M. Atz and M. Fratoni. "Impact of partitioning and transmutation on the back end of the fuel cycle". In: *Proceedings of the 15th International Exchange Meeting on Actinide and Fission Product Partitioning and Transmutation*. Manchester, UK, Oct. 2018.

[92] K. D. Huff. "An Integrated Used Fuel Disposition and Generic Repository Model for Fuel Cycle Analysis". PhD thesis. University of Wisonsin, Madison, 2013.

[93] M. Atz et al. "Assessment of the potential for criticality in the far field of a used nuclear fuel repository". In: *Annals of Nuclear Energy* 124 (2019). DOI: 10.1016/j.anucene.2018.09.028.

[94] K. Pietrak and T. S. Wisniewski. "A review of models for effective thermal conductivity of composite materials". In: *Journal of Power Technologies* 95 (1 2015), pp. 14–24.

[95] S. Singh, P. K. Jain, and R. Uddin. "Analytical solution of time-dependent multilayer heat conduction problems for nuclear applications". In: *Proceedings of the 1st International Nuclear and Renewable Energy Conference (INREC10)*. Amman, Jordan, Mar. 2010.

[96] *COMSOL Multiphysics*. v. 5.4. www.comsol.com. COMSOL AB. Stockholm, Sweden, 2018.

[97] *Heat Transfer Module User's Guide*. COMSOL AB. Stockholm, Sweden, 2018.

[98] M. Plotze et al. "Thermophysical properties of bentonite". In: *Clays in Natural & Engineered Barriers for Radioactive Waste Confinement*. Lille, France, 2007, pp. 579–580.

Appendix A

Footprint model assumptions

The analytical heat conduction solutions employed in the repository footprint model rely on many assumptions required for validity. The first step of the model relies on the superposition of time-dependent heat contributions from outlying sources to a central point in the array. In the second step, the temperature history at that central point is used as the outer boundary condition by which the central waste package temperature is evaluated.

In this appendix, those assumptions are explored to ensure that they are appropriate for this analysis. The first section examines the assumptions employed in the first step of the model and whether they remain valid as the sources are moved closer together. The second section discusses the quasi-steady-state assumption required for the second step of the footprint model.

A.1 Analytical solutions and heat source spacing

In the repository footprint model the heat sources are moved closer together, challenging two of the assumptions required for the use of analytical solutions. In previous applications of these models, the spacing of heat sources was fixed at distances large enough that the host rock was the primary medium for heat conduction. The fact that heat needed to be transferred through a (generally more thermally resistive) EBS system before it could be conducted through rock was not significant.

The first issue arising from decreasing the spacing between heat sources surrounded by thermally resistive layers is that the time-dependent contribution from different sources in the array is calculated as conduction through solid, infinite host rock. As sources are moved closer to the evaluation point, the relative amount of host rock (as opposed to EBS materials) decreases. The question is what happens

when a greater share of the heat transfer takes place through the more resistive EBS material. An example is the bentonite-granite system, where the host rock ($k = 2.5$ W/m-K) is over four times more thermally conductive than the EBS ($k = 0.6$ W/m-K).

The second issue is that the time-dependent contributions of heat from those sources are calculated independently. However, as they are moved closer together, the overall density of heat near the evaluation point is increased. Is it reasonable (or conservative) to calculate the contribution of heat from independent, individual sources?

To study these assumptions, I explored simple analytical and numerical models to study heat conduction through composite media. My goal was to understand whether the assumptions would hold as implemented, and if not, whether modifications to the model would make it appropriate. I performed these analyses focusing on the granite generic repository concept in which was packages are surrounded by bentonite buffer in vertical boreholes in the granite host rock. Of the generic repository concepts I studied in this thesis, this one features the greatest difference between EBS and host rock heat transfer properties. Therefore, if the assumptions hold, or if some adjustments can be made to account for any differences, they should also be able to work for the other repository concepts.

A.1.1 Effective medium theories

Effective medium theories attempt to use analytical correlations to modify the heat transfer properties of mixtures of material by accounting for the properties of the constituent materials. A common application of these methods is for heat conduction through foams or suspensions, in which a secondary phase with different thermal properties exists within a bulk material. The simplest models approximate the thermal conductivity of the bulk material by weighting the thermal properties of each material [94]. In particular, Maxwell's model is appropriate for heterogeneous systems in which the filler material is limited to volume fractions of less than 25%. In Equation A.1, k_m and k_1 are the thermal conductivities of the matrix and filler materials, respectively, and ϕ is the volume fraction of the filler material in the matrix.

$$\frac{k_{eff}}{k_m} = 1 + \frac{3\phi}{\frac{k_1+2k_m}{k_1-k_m} - \phi}. \tag{A.1}$$

Relationships such as the one in Equation A.1 offer a simple means to account for the presence of multiple phases in the bulk material. In theory, an application to the repository footprint model would affect the thermal conductivity calculation

based on how the density of the heat sources. Denser spacing means higher density of non-rock materials which are generally more thermally resistive, so the effective thermal conductivity should be higher.

Although simple, application of these theories is not necessarily appropriate in this case. If the independence of heat sources is taken as appropriate, than each heat source can be modeled as a spherical composite system in which heat is released into an inner sphere (the EBS) and conducted into an outer sphere (the host rock), eventually reaching the evaluation point. Simple effective medium theories do not reflect the fact that for an individual heat source, heat is always transferred through both the EBS material and the host rock in series rather than through a bulk medium in parallel.

A.1.2 Analytical models for heat conduction in composite materials

Analytical unsteady heat conduction problems in composite materials are generally easy to formulate but difficult to solve. Although the heat equation and its initial and boundary conditions are simple, solving the system coupled in different media is not trivial. Even today, it is the subject of ongoing research, and academic papers demonstrating analytical solutions to unsteady composite heat conduction problems are still published and presented. A recent example in nuclear research is the application to the conduction of heat from fuel pebbles to coolant in pebble-bed nuclear reactors [95].

Although analytical unsteady heat conduction in composites are difficult, we can study properties of simple composite systems by applying one-dimensional, steady-state analytical models. In this section, this analysis is applied to a simple, two-component composite system. At $x = 0$, a heat flux q is released into material m_1, a thermally resistive layer which is in perfect contact with a more thermally conductive layer, material m_2, at $x = x_{int}$. At some distance away, x_b, a zero-temperature boundary is applied. Given this simple system, the solution for temperature in each region as a function of x_{int} and x_b is given by the following equations:

$$T(x) = \begin{cases} T(x) = -\frac{q}{k_1}x + \left(\frac{q}{k_1}x_{int} - \frac{q}{k2}(x_{int} + b)\right), & 0 < x \leq x_{int}, \\ T(x) = -\frac{q}{k_2}x - \frac{q}{k_2}x_b, & x_{int} < x \leq x_b. \end{cases} \tag{A.2}$$

(A.3)

Examining these simple, linear equations can tell us a good amount about heat transfer through the composite system when the volume fractions of the layers are changing. In particular, the slope of both equations depends only on the heat flux q and the thermal conductivity of the material, not the thickness of the layer. Therefore, even if the layer is thicker, the temperature drop as a function of distance will be constant. We can show this with a simple numerical example. Four cases are considered, all using $q = 10.0$, $k_1 = 0.6$, $k_2 = 2.5$, and $x_b = 100.0$, loosely approximating an infinite temperature boundary condition. In each case, x_{int} is varied to produce systems with different volume fractions of layers 1 and 2. The result for the temperature through the system is plotted in Figure A.1.

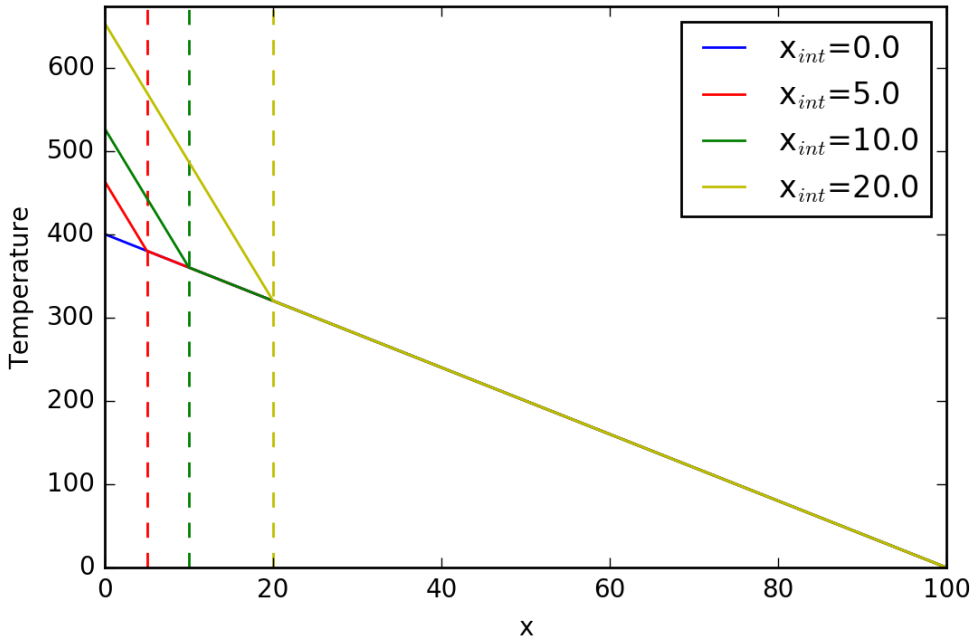

Figure A.1: Illustration and terminology for a generic engineered barrier system.

In Figure A.1, as the share of the first layer increases, the slope of the temperature through the layer does not change because the heat flux is the same and is not dependent on the the layer geometry. However, the temperature increases at $x = 0$ as the layer grows because the intercept in the linear equation for temperature depends on the layer width. The temperature at the interface between the two layers is decreases as the thickness of the first layer increases. The temperature in the second layer is the same in all cases because the temperature is fixed at

$x = 100.0$. If the thickness of the second layer were to remain constant (in other words, $x_b = x_{int} + \text{constant}$, the temperature at the interface would still be the same for all cases, and the temperature in the second layer would be slightly offset.

Because the primary effect of changing x_{int} is to change the temperature at $x = 0$ and not the temperatures in the second layer, this gives confidence that heat sources can be located relatively close together without violating the assumptions that make possible the use of analytical solutions.

A.1.3 Numerical modeling

To expand on the 1D model studied in the previous section, numerical models for heat conduction were simulated in COMSOL 5.3 [96] using the Heat Transfer module [97]. Considering the granite generic repository design concept, the package and EBS are modeled as concentric spheres in perfect contact. The radius of the sphere for the waste package is determined assuming the sphere has the same volume as the cylindrical package. The radius of the buffer is determined assuming a constant thickness of 0.35 m. A large sphere (r=50.0) is used to simulate the surrounding rock mass, with a zero-temperature external boundary condition. Heat is generated within the central sphere using an interpolation of the decay heat data for a 4-assembly PWR package.

Table A.1: Material thermal properties used in the COMSOL models

Component	Material	Radius (m)	Thermal conductivity (W/m-K)	Density (m^3/kg)	Heat capacity (J/kg-K)
Package	Steel	0.85	53.0	7833	465
Buffer	Bentonite	1.2	0.60	2290	650
Host rock	Granite	50	2.50	2766	800

Using this setup, two studies were performed to probe the effect of including the buffer material, shown in Figure A.2. The first model is a single source located at the center of the spherical rock mass, used to study the maximum temperature increase as a function of radial position with and without the bentonite buffer.

The second model is a square 3x3 array of sources (arranged in the X-Y plane). The center-to-center spacing between the sources, equal in the X and Y dimensions, is varied to determine the temperature increase at the "evaluation point" as a function of time and source-spacing with and without the bentonite buffer. The evaluation point is the interface between the buffer and host rock located directly above the central source. In Cartesian coordinates, this corresponds to (X=0, Y=0, Z=1.2).

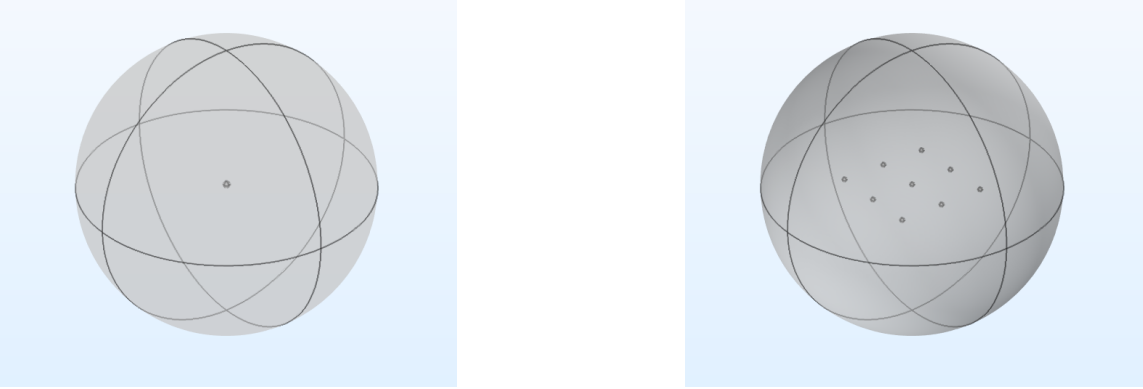

(a) Model 1 (b) Model 2

Figure A.2: Geometry of the two numerical models simulated in COMSOL. The large sphere simulates the rock mass, while the smaller spheres inside are the packages and EBS systems.

The peak temperature increase as a function of position for the single-source system with and without the bentonite buffer is plotted in Figure XX. The dotted lines indicate the location of the buffer. The temperature distributions in the rock region are nearly identical, demonstrating that the presence of the resistive buffer layer primarily affects the temperature in the waste package. This confirms the result and insights from the analytical 1D steady-state model.

The temperature at the evaluation point for the 3x3 array is shown as a function of source spacing with and without the buffer material in Figure A.4. The temperature increase at the evaluation point is greater when the sources are closer together and decreases as they are separated further. Spacing of $d = 2.4$ m means that the buffer spheres ($r = 1.2$ m) are touching. In this configuration, the temperature increase is slightly greater when the buffer is included. When $d = 4$ m, the effect of the buffer is insignificant and the result is the same if no buffer is considered. For greater spacing between packages, neglecting the buffer actually yields a higher temperature increase.

This result indicates that there is some lower limit to package spacing that should be applied to ensure that the assumptions enabling the use of the analytical models hold. In early applications of the footprint model, the lower bounds for the center-to-center drift spacing s_d and package spacing s_p were set to be $2r_d$ and $2L_{wp}$, respectively, corresponding to two drifts located right next to each other and waste packages placed end-to-end. Because $2r_d < 2L_{wp}$ and $L_{wp} \approx 5$m, small values for drift spacing are more likely to create arrangements of sources where use of the

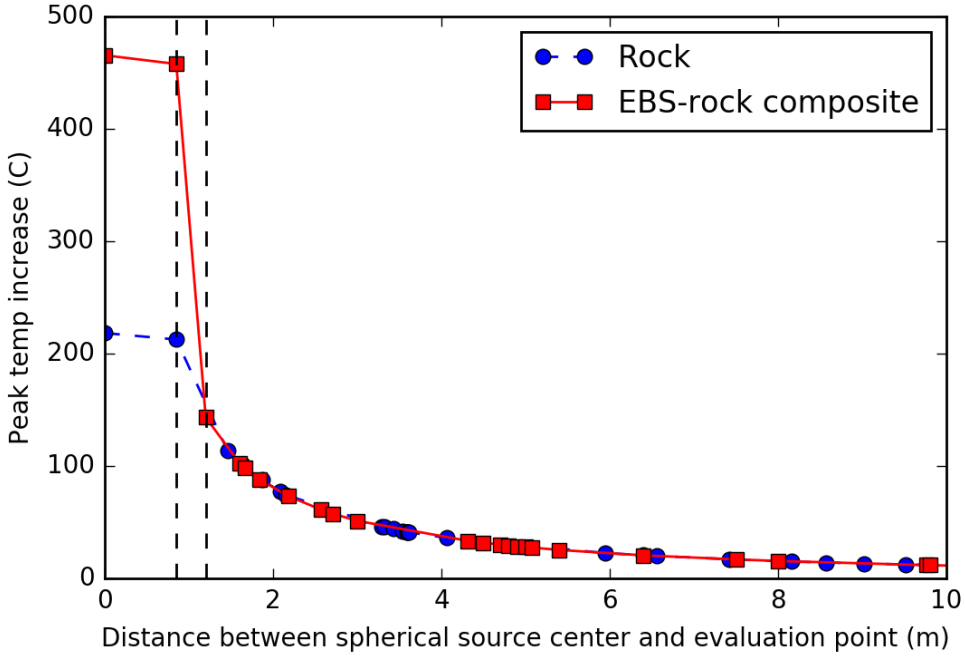

Figure A.3: Peak temperature increase as a function of position for the single-source system with and without the bentonite buffer. The radial location of the buffer is indicated in the figure by the dotted lines.

analytical models is inappropriate.

Rather than limit the drift spacing to a fixed value, an empirical relationship was used to generate a new constraint: $s_d > s_p$. This is empirically true for all proposed repository designs; in general, s_d is at least two times larger than s_p. It also makes sense conceptually, because drilling many sparsely filled drifts very close to one another would be much more expensive and difficult than cramming many packages into drifts located far from one another. It is expected that this constraint should limit the spacing of sources in the array to an extent that the assumptions required for the use of the analytical models are satisfied.

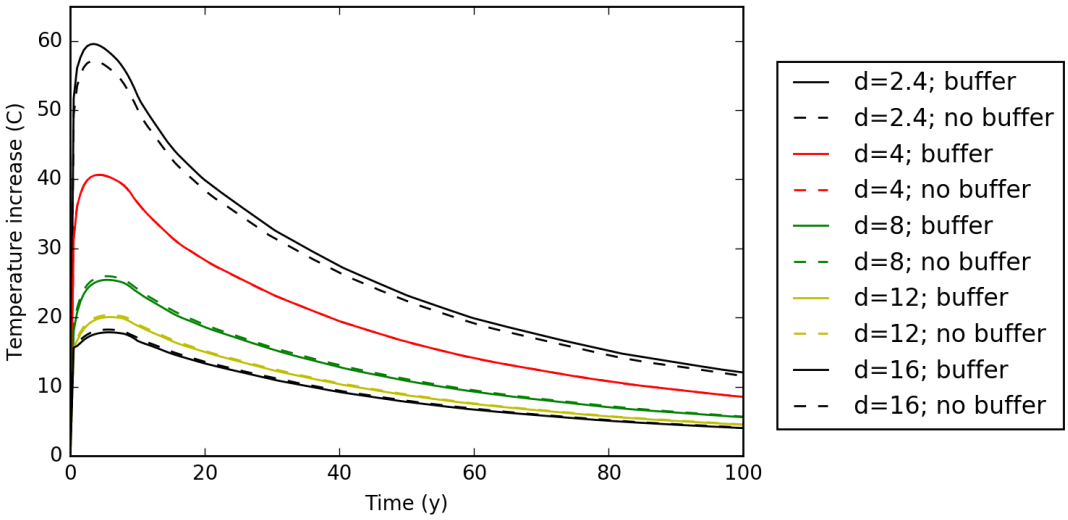

Figure A.4: Temperature increase as a function of position for the single-source system with and without the bentonite buffer. The radial location of the buffer is indicated in the figure by the dotted lines.

A.2 Quasi-steady-state conduction through the EBS

After the temperature history at the interface of the host rock and EBS is determined for the central package in the array, the footprint model assumes steady-state conduction through the EBS to determine the waste package temperature. This assumption relies on heat transfer taking place more quickly relative to the heat transfer through the host rock, except for the period immediately after emplacement when temperatures in the EBS are changing quickly.

The primary method to test this assumption is to check the validity of lumped capacitance in the system, which indicates whether the cylindrical shells can be approximated as isothermal by comparing their thermal resistance to that of the host rock. Because the same heat flux passes through both, this should determine the fraction of the temperature drop that occurs across the rock versus across the EBS. Lumped capacitance is indicated by the Biot number, the ratio of the thermal resistances of adjacent materials. In this system, if the thermal resistance of the EBS is significantly less than the resistance of the host rock, the EBS could be modeled as isothermal.

$$Bi = \frac{R_{\text{EBS}}}{R_{\text{rock}}}. \tag{A.4}$$

The resistance of the EBS can be modeled using the equation for resistance of a cylindrical shell. In Equation A.5, r_o and r_i are the outer and inner radii of the EBS shell, k is the thermal conductivity (W/m-K), and L is the cylinder length.

$$R_{\text{cyl}} = \frac{\ln\left(r_o/r_i\right)}{2\pi kL}. \tag{A.5}$$

Spherical resistance is used for the rock because as time goes on, the heat will conduct very far away and the package appears as a spherical point source.

$$R_{\text{sph}} = \frac{1/r_i - 1/r_o}{4\pi k}. \tag{A.6}$$

In Equation A.6, r_i and r_o are the inner and outer radii of the sphere, and k is the thermal conductivity of the host rock (W/m-K). Because the host rock is taken to be infinite, setting r_o to ∞ causes the second term to become zero, yielding the following form in Equation A.7.

$$R_{\text{sph}} = \frac{1}{4\pi k r_i}. \tag{A.7}$$

The Biot number is evaluated using constants taken from the 4-assembly SNF package disposal concept in granite host rock [7]. In that system, the EBS is thermally resistant bentonite clay ($k = 0.60$ W/m-K dry). This system was selected as a bounding case for the application of lumped capacitance. Because the EBS in this disposal concept is more thermally resistive than for others, if lumped capacitance holds it should be applicable to other concepts. Table A.2 shows the key values characterizing the EBS and host rock.

Using these values, Bi(granite, SNF) = 0.76. In this case, Bi is not significantly smaller than unity. If it were, it would be possible to say that the greater temperature drop occurs across the rock and the EBS can be modeled as isothermal. However, two time constants can be evaluated to validate the assumption.

First, the lumped capacitance thermal time constant, τ, is the exponential decay rate at which temperature in the system would relax to the equilibrium temperature if heat generation was turned off. Qualitatively, the time constant can be compared to the timescale of interest for the problem. If $\tau << t_{\text{problem}}$, then the EBS thermal response is fast compared to other processes, so the system can be justified as being quasi-steady-state, since the transient is very short. Even if $Bi > 1$, the lumped-capacitance time constant indicates whether the EBS acts as a "thermal capacitor."

Table A.2: Parameters characterizing the 4-asm. SNF package granite disposal concept

Region	Parameter	Value
EBS	r_i	0.48 m
EBS	r_o	0.83 m
EBS	L	5.0 m
EBS	k_{EBS}	0.60 W/m-K
Rock	r_i	0.83 m
Rock	k_{rock}	2.5 W/m-K

If τ is large, a significant amount of heat goes into "charging up" the EBS and thus would not be released into the rock for a long time.

$$\tau_{\text{EBS}} = \frac{\rho_{\text{EBS}} V_{\text{EBS}} c_p^{\text{EBS}}}{R_{rock}^{-1}}. \tag{A.8}$$

Using values from Table A.2 as well as that $\rho = 2290$ kg/m^3 and $c_p = 650$ J/kg-K [98] for bentonite, $\tau_{\text{EBS}} = 411131$ s $= 0.013$ y. This is very short compared to the timescale of the problem, which is on the order of tens to hundreds of years, indicating that EBS holds back heat (while thermally charging) only in the very early period after package emplacement.

The second time constant of interest is the diffusion time constant, which accounts for the finite time it takes for temperature changes to diffuse through the EBS. This requires determining the thermal diffusivity of the EBS, α.

$$\alpha_{\text{EBS}} = \frac{k}{\rho_{\text{EBS}} c_p^{\text{EBS}}}. \tag{A.9}$$

Based on this, the thermal diffusion time constant is defined. This reflects the characteristic time it takes a temperature change at the inside of the EBS to propagate through the EBS to the outside. Since it is a diffusion process, the time is characteristic rather than exact since the diffusing heat does not travel as a packet with well-defined velocity.

$$\tau_{\text{EBS}}^{d} = \frac{(r_o - r_i)^2}{\alpha_{\text{EBS}}}. \tag{A.10}$$

Although this is not the same as knowing how long it takes the heat to propagate through the EBS, by knowing how quickly the temperature responds one can infer

how quickly the temperature gradient in the EBS responds, supporting the assumption of a constant heat flux across the EBS. Using the values in Table A.2 as well as the values for ρ and c_p for bentonite, the thermal diffusion time constant is calculated to be $\tau_{\text{EBS}} = 303895$ s $= 0.01$ y.

Appendix B

Waste stream material attractiveness

This appendix presents the results for the material attractiveness FOM (FOM) described in Chapter 2 Section 2.1.3 for the Fuel Cycle Evaluation and Screening analysis examples introduced in Chapter 3. The results presented in Chapter 4 are generated based on these data.

B.1 Summary tables

This section presents tables that summarize the metric data presented in Chapter 4. Table B.1 shows the two most distinctive and comprehensive metrics: the time before recovered material becomes attractive and the number of packages required to obtain a critical mass of attractive material at the time the material becomes attractive, as well as the number of packages of each waste form produced per unit energy for each fuel cycle.

Table B.1: Time before material attractiveness and packages required to obtain critical mass

Fuel cycle identifier	Waste form	N_{pkgs}/ GWe-y	t(FOM>1) (y)			N_{pkgs}(CM; t(FOM>1)		
			Pu	TRU	U	Pu	TRU	U
1.OT—PWR—U	SNF	12	101	102	—	1	1	—
2.OT—HTGR—U	SNF	47	45.2	47.2	—	7	7	—
3.OT—HWR—U	SNF	25	59.2	59.5	—	1	1	—
4.OT—SFR—U	SNF	5	117	117	—	1	1	—
5.OT—HTGR—U/Th	SNF	59	38.8	40.8	—	16	16	—
6.OT—FFH—Th	Ceramic	22	146	130	121	8260	4280	3
7.OT—ADS—U	SNF	295	5.0	5.0	—	2	2	—
8.OT—FFH—Th	SNF	1	225	223	211	10	8	2
9.LR—SFR—U/TRU	Batch 3 skull	1	46.6	48.2	—	2	2	—
	Batch 5 skull	1	51.5	53.9	—	3	3	—
	Batch 7 skull	1	52.9	55.8	—	4	3	—
	Batch 8 SNF	2	78.5	78.7	—	1	1	—

Table B.1: Time before material attractiveness and packages required to obtain critical mass

Fuel cycle identifier	Waste form	N_{pkgs}/ GWe-y	t(FOM>1) (y)			N^{CM}_{pkgs}; t(FOM>1)		
			Pu	TRU	U	Pu	TRU	U
10.LR—MSR—Th/U3	Ceramic	327	5.0	5.0	5.0	1.49e6	8470	4
11.LR—SFR—U/Th/U3	Batch 1 SNF	4	88.2	88.2	—	1	1	—
	Batch 3 skull	2	24.8	15.5	10.5	4.76e6	2.20e6	17
	Batch 4 skull	2	30.8	23.2	18.5	2.68e5	1.65e5	14
	Batch 5 skull	2	42	29.6	23.5	4.92e4	3.39e4	14
	Batch 8 SNF	2	152	141	129	421	242	1
12.LR—HWR/PWR—U/Pu	Glass	3	201	205	—	10	8	—
	SNF	3	101	102	—	1	1	—
13.LR—PWR/PWR—U/Pu	Glass	4	205	213	—	21	7	—
	SNF	2	101	103	—	1	1	—
14.LR—SFR/PWR—U/Pu	Ceramic	3	213	218	—	3	3	—
	SNF	4	96.1	97.6	—	1	1	—
15.LR—PWR/SFR—U/Pu	Glass	4	205	214	—	21	8	—
	SNF	3	62.6	63.3	—	1	1	—

Table B.1: Time before material attractiveness and packages required to obtain critical mass

Fuel cycle identifier	Waste form	N_{pkgs}/	t(FOM>1) (y)			N^{CM}_{pkgs}; t(FOM>1)		
		GWe-y	Pu	TRU	U	Pu	TRU	U
16.LR—PWR/ADS—U/Pu	Glass	4	205	213	—	21	7	—
	SNF	7	31.8	33.1	33.9	1	2	816
17.LR—PWR/PWR—U/Th/Pu	Glass	4	205	213	—	21	7	—
	SNF	2	114	117	112	1	1	1
18.LR—PWR/PWR—U/Th/U3	Glass	4	203	204	2810	1	1	64
	SNF	4	121	122	6.31e4	1	1	171
19.CR—HWR—U/Pu	Glass	5	195	205	—	7	5	—
20.CR—HWR—U/TRU	Glass	5	201	201	—	6	6	—
21.CR—PWR—U/Pu	Glass	7	186	197	—	10	5	—
22.CR—PWR—U/TRU	Glass	4	210	212	—	7	7	—
23.CR—SFR—U/Pu	Ceramic (blanket)	1	198	198	—	3	3	—
	Ceramic (driver)	3	220	225	—	3	3	—

Table B.1: Time before material attractiveness and packages required to obtain critical mass

Fuel cycle identifier	Waste form	N_{pkgs}/	t(FOM>1) (y)			N^{CM}_{pkgs}; t(FOM>1)		
		GWe-y	Pu	TRU	U	Pu	TRU	U
24.CR—SFR—U/TRU	Ceramic	3	222	222	—	3	3	—
25.CR—PWR—U/TRU/Th/U3	Glass (blanket)	3	220	211	205	1.16e4	5100	9
	Glass (driver)	2	212	214	—	20	20	—
26.CR—MSR—Th/U3/TRU	Ceramic	312	41.3	26.4	6.5	4340	3060	4
27.CR—SFR—U/Th/U3	Ceramic	7	176	176	794	1	1	24
28.CR—SFR—Th/U3	Ceramic	5	205	202	196	578	396	3
29.CR—SFR/PWR—U/Pu	Ceramic	2	213	218		3	3	90
	Glass	3	184	203	1.20e5	6	2	21
30.CR—SFR/PWR—U/TRU	Ceramic	3	218	218	—	3	3	134
	Glass	1	212	213	—	5	5	—
31.CR—PWR/SFR—U/Pu	Glass	2	204	220	2.19e4	5	3	73

Table B.1: Time before material attractiveness and packages required to obtain critical mass

Fuel cycle identifier	Waste form	N_{pkgs}/ GWe-y	t(FOM>1) (y)			N^{CM}_{pkgs}; t(FOM>1)		
			Pu	TRU	U	Pu	TRU	U
32.CR—PWR/SFR—U/TRU	Ceramic	1	227	228	—	4	4	—
	Glass	3	210	211	—	24	25	—
33.CR—ADS/PWR—U/Pu	Ceramic (blanket)	1	181	181	—	2	2	—
	Ceramic (driver)	3	219	224	—	2	2	—
	Glass	2	177	194	1.62e5	6	3	27
34.CR—ADS/PWR—U/TRU	Ceramic (blanket)	1	180	180	—	2	2	—
	Ceramic (driver)	3	221	221	—	2	3	—
	Glass	1	212	214	—	5	5	—
35.CR—PWR/ADS—U/Pu	Ceramic	1	222	242	227	3	2	514
	Glass	4	205	213	—	22	7	—
36.CR—PWR/ADS—U/Pu/MA	Ceramic	1	231	234	230	4	3	48
	Glass	4	210	211	—	13	13	—
37.CR—PWR/SFR/PWR—U/TRU/Th/U3	Glass	2	209	209	—	25	25	—
	Glass (blanket)	1	234	210	206	7.02e6	9.12e5	2
	Glass (driver)	2	218	219	—	3	3	—

Table B.1: Time before material attractiveness and packages required to obtain critical mass

Fuel cycle identifier	Waste form	N_{pkgs}/ GWe-y	t(FOM>1) (y) Pu	TRU	U	N^{CM}_{pkgs}; t(FOM>1) Pu	TRU	U
38.CR—SFR/PWR—Th/U3	Ceramic	5	199	194	187	1590	927	3
	Glass	1	219	216	206	311	230	14
39.CR—PWR/PWR/ADS—U/TRU/Th/U3	Ceramic	1	230	231	230	3	3	48
	Glass	2	218	211	203	2170	1220	18
	Glass (blanket)	2	223	213	207	2.19e5	8.72e4	14
	Glass (driver)	2	217	218	—	34	33	—
40.CR—ADS/PWR—Th/U3	Ceramic	1	228	214	208	872	260	6
	Glass	4	219	212	205	38	21	17

B.2 Individual fuel cycles

For each fuel cycle, the mass per waste package and fissile fraction of the potentially attractive material — separated Pu, TRU, and/or U — is assessed. The FOM and the values required to calculate it — the critical mass (kg) and decay heat content (W/kg) of the separated material and the dose rate (rad/hr) of the material in the waste package — are shown as well. Figures for 1.OT—PWR—U and 23.CR—SFR—U/Pu are presented in Chapter 4 Section 4.3.

For the most part, colors are used to differentiate among different potentially attractive materials and marker styles are used to differentiate among waste streams, including wastes from different fuel cycle stages. For a few fuel cycles that generate too many waste streams to show the characterization of all potentially attractive fissile materials together on a single plot, the colors indicate the streams and only a single material characterization is shown. These are:

- 9.LR—SFR—U/TRU,
- 11.LR—SFR—U/Th/U3,
- 37.CR—PWR/SFR/PWR—U/TRU/Th/U3, and
- 39.CR—PWR/PWR/ADS—U/TRU/Th/U3.

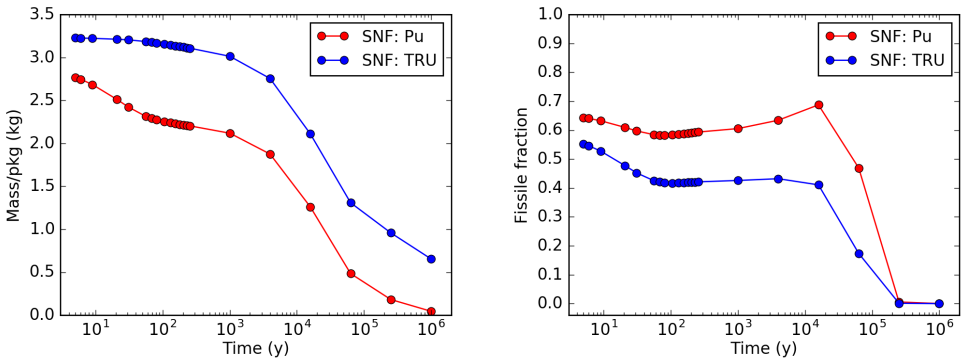

Figure B.1: Pu and TRU package inventory and fissile fraction in SNF from 2.OT—HTGR—U.

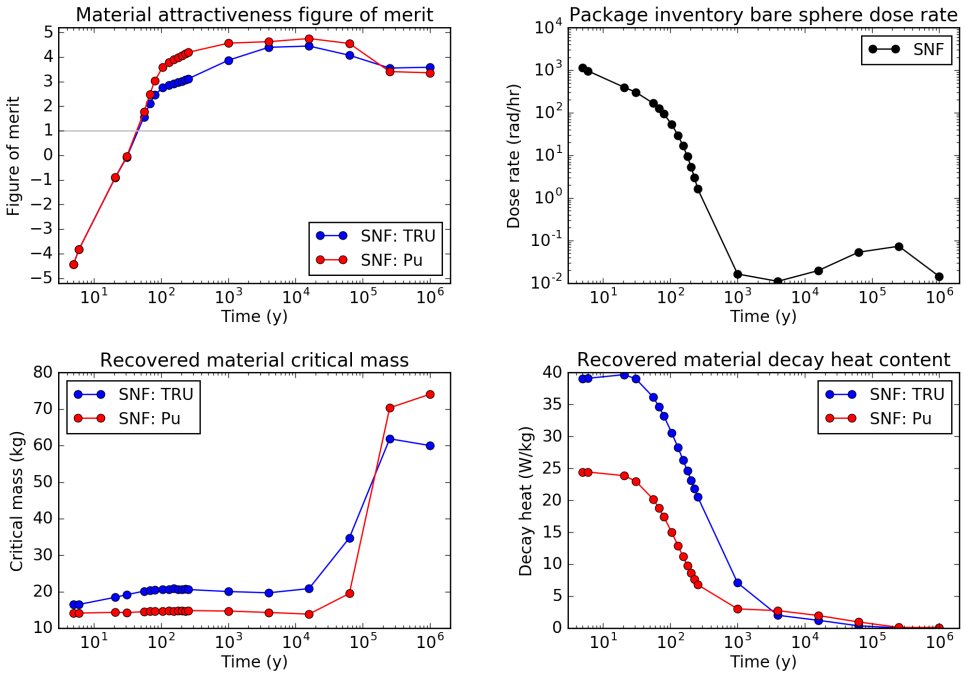

Figure B.2: FOM evaluation for Pu and TRU in SNF from 2.OT—HTGR—U.

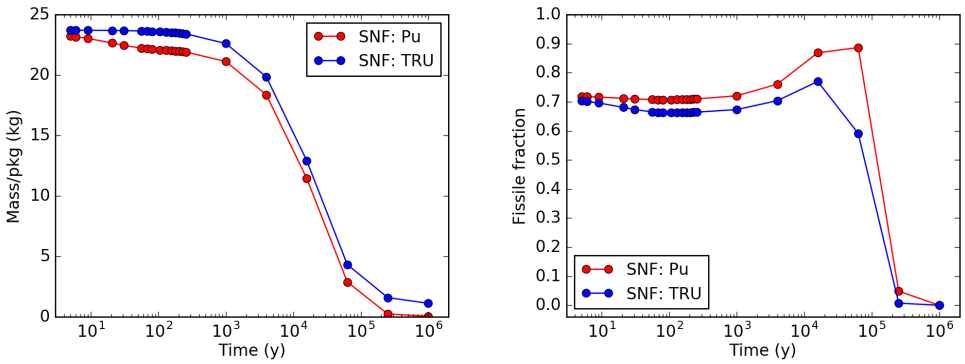

Figure B.3: Pu and TRU package inventory and fissile fraction in SNF from 3.OT—HWR—U.

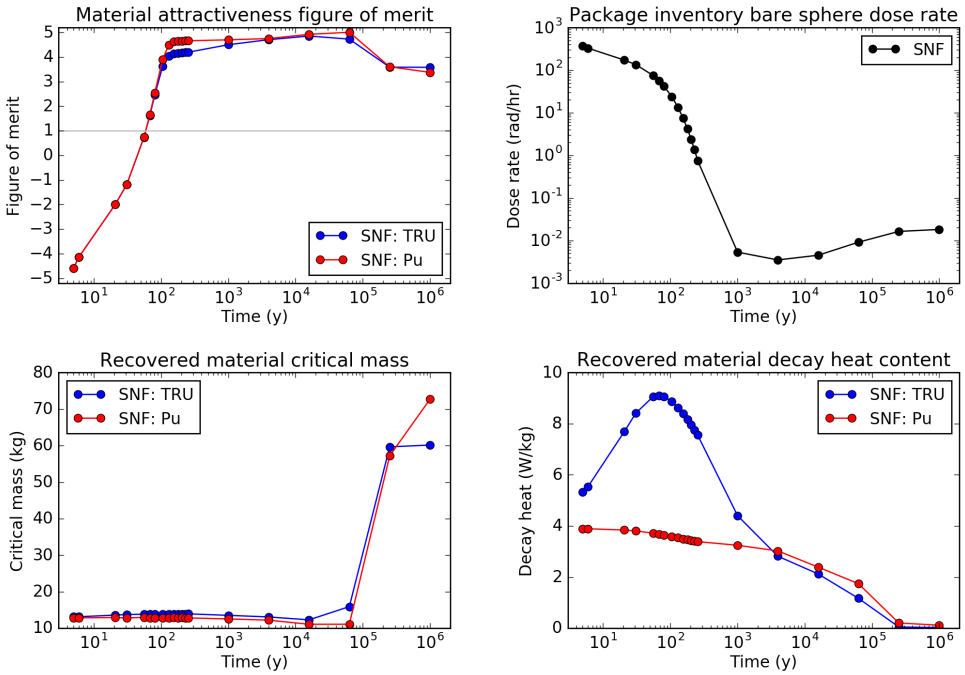

Figure B.4: FOM evaluation for Pu and TRU in SNF from 3.OT—HWR—U.

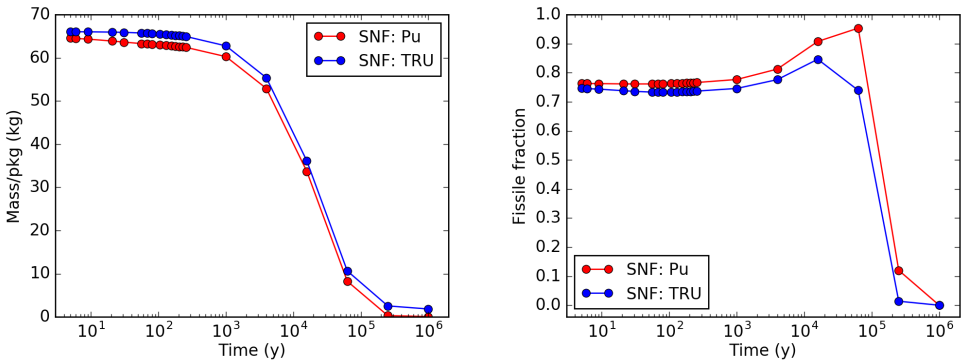

Figure B.5: Pu and TRU package inventory and fissile fraction in SNF from 4.OT—SFR—U.

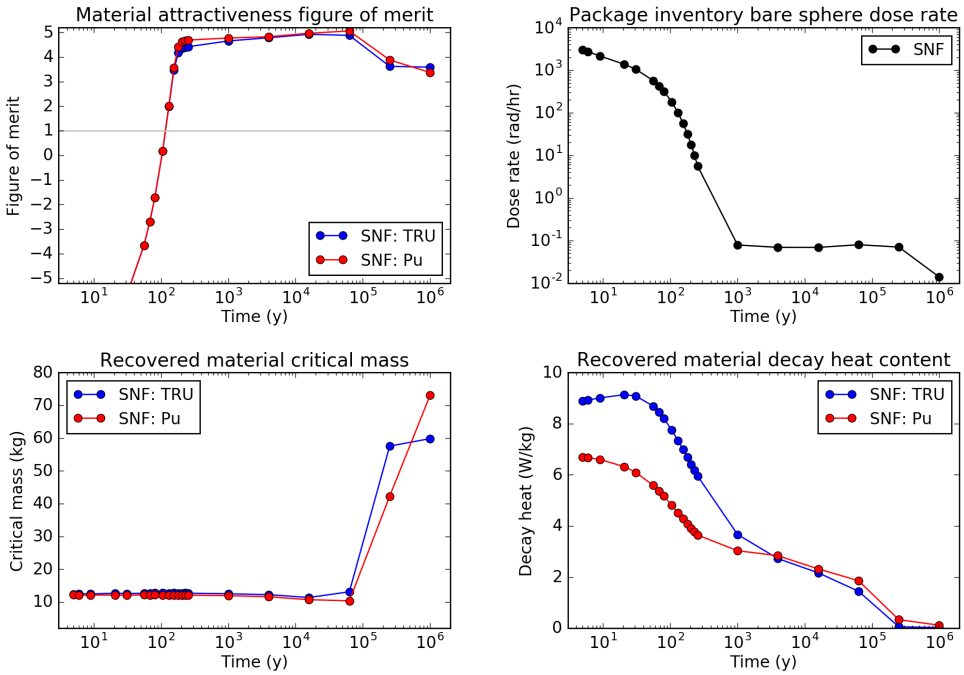

Figure B.6: FOM evaluation for Pu and TRU in SNF from 4.OT—SFR—U.

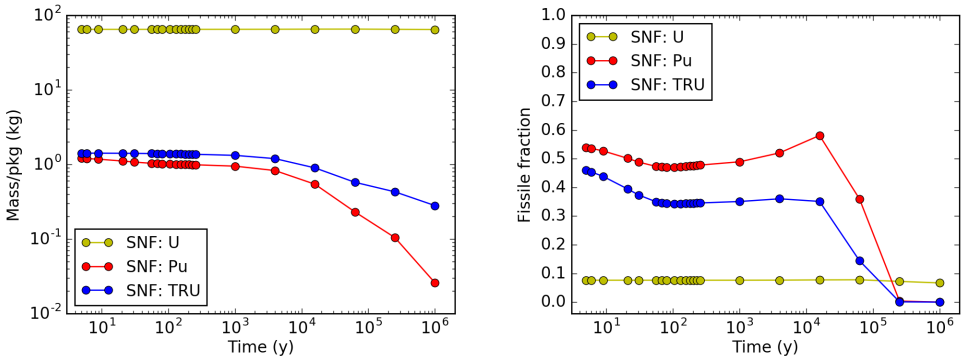

Figure B.7: U, Pu, and TRU package inventory and fissile fraction in SNF from 5.OT—HTGR—U/Th.

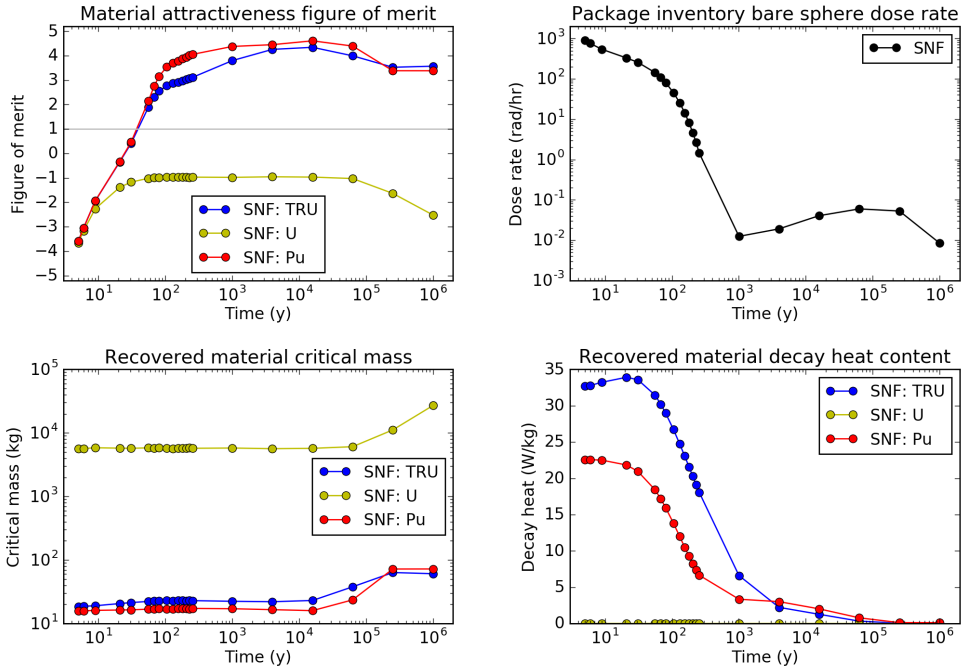

Figure B.8: FOM evaluation for U, Pu, and TRU in SNF from 5.OT—HTGR—U/Th.

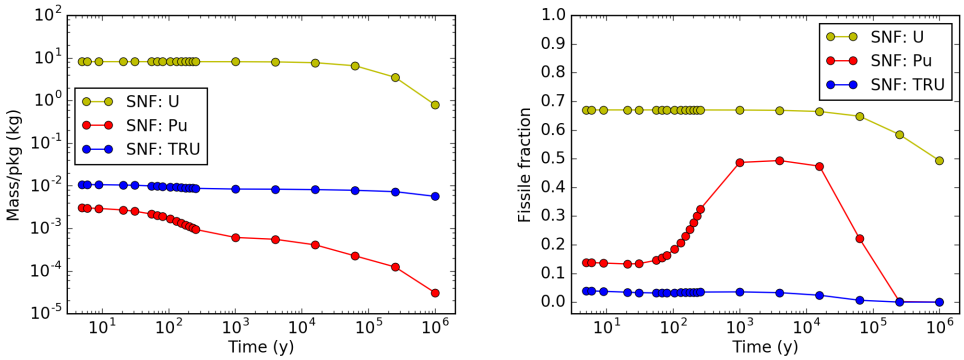

Figure B.9: U, Pu, and TRU package inventory and fissile fraction in SNF (discharged molten salt encapsulated in ceramic) from 6.OT—FFH—Th.

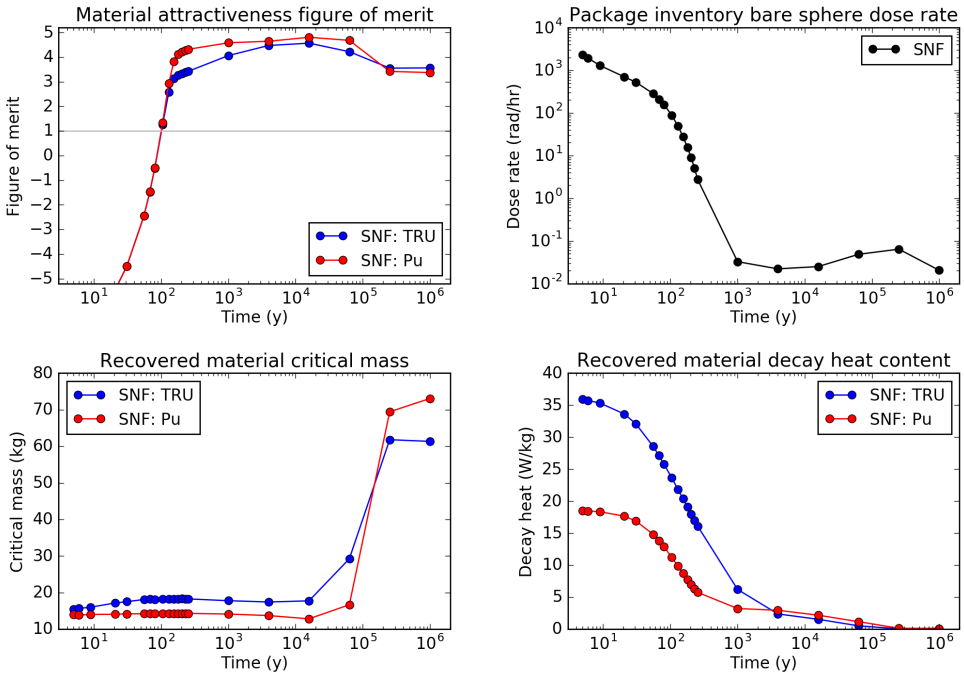

Figure B.10: FOM evaluation for U, Pu, and TRU in SNF (discharged molten salt encapsulated in ceramic) from 6.OT—FFH—Th.

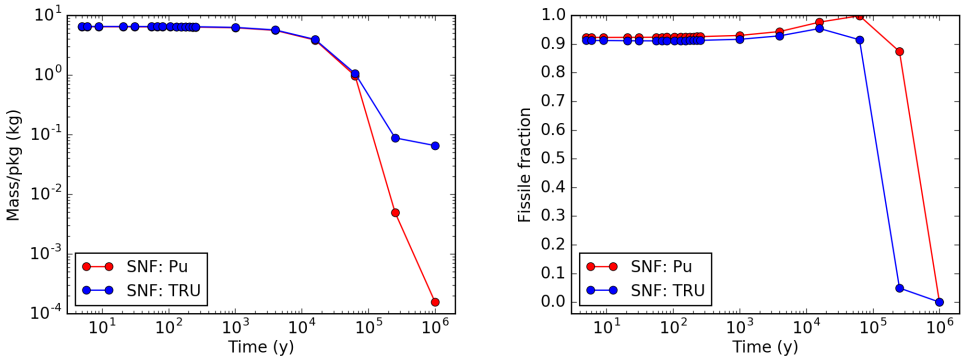

Figure B.11: Pu and TRU package inventory and fissile fraction in SNF from 7.OT—ADS—U.

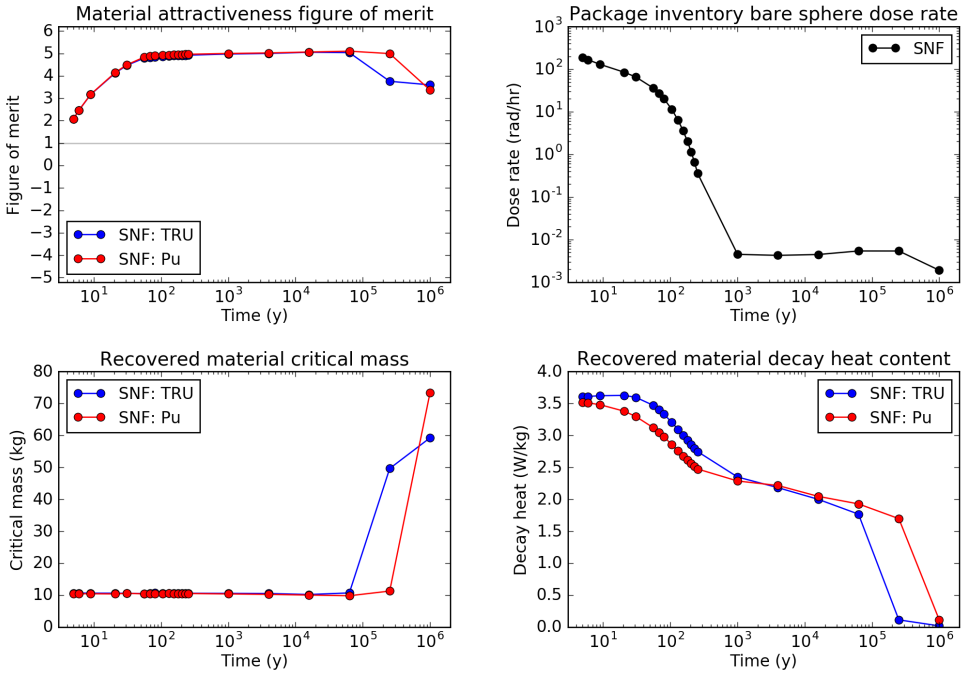

Figure B.12: FOM evaluation for Pu and TRU in SNF from 7.OT—ADS—U.

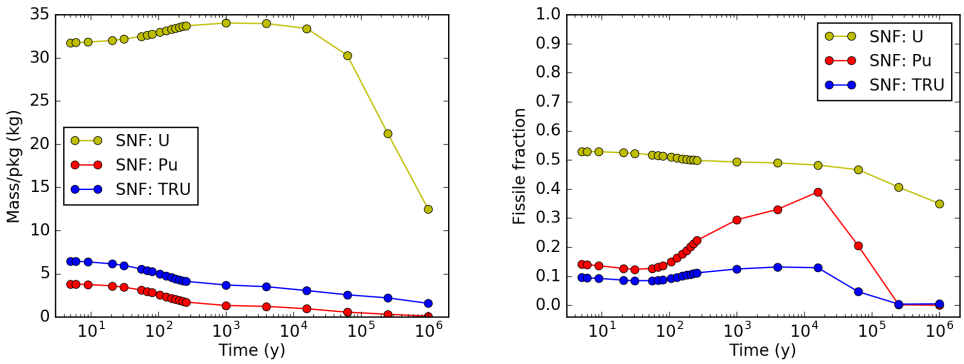

Figure B.13: U, Pu, and TRU package inventory and fissile fraction in SNF from 8.OT—FFH—Th.

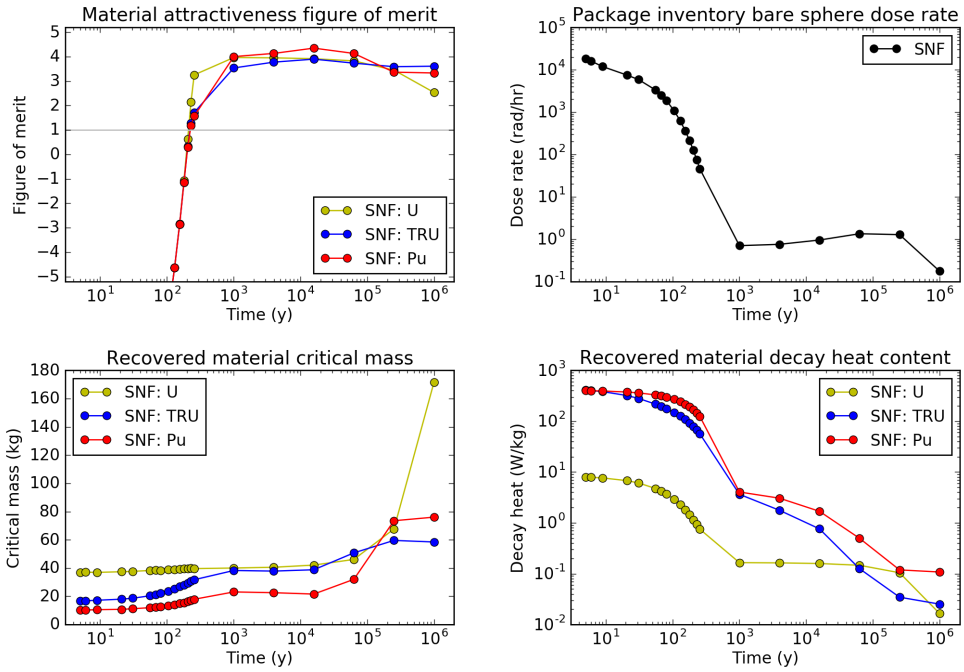

Figure B.14: FOM evaluation for U, Pu, and TRU in SNF from 8.OT—FFH—Th.

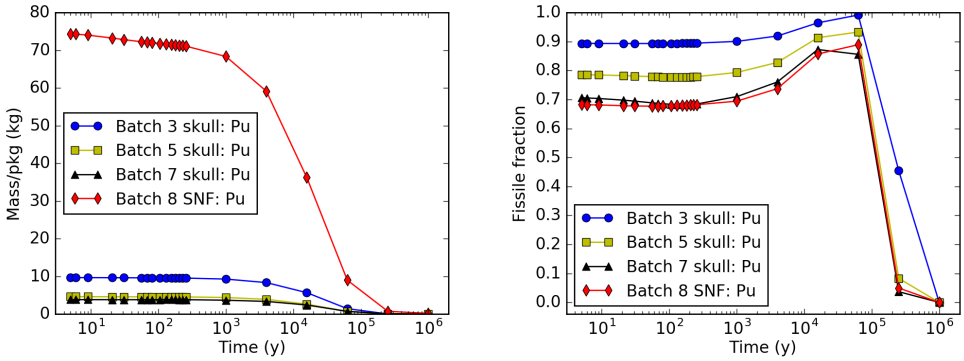

Figure B.15: Pu package inventory and fissile fraction for wastes from 9.LR—SFR—U/TRU.

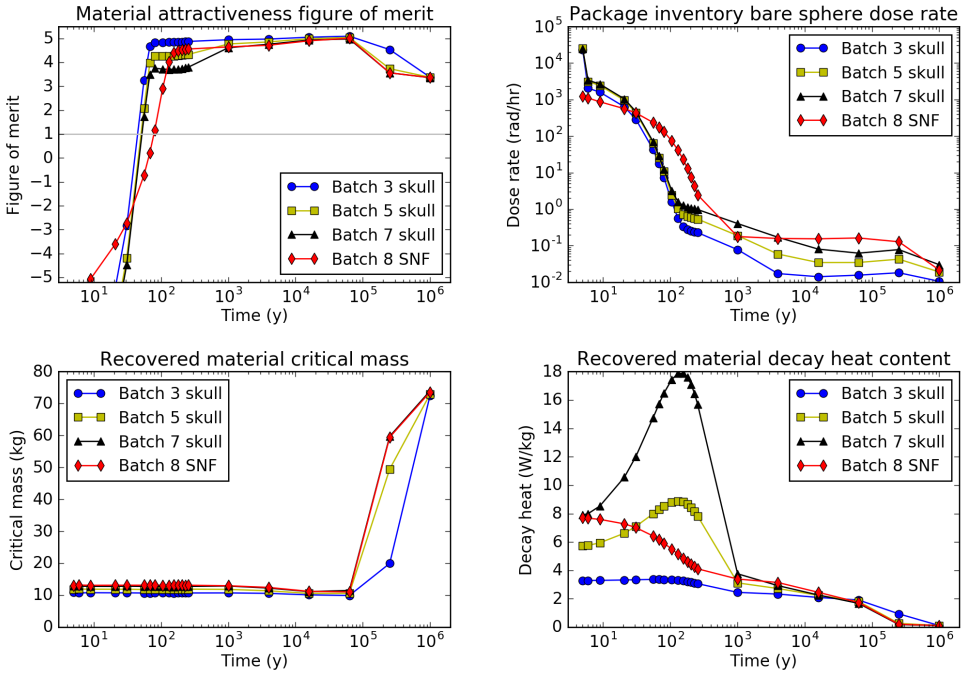

Figure B.16: FOM evaluation for Pu in wastes from 9.LR—SFR—U/TRU.

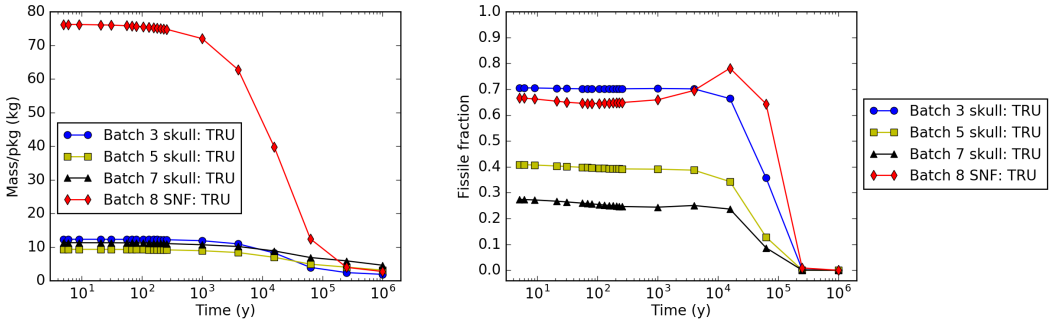

Figure B.17: TRU package inventory and fissile fraction for wastes from 9.LR—SFR—U/TRU.

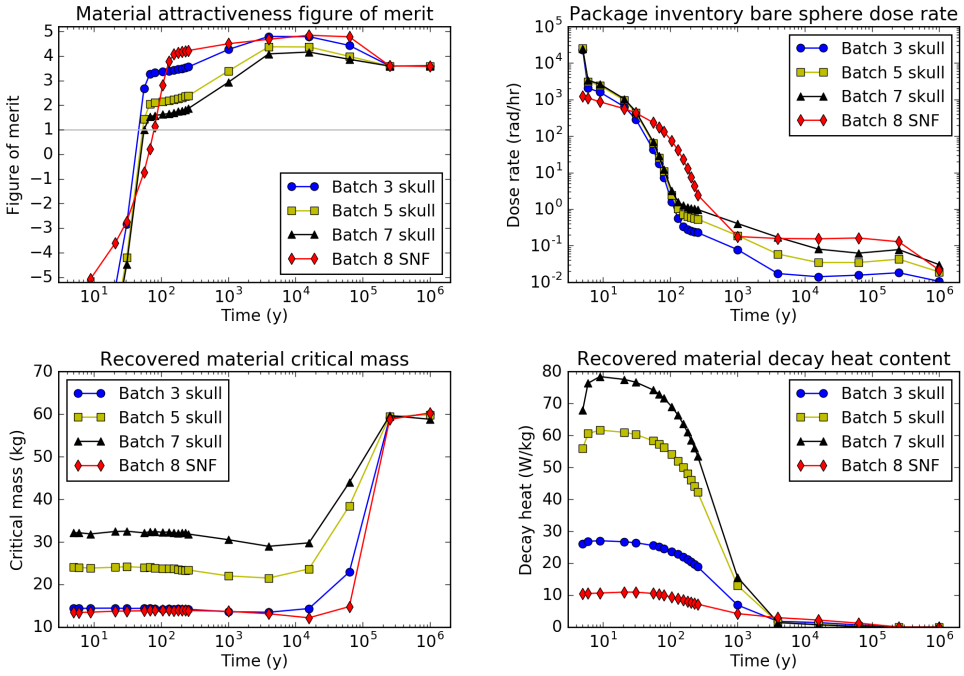

Figure B.18: FOM evaluation for TRU in wastes from 9.LR—SFR—U/TRU.

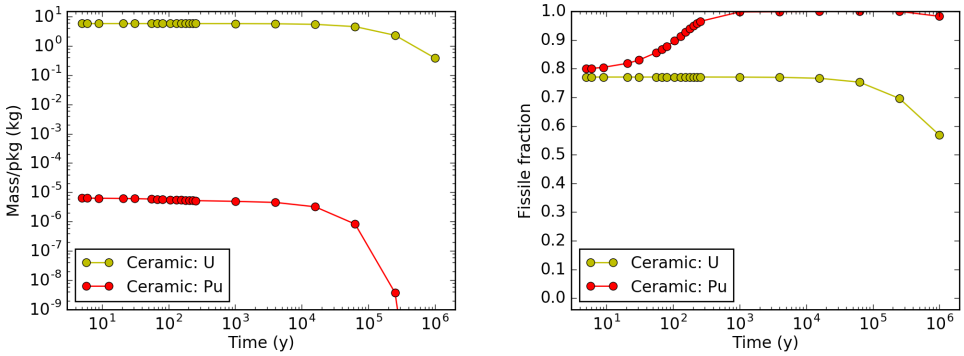

Figure B.19: U and Pu package inventory and fissile fraction in ceramic waste from processing molten salt in 10.LR—MSR—Th/U3.

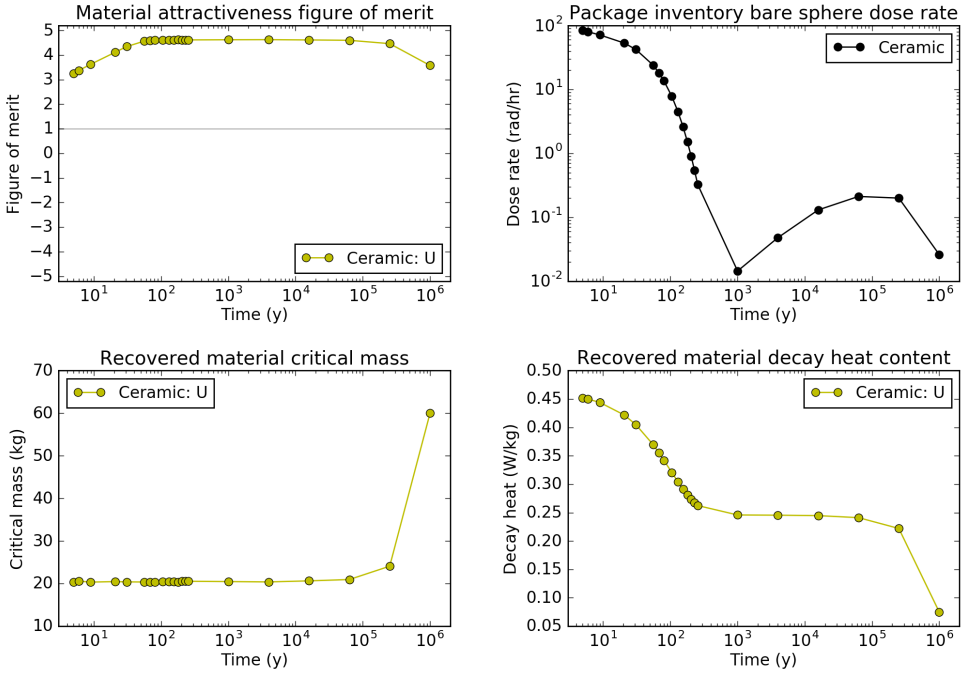

Figure B.20: FOM evaluation for U in ceramic waste from processing molten salt in 10.LR—MSR—Th/U3 (insignificant Pu produced).

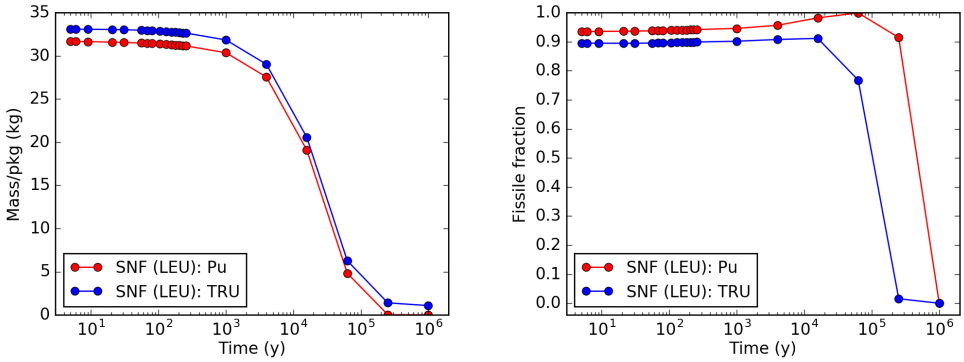

Figure B.21: Pu and TRU package inventory and fissile fraction for LEU SNF generated in 11.LR—SFR—U/Th/U3.

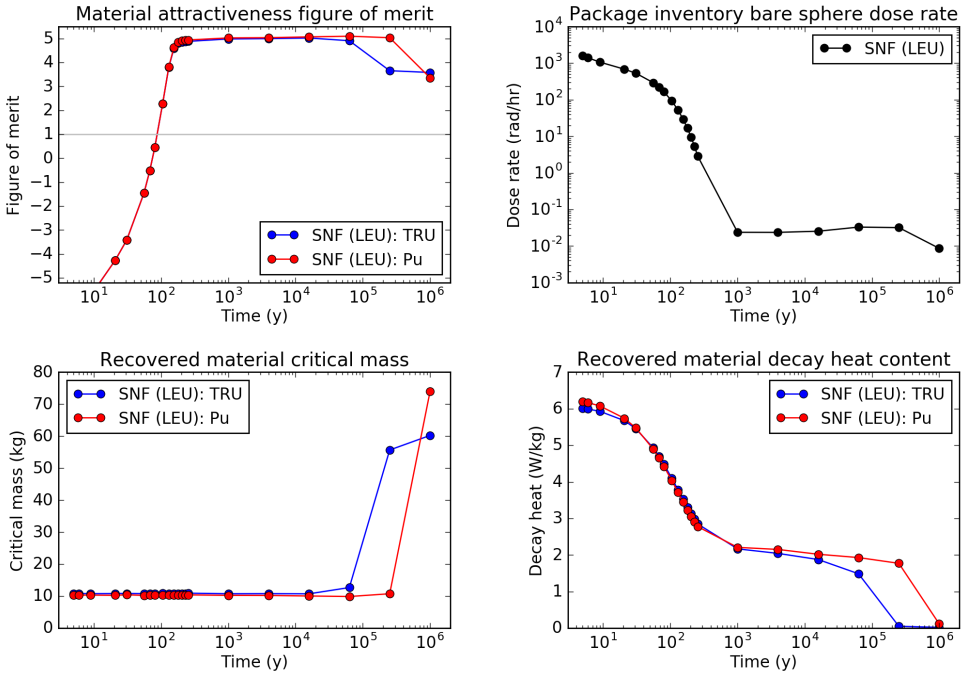

Figure B.22: FOM evaluation for Pu and TRU from LEU SNF generated in 11.LR—SFR—U/Th/U3.

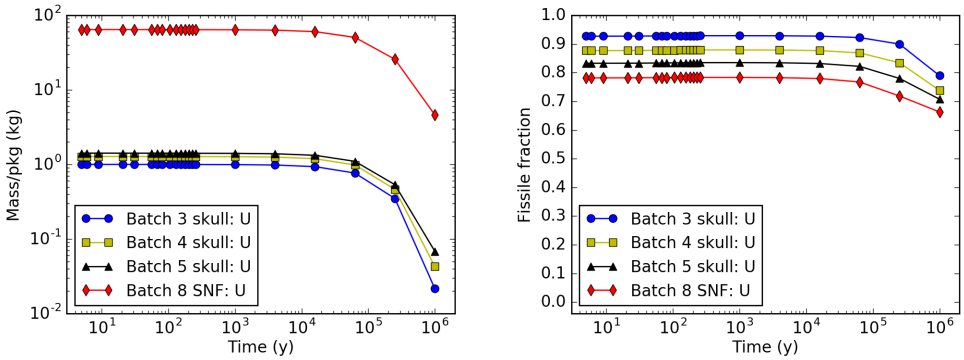

Figure B.23: U package inventory and fissile fraction for breed-and-burn wastes generated in 11.LR—SFR—U/Th/U3.

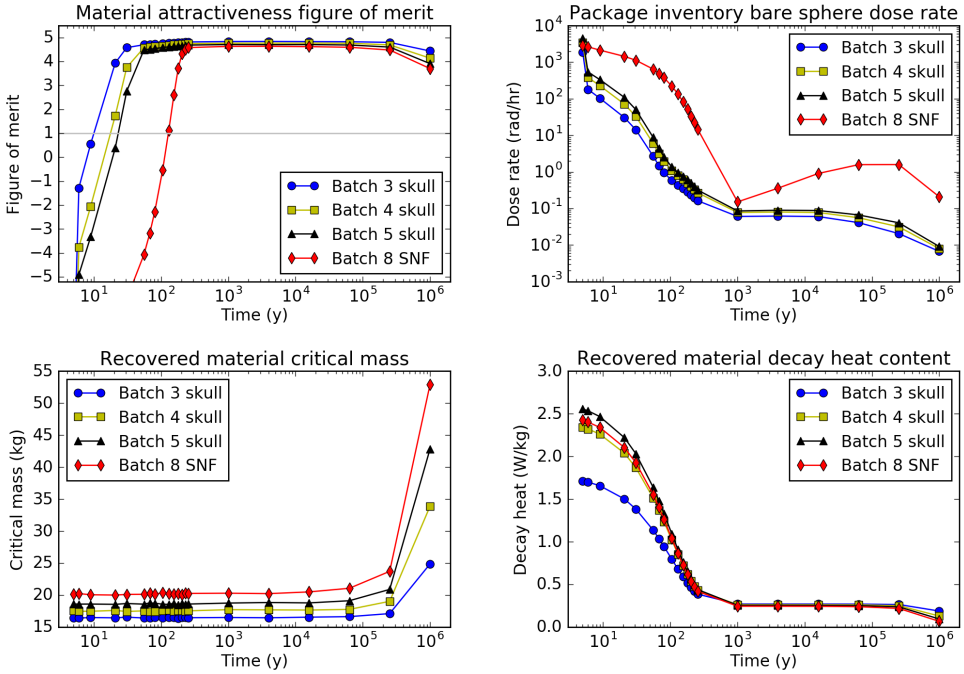

Figure B.24: FOM evaluation for U in breed-and-burn wastes generated in 11.LR—SFR—U/Th/U3.

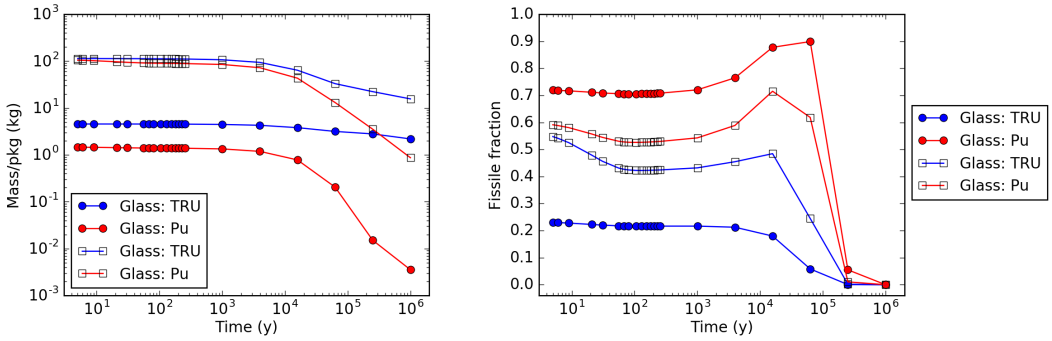

Figure B.25: Pu and TRU package inventory and fissile fraction in HLW glass and SNF from 12.LR—HWR/PWR—U/Pu.

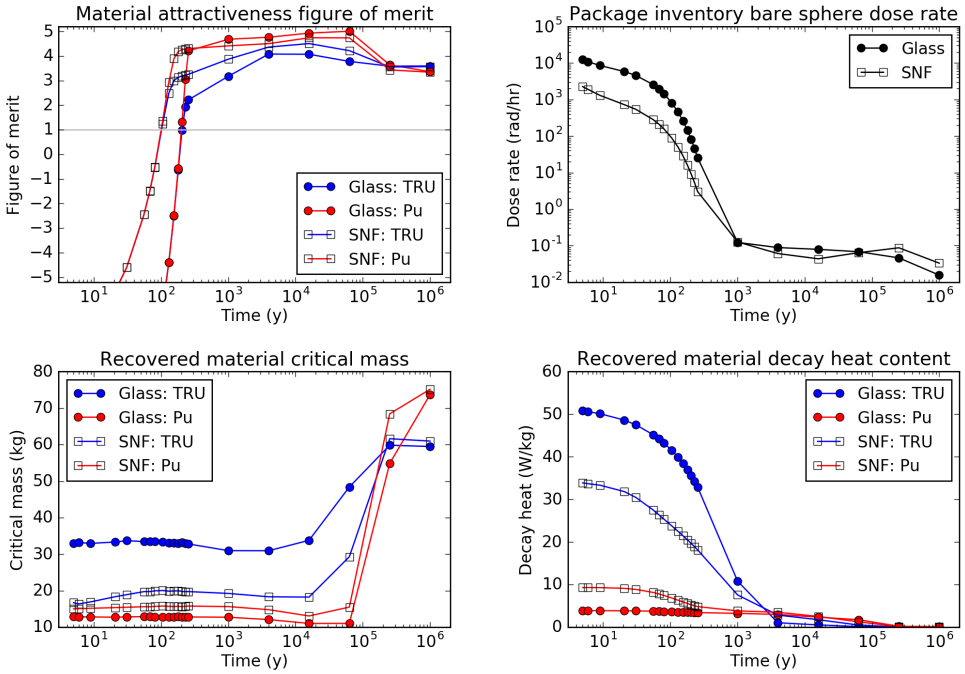

Figure B.26: FOM evaluation for Pu and TRU in HLW glass and SNF from 12.LR—HWR/PWR—U/Pu.

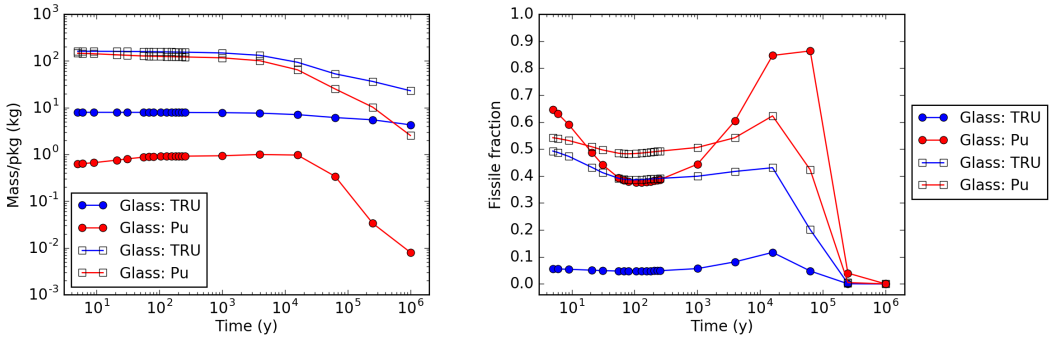

Figure B.27: Pu and TRU package inventory and fissile fraction in HLW glass and SNF from 13.LR—PWR/PWR—U/Pu.

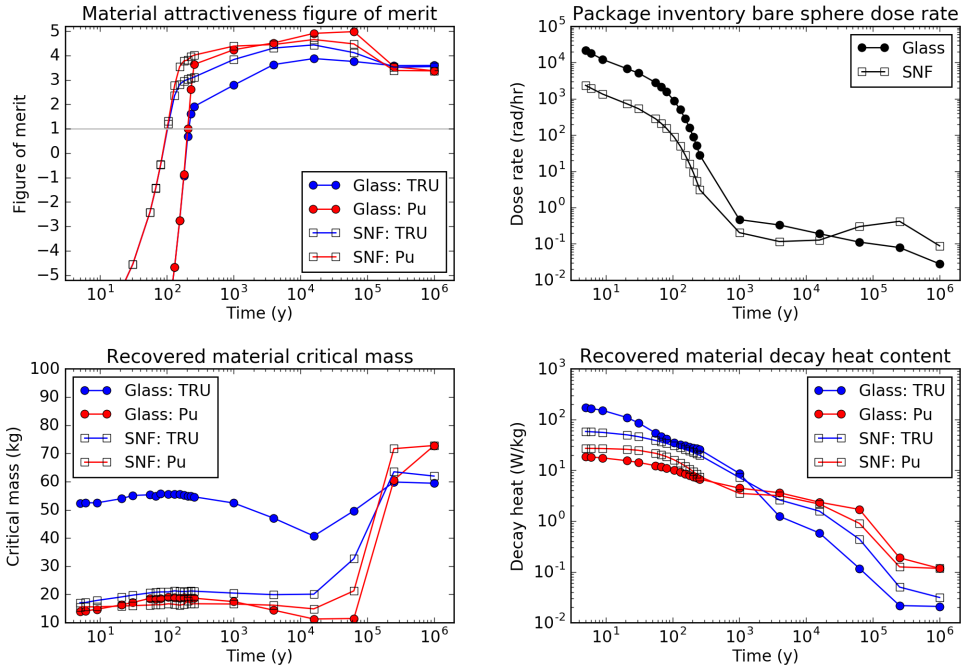

Figure B.28: FOM evaluation for Pu and TRU in HLW glass and SNF from 13.LR—PWR/PWR—U/Pu.

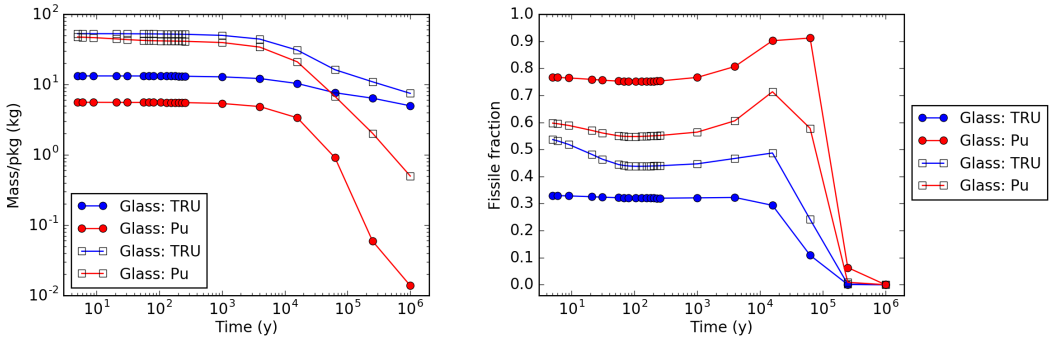

Figure B.29: Pu and TRU package inventory and fissile fraction in HLW ceramic and SNF from 14.LR—SFR/PWR—U/Pu.

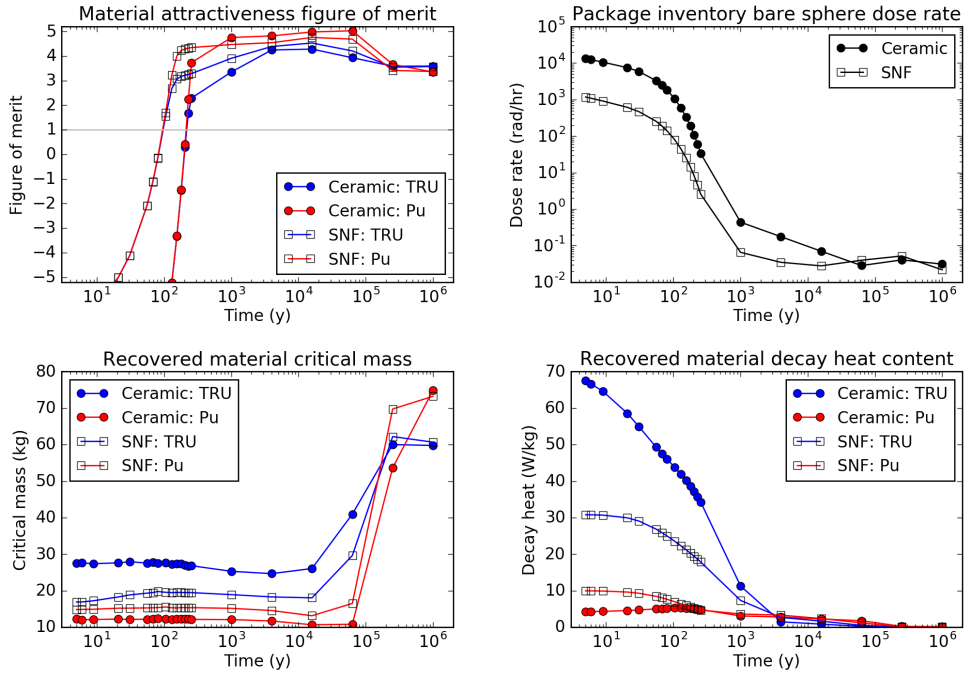

Figure B.30: FOM evaluation for Pu and TRU in HLW ceramic and SNF from 14.LR—SFR/PWR—U/Pu.

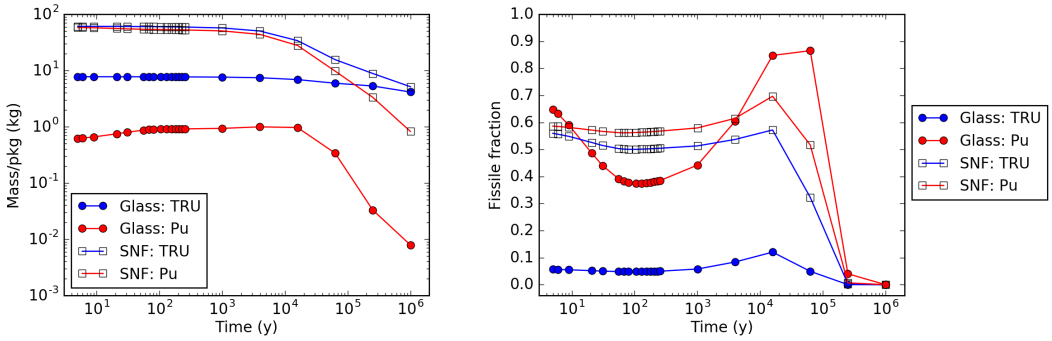

Figure B.31: Pu and TRU package inventory and fissile fraction in HLW glass and SNF from 15.LR—PWR/SFR—U/Pu.

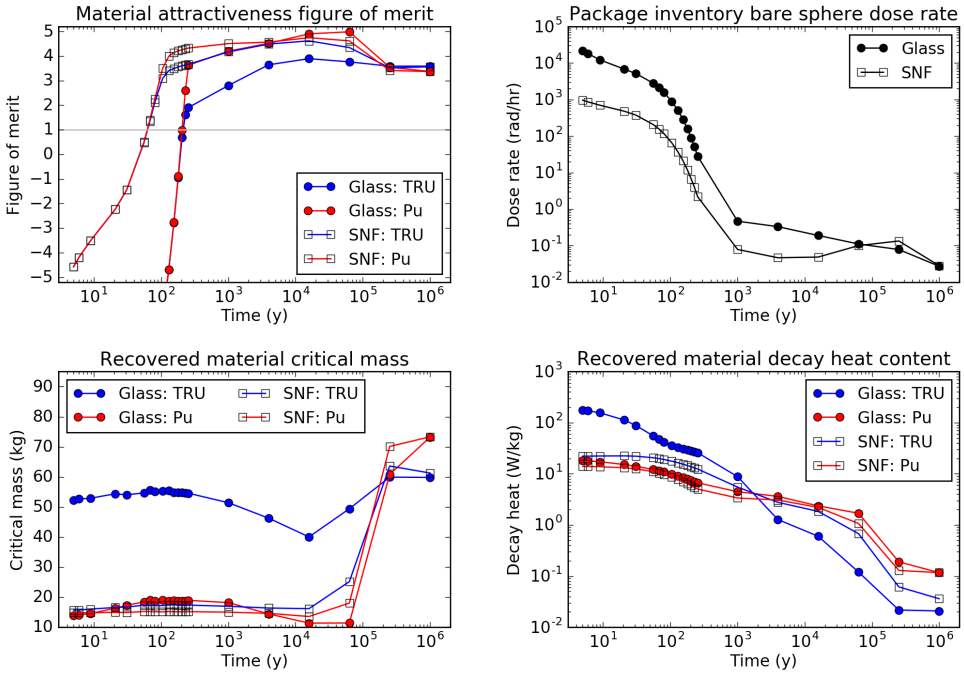

Figure B.32: FOM evaluation for Pu and TRU in HLW glass and SNF from 15.LR—PWR/SFR—U/Pu.

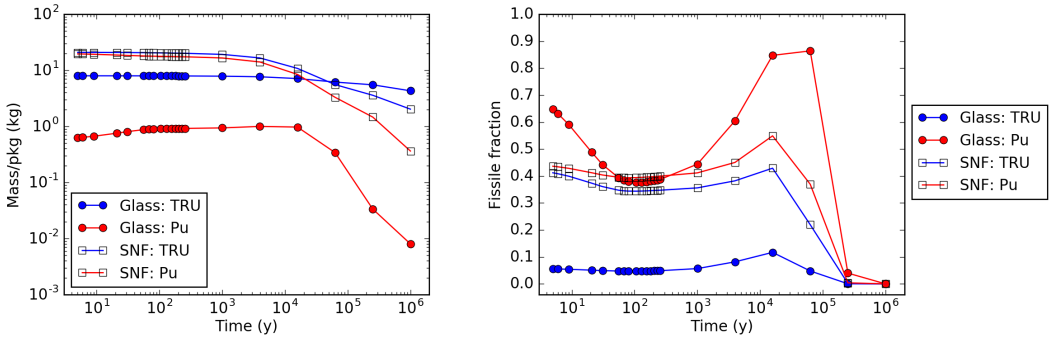

Figure B.33: Pu and TRU package inventory and fissile fraction in HLW glass and SNF from 16.LR—PWR/ADS—U/Pu.

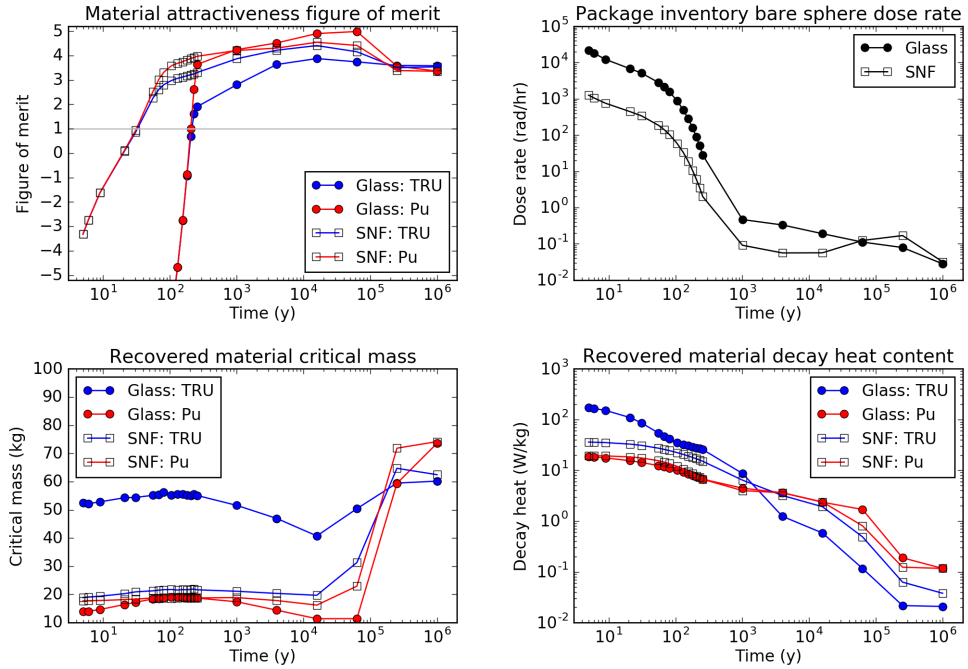

Figure B.34: FOM evaluation for Pu and TRU in HLW glass and SNF from 16.LR—PWR/ADS—U/Pu.

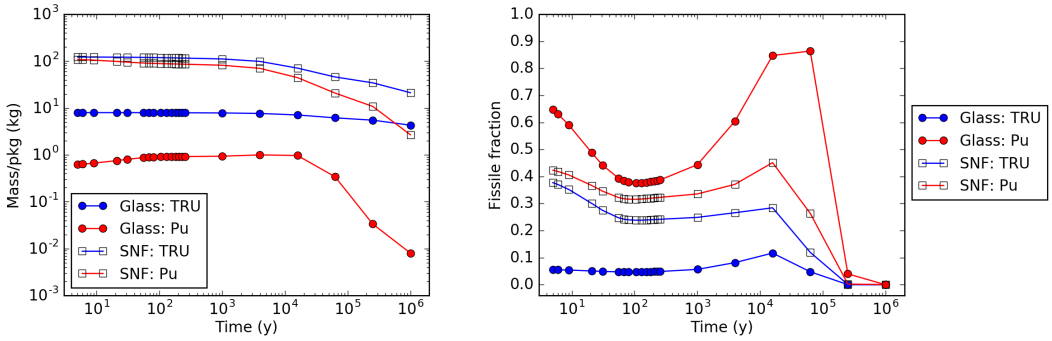

Figure B.35: Pu and TRU package inventory and fissile fraction in HLW glass and SNF from 17.LR—PWR/PWR—U/Th/Pu.

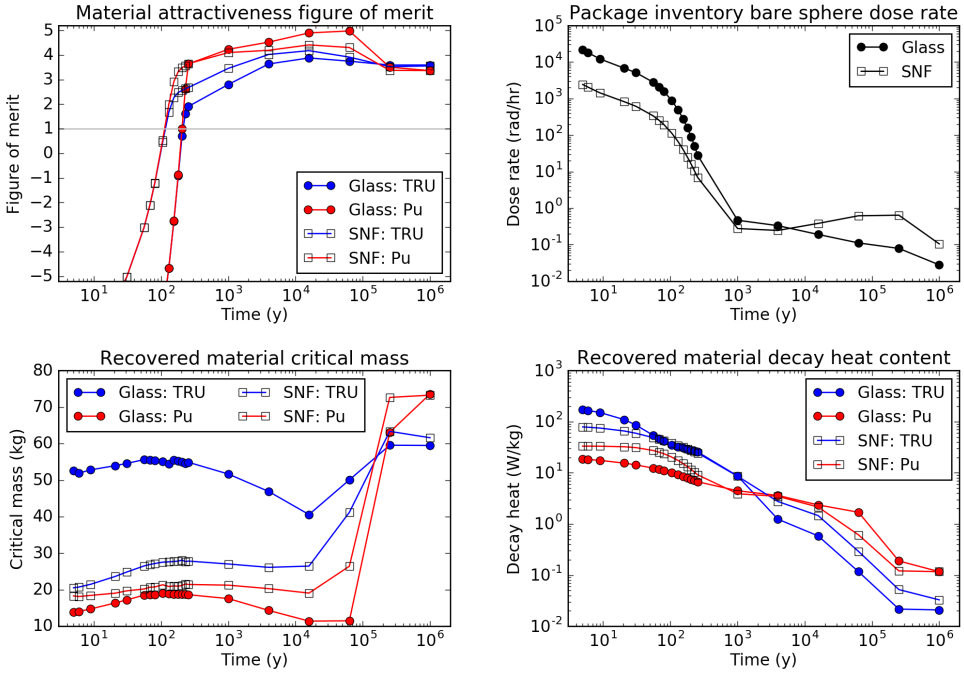

Figure B.36: FOM evaluation for Pu and TRU in HLW glass and SNF from 17.LR—PWR/PWR—U/Th/Pu.

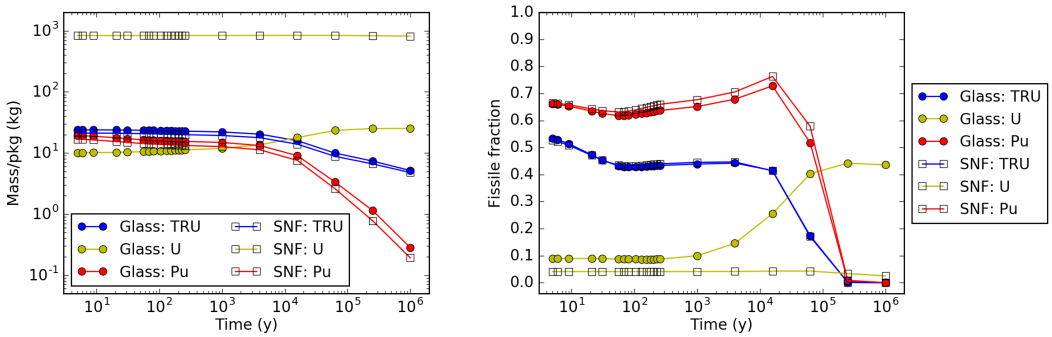

Figure B.37: U, Pu, and TRU package inventory and fissile fraction in HLW glass and SNF from 18.LR—PWR/PWR—U/Th/U3.

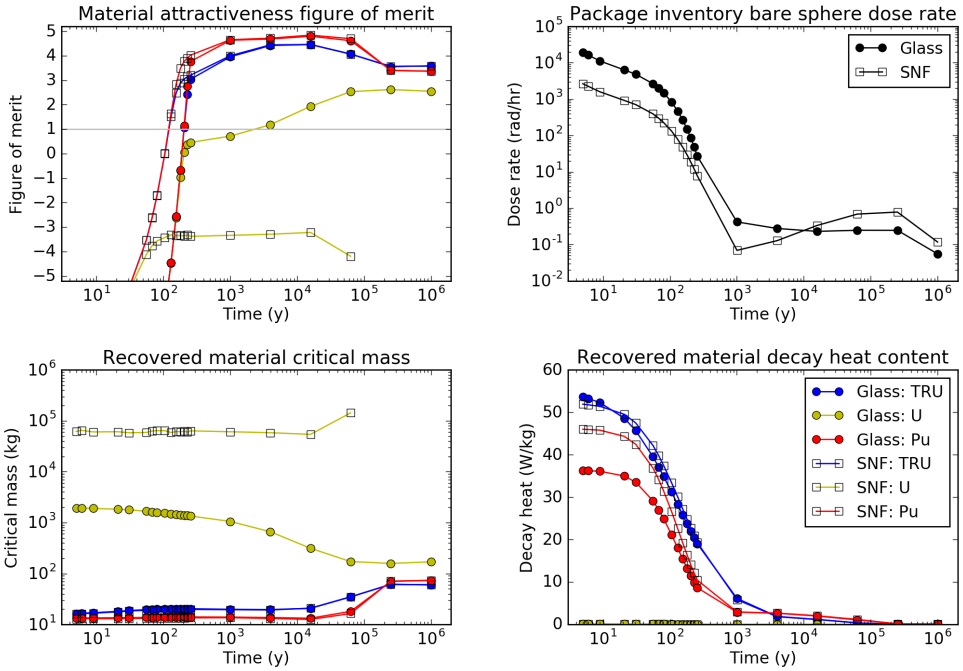

Figure B.38: FOM evaluation for U, Pu, and TRU in HLW glass and SNF from 18.LR—PWR/PWR—U/Th/U3.

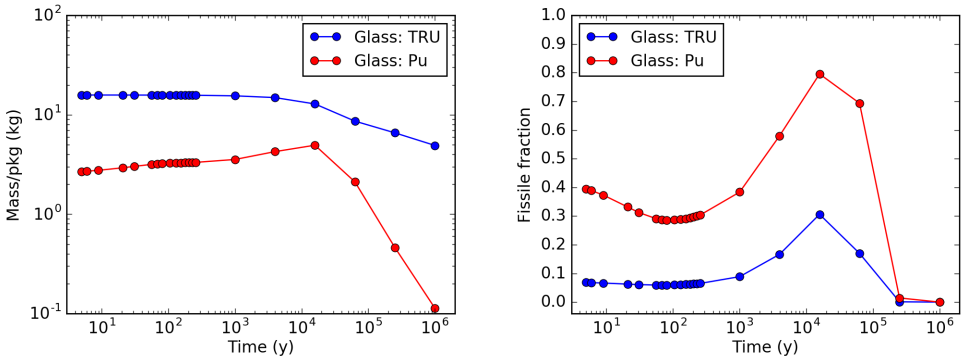

Figure B.39: Pu and TRU package inventory and fissile fraction in HLW glass from 19.CR—HWR—U/Pu.

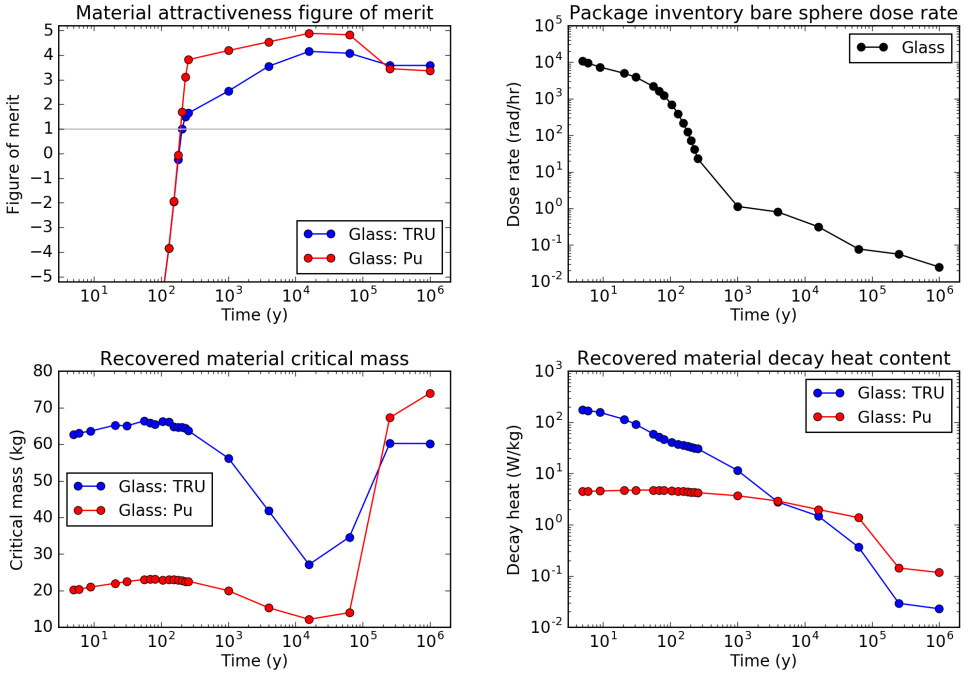

Figure B.40: FOM evaluation for Pu and TRU in HLW glass from 19.CR—HWR—U/Pu.

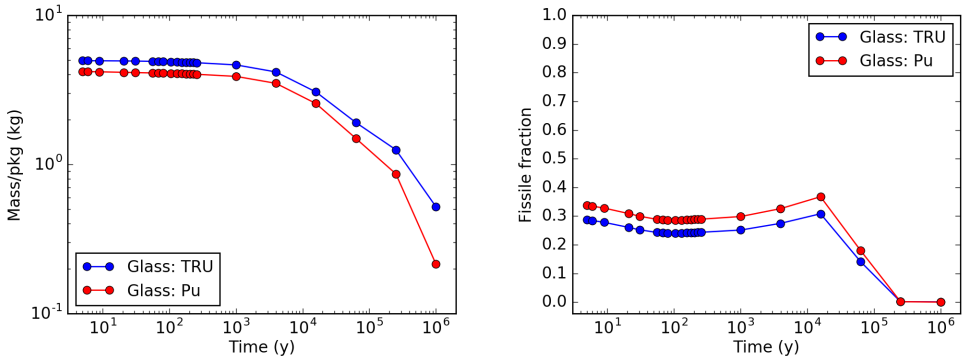

Figure B.41: Pu and TRU package inventory and fissile fraction in HLW glass from 20.CR—HWR—U/TRU.

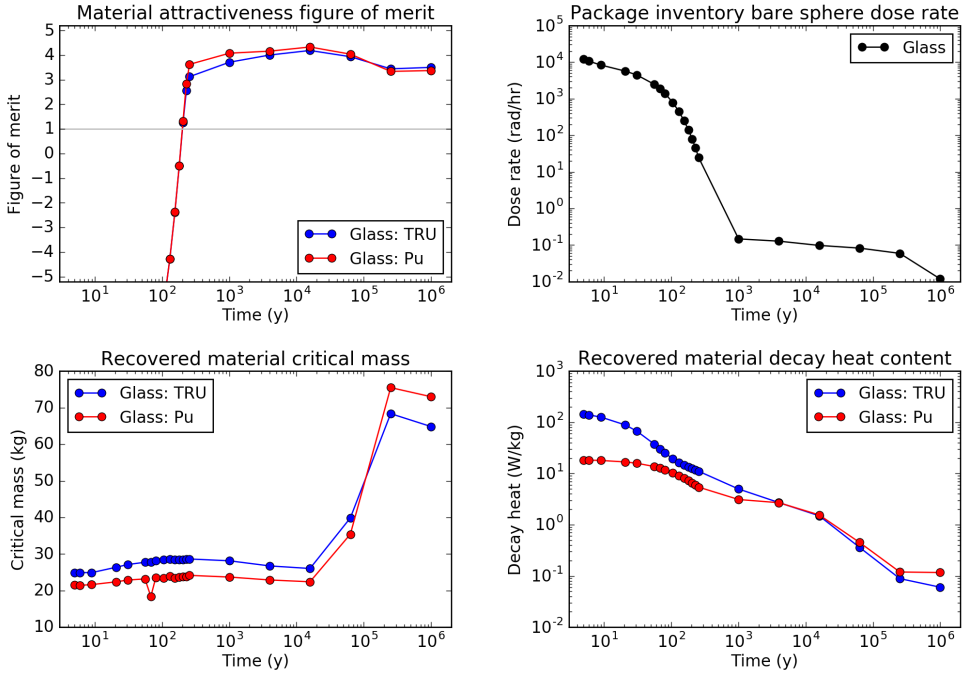

Figure B.42: FOM evaluation for Pu and TRU in HLW glass from 20.CR—HWR—U/TRU.

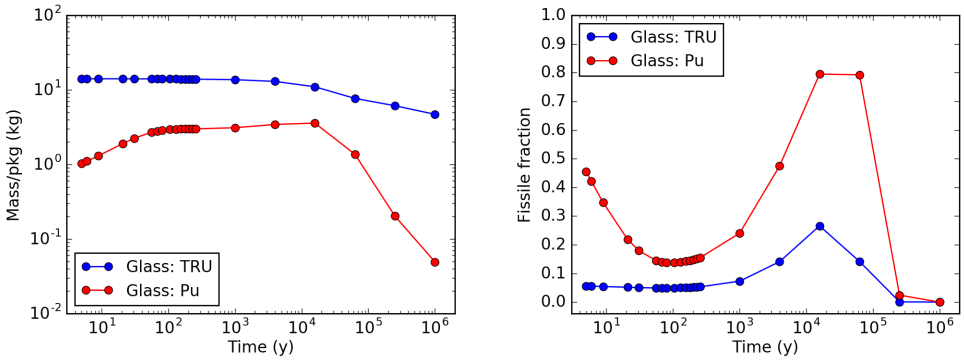

Figure B.43: Pu and TRU package inventory and fissile fraction in HLW glass from 21.CR—PWR—U/Pu.

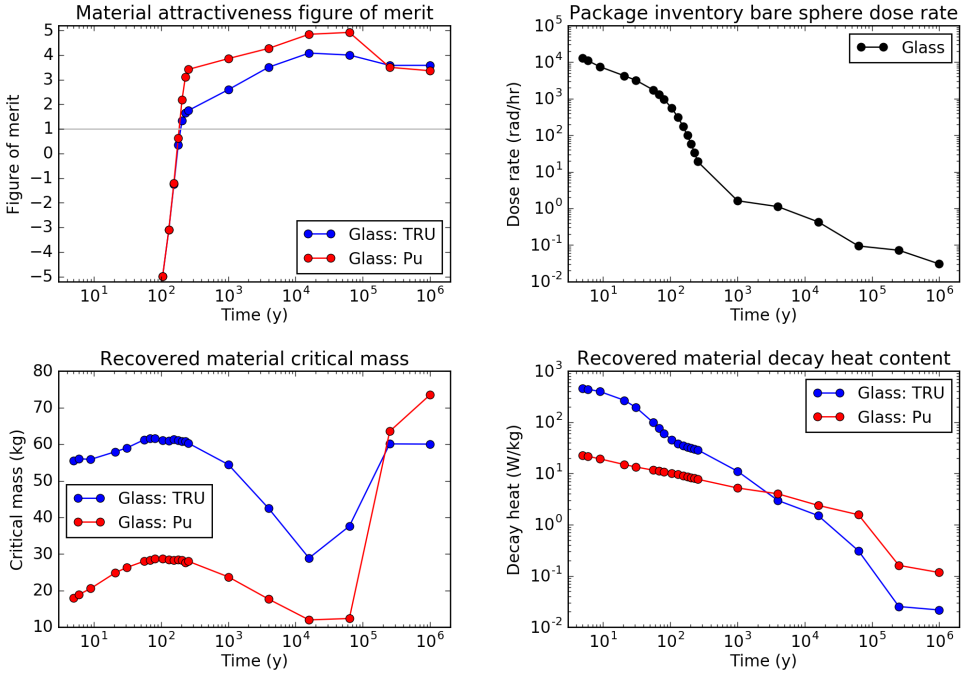

Figure B.44: FOM evaluation for Pu and TRU in HLW glass from 21.CR—PWR—U/Pu.

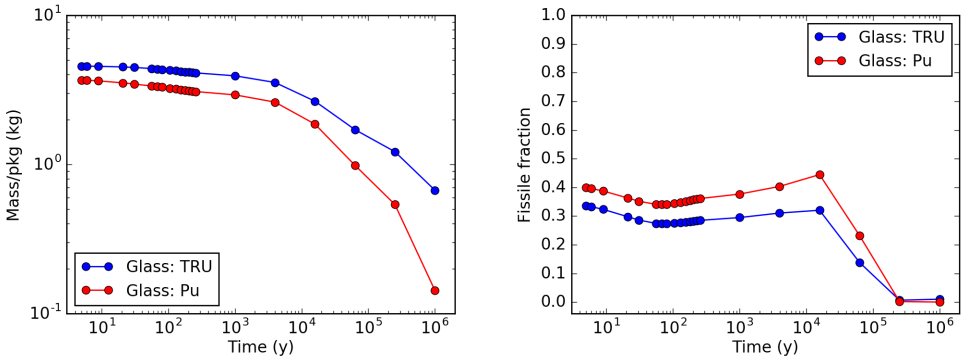

Figure B.45: Pu and TRU package inventory and fissile fraction in HLW glass from 22.CR—PWR—U/TRU.

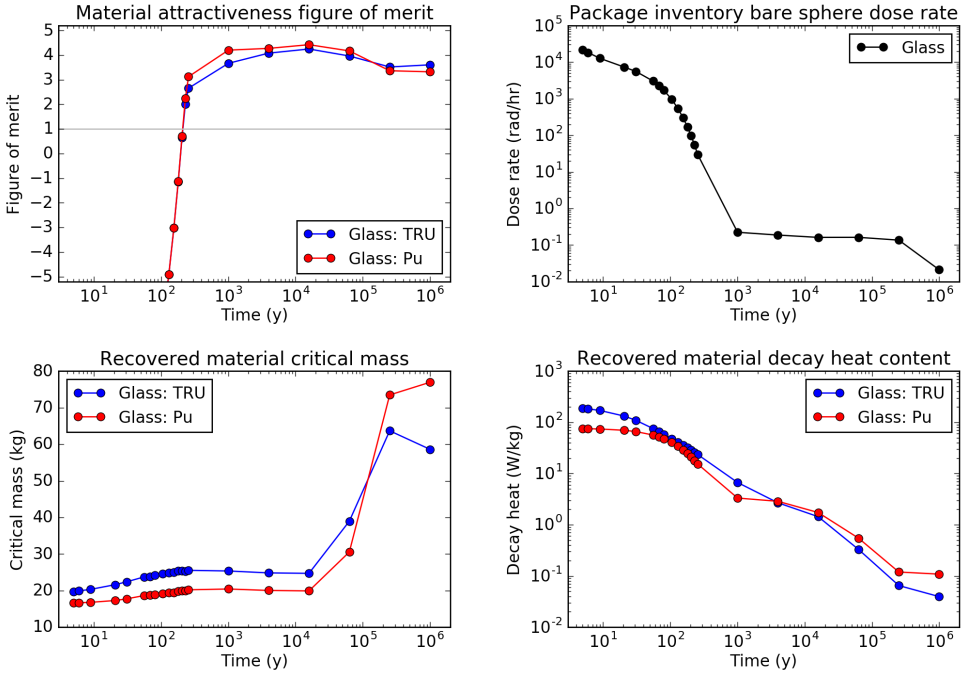

Figure B.46: FOM evaluation for Pu and TRU in HLW glass from 22.CR—PWR—U/TRU.

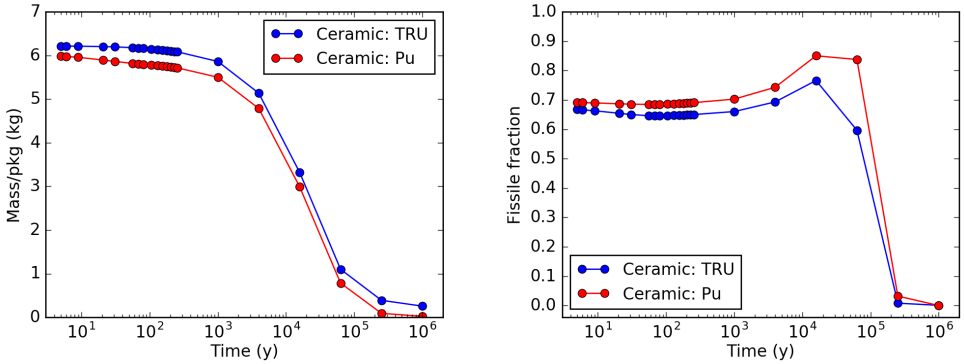

Figure B.47: Pu and TRU package inventory and fissile fraction in HLW ceramic from 24.CR—SFR—U/TRU.

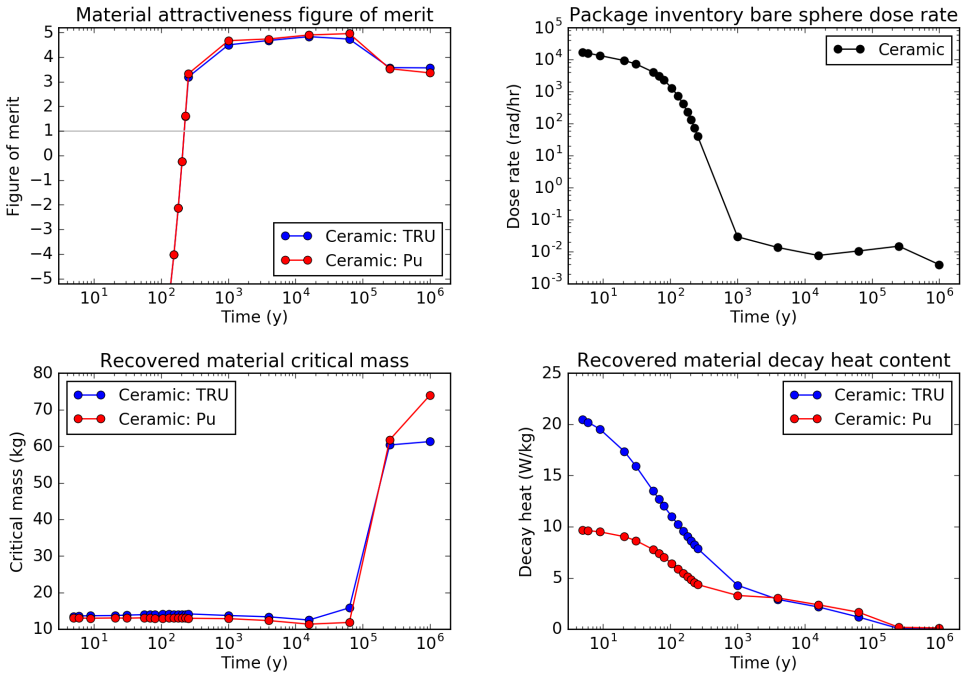

Figure B.48: FOM evaluation for Pu and TRU in HLW ceramic from 24.CR—SFR—U/TRU.

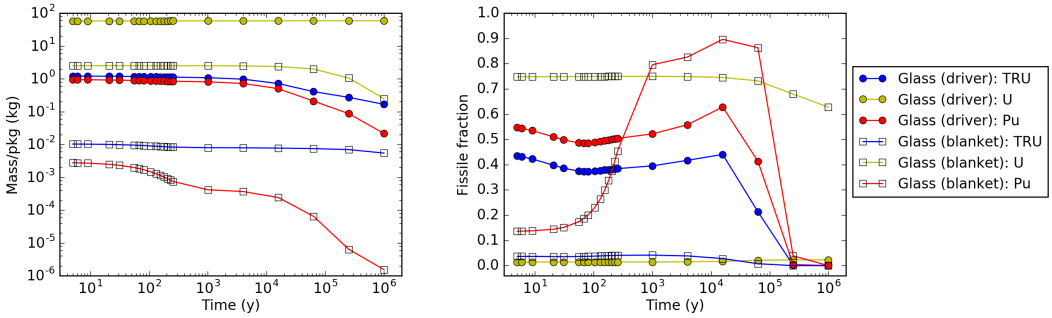

Figure B.49: U, Pu, and TRU package inventory and fissile fraction in HLW glass from 25.CR—PWR—U/TRU/Th/U3.

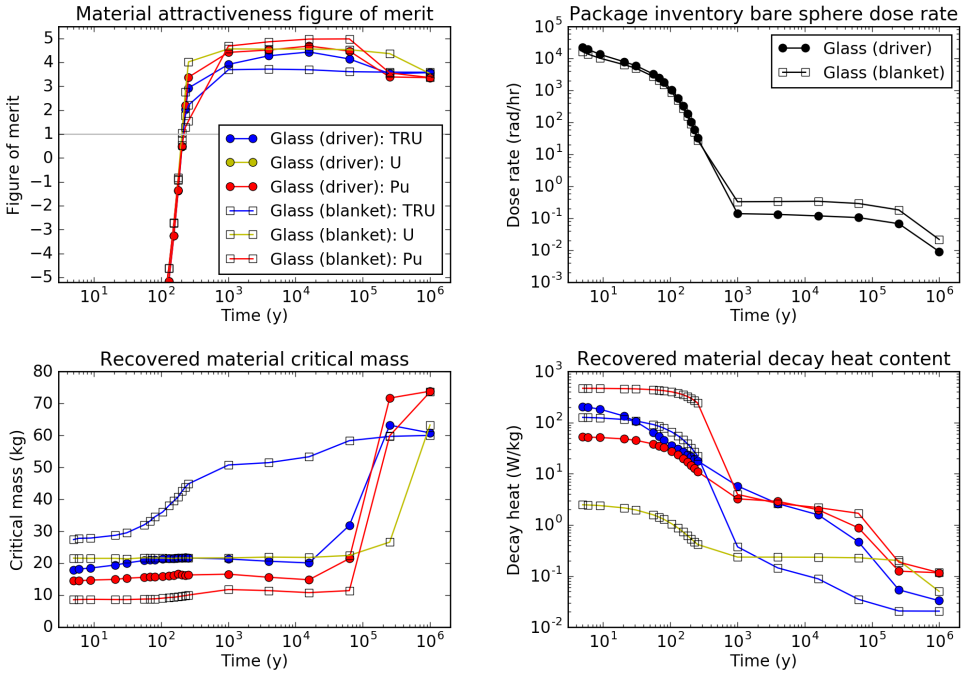

Figure B.50: FOM evaluation for U, Pu and TRU in HLW glass from 25.CR—PWR—U/TRU/Th/U3.

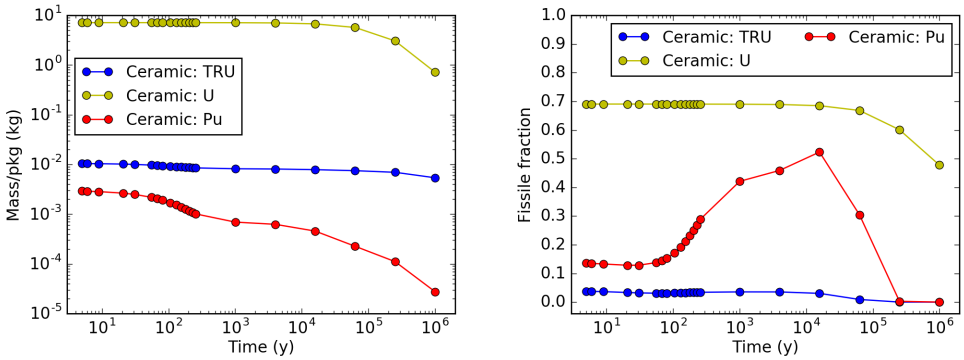

Figure B.51: U, Pu, and TRU package inventory and fissile fraction in HLW ceramic from 26.CR—MSR—Th/U3/TRU.

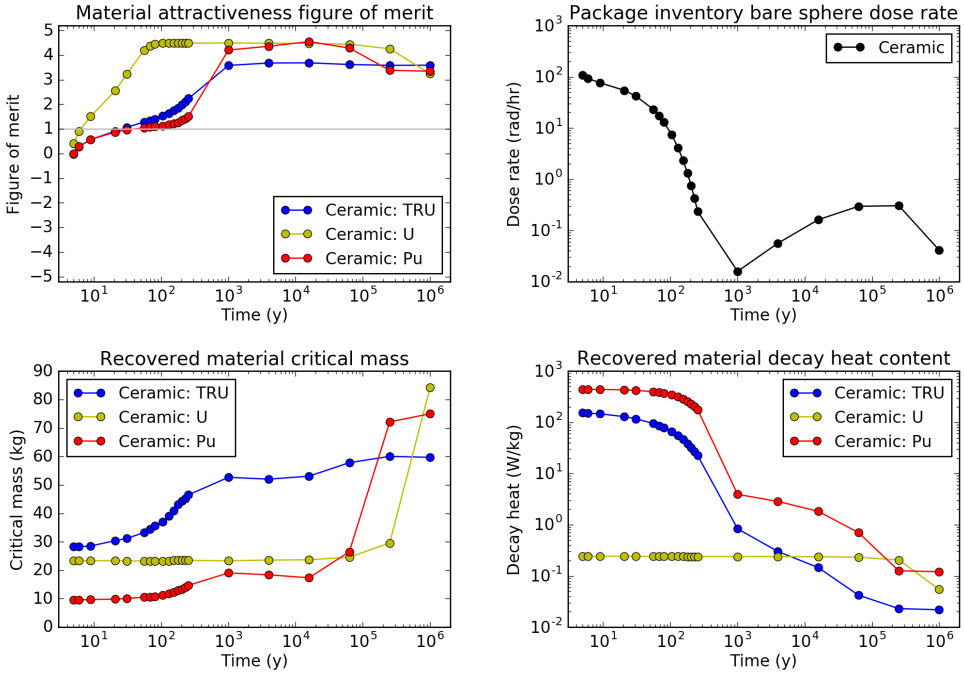

Figure B.52: FOM evaluation for U, Pu, and TRU in HLW ceramic from 26.CR—MSR—Th/U3/TRU.

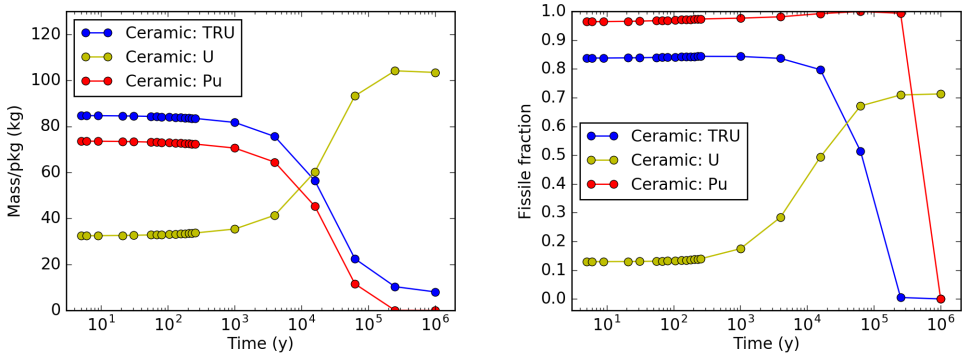

Figure B.53: U, Pu, and TRU package inventory and fissile fraction in HLW ceramic from 27.CR—SFR—U/Th/U3.

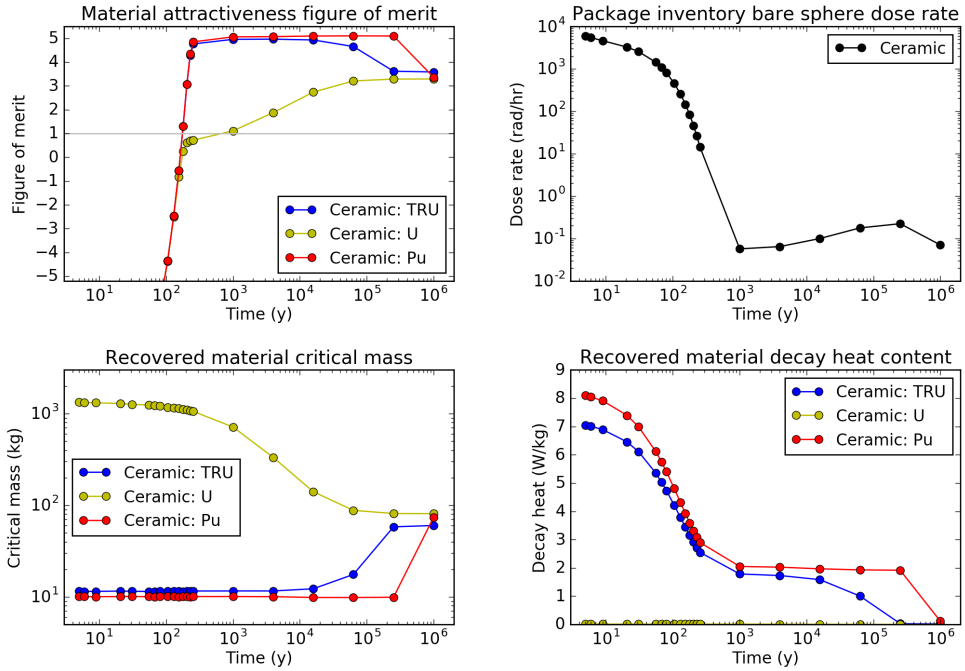

Figure B.54: FOM evaluation for U, Pu, and TRU in HLW ceramic from 27.CR—SFR—U/Th/U3.

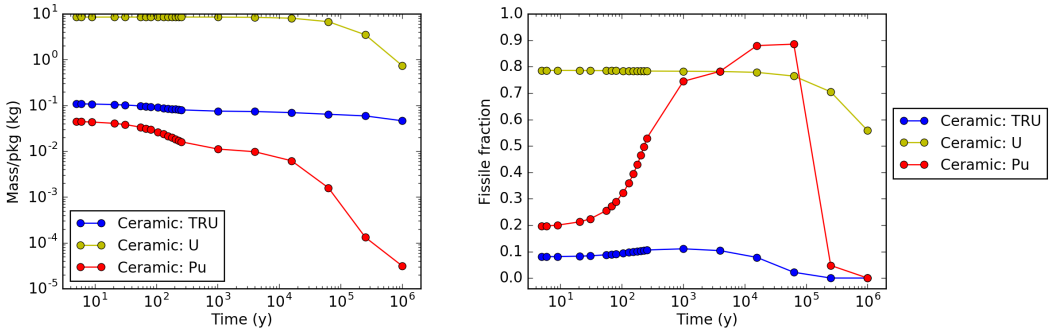

Figure B.55: U, Pu, and TRU package inventory and fissile fraction in HLW ceramic from 28.CR—SFR—Th/U3.

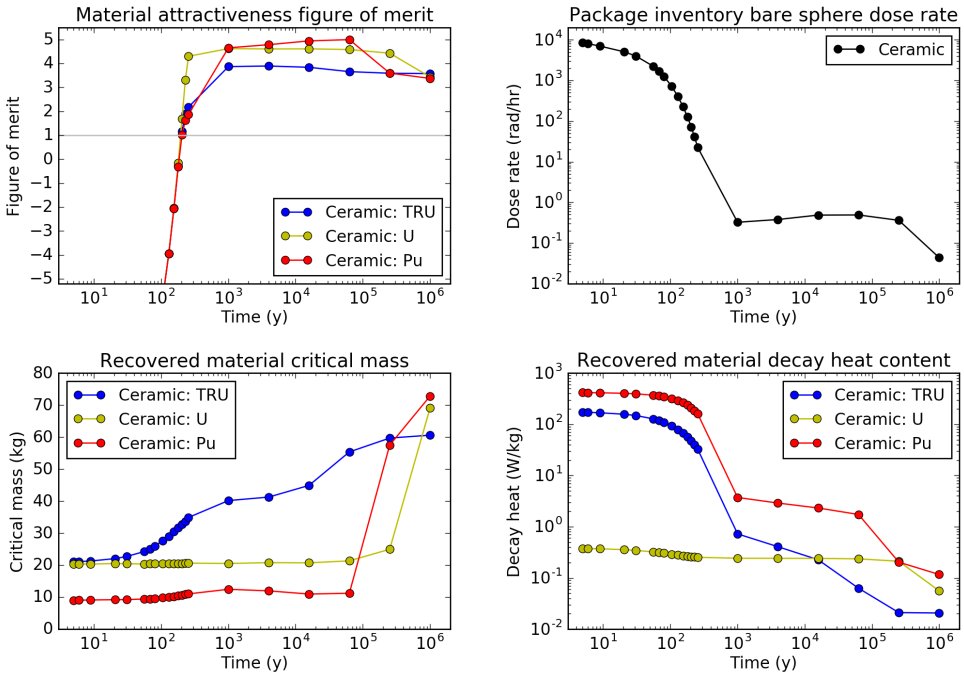

Figure B.56: FOM evaluation for U, Pu, and TRU in HLW ceramic from 28.CR—SFR—Th/U3.

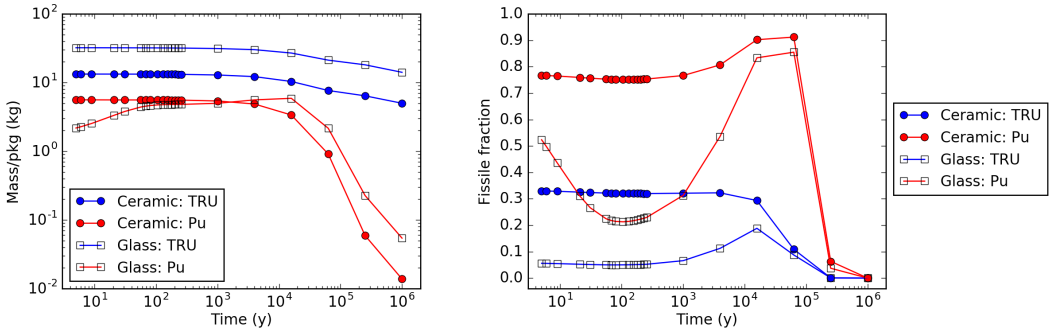

Figure B.57: Pu and TRU package inventory and fissile fraction in HLW ceramic and glass from 29.CR—SFR/PWR—U/Pu.

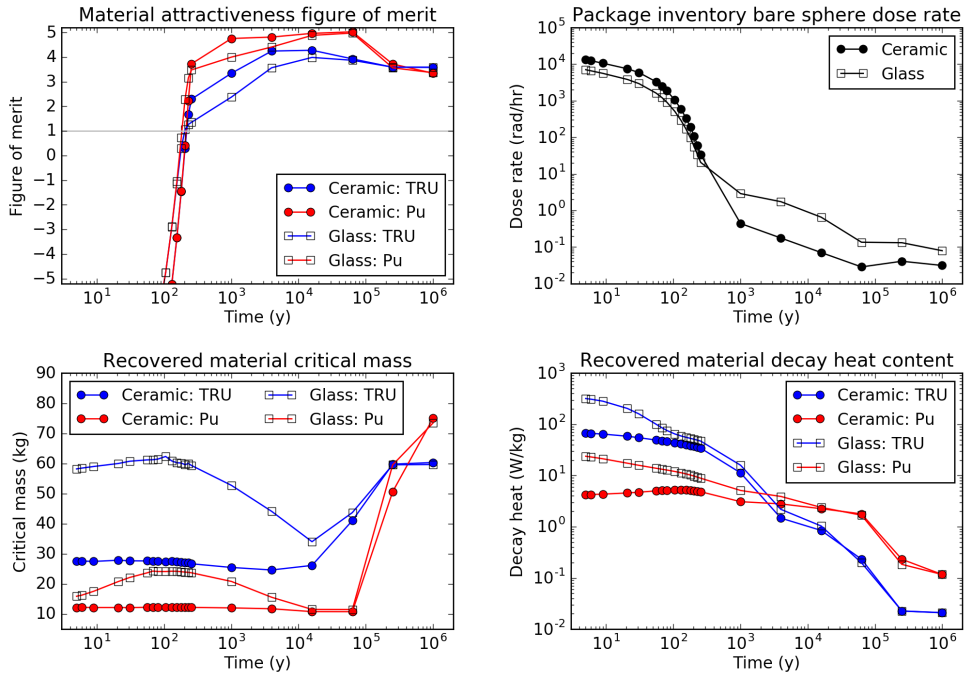

Figure B.58: FOM evaluation for Pu and TRU in HLW ceramic and glass from 29.CR—SFR/PWR—U/Pu.

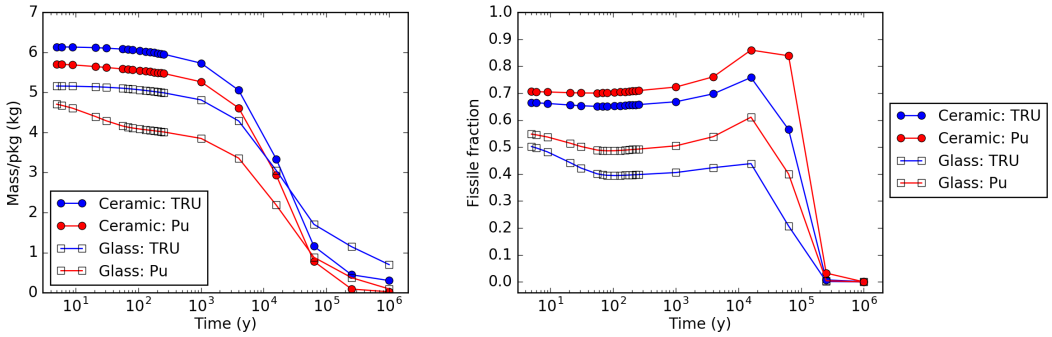

Figure B.59: Pu and TRU package inventory and fissile fraction in HLW ceramic and glass from 30.CR—SFR/PWR—U/TRU.

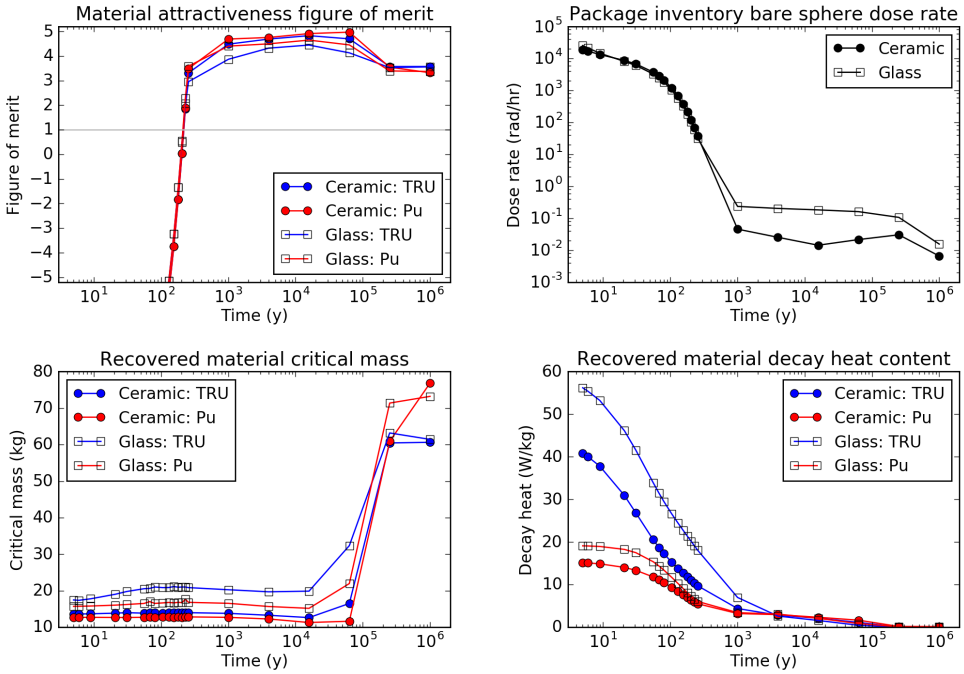

Figure B.60: FOM evaluation for Pu and TRU in HLW ceramic and glass from 30.CR—SFR/PWR—U/TRU.

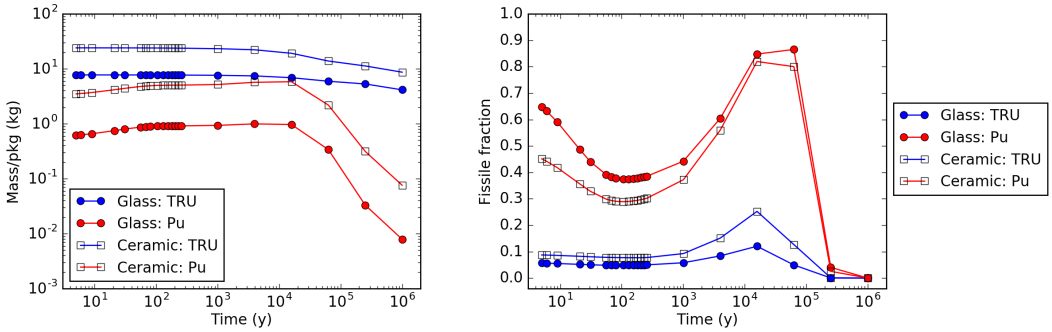

Figure B.61: Pu and TRU package inventory and fissile fraction in HLW glass and ceramic from 31.CR—PWR/SFR—U/Pu.

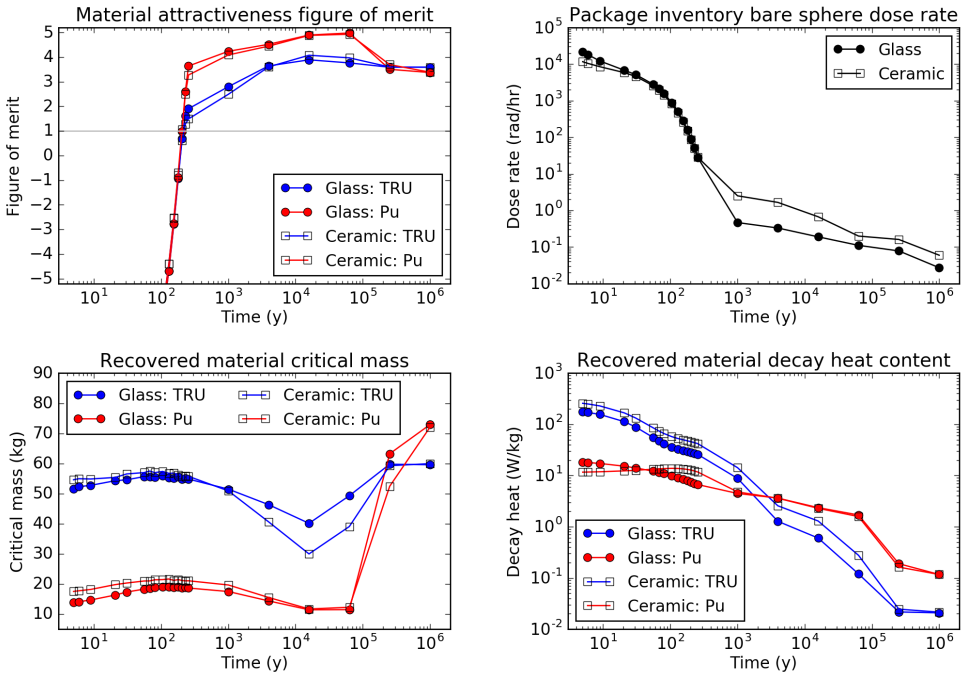

Figure B.62: FOM evaluation for Pu and TRU in HLW glass and ceramic from 31.CR—PWR/SFR—U/Pu.

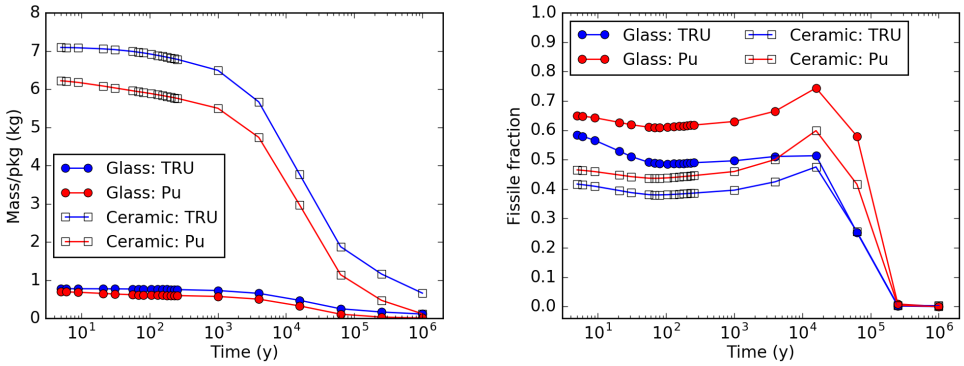

Figure B.63: Pu and TRU package inventory and fissile fraction in HLW glass and ceramic from 32.CR—PWR/SFR—U/TRU.

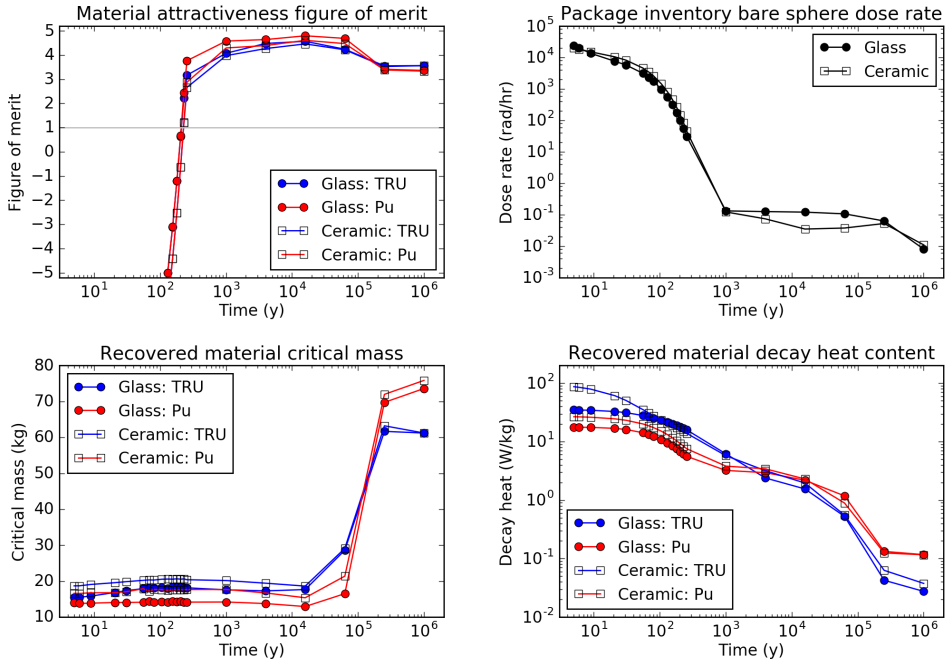

Figure B.64: FOM evaluation for Pu and TRU in HLW glass and ceramic from 32.CR—PWR/SFR—U/TRU.

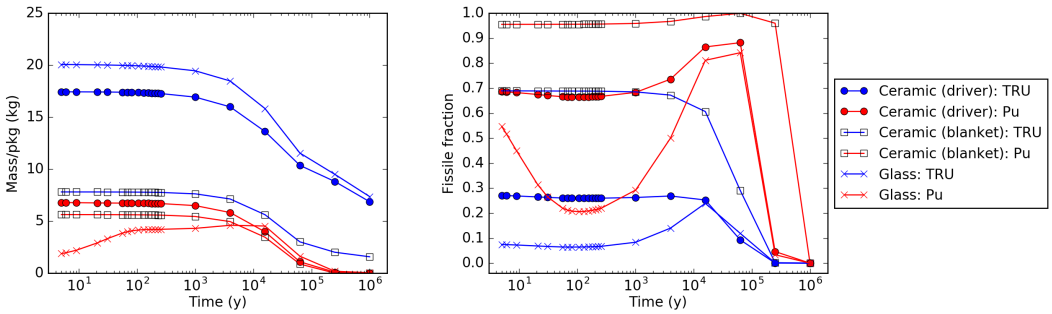

Figure B.65: Pu and TRU package inventory and fissile fraction in HLW ceramic and glass from 33.CR—ADS/PWR—U/Pu.

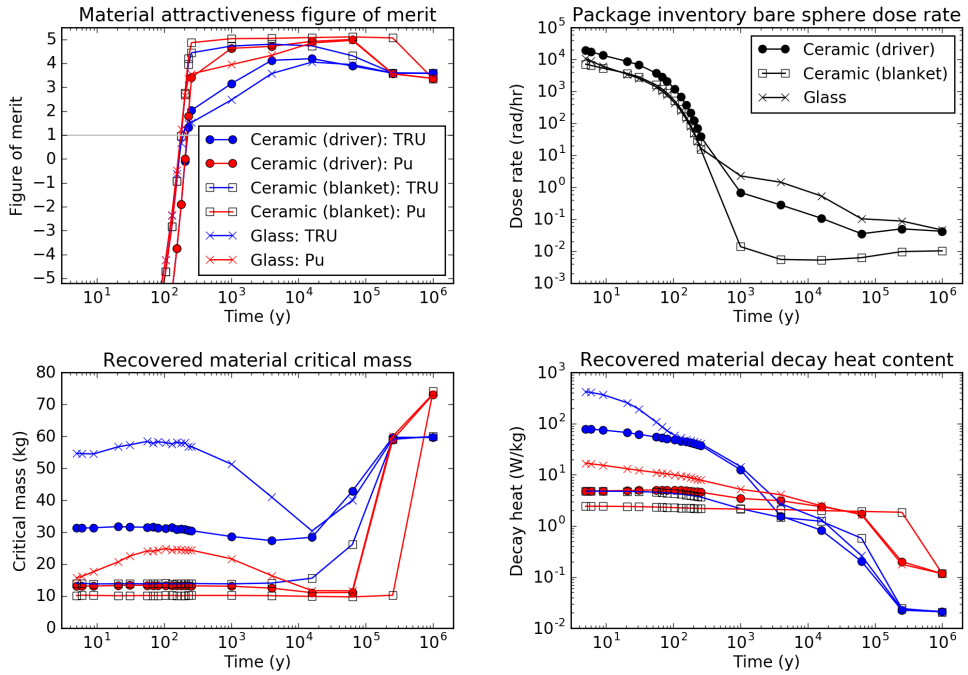

Figure B.66: FOM evaluation for Pu and TRU in HLW ceramic and glass from 33.CR—ADS/PWR—U/Pu.

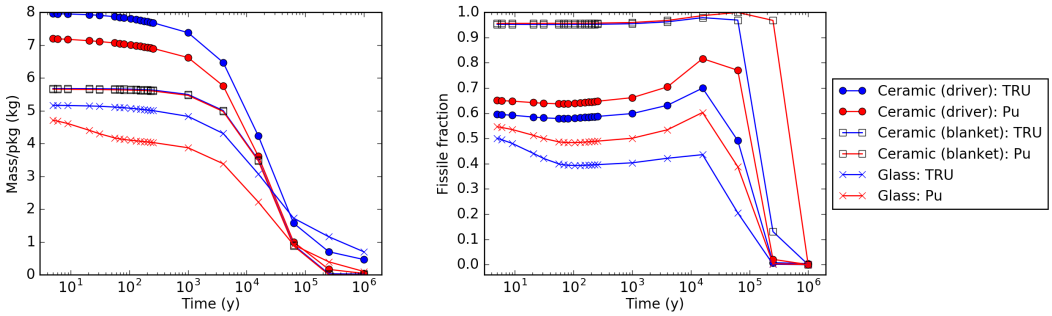

Figure B.67: Pu and TRU package inventory and fissile fraction in HLW ceramic and glass from 34.CR—ADS/PWR—U/TRU.

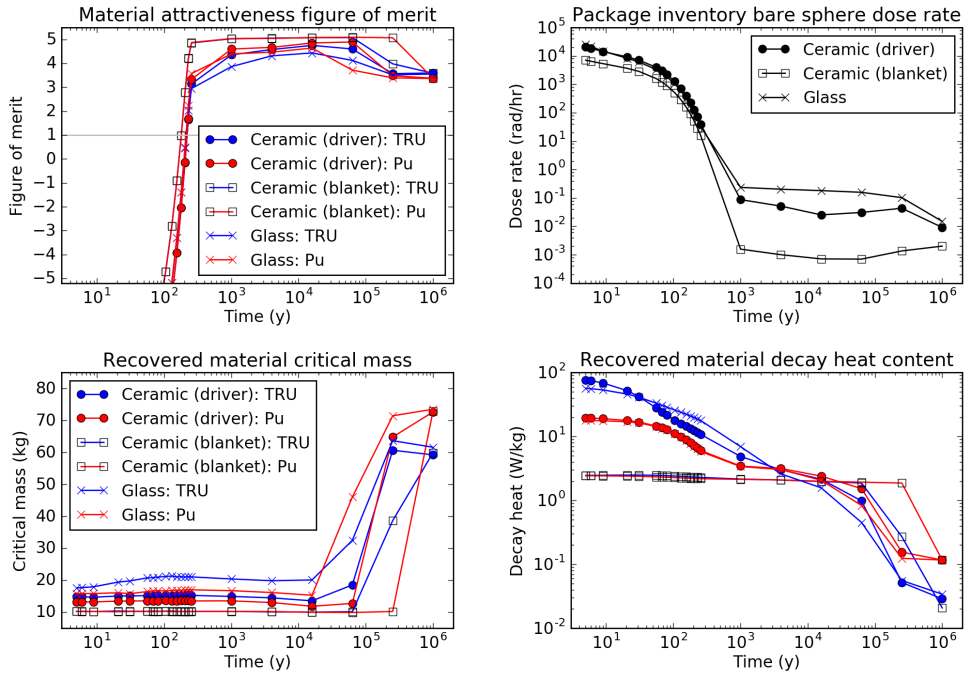

Figure B.68: FOM evaluation for Pu and TRU in HLW ceramic and glass from 34.CR—ADS/PWR—U/TRU.

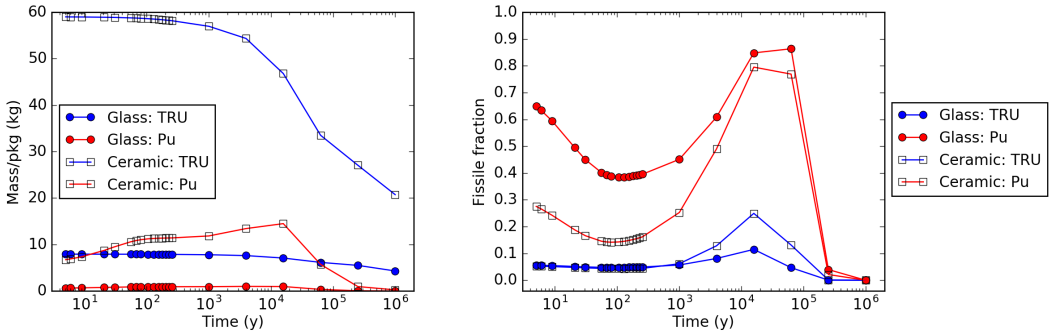

Figure B.69: Pu and TRU package inventory and fissile fraction in HLW glass and ceramic from 35.CR—PWR/ADS—U/Pu.

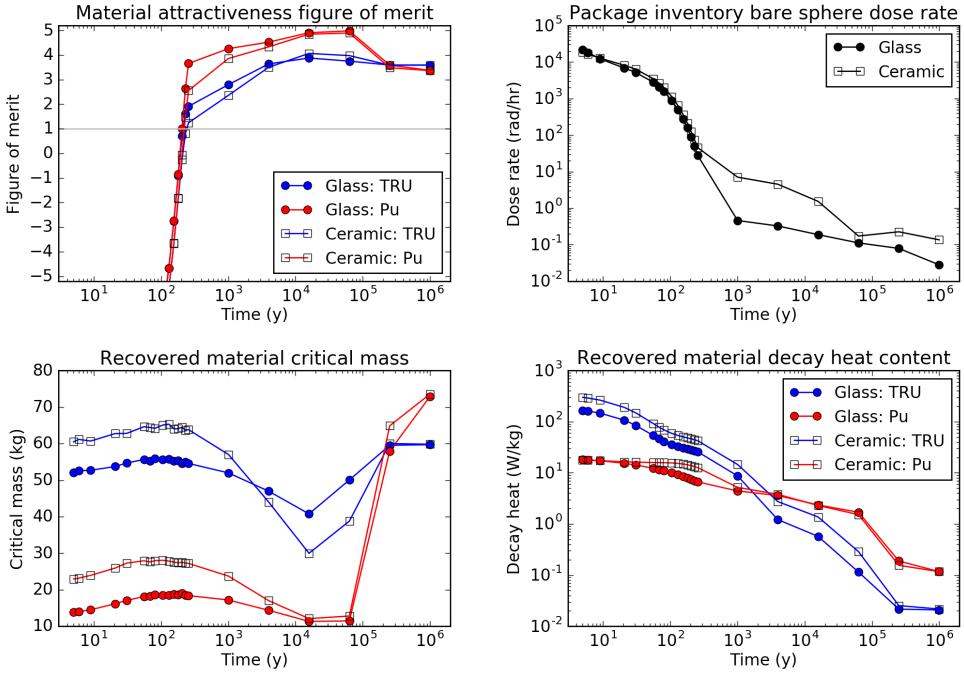

Figure B.70: FOM evaluation for Pu and TRU in HLW glass and ceramic from 35.CR—PWR/ADS—U/Pu.

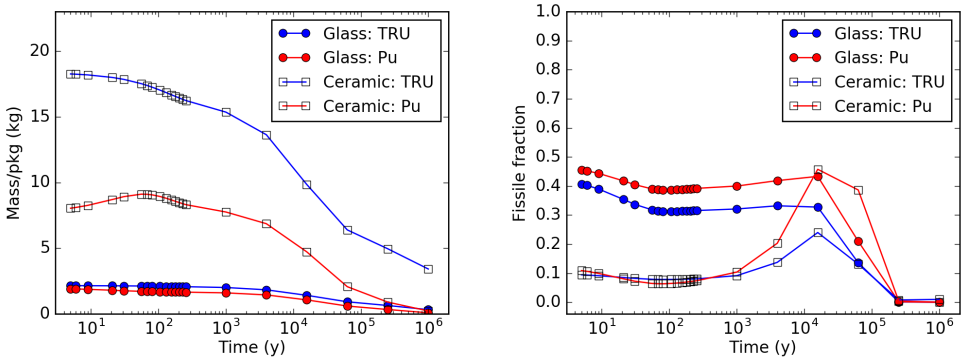

Figure B.71: Pu and TRU package inventory and fissile fraction in HLW glass and ceramic from 36.CR—PWR/ADS—U/Pu/MA.

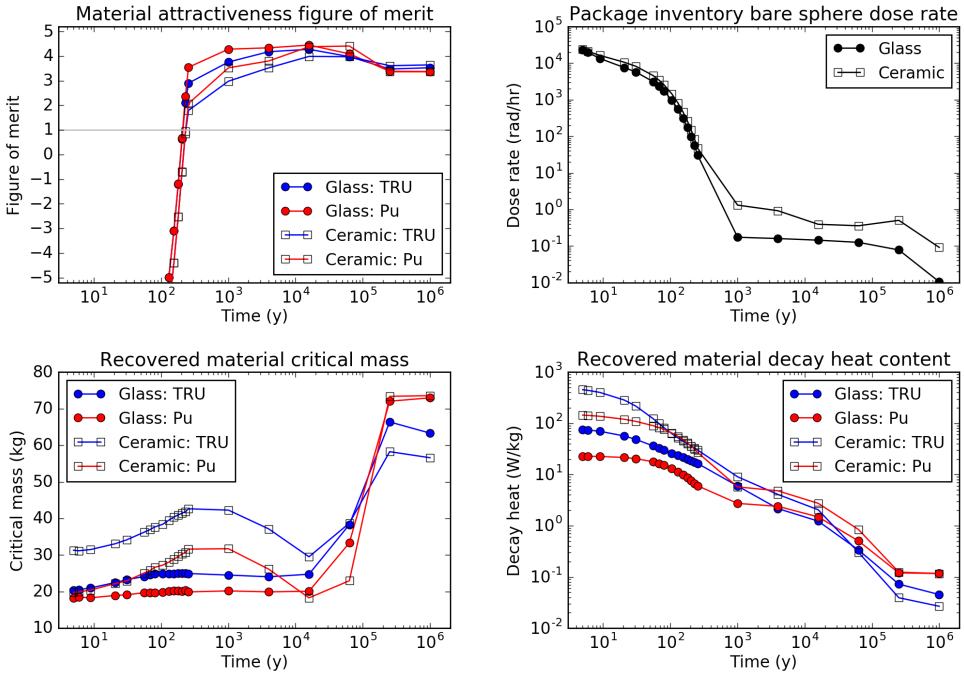

Figure B.72: FOM evaluation for Pu and TRU in HLW glass and ceramic from 36.CR—PWR/ADS—U/Pu/MA.

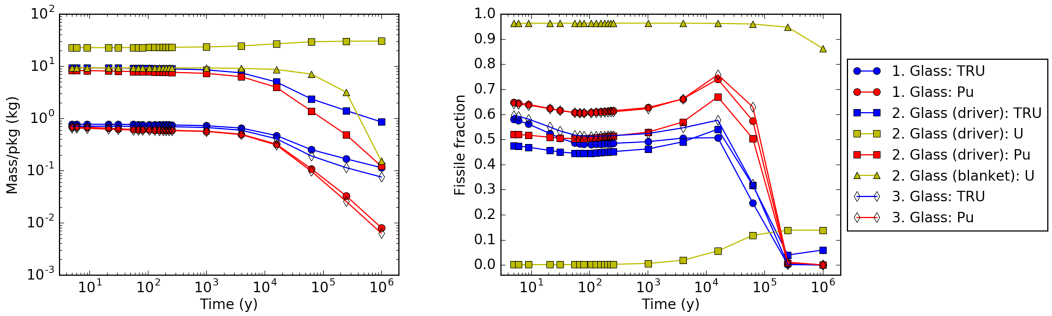

Figure B.73: U, Pu, and TRU package inventory and fissile fraction in HLW glass from 37.CR—PWR/SFR/PWR—U/TRU/Th/U3.

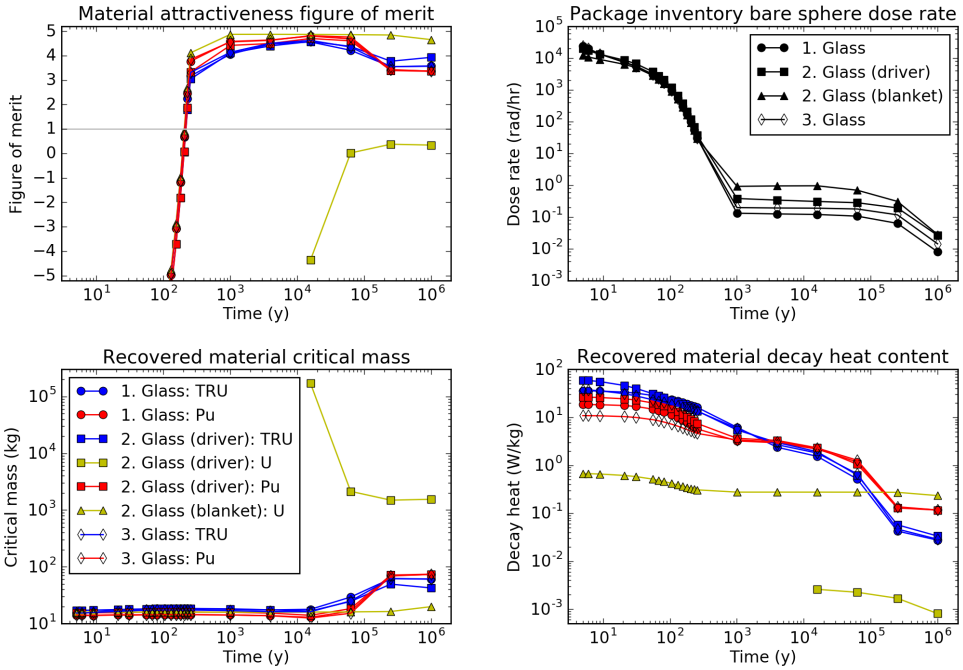

Figure B.74: FOM evaluation for U, Pu, and TRU in HLW glass from 37.CR—PWR/SFR/PWR—U/TRU/Th/U3.

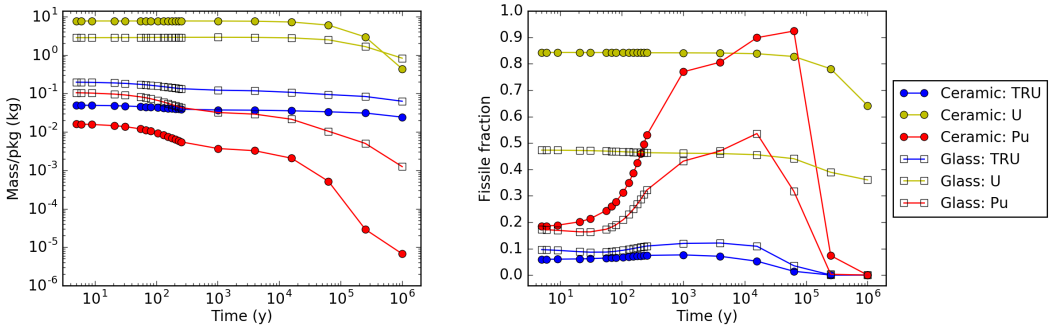

Figure B.75: U, Pu, and TRU package inventory and fissile fraction in HLW ceramic and glass from 38.CR—SFR/PWR—Th/U3.

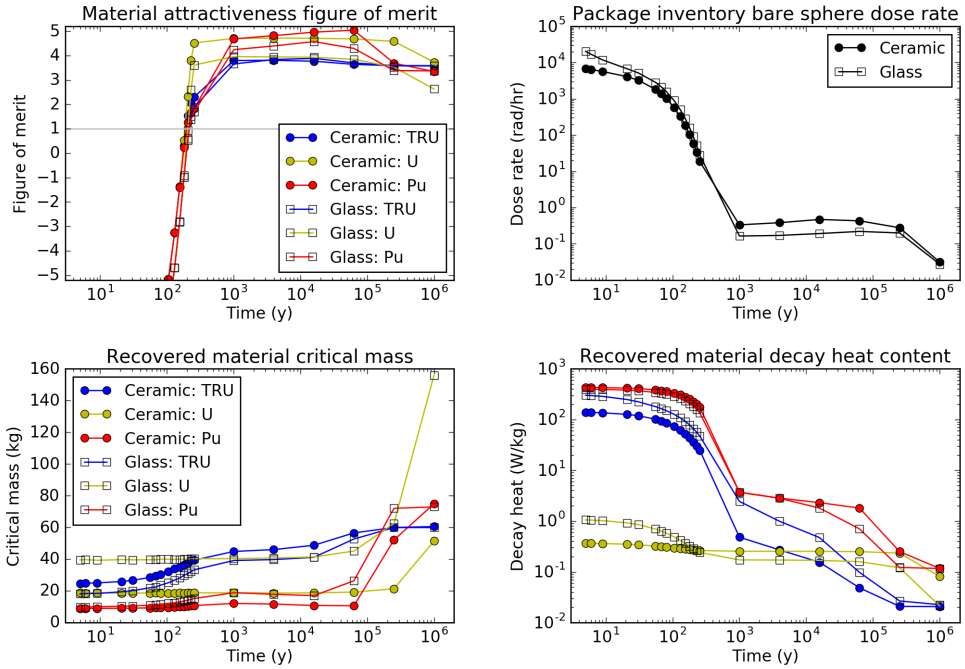

Figure B.76: FOM evaluation for U, Pu, and TRU in HLW ceramic and glass from 38.CR—SFR/PWR—Th/U3.

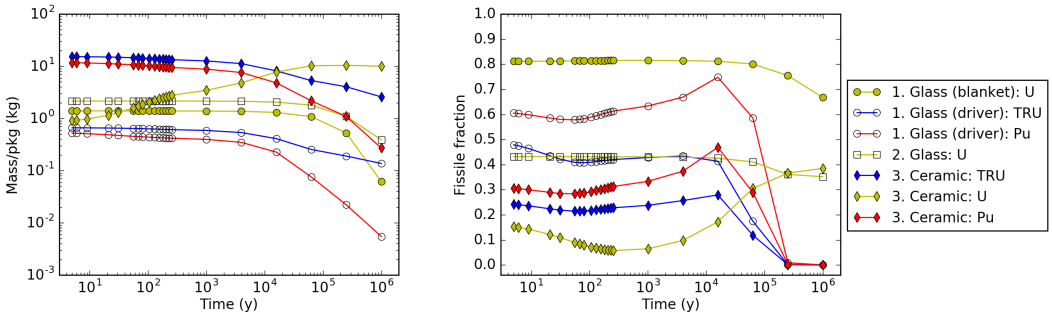

Figure B.77: U, Pu, and TRU package inventory and fissile fraction in HLW glass and ceramic from 39.CR—PWR/PWR/ADS—U/TRU/Th/U3.

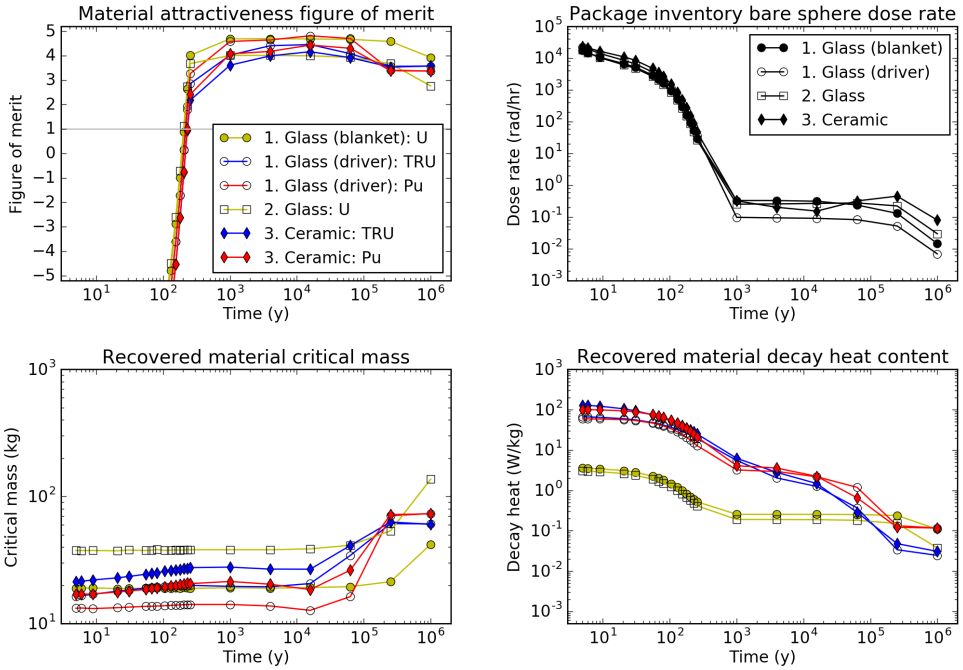

Figure B.78: FOM evaluation for U, Pu, and TRU in HLW glass and ceramic from 39.CR—PWR/PWR/ADS—U/TRU/Th/U3.

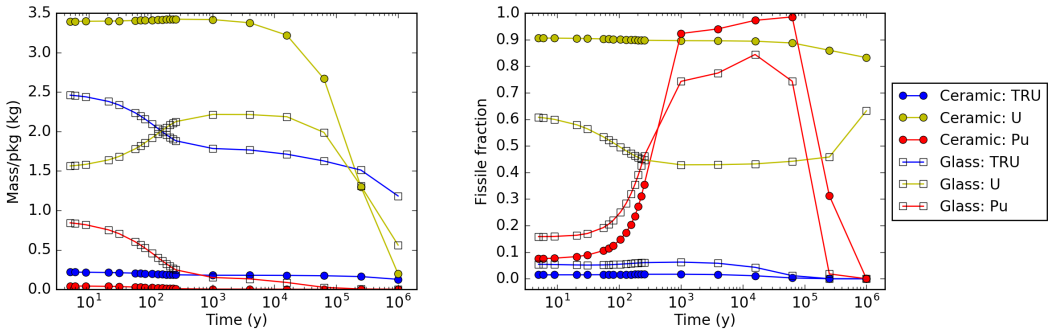

Figure B.79: U, Pu, and TRU package inventory and fissile fraction in HLW glass and ceramic from 40.CR—ADS/PWR—Th/U3.

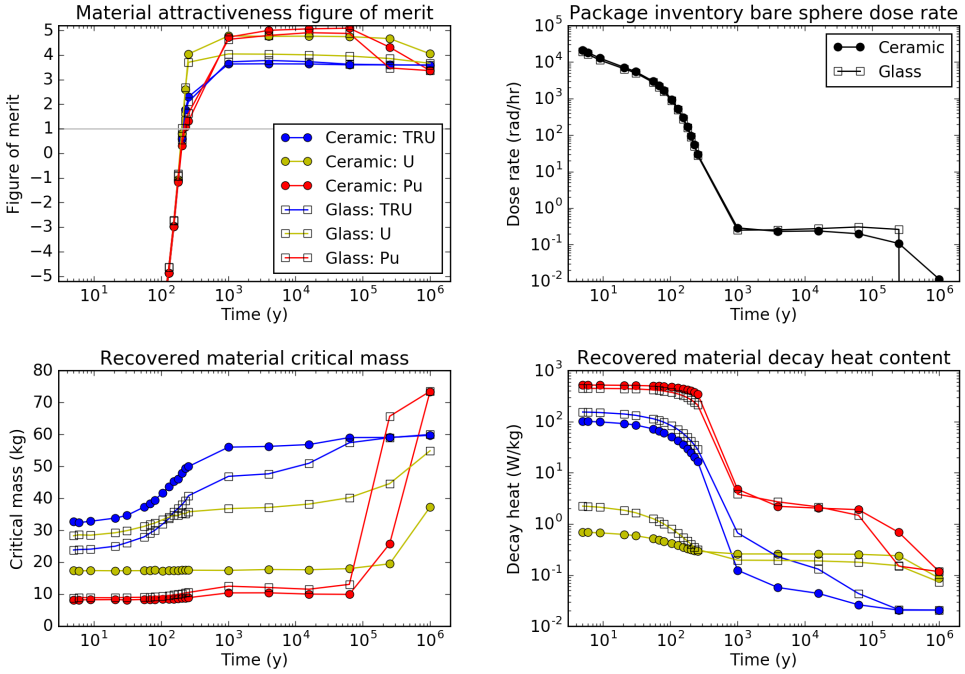

Figure B.80: FOM evaluation for U, Pu, and TRU in HLW glass and ceramic from 40.CR—ADS/PWR—Th/U3.

Appendix C

Waste stream repository footprint

This appendix presents results for disposal area required for each fuel cycle waste stream plotted against surface storage time and parameterized by waste package loading (for SNF) and waste form loading (for HLW). The legend indicates waste package and waste form loading options and the package inventory produced for the fuel cycle to generate 1 GWe-y of electricity. Because some fuel cycles produce multiple waste streams, the figures are split by un-numbered sections. Figures for 1.OT—PWR—U, 13.LR—PWR/PWR—U/Pu, and 23.CR—SFR—U/Pu (ceramic HLW) are included in Chapter 4 Section 4.4.

In some cases, different waste package or waste form loading options are shown to require different disposal areas despite the legend indicating that they produce the same number of packages. This is due to rounding — the repository footprint calculation was performed on the basis of 100 GWe-y and was renormalized to 1 GWe-y. For example, two different options for HLW loading fractions for the same waste form (say, $x_w = 0.3$ and $x_w = 0.4$) should produce different number of packages. If the number of packages is sufficiently small (say, 1.0 and 0.75 packages per 100 GWe-y), then per GWe-y the result for both cases would round to 0.01 packages/GWe-y.

2.OT—HTGR—U

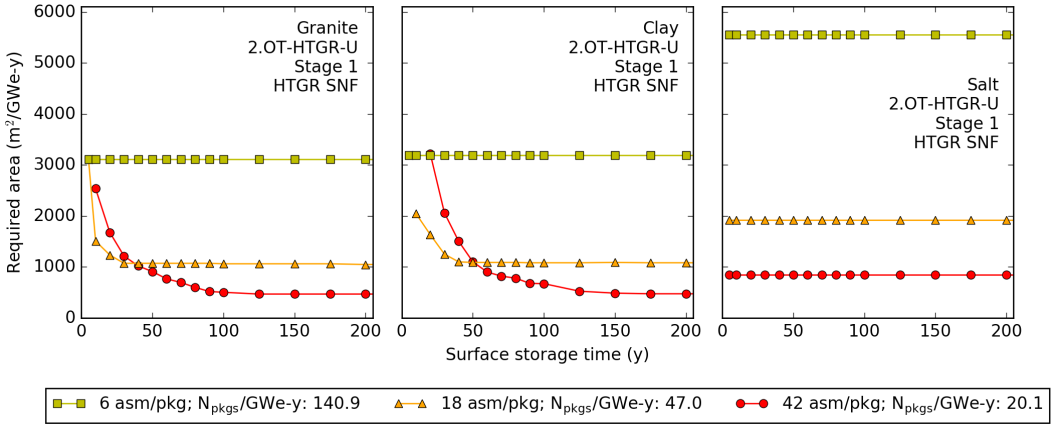

Figure C.1: Repository area versus surface storage time for disposal of SNF from 2.OT—HTGR—U.

3.OT—HWR—U

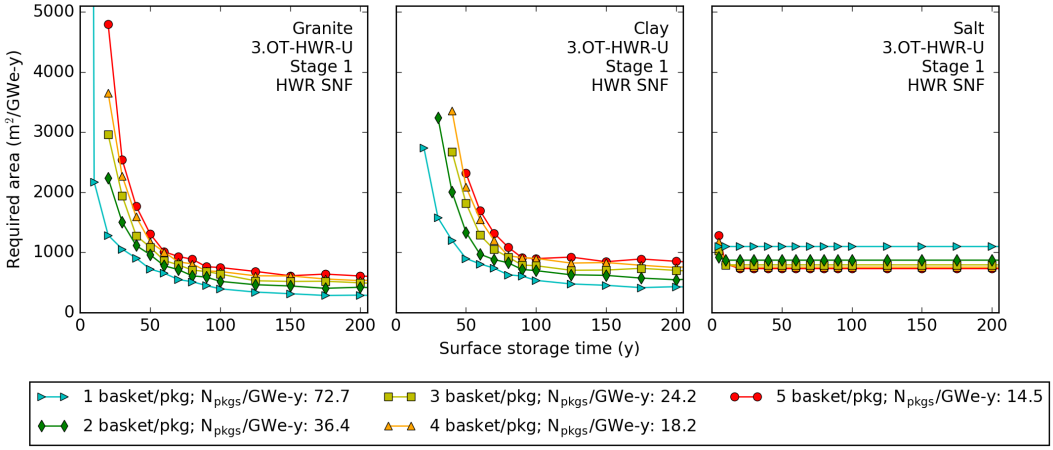

Figure C.2: Repository area versus surface storage time for disposal of SNF from 3.OT—HWR—U.

4.OT—SFR—U

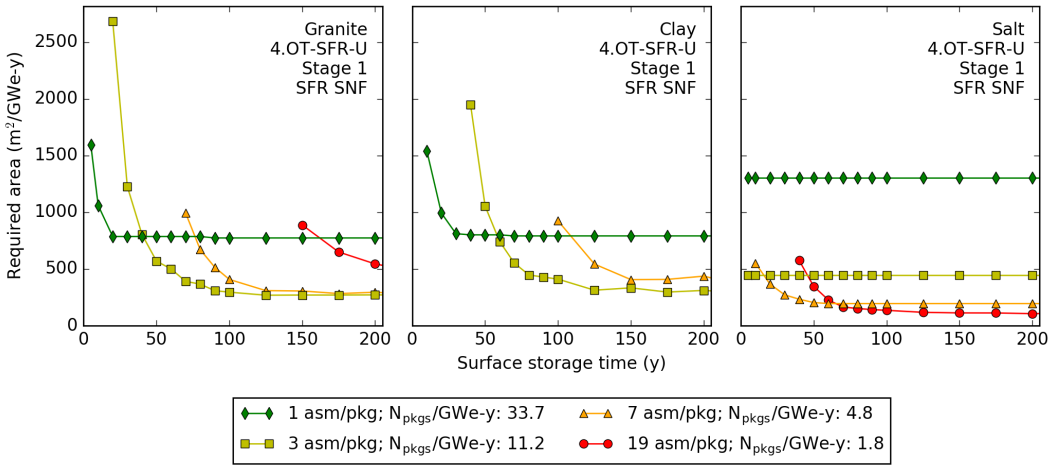

Figure C.3: Repository area versus surface storage time for disposal of SNF from 4.OT—SFR—U.

5.OT—HTGR—U/Th

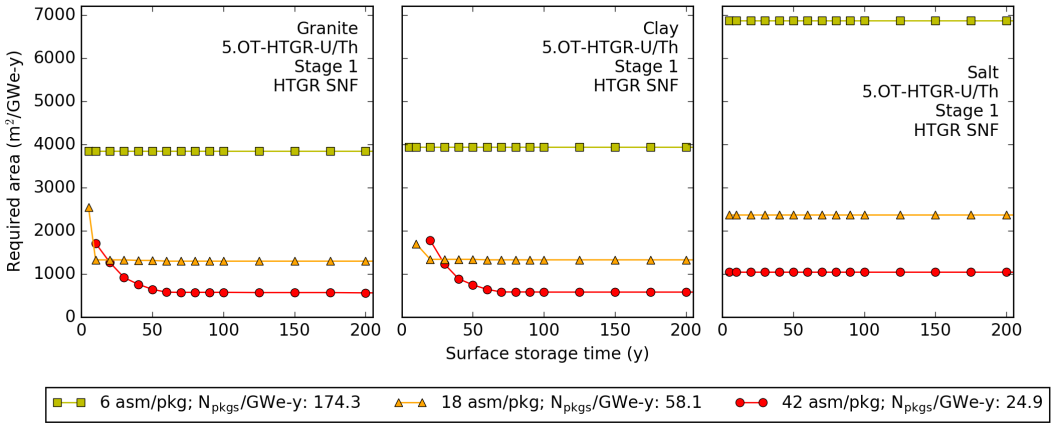

Figure C.4: Repository area versus surface storage time for disposal of SNF from 5.OT—HTGR—U/Th.

6.OT—FFH—Th

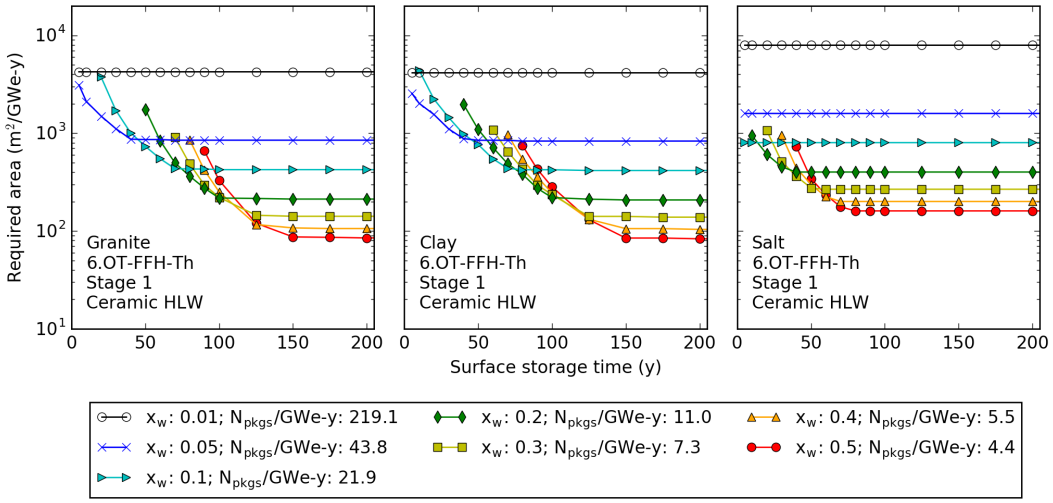

Figure C.5: Repository area versus surface storage time for disposal of ceramic HLW from 6.OT—FFH—Th.

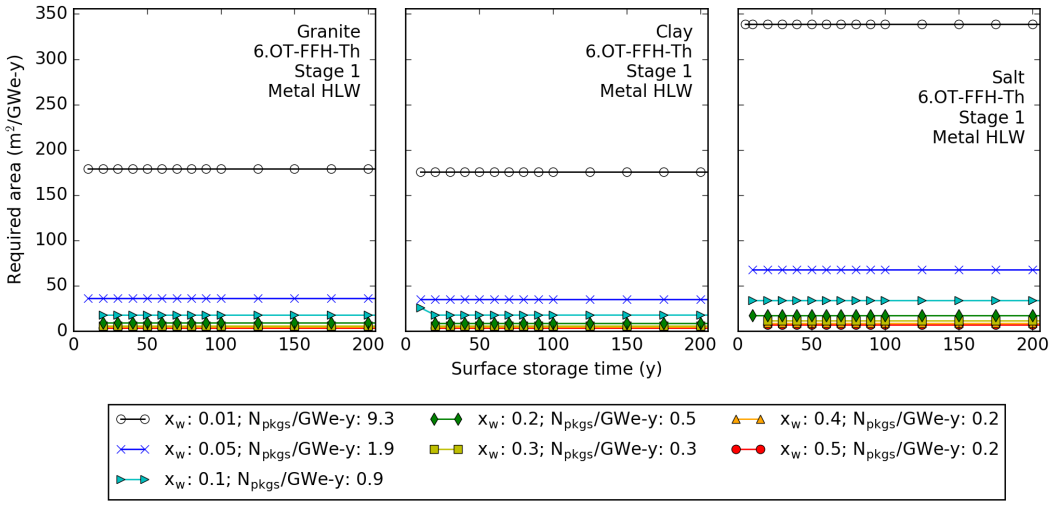

Figure C.6: Repository area versus surface storage time for disposal of metal HLW from 6.OT—FFH—Th.

7.OT—ADS—U

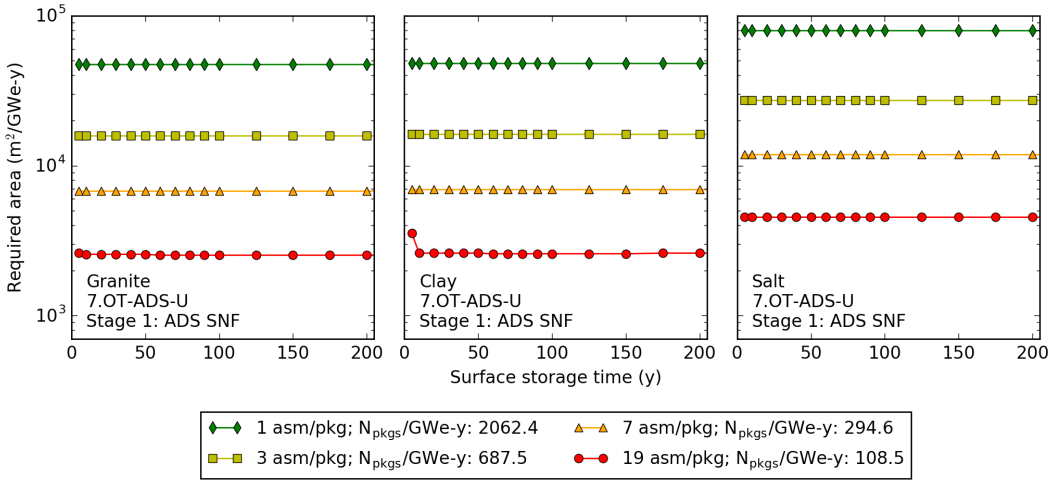

Figure C.7: Repository area versus surface storage time for disposal of SNF from 7.OT—ADS—U.

8.OT—FFH—Th

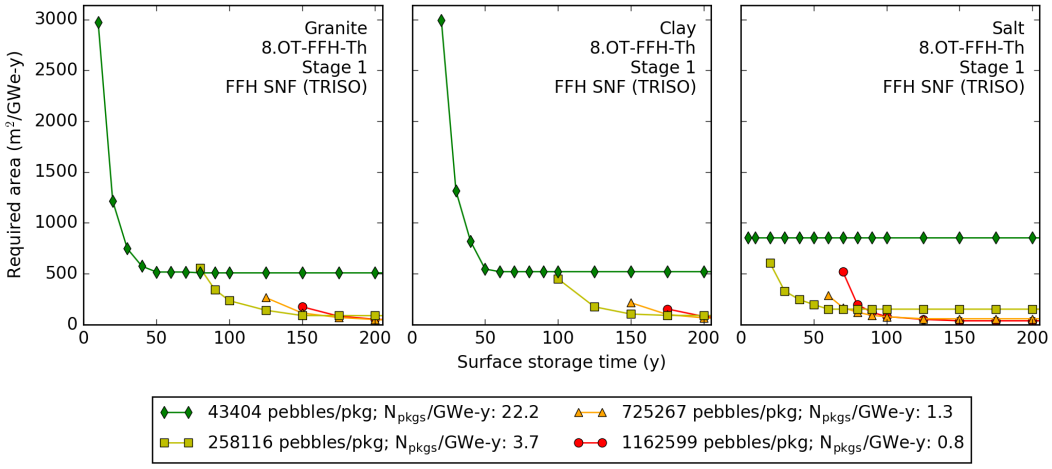

Figure C.8: Repository area versus surface storage time for disposal of SNF from 8.OT—FFH—Th.

9.LR—SFR—U/TRU

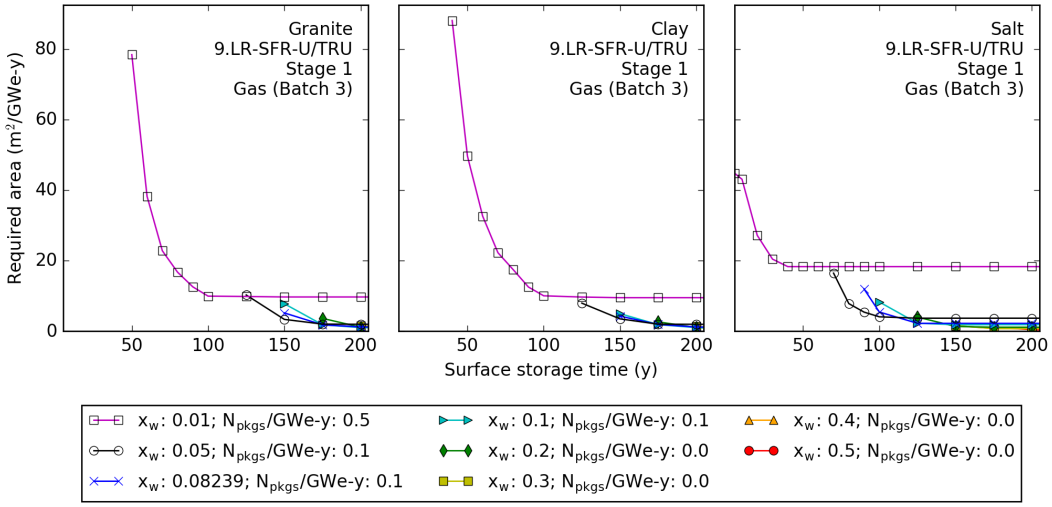

Figure C.9: Repository area versus surface storage time for disposal of gas HLW (Batch 3) from 9.LR—SFR—U/TRU.

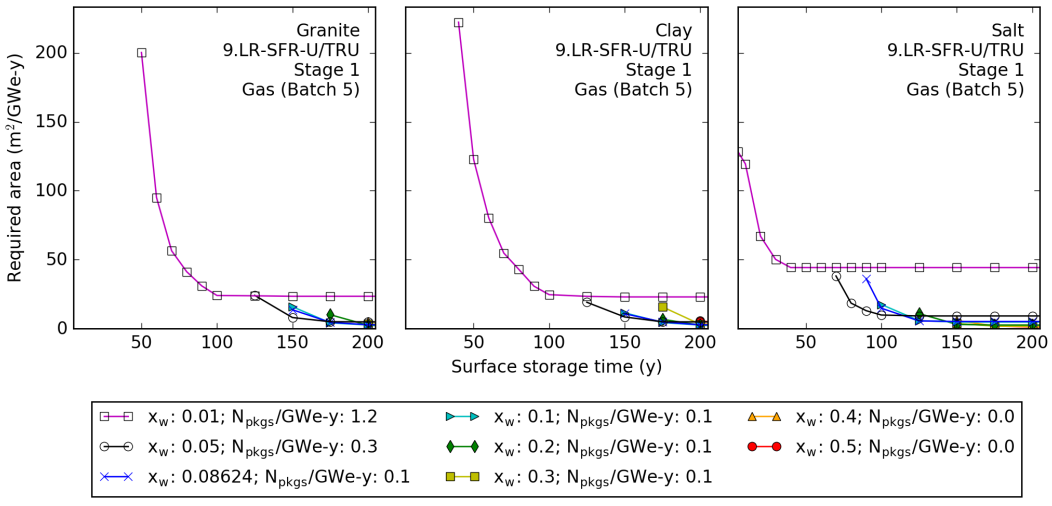

Figure C.10: Repository area versus surface storage time for disposal of gas HLW (Batch 5) from 9.LR—SFR—U/TRU.

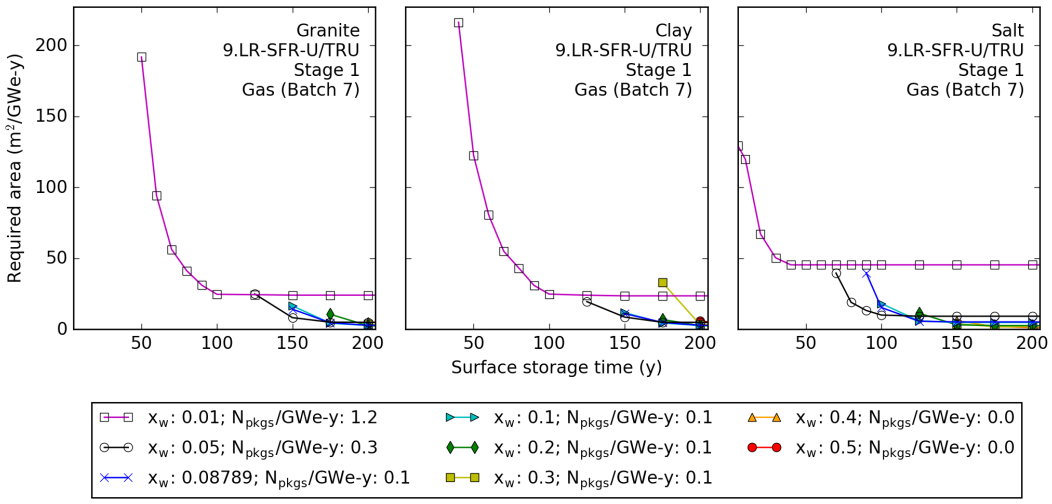

Figure C.11: Repository area versus surface storage time for disposal of gas HLW (Batch 7) from 9.LR—SFR—U/TRU.

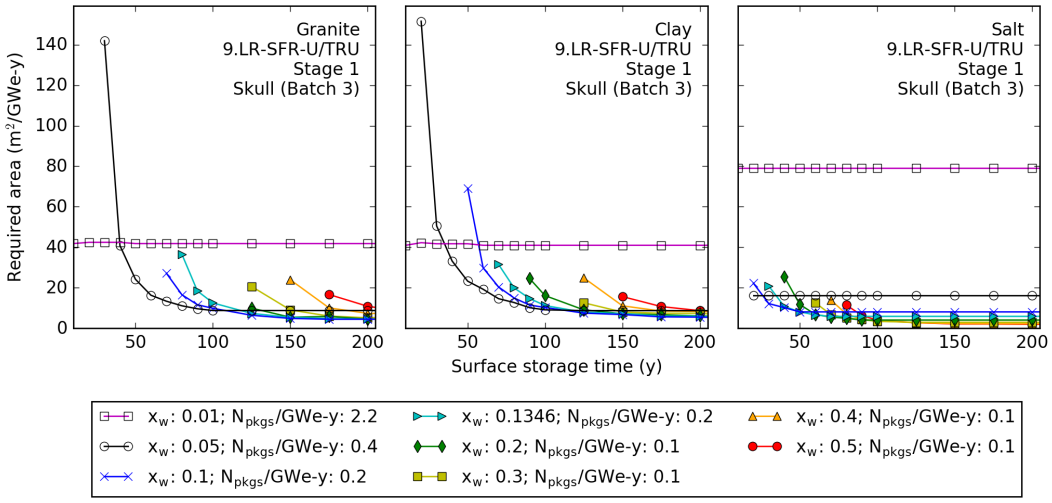

Figure C.12: Repository area versus surface storage time for disposal of HLW skull (Batch 3) from 9.LR—SFR—U/TRU.

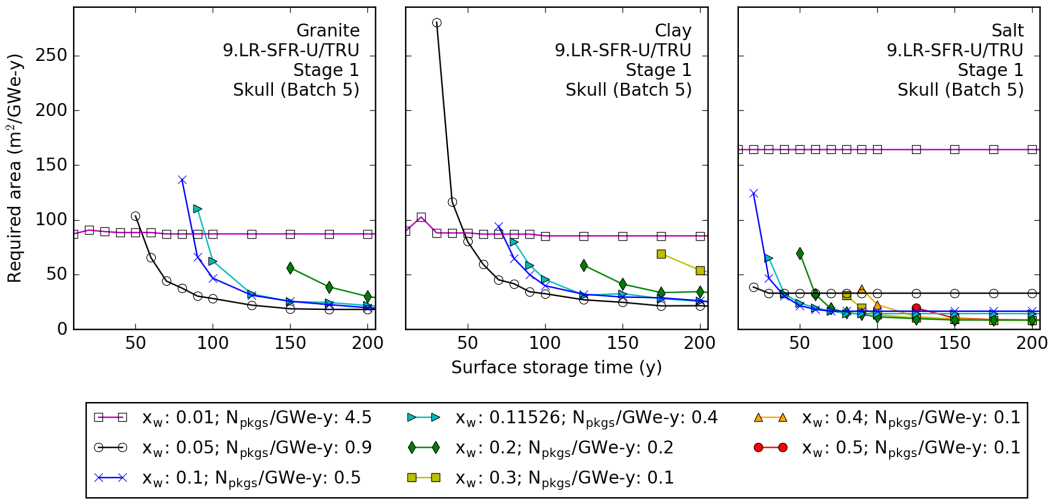

Figure C.13: Repository area versus surface storage time for disposal of HLW skull (Batch 5) from 9.LR—SFR—U/TRU.

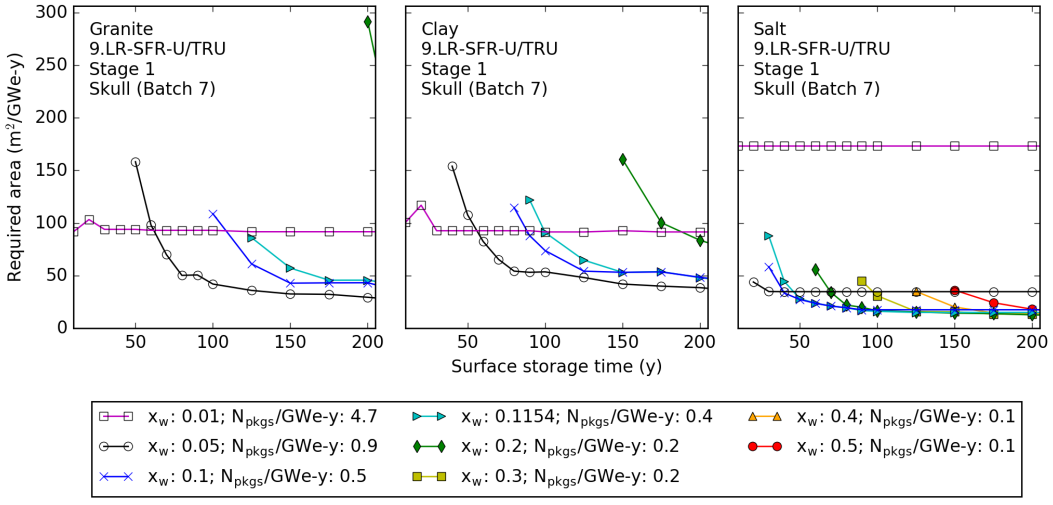

Figure C.14: Repository area versus surface storage time for disposal of HLW skull (Batch7) from 9.LR—SFR—U/TRU.

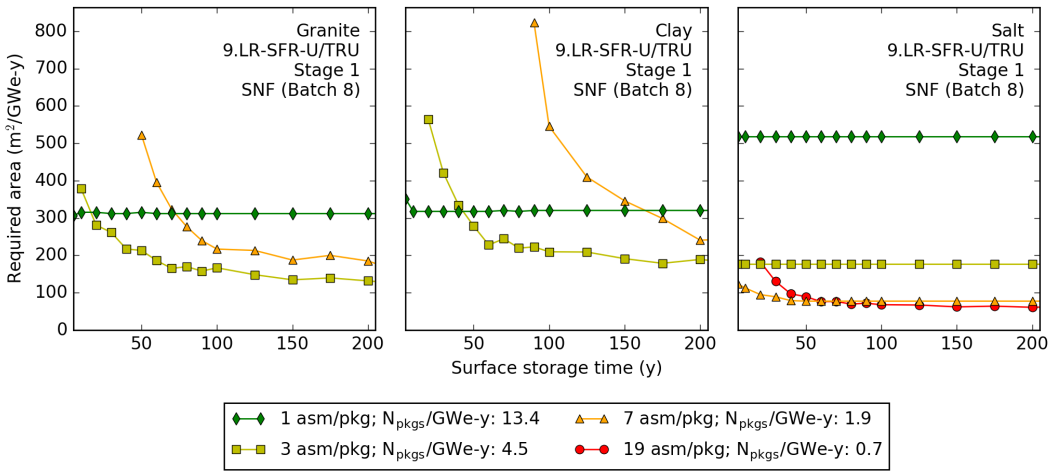

Figure C.15: Repository area versus surface storage time for disposal of SNF (Batch 8) from 9.LR—SFR—U/TRU.

10.LR—MSR—Th/U3

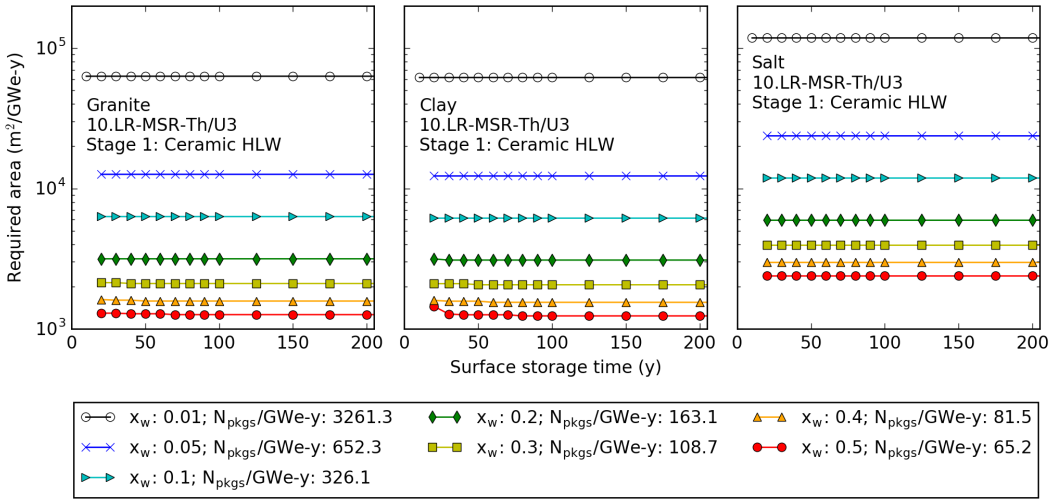

Figure C.16: Repository area versus surface storage time for disposal of ceramic HLW from 10.LR—MSR—Th/U3.

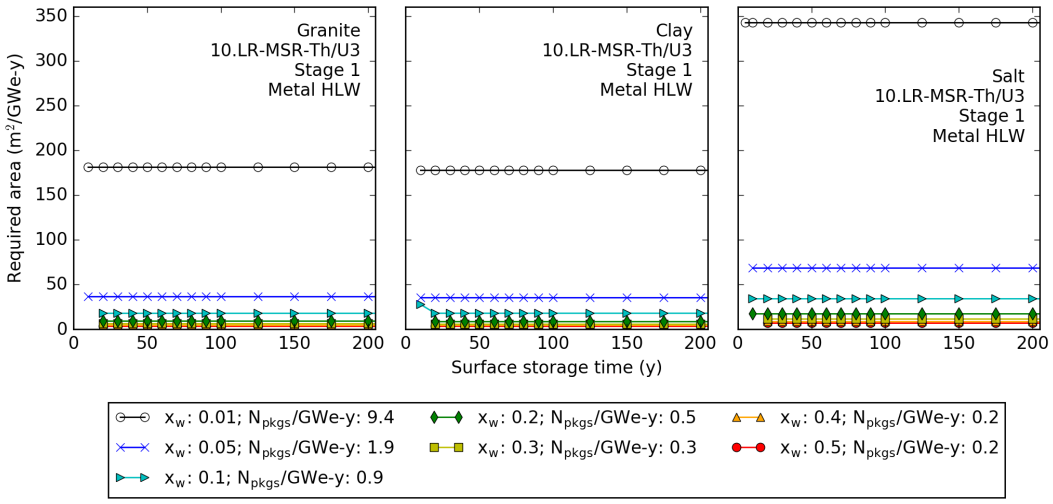

Figure C.17: Repository area versus surface storage time for disposal of metal HLW from 10.LR—MSR—Th/U3.

11.LR—SFR—U/Th/U3

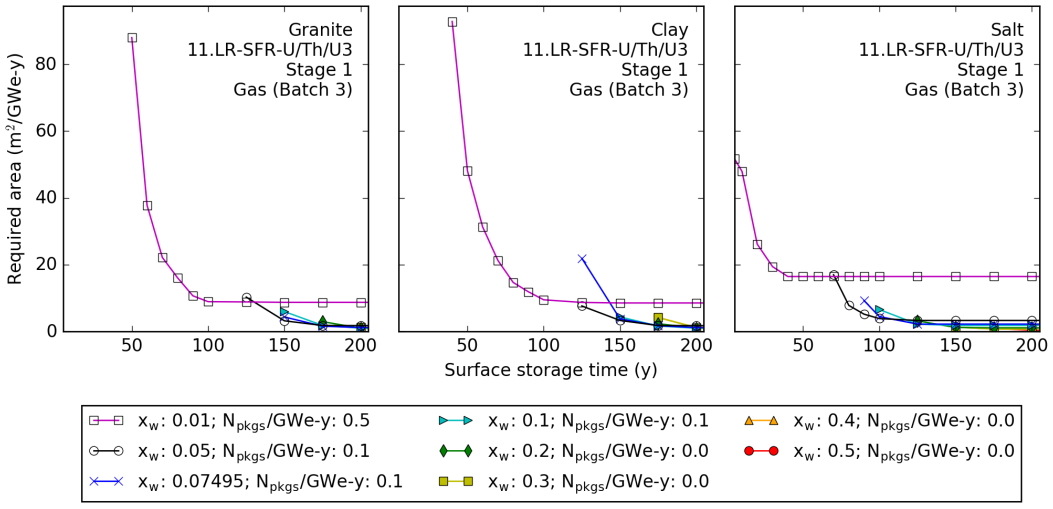

Figure C.18: Repository area versus surface storage time for disposal of gas HLW (Batch 3) from 11.LR—SFR—U/Th/U3.

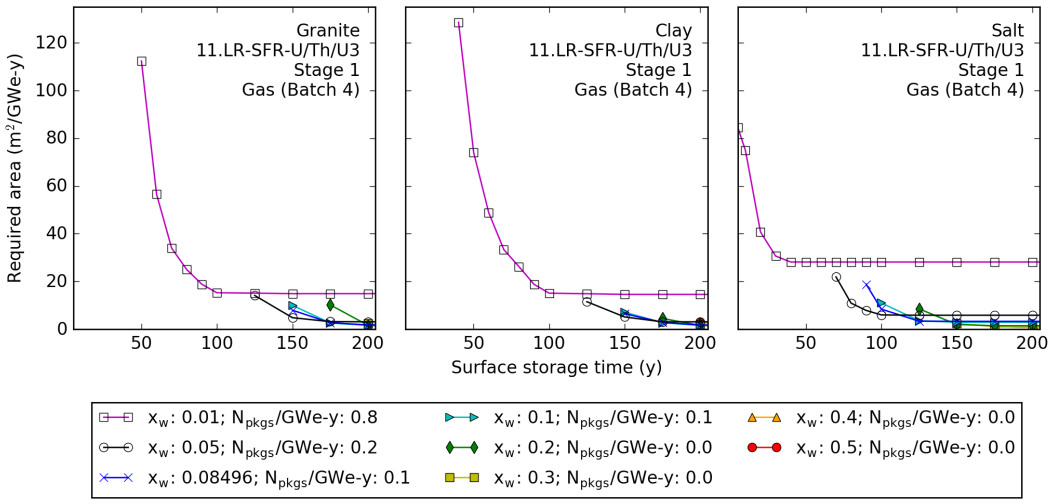

Figure C.19: Repository area versus surface storage time for disposal of gas HLW (Batch 4) from 11.LR—SFR—U/Th/U3.

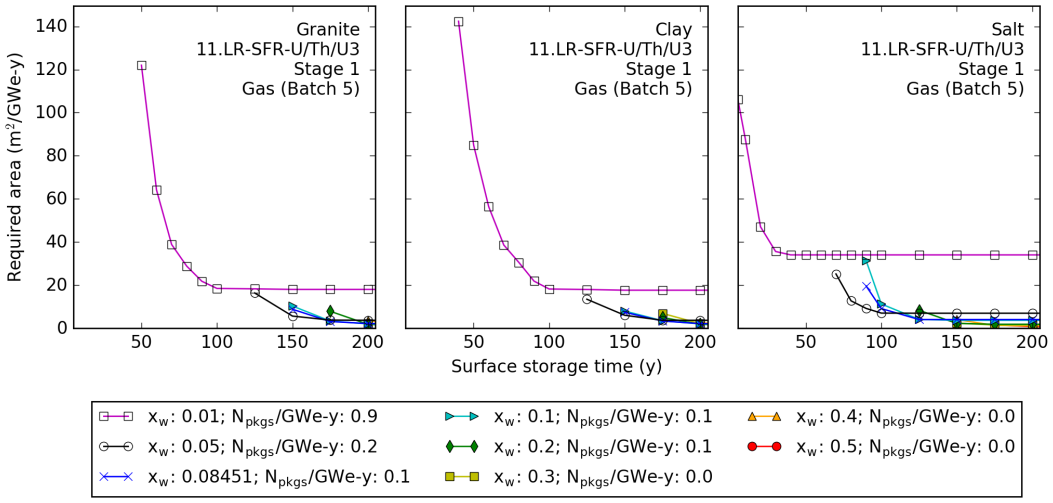

Figure C.20: Repository area versus surface storage time for disposal of gas HLW (Batch 5) from 11.LR—SFR—U/Th/U3.

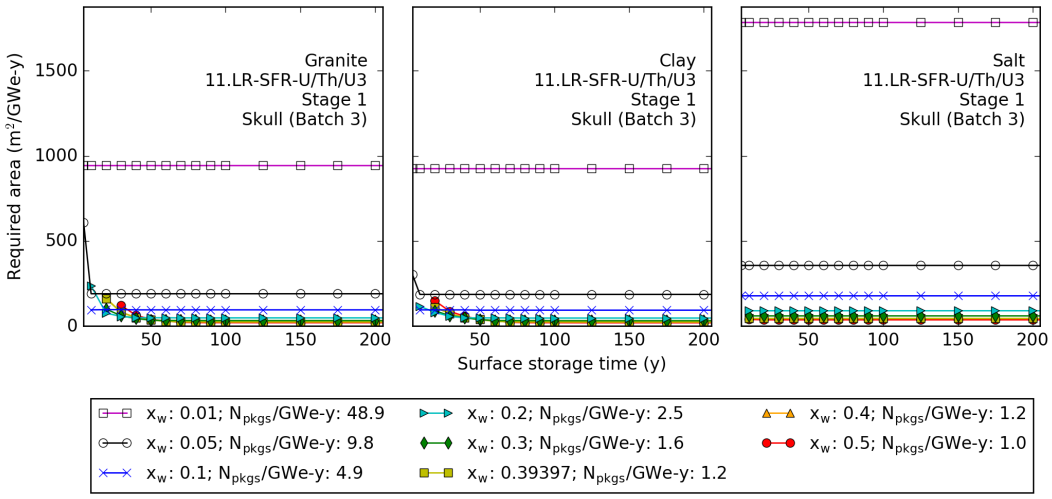

Figure C.21: Repository area versus surface storage time for disposal of HLW skull (Batch 3) from 11.LR—SFR—U/Th/U3.

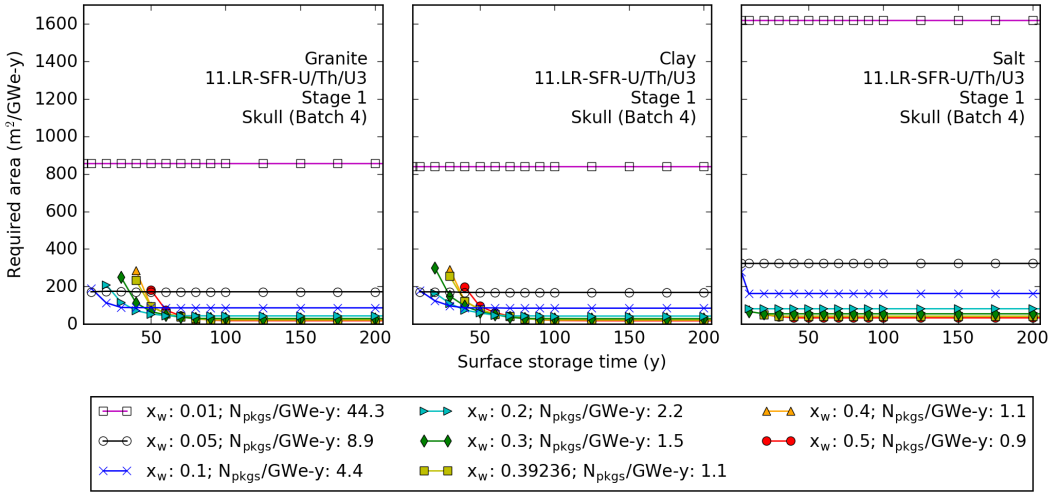

Figure C.22: Repository area versus surface storage time for disposal of HLW skull (Batch 4) from 11.LR—SFR—U/Th/U3.

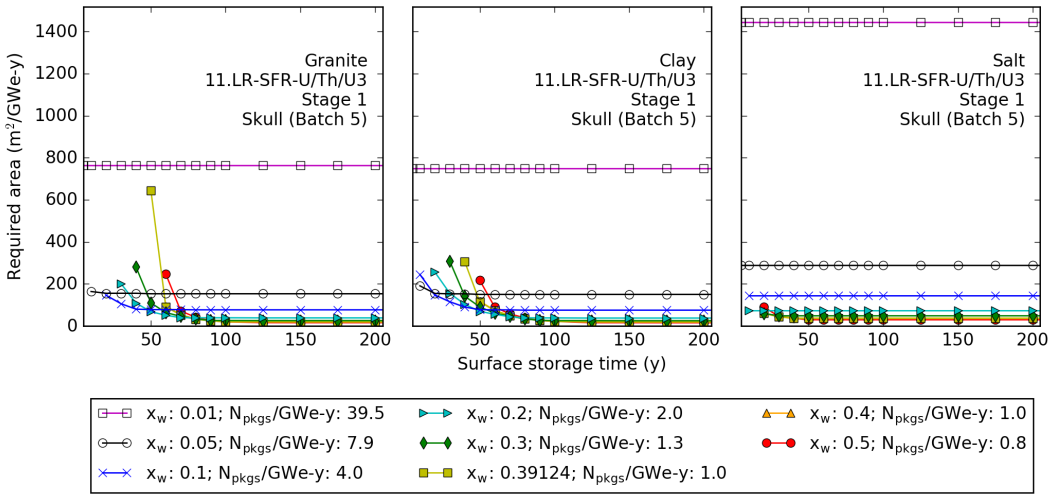

Figure C.23: Repository area versus surface storage time for disposal of HLW skull (Batch 5) from 11.LR—SFR—U/Th/U3.

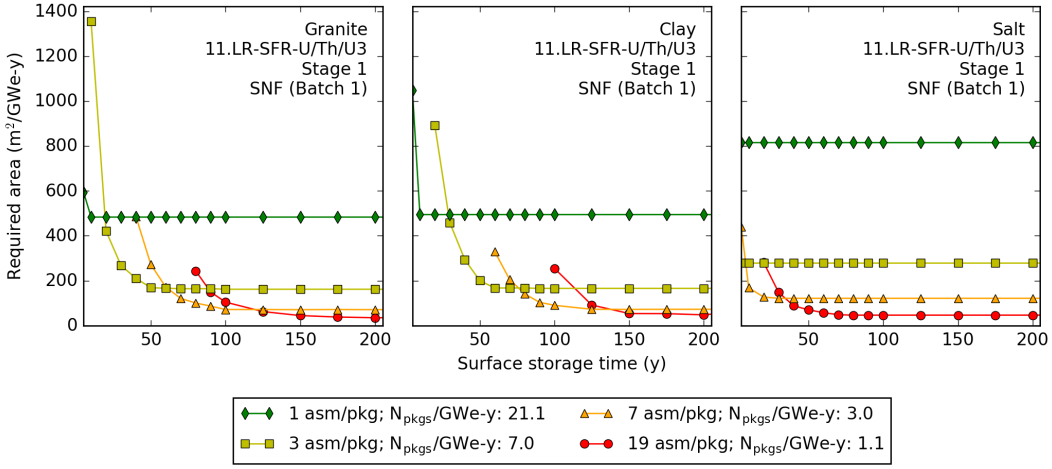

Figure C.24: Repository area versus surface storage time for disposal of SNF (Batch 1) from 11.LR—SFR—U/Th/U3.

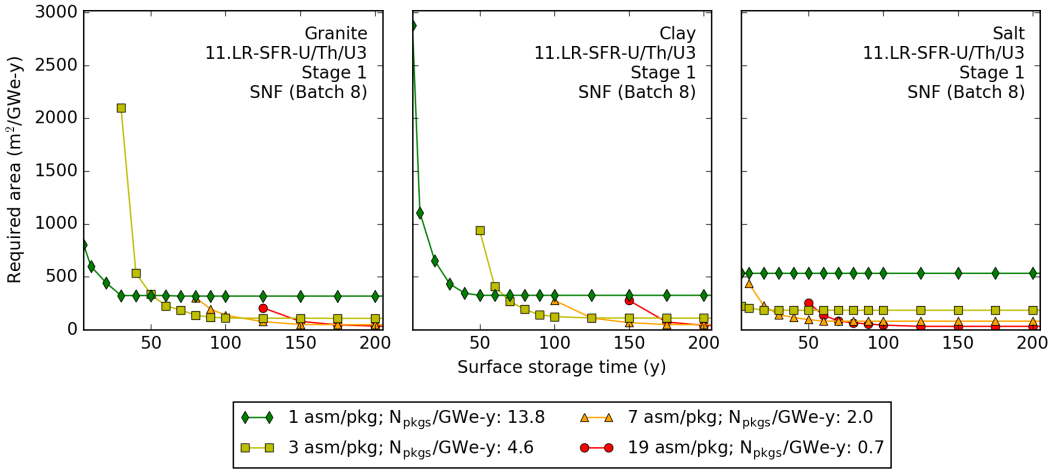

Figure C.25: Repository area versus surface storage time for disposal of SNF (Batch 8) from 11.LR—SFR—U/Th/U3.

12.LR—HWR/PWR—U/Pu

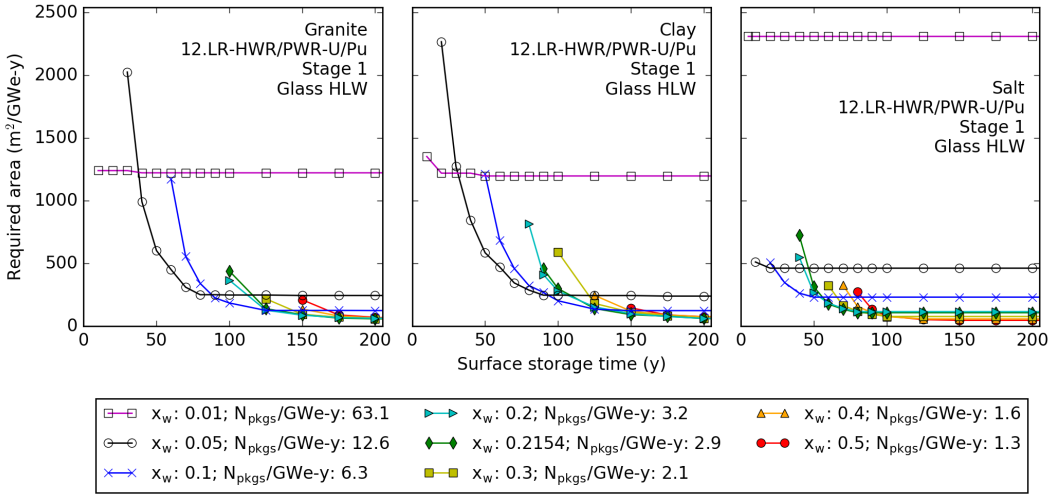

Figure C.26: Repository area versus surface storage time for disposal of glass HLW from 12.LR—HWR/PWR—U/Pu.

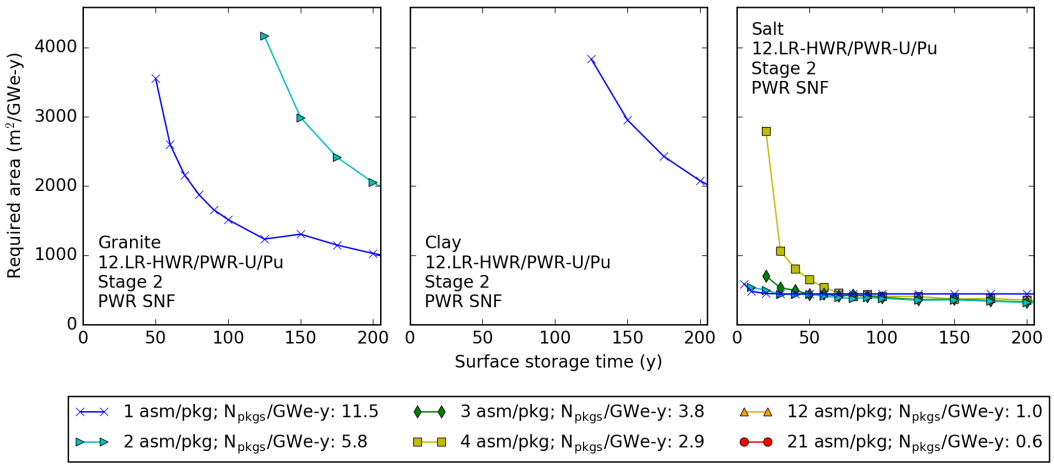

Figure C.27: Repository area versus surface storage time for disposal of SNF from 12.LR—HWR/PWR—U/Pu.

14.LR—SFR/PWR—U/Pu

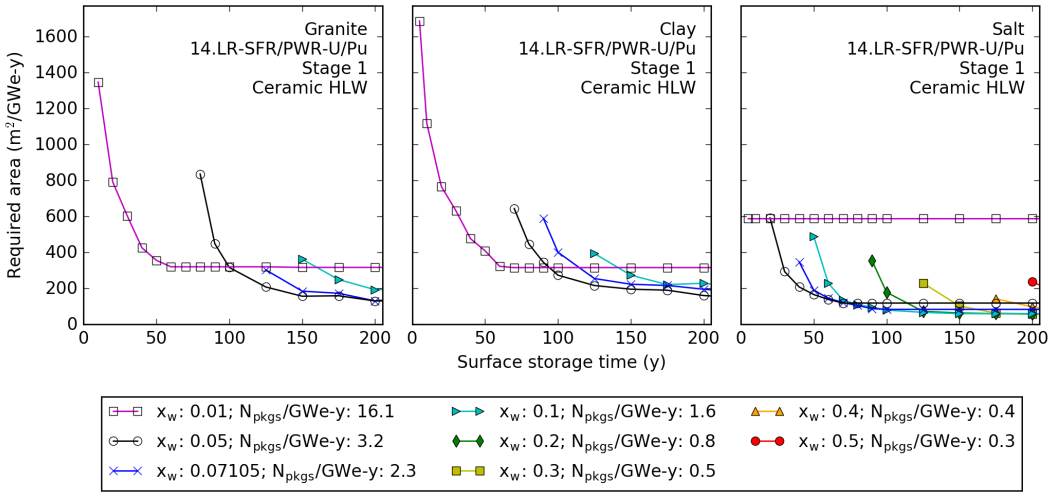

Figure C.28: Repository area versus surface storage time for disposal of ceramic HLW from 14.LR—SFR/PWR—U/Pu.

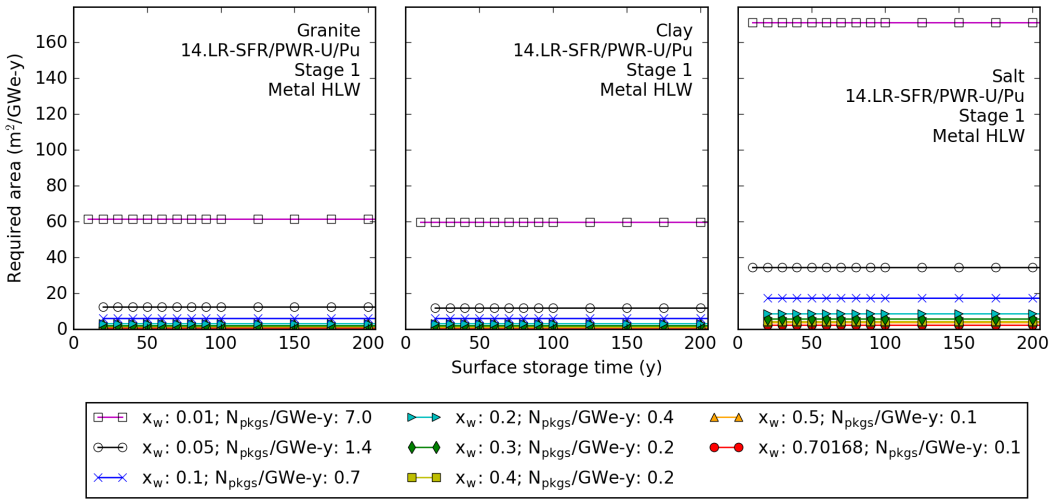

Figure C.29: Repository area versus surface storage time for disposal of metal HLW from 14.LR—SFR/PWR—U/Pu.

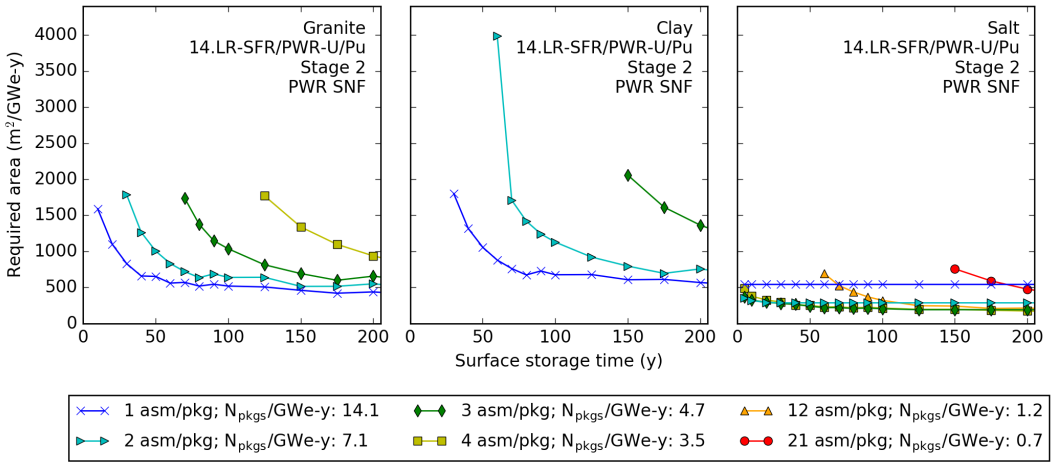

Figure C.30: Repository area versus surface storage time for disposal of SNF from 14.LR—SFR/PWR—U/Pu.

15.LR—PWR/SFR—U/Pu

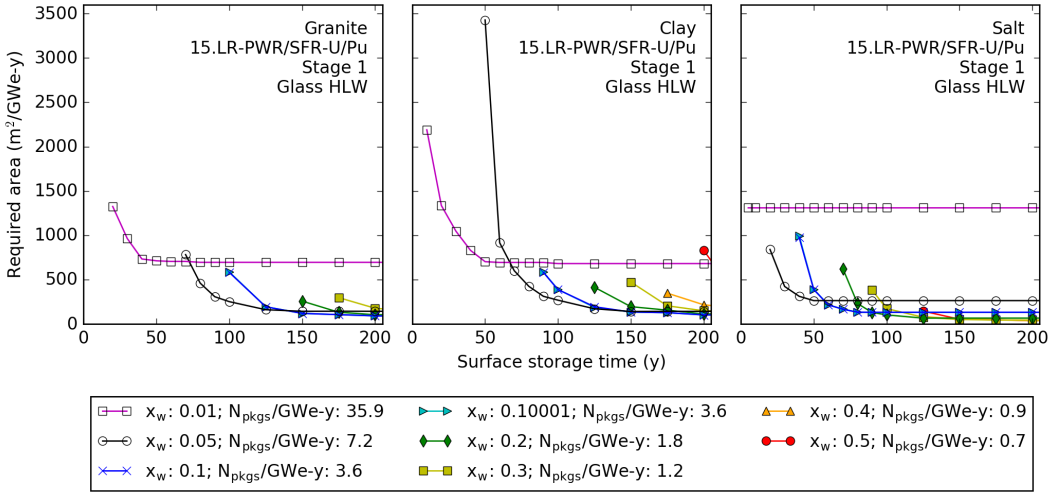

Figure C.31: Repository area versus surface storage time for disposal of glass HLW from 15.LR—PWR/SFR—U/Pu.

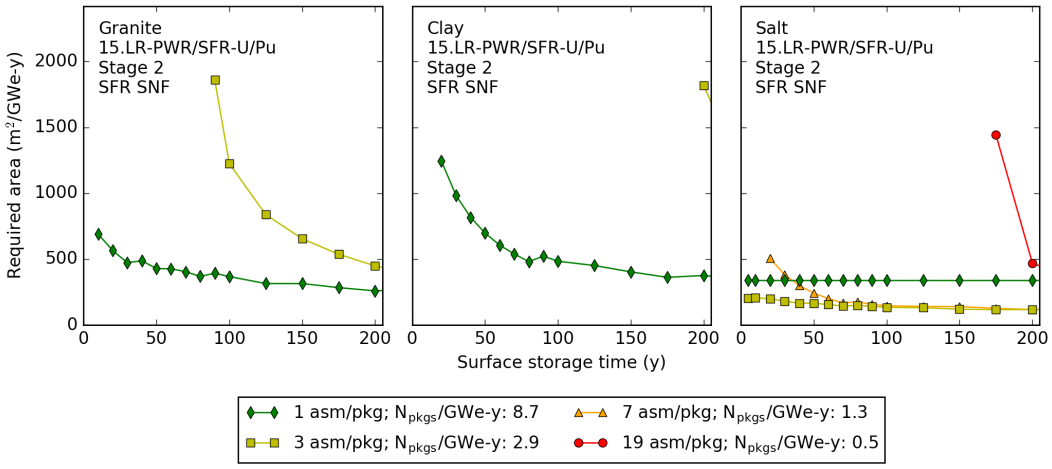

Figure C.32: Repository area versus surface storage time for disposal of SNF from 15.LR—PWR/SFR—U/Pu.

16.LR—PWR/ADS—U/Pu

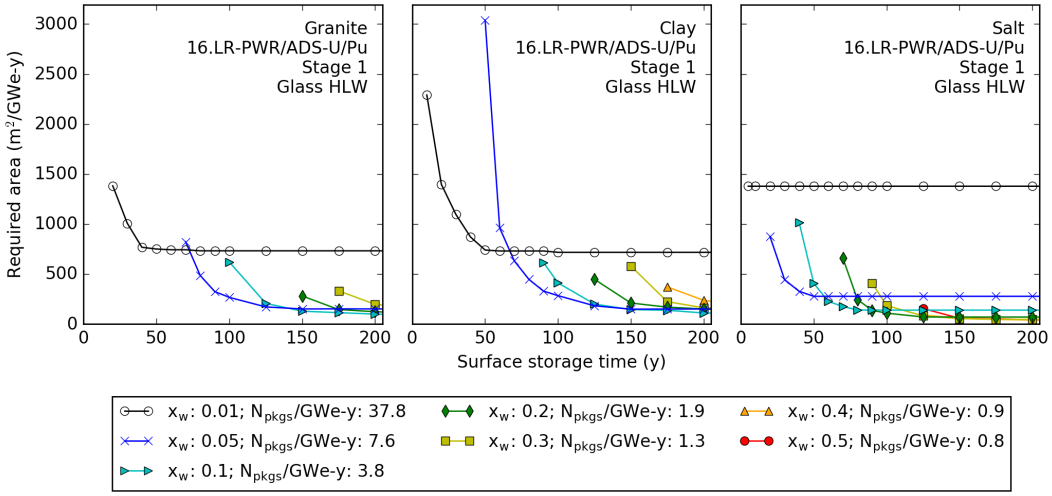

Figure C.33: Repository area versus surface storage time for disposal of glass HLW from 16.LR—PWR/ADS—U/Pu.

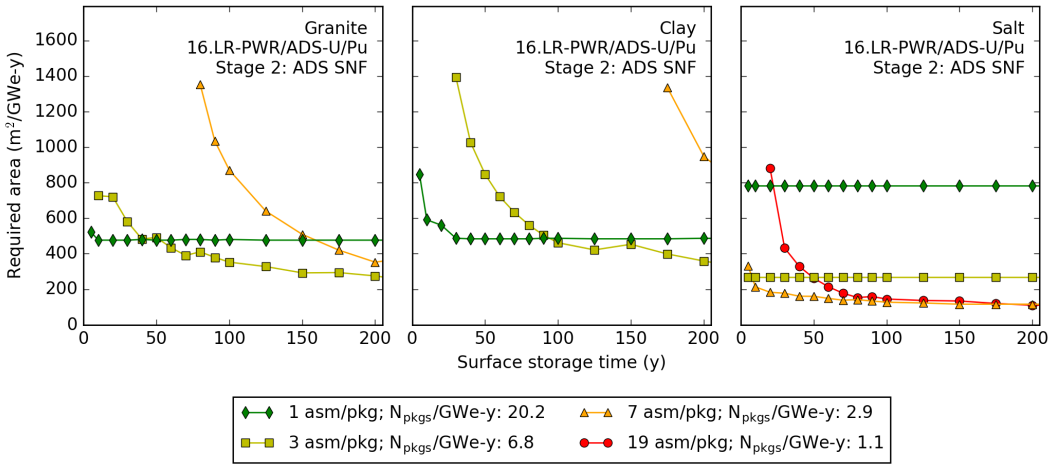

Figure C.34: Repository area versus surface storage time for disposal of SNF from 16.LR—PWR/ADS—U/Pu.

17.LR—PWR/PWR—U/Th/Pu

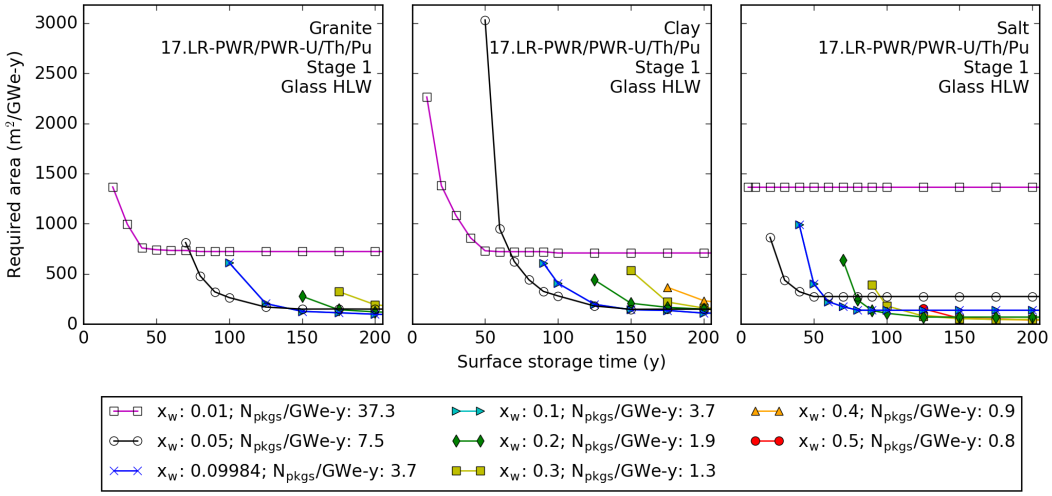

Figure C.35: Repository area versus surface storage time for disposal of glass HLW from 17.LR—PWR/PWR—U/Th/Pu.

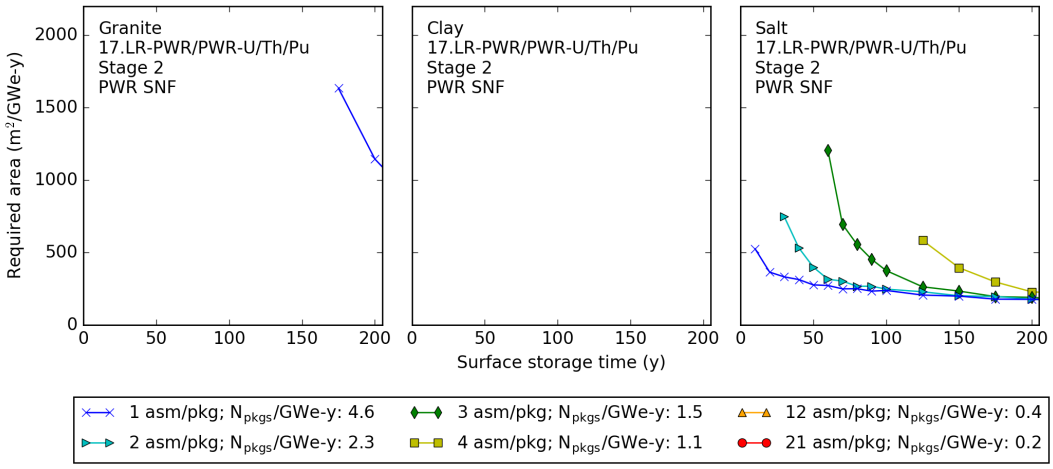

Figure C.36: Repository area versus surface storage time for disposal of SNF from 17.LR—PWR/PWR—U/Th/Pu.

18.LR—PWR/PWR—U/Th/U3

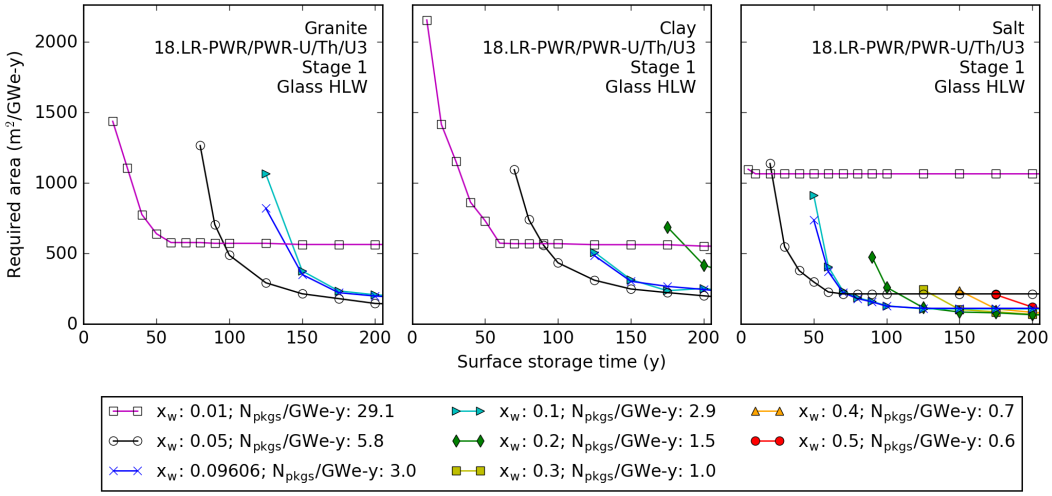

Figure C.37: Repository area versus surface storage time for disposal of glass HLW from 18.LR—PWR/PWR—U/Th/U3.

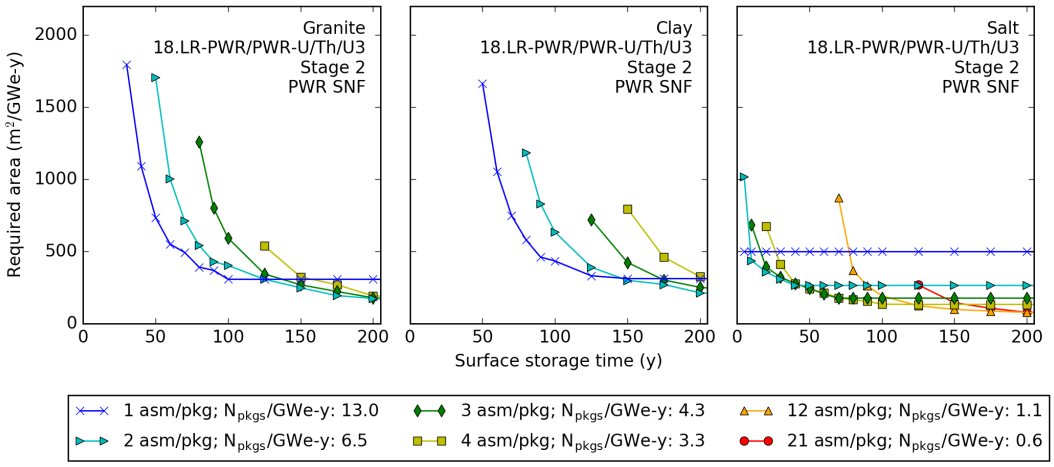

Figure C.38: Repository area versus surface storage time for disposal of SNF from 18.LR—PWR/PWR—U/Th/U3.

19.CR—HWR—U/Pu

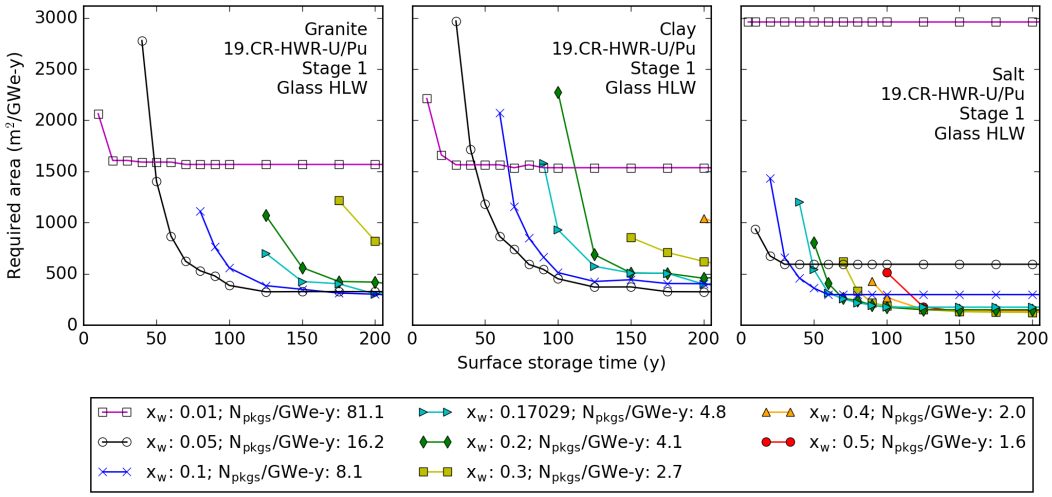

Figure C.39: Repository area versus surface storage time for disposal of glass HLW from 19.CR—HWR—U/Pu.

20.CR—HWR—U/TRU

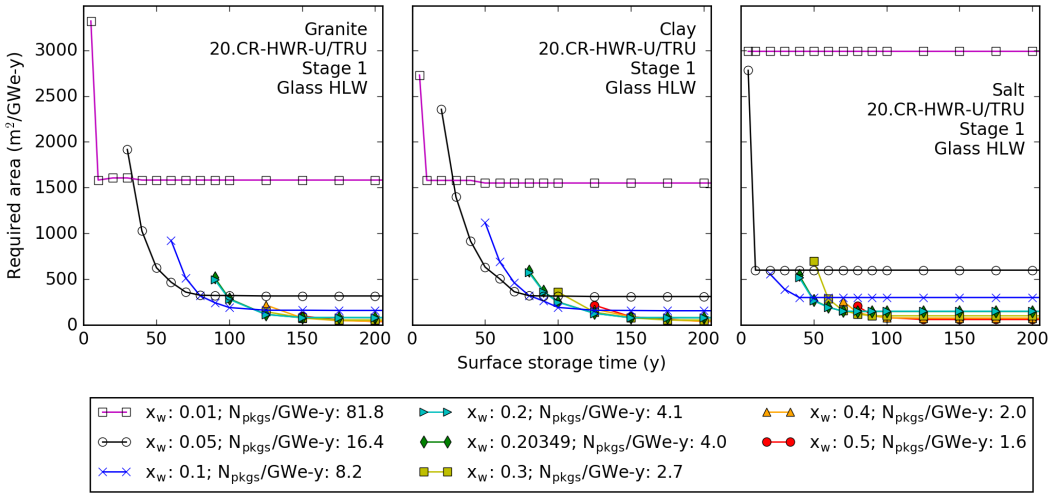

Figure C.40: Repository area versus surface storage time for disposal of glass HLW from 20.CR—HWR—U/TRU.

21.CR—PWR—U/Pu

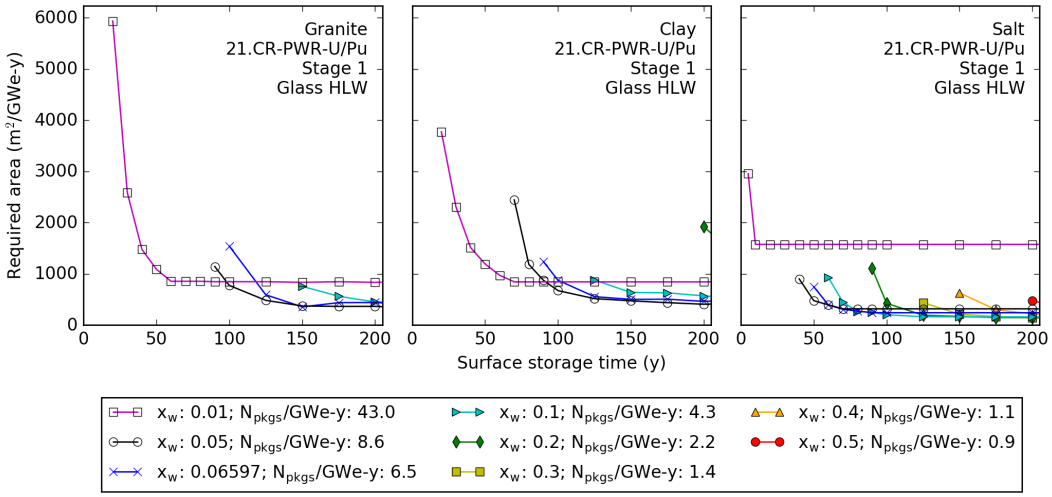

Figure C.41: Repository area versus surface storage time for disposal of glass HLW from 21.CR—PWR—U/Pu.

22.CR—PWR—U/TRU

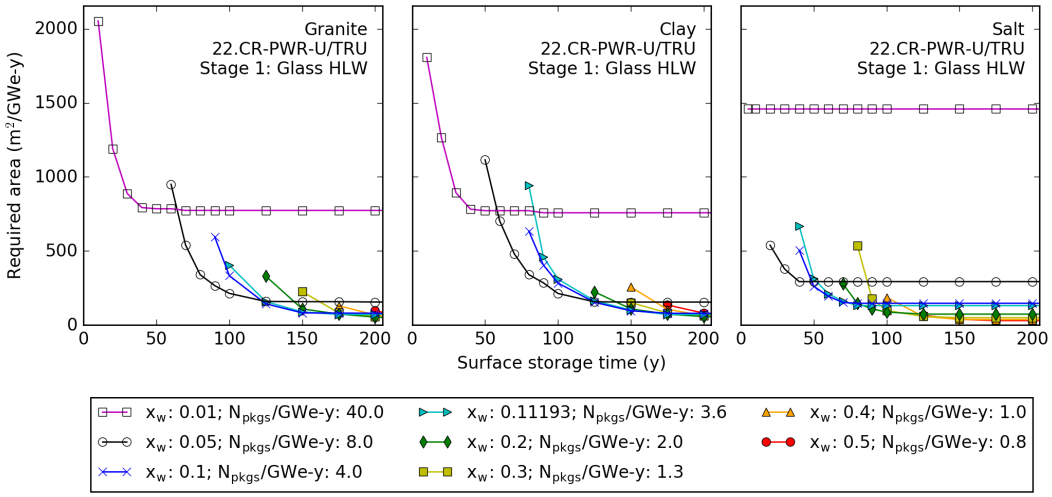

Figure C.42: Repository area versus surface storage time for disposal of glass HLW from 22.CR—PWR—U/TRU.

23.CR—SFR—U/Pu

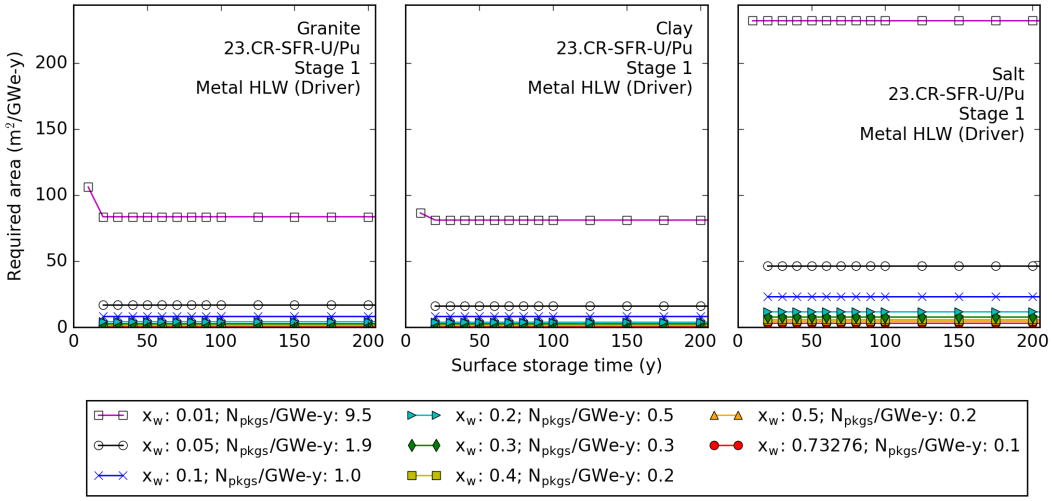

Figure C.43: Repository area versus surface storage time for disposal of metal HLW (driver) from 23.CR—SFR—U/Pu.

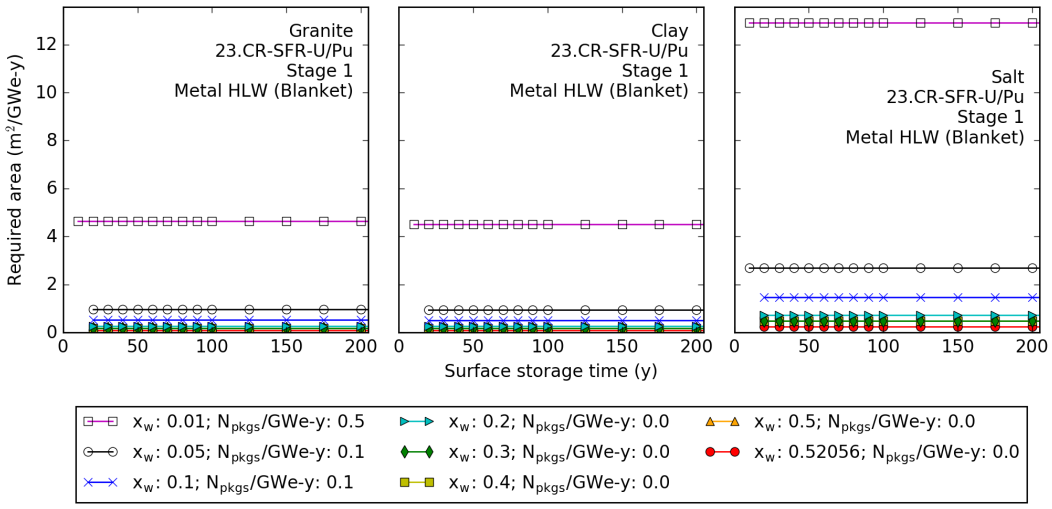

Figure C.44: Repository area versus surface storage time for disposal of metal HLW (blanket) from 23.CR—SFR—U/Pu.

24.CR—SFR—U/TRU

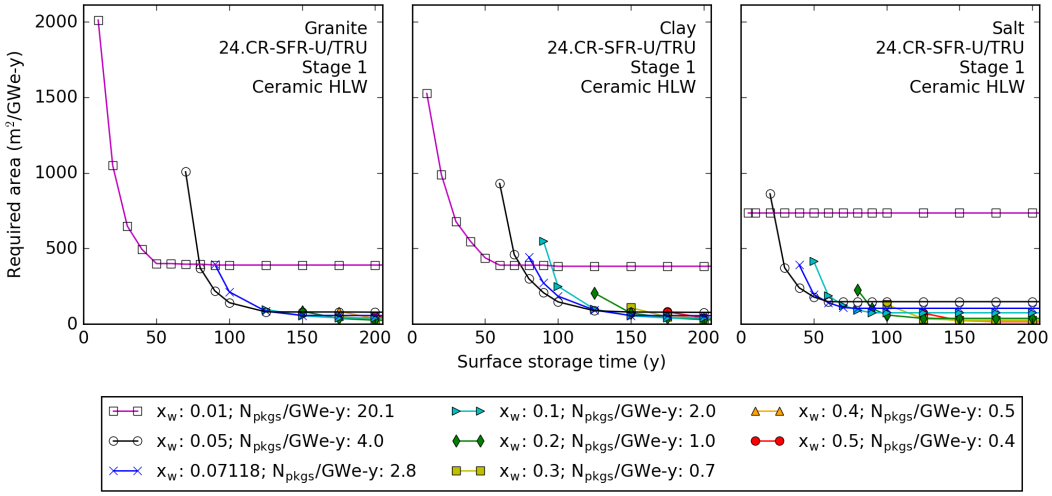

Figure C.45: Repository area versus surface storage time for disposal of ceramic HLW from 24.CR—SFR—U/TRU.

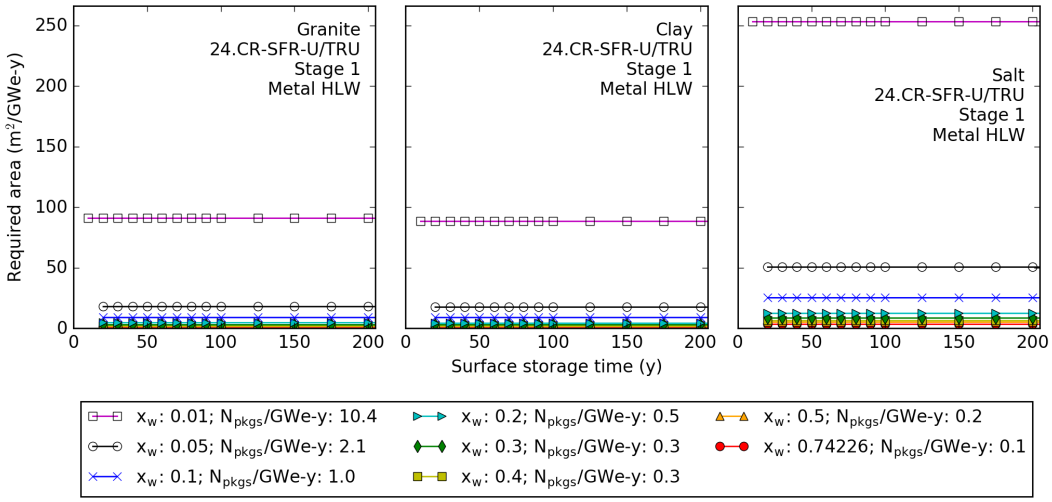

Figure C.46: Repository area versus surface storage time for disposal of metal HLW from 24.CR—SFR—U/TRU.

25.CR—PWR—U/TRU/Th/U3

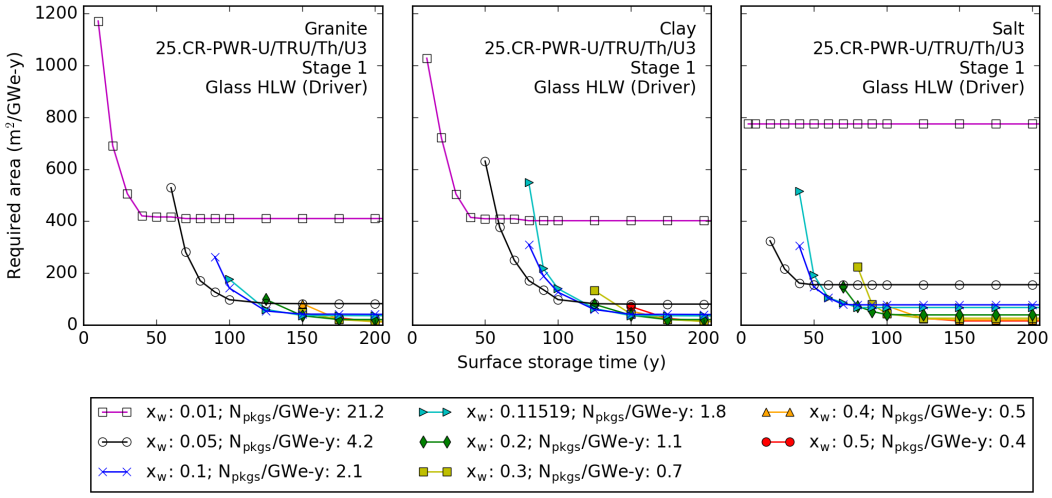

Figure C.47: Repository area versus surface storage time for disposal of glass HLW (driver) from 25.CR—PWR—U/TRU/Th/U3.

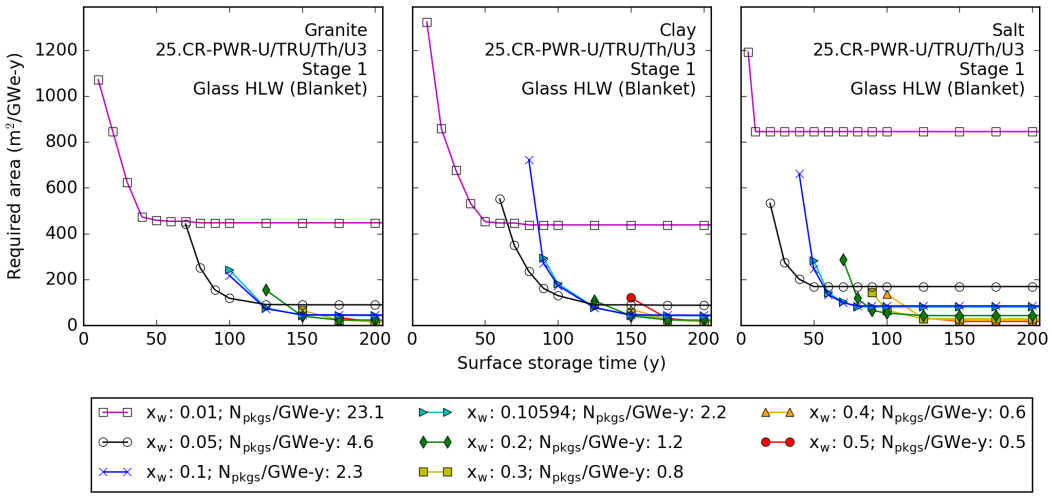

Figure C.48: Repository area versus surface storage time for disposal of glass HLW (blanket) from 25.CR—PWR—U/TRU/Th/U3.

26.CR—MSR—Th/U3/TRU

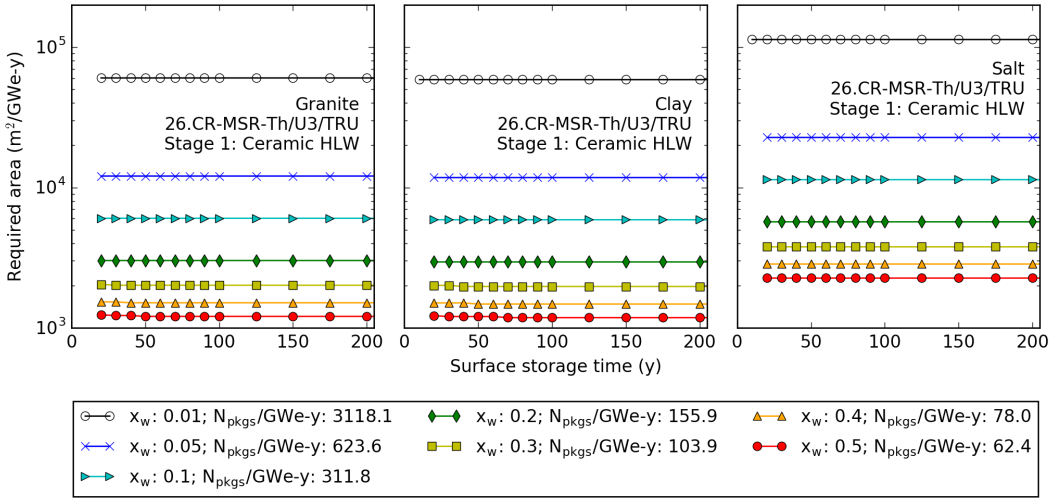

Figure C.49: Repository area versus surface storage time for disposal of ceramic HLW from 26.CR—MSR—Th/U3/TRU.

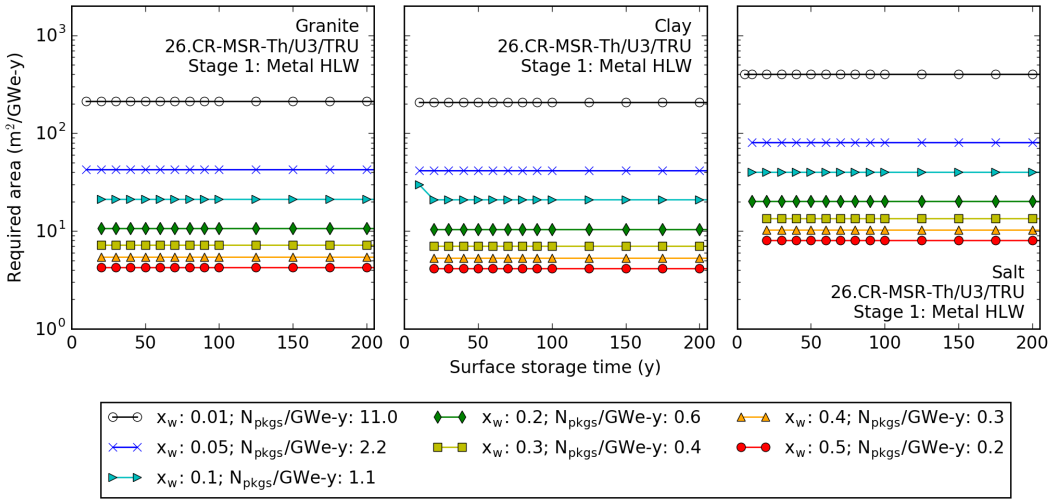

Figure C.50: Repository area versus surface storage time for disposal of metal HLW from 26.CR—MSR—Th/U3/TRU.

27.CR—SFR—U/Th/U3

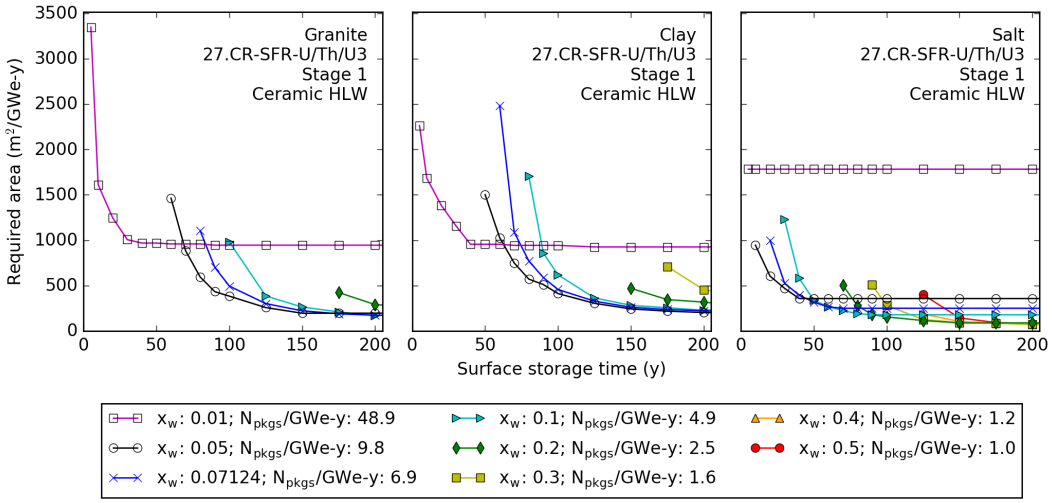

Figure C.51: Repository area versus surface storage time for disposal of ceramic HLW from 27.CR—SFR—U/Th/U3.

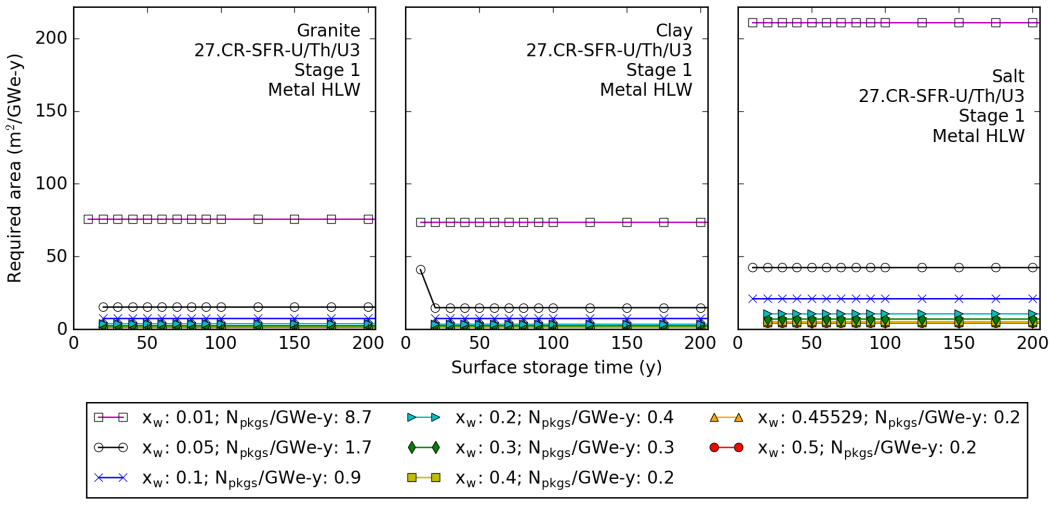

Figure C.52: Repository area versus surface storage time for disposal of metal HLW from 27.CR—SFR—U/Th/U3.

28.CR—SFR—Th/U3

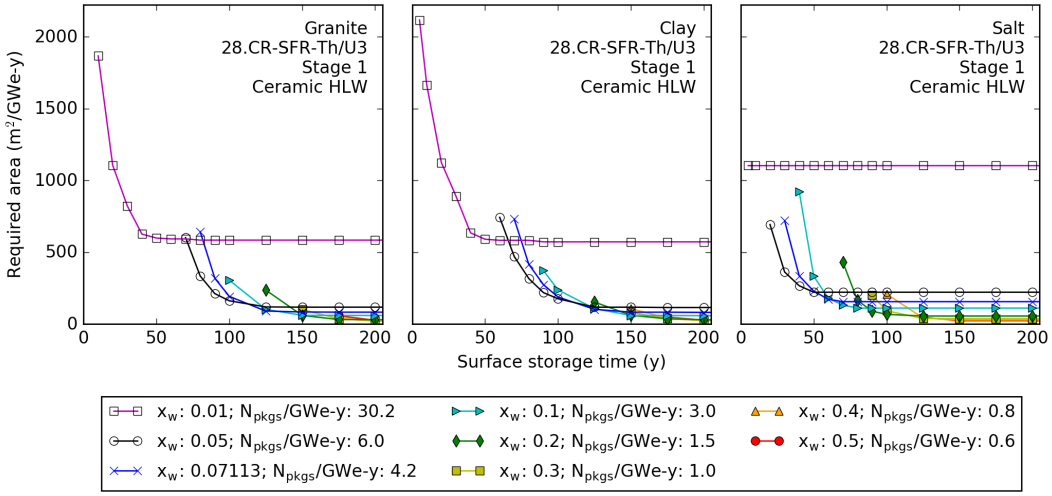

Figure C.53: Repository area versus surface storage time for disposal of ceramic HLW from 28.CR—SFR—Th/U3.

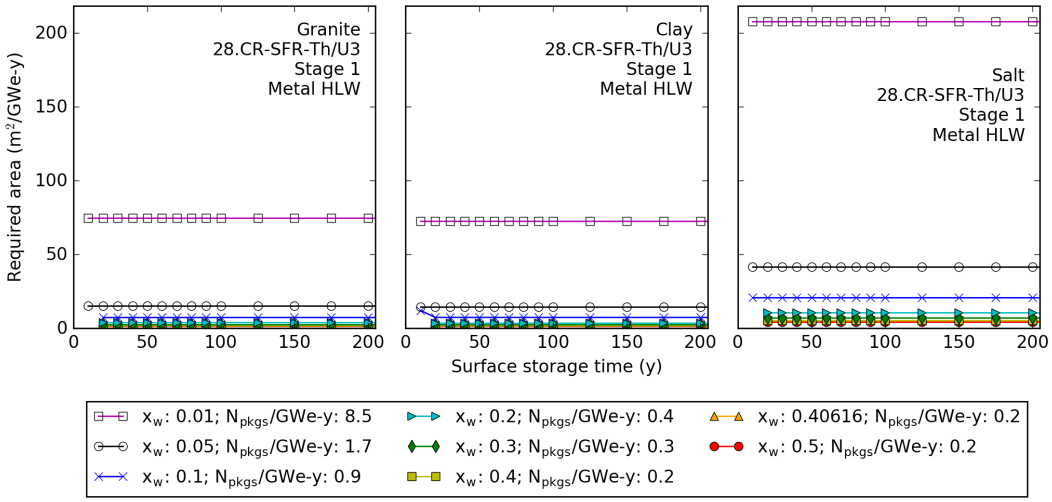

Figure C.54: Repository area versus surface storage time for disposal of metal HLW from 28.CR—SFR—Th/U3.

29.CR—SFR/PWR—U/Pu

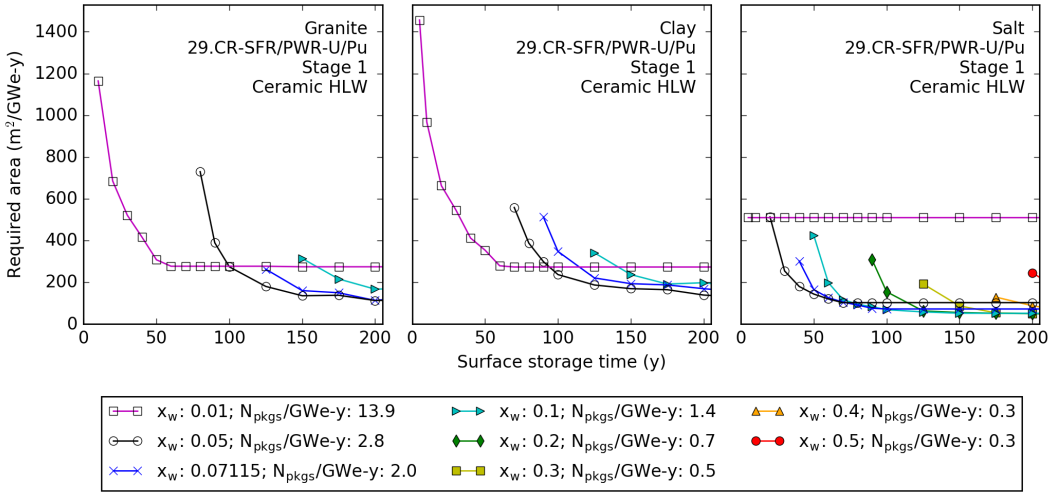

Figure C.55: Repository area versus surface storage time for disposal of ceramic HLW from 29.CR—SFR/PWR—U/Pu.

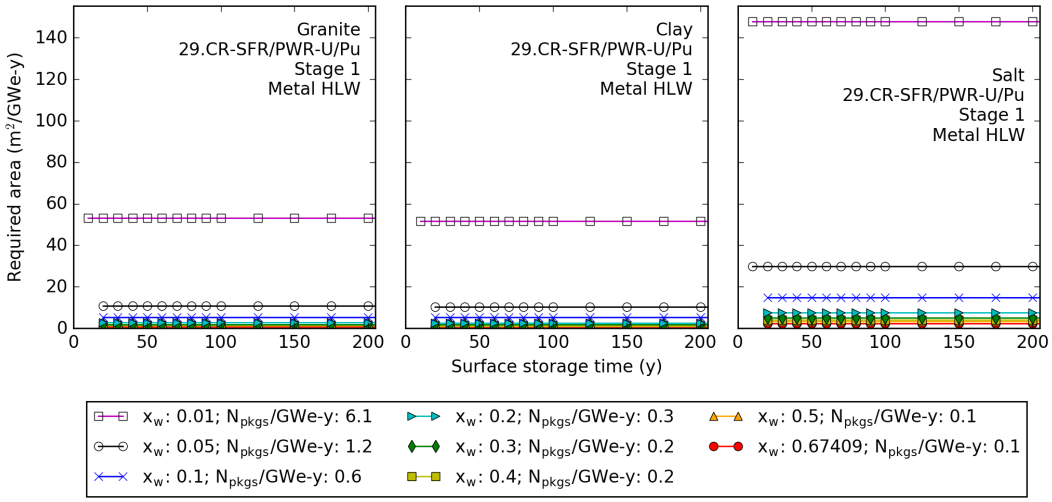

Figure C.56: Repository area versus surface storage time for disposal of metal HLW from 29.CR—SFR/PWR—U/Pu.

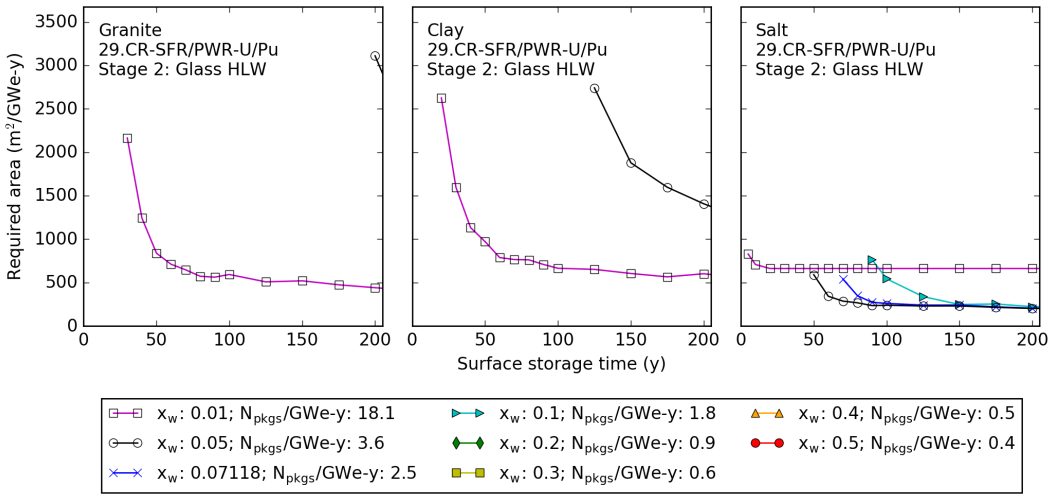

Figure C.57: Repository area versus surface storage time for disposal of glass HLW from 29.CR—SFR/PWR—U/Pu.

30.CR—SFR/PWR—U/TRU

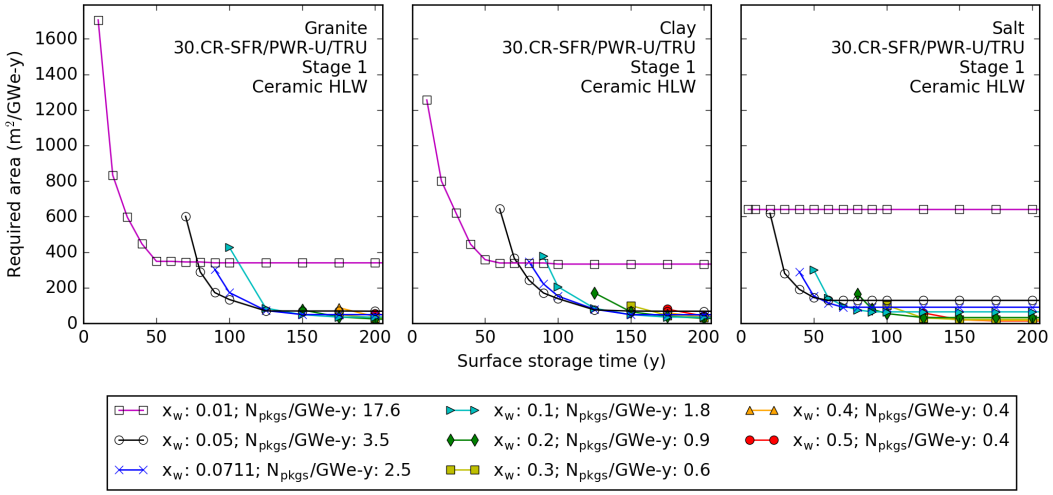

Figure C.58: Repository area versus surface storage time for disposal of ceramic HLW from 30.CR—SFR/PWR—U/TRU.

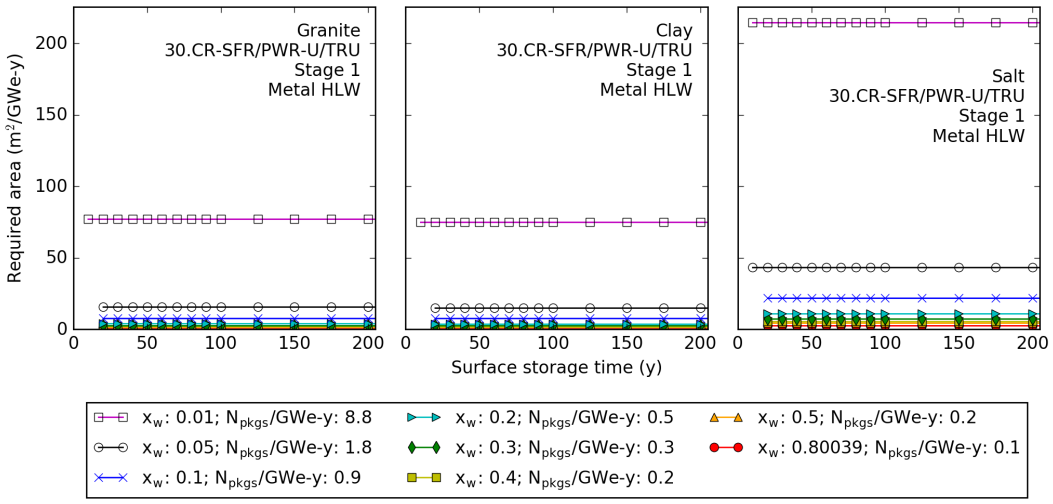

Figure C.59: Repository area versus surface storage time for disposal of metal HLW from 30.CR—SFR/PWR—U/TRU.

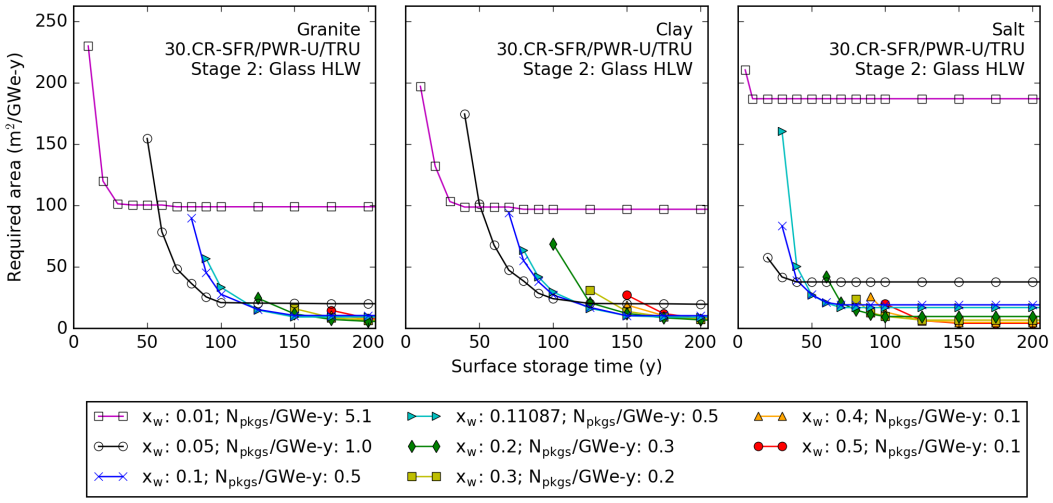

Figure C.60: Repository area versus surface storage time for disposal of glass HLW from 30.CR—SFR/PWR—U/TRU.

31.CR—PWR/SFR—U/Pu

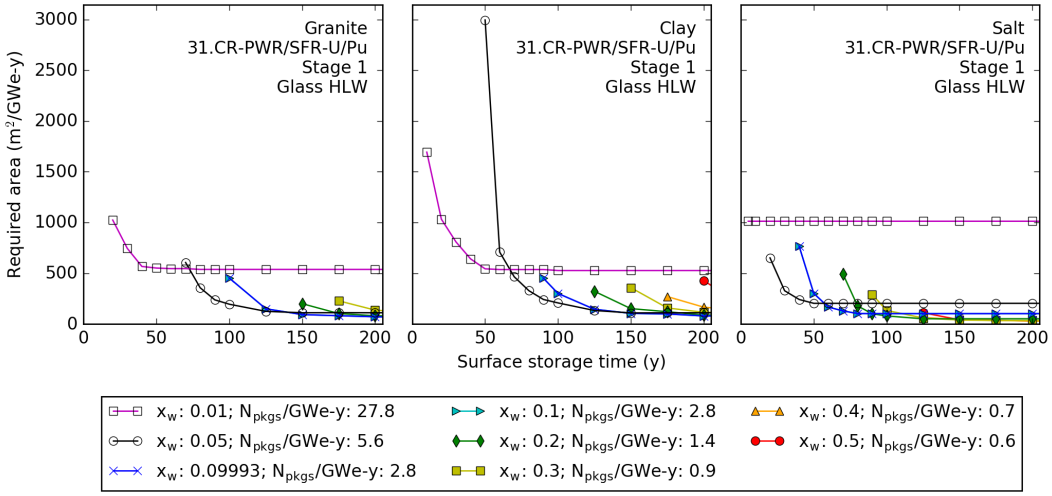

Figure C.61: Repository area versus surface storage time for disposal of glass HLW from Stage 1 of 31.CR—PWR/SFR—U/Pu.

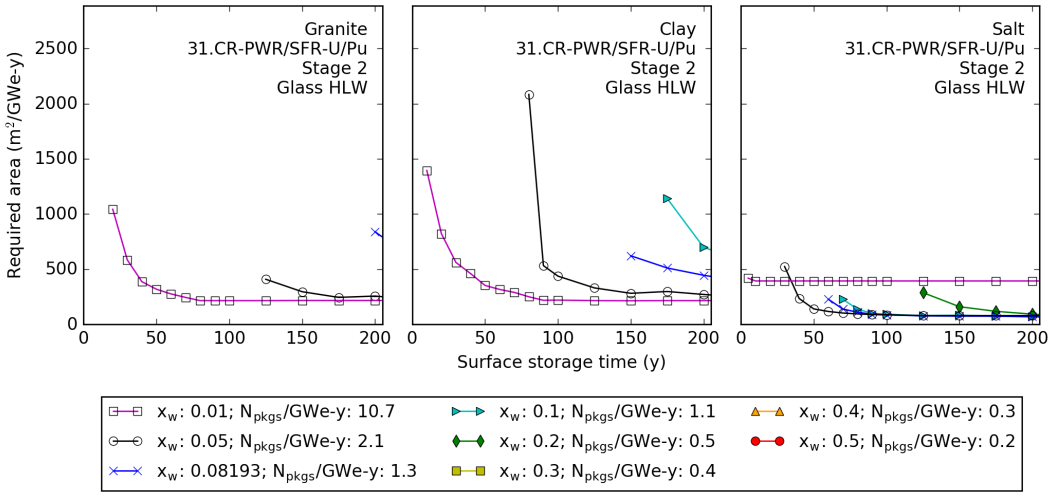

Figure C.62: Repository area versus surface storage time for disposal of glass HLW from Stage 2 of 31.CR—PWR/SFR—U/Pu.

32.CR—PWR/SFR—U/TRU

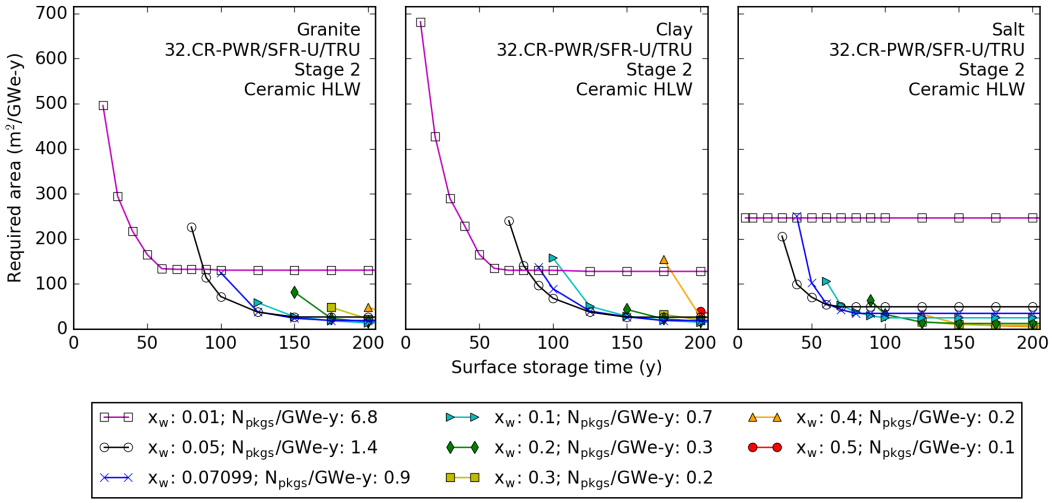

Figure C.63: Repository area versus surface storage time for disposal of ceramic HLW from 32.CR—PWR/SFR—U/TRU.

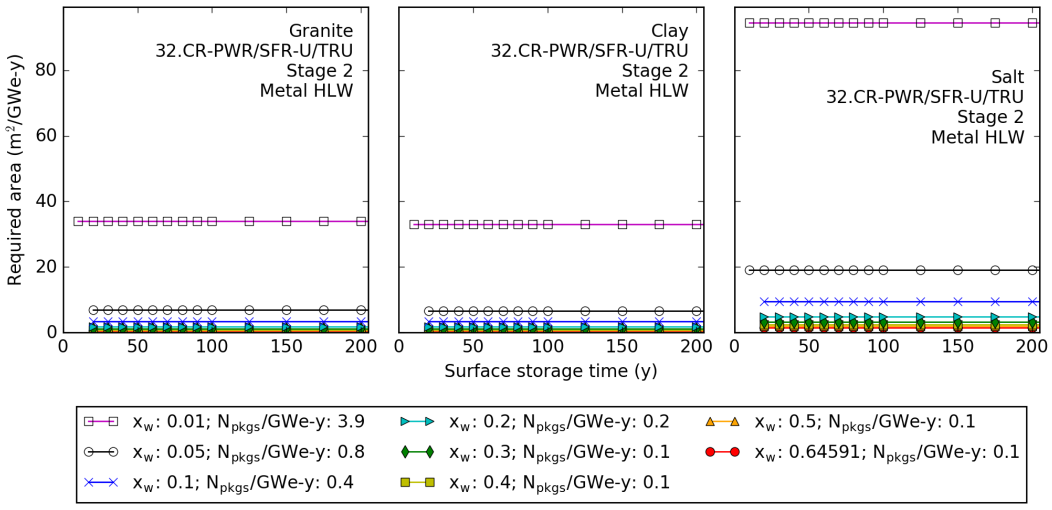

Figure C.64: Repository area versus surface storage time for disposal of metal HLW from 32.CR—PWR/SFR—U/TRU.

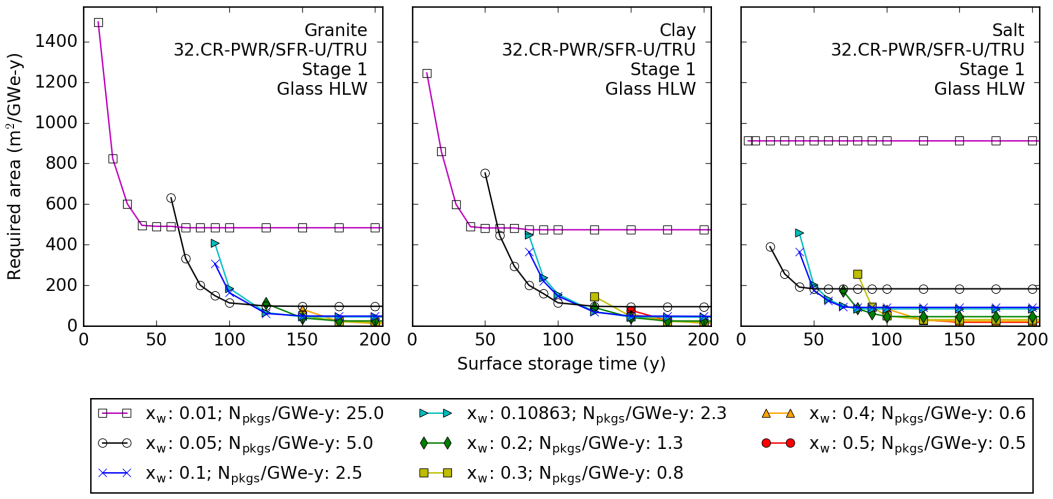

Figure C.65: Repository area versus surface storage time for disposal of glass HLW from 32.CR—PWR/SFR—U/TRU.

33.CR—ADS/PWR—U/Pu

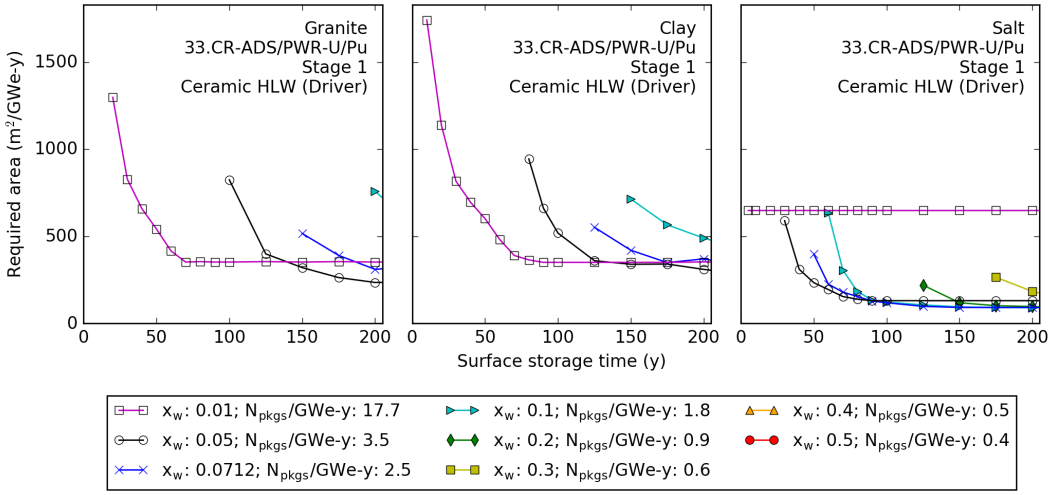

Figure C.66: Repository area versus surface storage time for disposal of ceramic HLW (driver) from 33.CR—ADS/PWR—U/Pu.

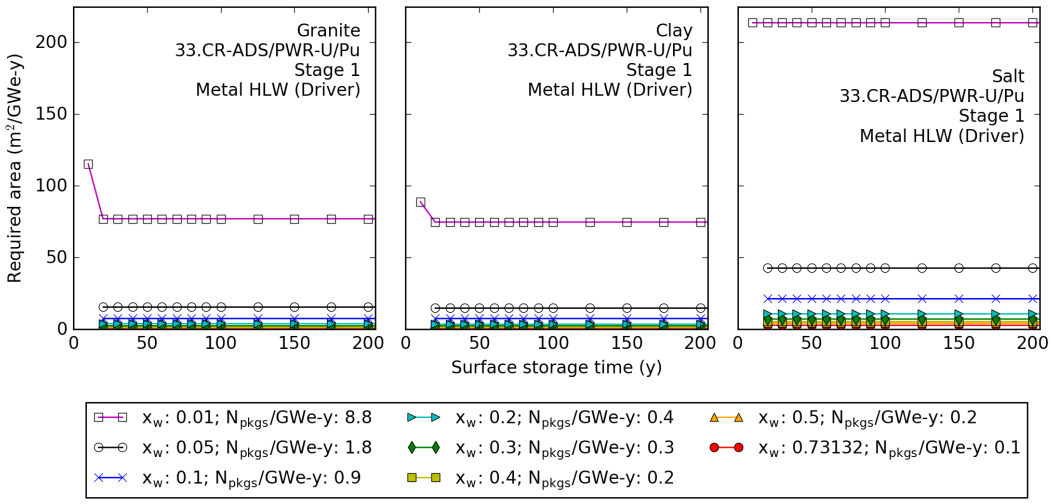

Figure C.67: Repository area versus surface storage time for disposal of metal HLW (driver) from 33.CR—ADS/PWR—U/Pu.

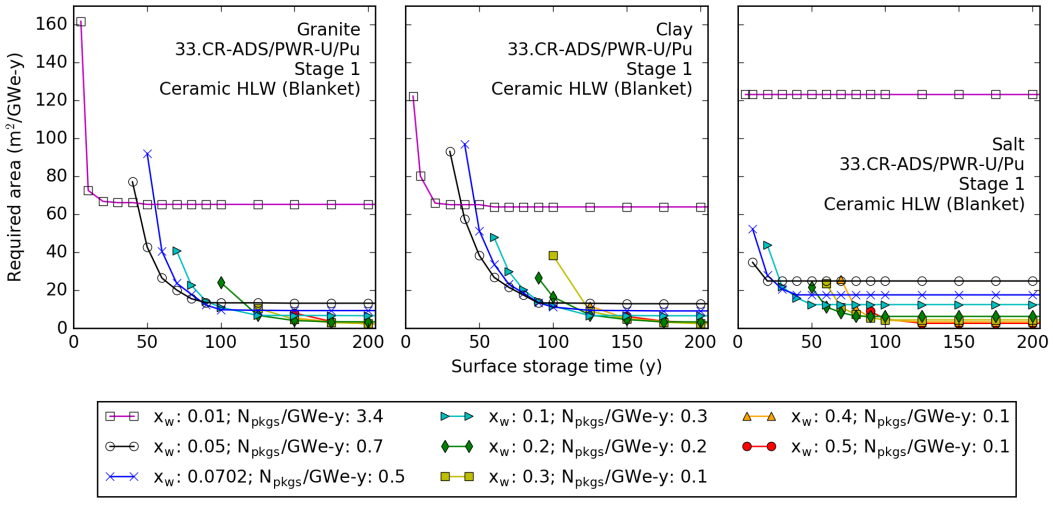

Figure C.68: Repository area versus surface storage time for disposal of ceramic HLW (blanket) from 33.CR—ADS/PWR—U/Pu.

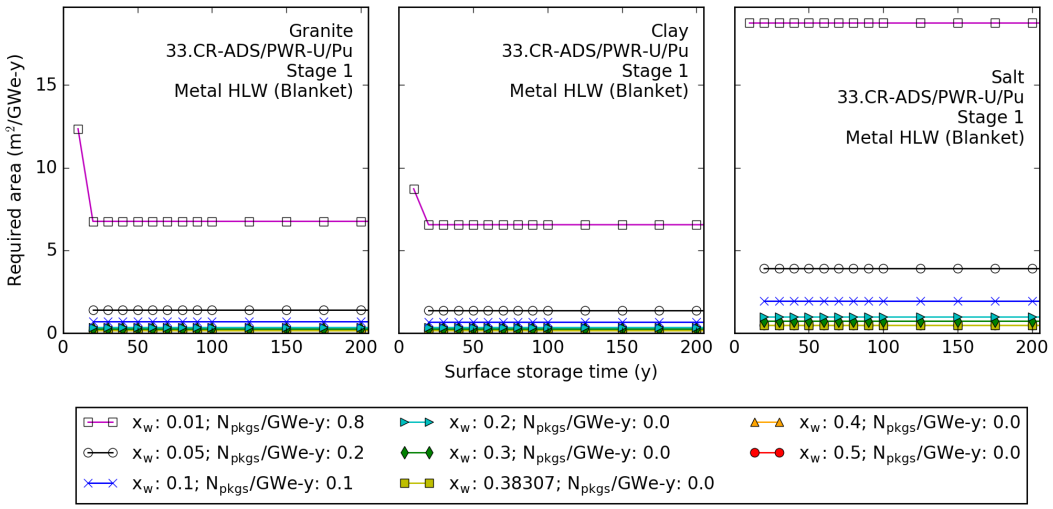

Figure C.69: Repository area versus surface storage time for disposal of metal HLW (blanket) from 33.CR—ADS/PWR—U/Pu.

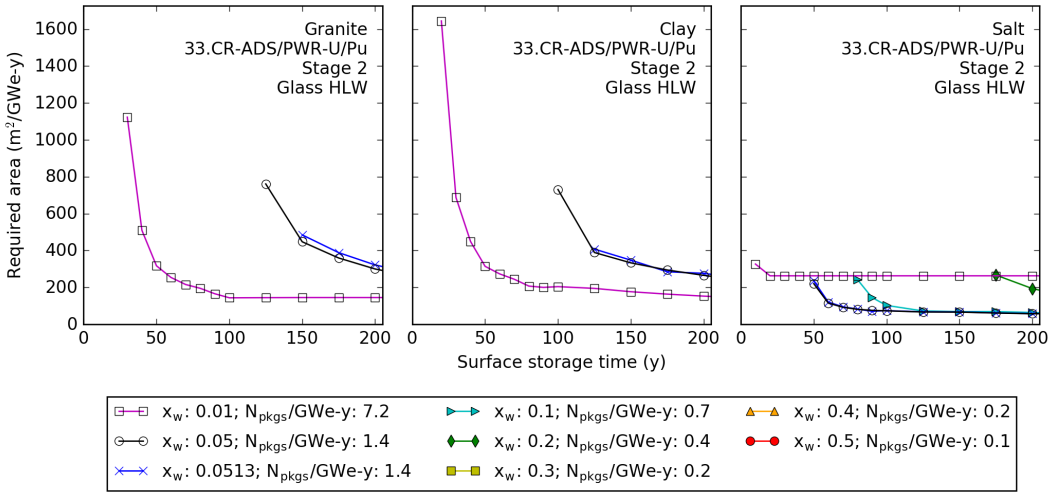

Figure C.70: Repository area versus surface storage time for disposal of glass HLW from 33.CR—ADS/PWR—U/Pu.

34.CR—ADS/PWR—U/TRU

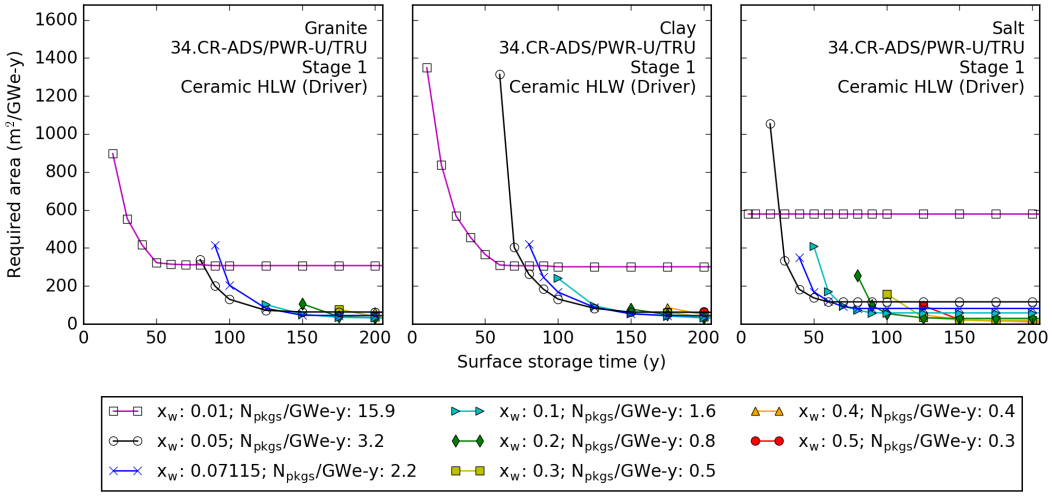

Figure C.71: Repository area versus surface storage time for disposal of ceramic HLW (blanket) from 34.CR—ADS/PWR—U/TRU.

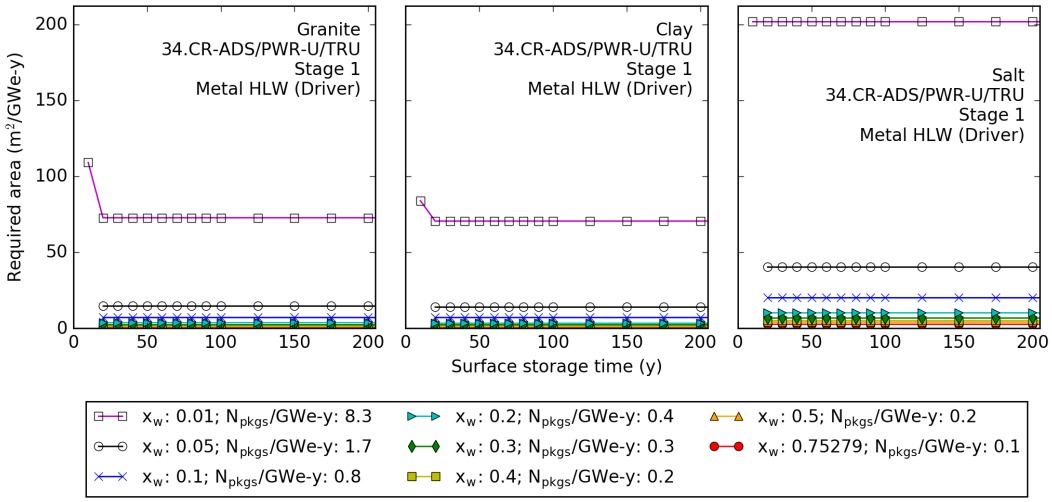

Figure C.72: Repository area versus surface storage time for disposal of HLW from 34.CR—ADS/PWR—U/TRU.

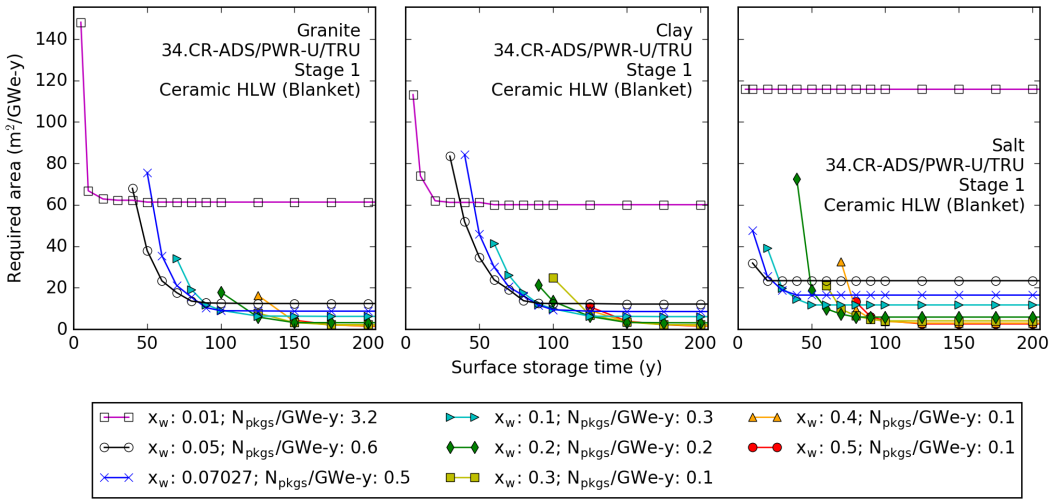

Figure C.73: Repository area versus surface storage time for disposal of ceramic HLW (blanket) from 34.CR—ADS/PWR—U/TRU.

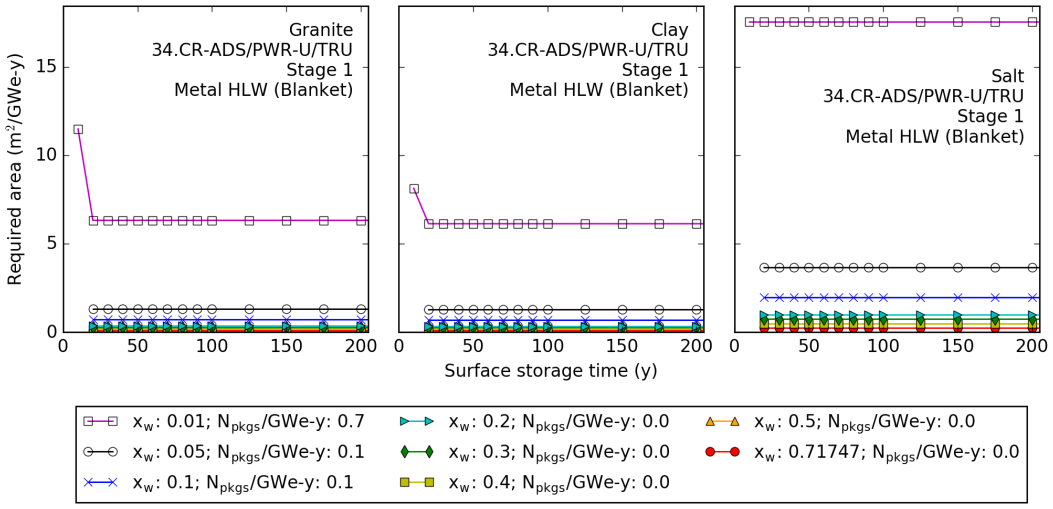

Figure C.74: Repository area versus surface storage time for disposal of metal HLW (blanket) from 34.CR—ADS/PWR—U/TRU.

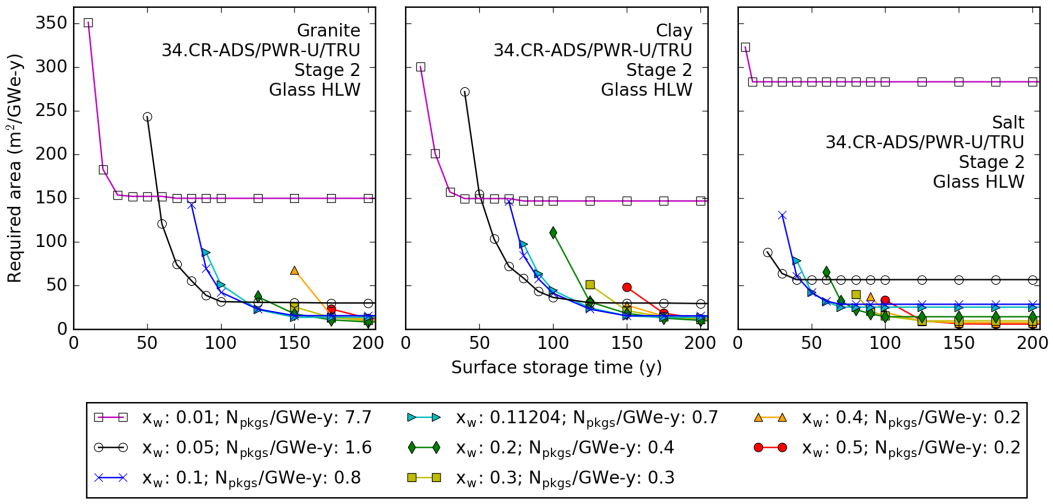

Figure C.75: Repository area versus surface storage time for disposal of glass HLW from 34.CR—ADS/PWR—U/TRU.

35.CR—PWR/ADS—U/Pu

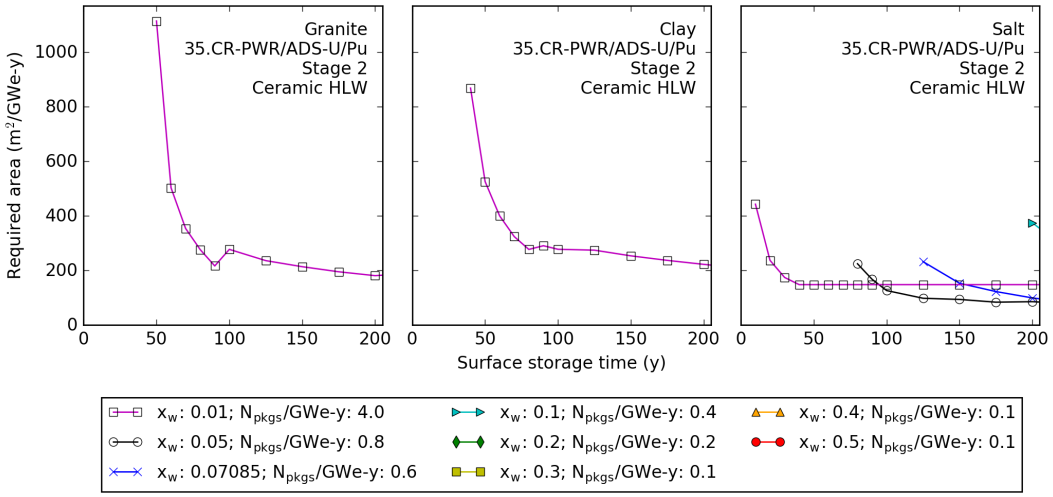

Figure C.76: Repository area versus surface storage time for disposal of ceramic HLW from 35.CR—PWR/ADS—U/Pu.

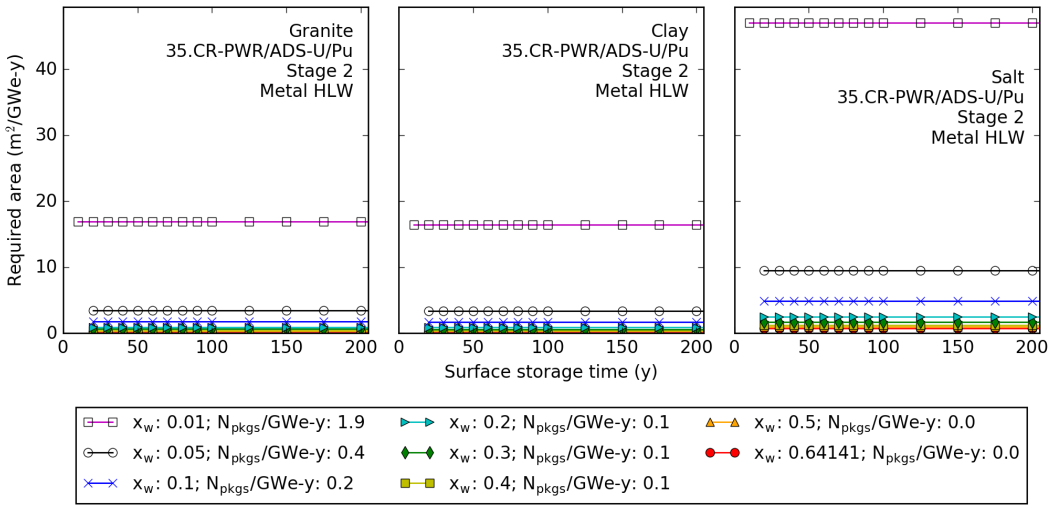

Figure C.77: Repository area versus surface storage time for disposal of metal HLW from 35.CR—PWR/ADS—U/Pu.

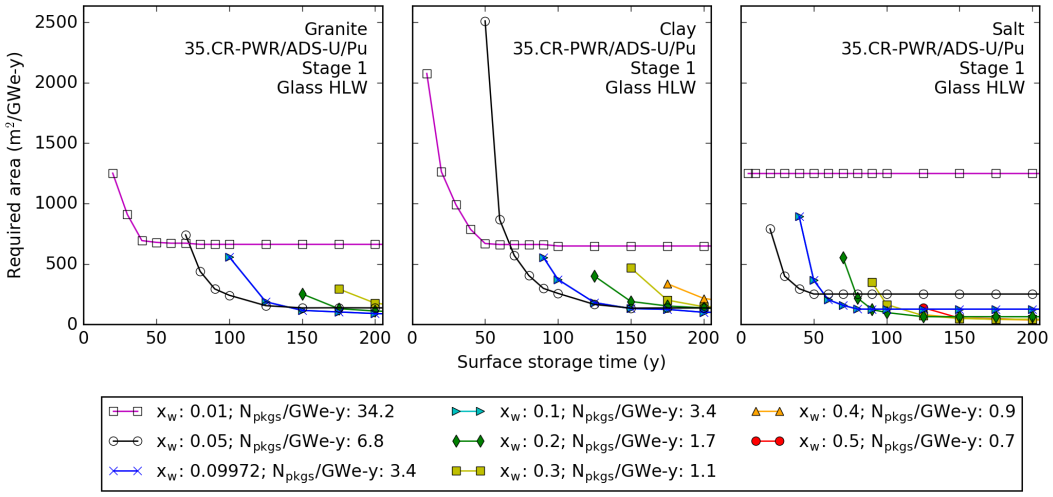

Figure C.78: Repository area versus surface storage time for disposal of glass HLW from 35.CR—PWR/ADS—U/Pu.

36.CR—PWR/ADS—U/Pu/MA

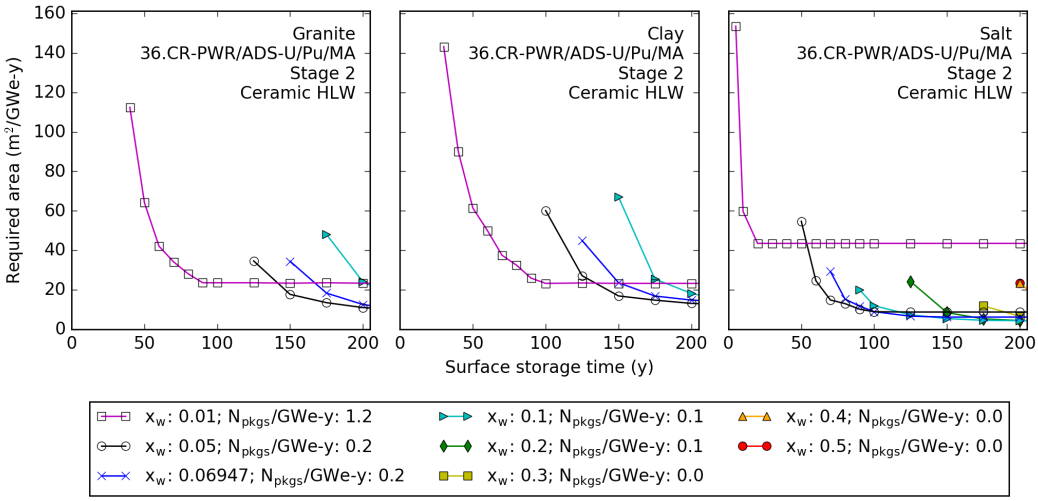

Figure C.79: Repository area versus surface storage time for disposal of ceramic HLW from 36.CR—PWR/ADS—U/Pu/MA.

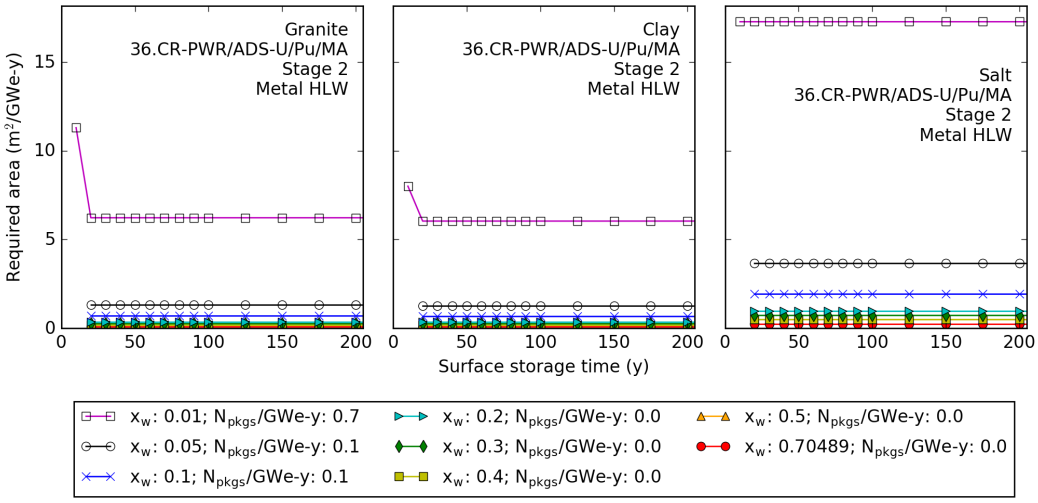

Figure C.80: Repository area versus surface storage time for disposal of metal HLW from 36.CR—PWR/ADS—U/Pu/MA.

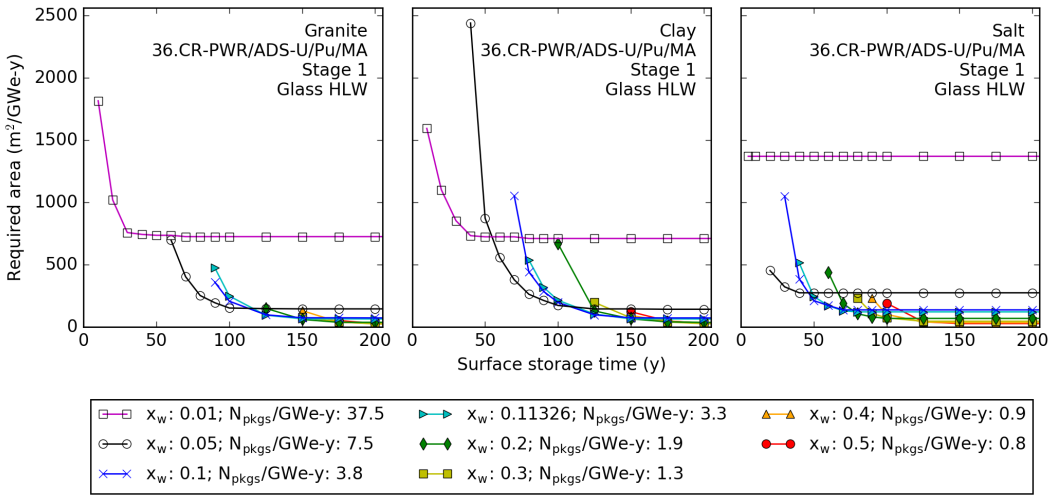

Figure C.81: Repository area versus surface storage time for disposal of glass HLW from 36.CR—PWR/ADS—U/Pu/MA.

37.CR—PWR/SFR/PWR—U/TRU/Th/U3

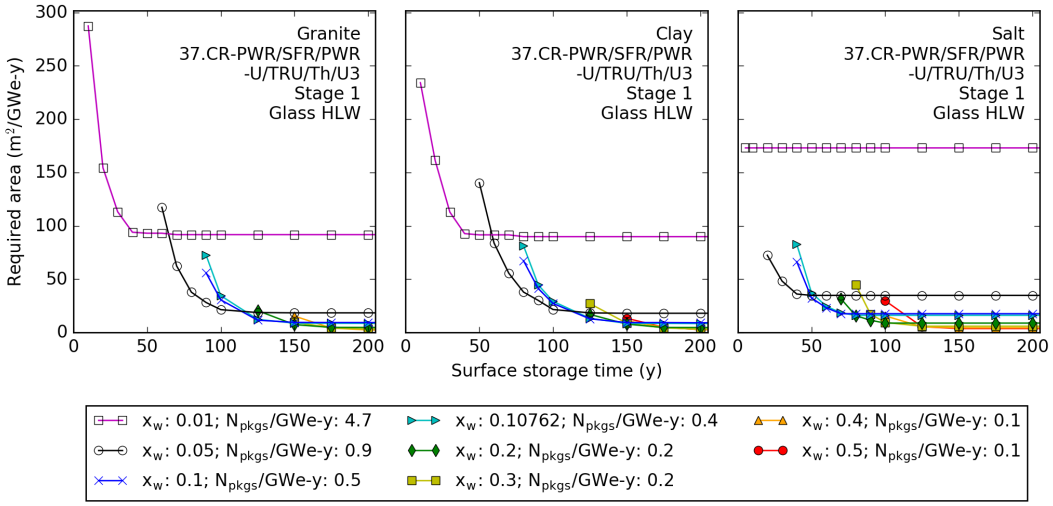

Figure C.82: Repository area versus surface storage time for disposal of glass HLW from Stage 1 of 37.CR—PWR/SFR/PWR—U/TRU/Th/U3.

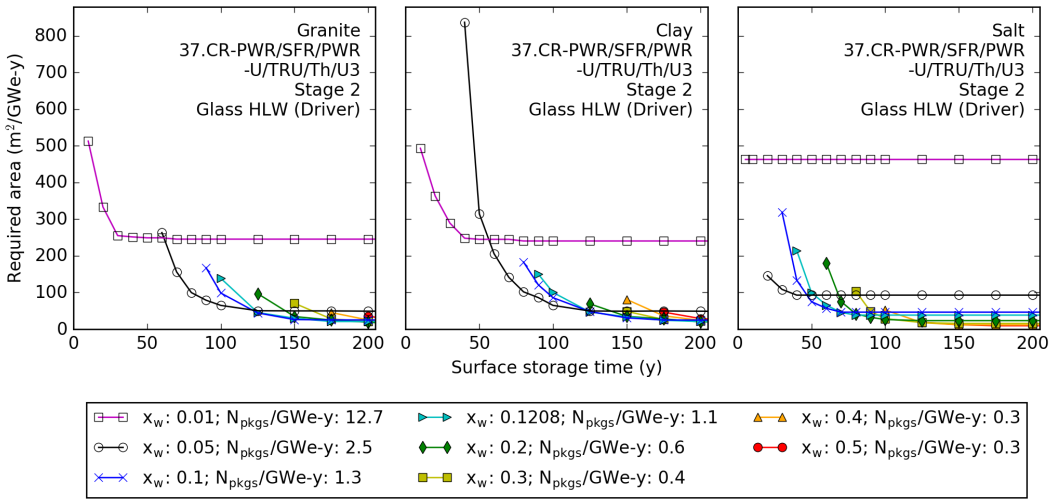

Figure C.83: Repository area versus surface storage time for disposal of glass HLW (driver) from Stage 2 of 37.CR—PWR/SFR/PWR—U/TRU/Th/U3.

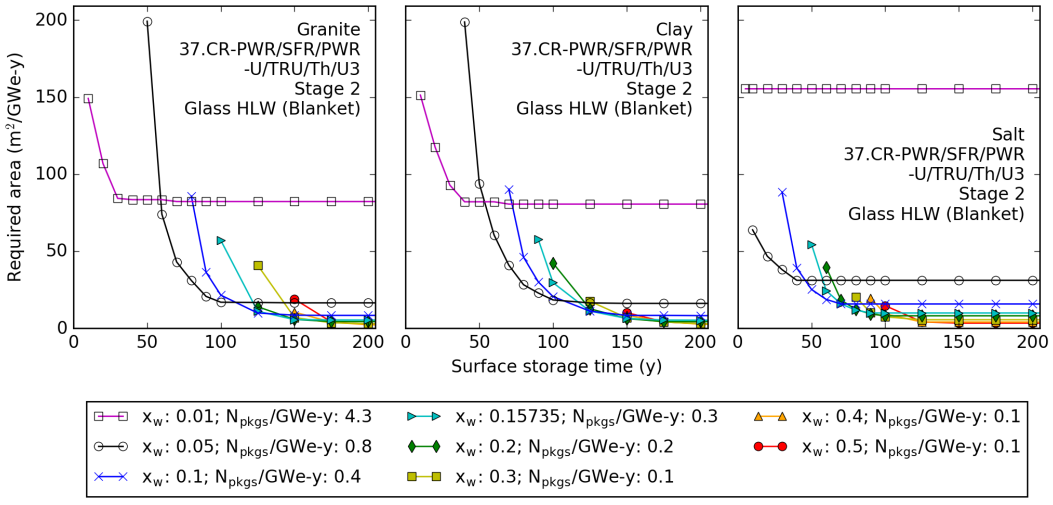

Figure C.84: Repository area versus surface storage time for disposal of glass HLW (blanket) from Stage 2 of 37.CR—PWR/SFR/PWR—U/TRU/Th/U3.

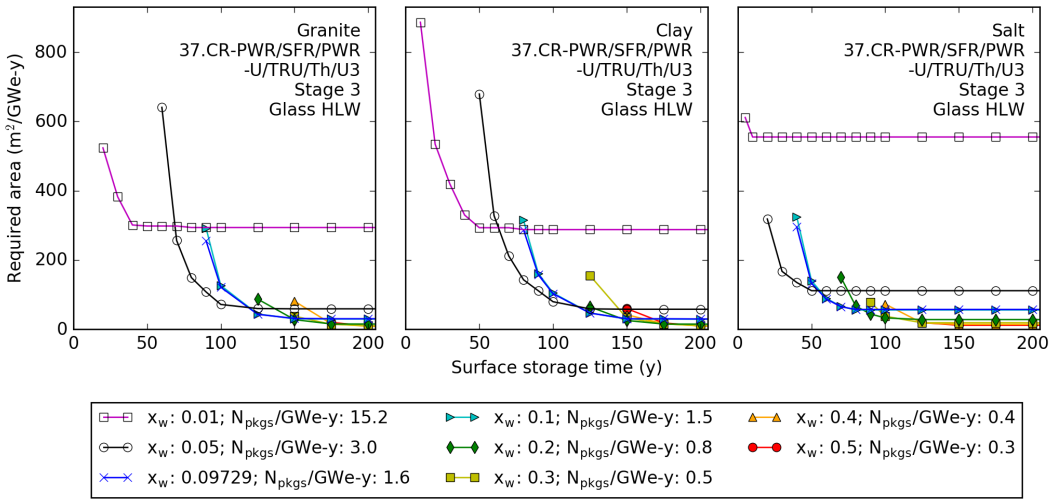

Figure C.85: Repository area versus surface storage time for disposal of glass HLW from Stage 3 of 37.CR—PWR/SFR/PWR—U/TRU/Th/U3.

38.CR—SFR/PWR—Th/U3

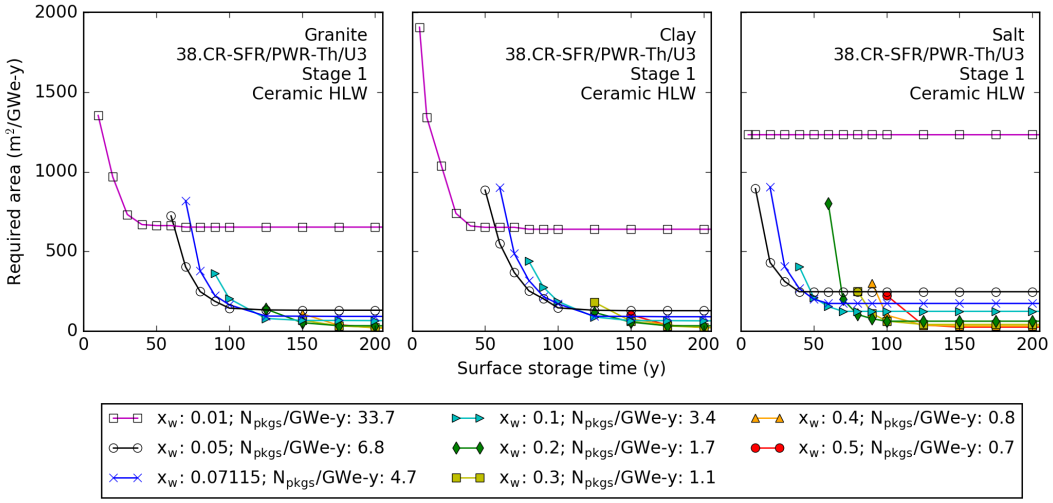

Figure C.86: Repository area versus surface storage time for disposal of ceramic HLW from 38.CR—SFR/PWR—Th/U3.

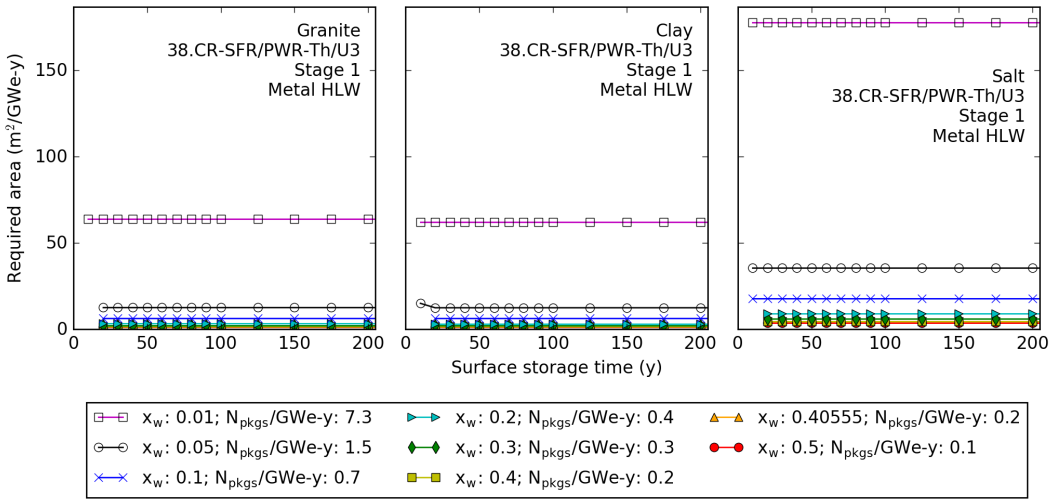

Figure C.87: Repository area versus surface storage time for disposal of metal HLW from 38.CR—SFR/PWR—Th/U3.

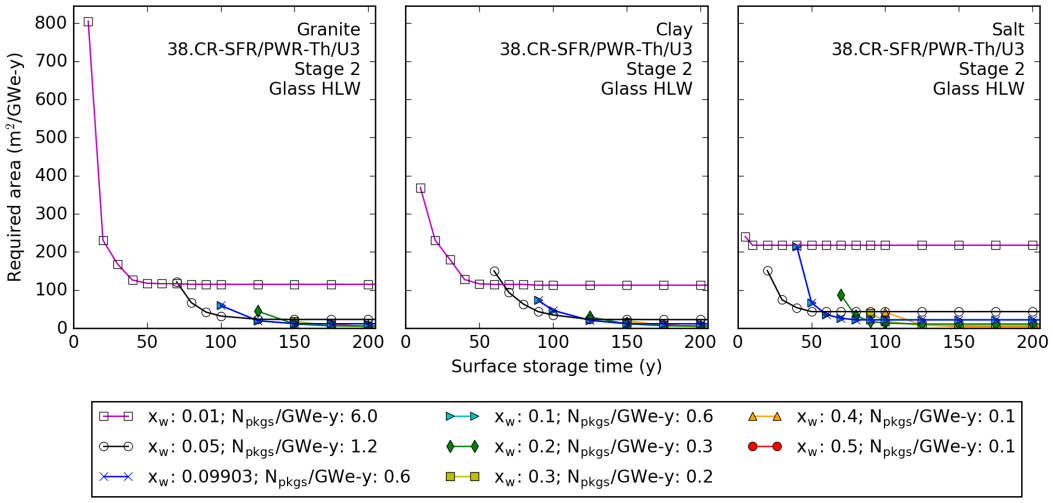

Figure C.88: Repository area versus surface storage time for disposal of glass HLW from 38.CR—SFR/PWR—Th/U3.

39.CR—PWR/PWR/ADS—U/TRU/Th/U3

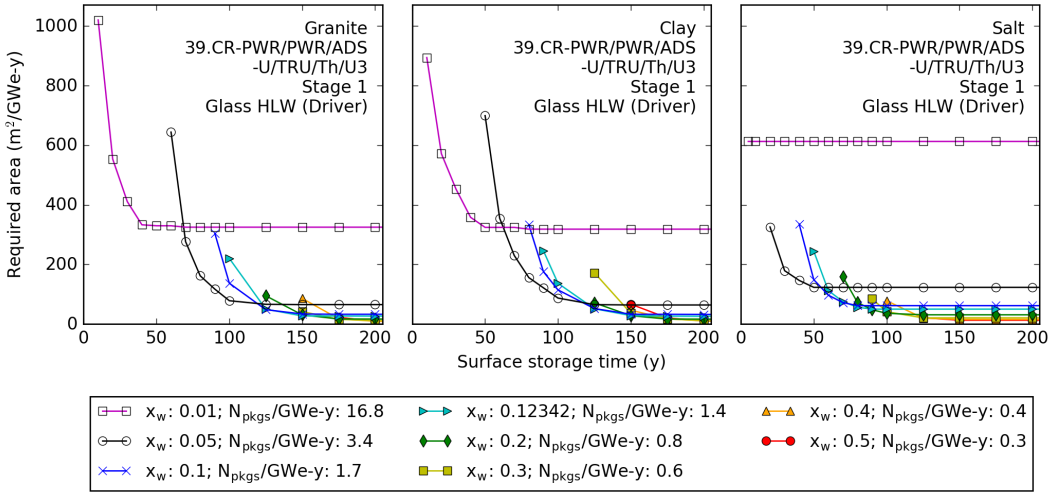

Figure C.89: Repository area versus surface storage time for disposal of glass HLW (driver) from Stage 1 of 39.CR—PWR/PWR/ADS—U/TRU/Th/U3.

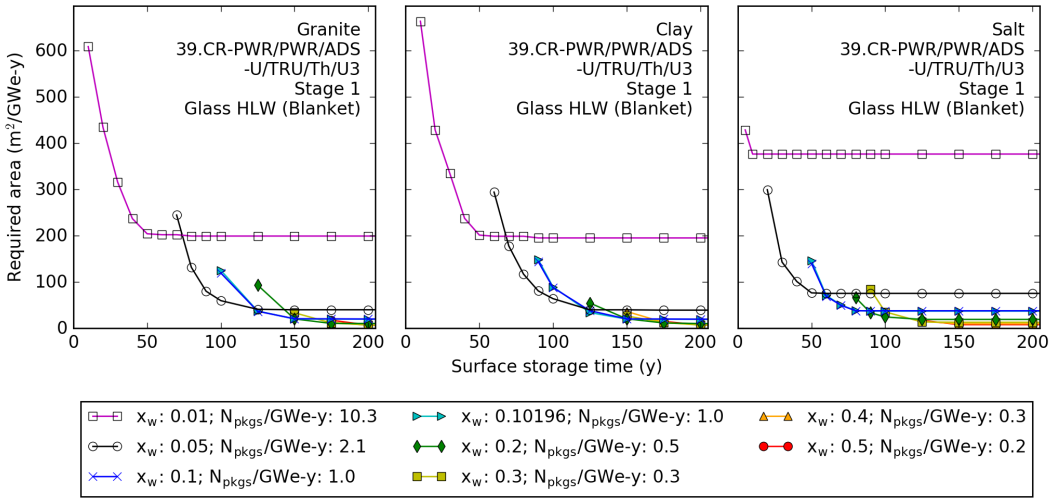

Figure C.90: Repository area versus surface storage time for disposal of glass HLW (blanket) from 39.CR—PWR/PWR/ADS—U/TRU/Th/U3.

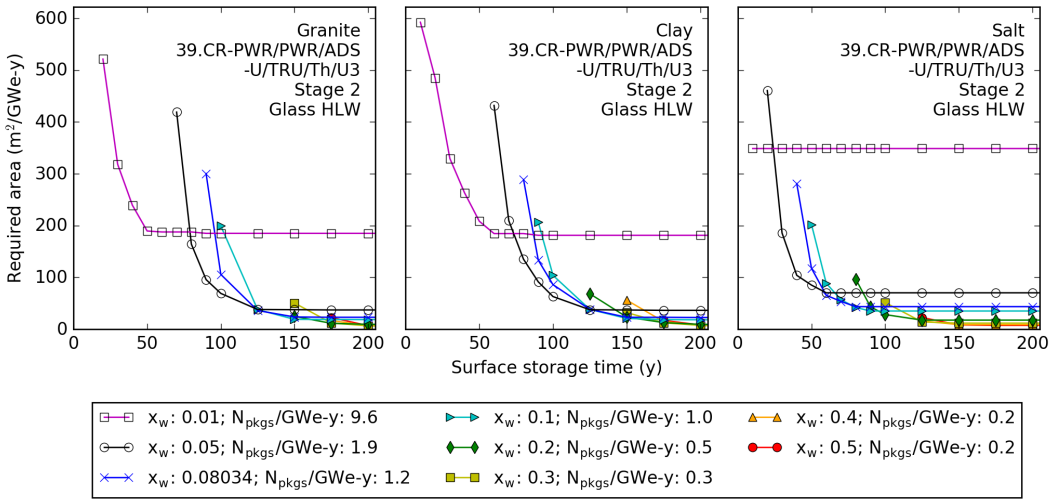

Figure C.91: Repository area versus surface storage time for disposal of glass HLW from Stage 2 of 39.CR—PWR/PWR/ADS—U/TRU/Th/U3.

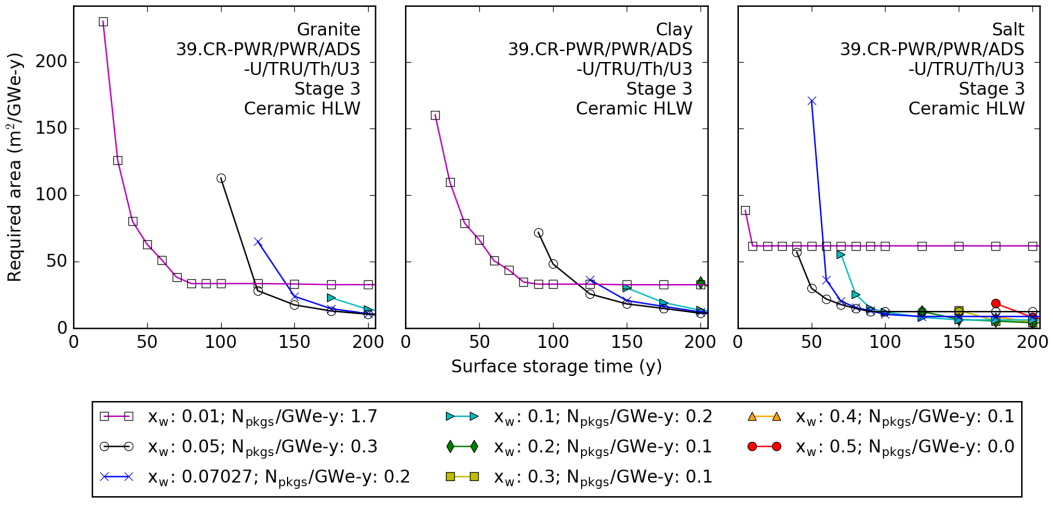

Figure C.92: Repository area versus surface storage time for disposal of ceramic HLW from Stage 3 of 39.CR—PWR/PWR/ADS—U/TRU/Th/U3.

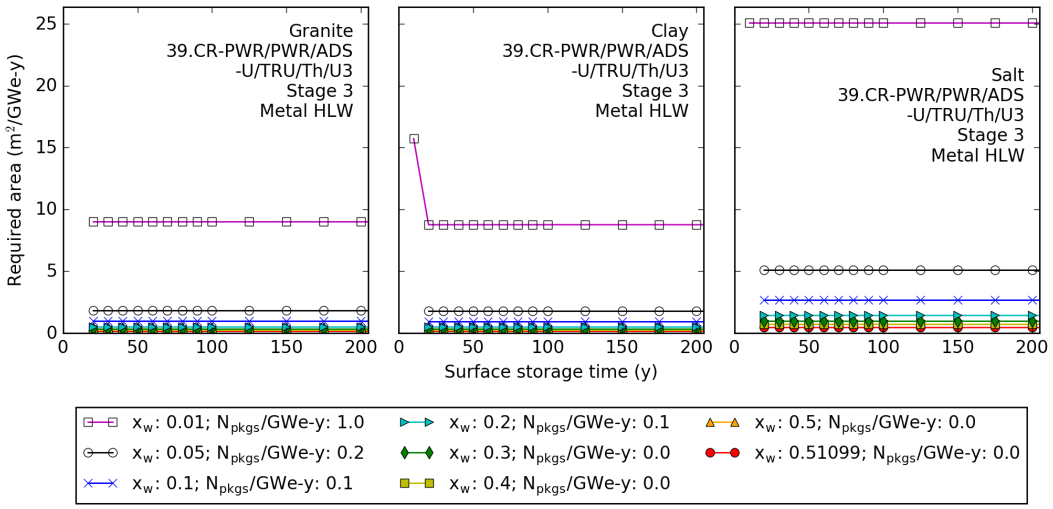

Figure C.93: Repository area versus surface storage time for disposal of metal HLW from Stage 3 of 39.CR—PWR/PWR/ADS—U/TRU/Th/U3.

40.CR—ADS/PWR—Th/U3

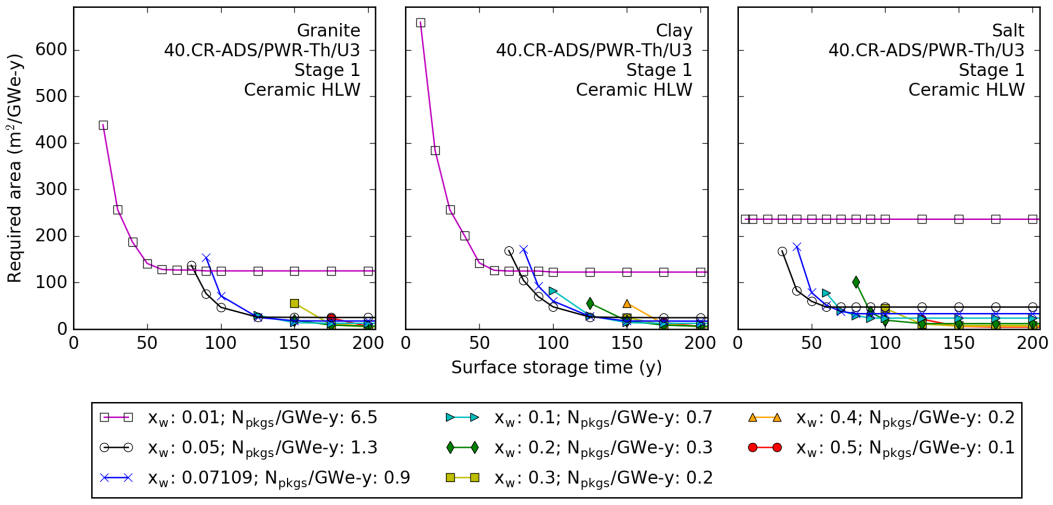

Figure C.94: Repository area versus surface storage time for disposal of ceramic HLW from 40.CR—ADS/PWR—Th/U3.

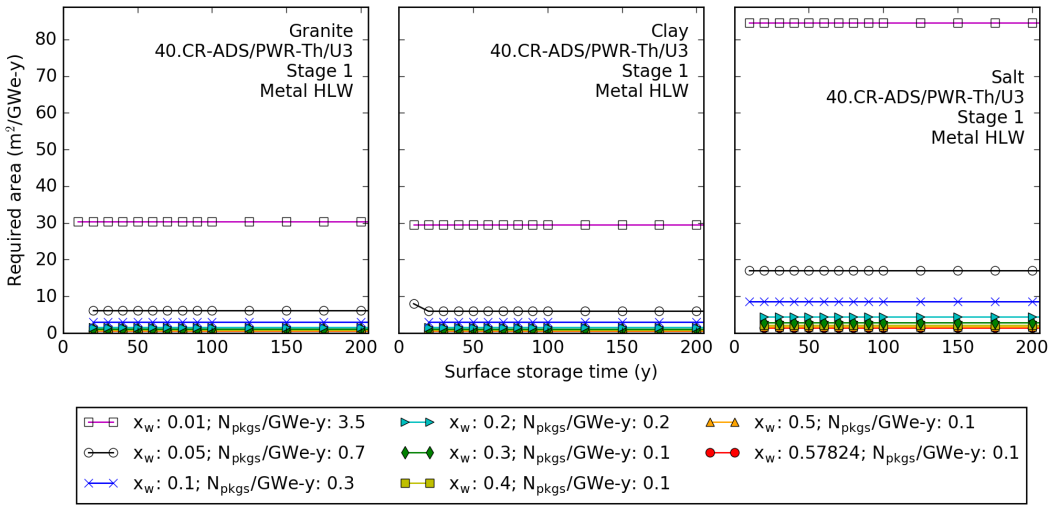

Figure C.95: Repository area versus surface storage time for disposal of metal HLW from 40.CR—ADS/PWR—Th/U3.

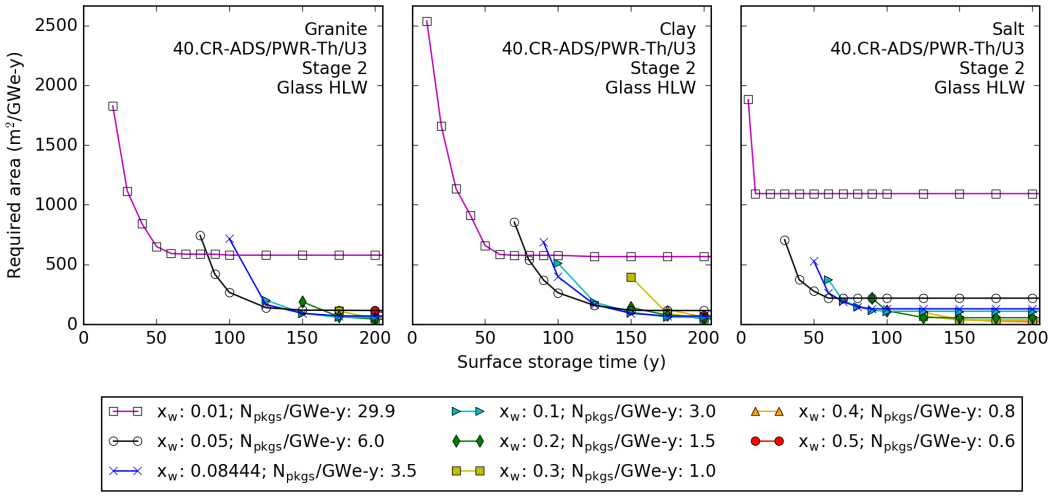

Figure C.96: Repository area versus surface storage time for disposal of glass HLW from 40.CR—ADS/PWR—Th/U3.

Appendix D

Minimum repository footprint

This appendix presents the results for the minimum required repository area as a function of surface storage time for disposal in each repository environment — granite, clay, and salt. The minimum is taken with respect to all possible options of waste package (for SNF) or waste form (for HLW) loading, which can lead to the appearance of flat sections and/or disjoints in the plotted lines. Figures for 1.OT—PWR—U, 13.LR—PWR/PWR—U/Pu, and 23.CR—SFR—U/Pu are included in Chapter 4 Section 4.4.

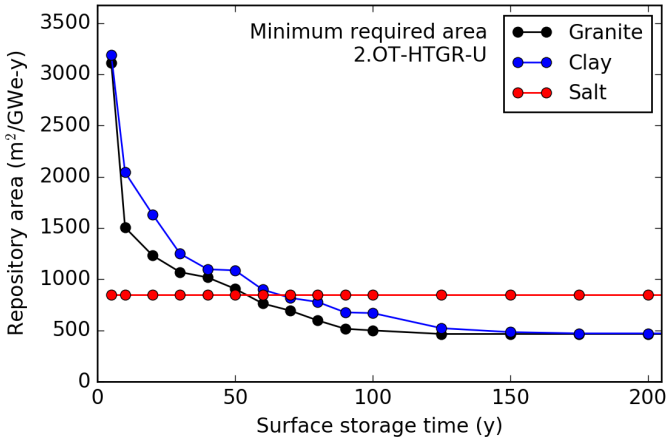

Figure D.1: Minimum required repository area (m^2/GWe-y) versus surface storage time for disposal of SNF generated from 2.OT—HTGR—U.

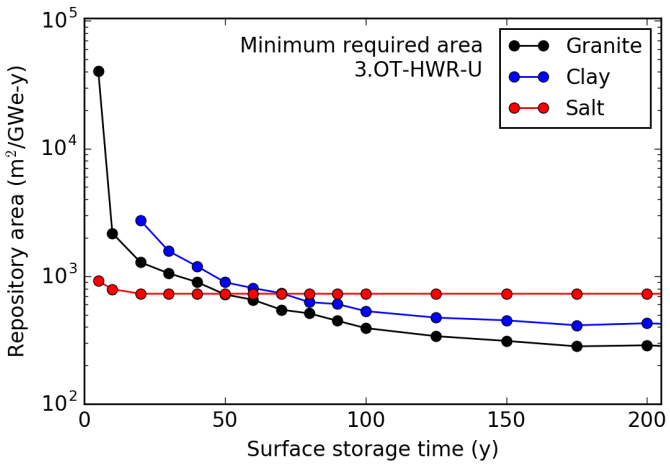

Figure D.2: Minimum required repository area (m^2/GWe-y) versus surface storage time for disposal of SNF generated from 3.OT—HWR—U.

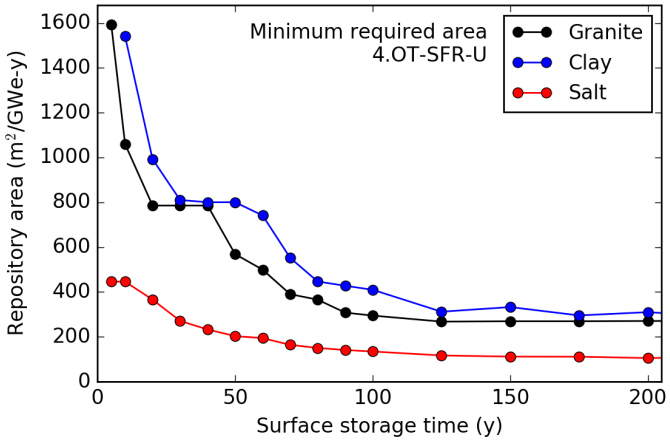

Figure D.3: Minimum required repository area (m^2/GWe-y) versus surface storage time for disposal of SNF generated from 4.OT—SFR—U.

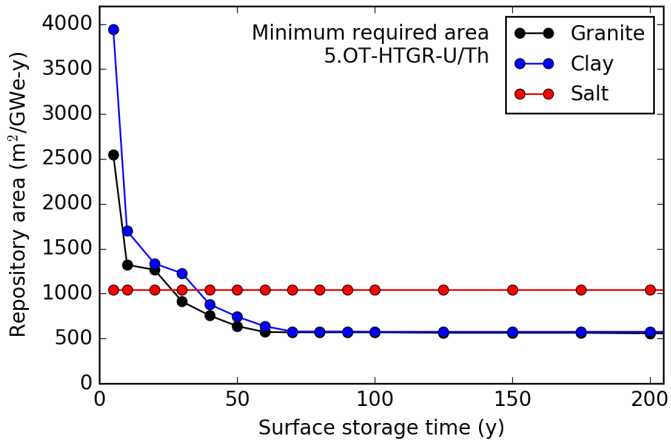

Figure D.4: Minimum required repository area (m^2/GWe-y) versus surface storage time for disposal of SNF generated from 5.OT—HTGR—U/Th.

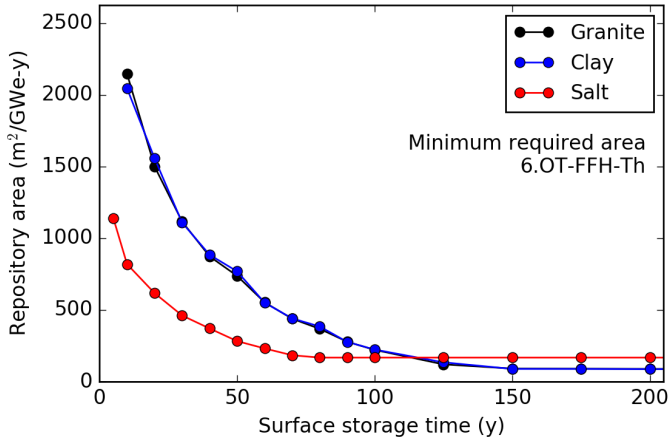

Figure D.5: Minimum required repository area (m^2/GWe-y) versus surface storage time for disposal of HLW generated from 6.OT—FFH—Th.

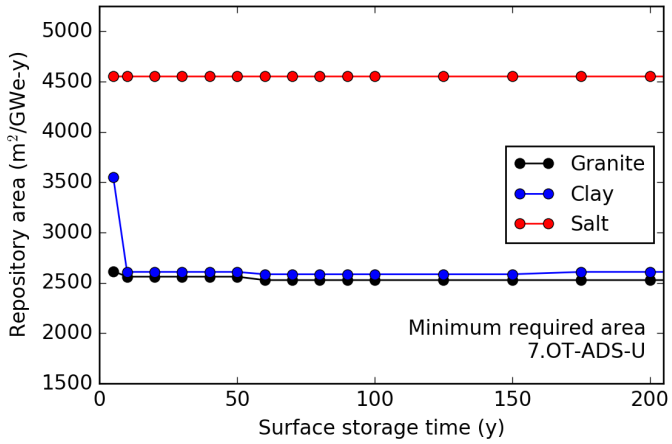

Figure D.6: Minimum required repository area (m^2/GWe-y) versus surface storage time for disposal of SNF generated from 7.OT—ADS—U.

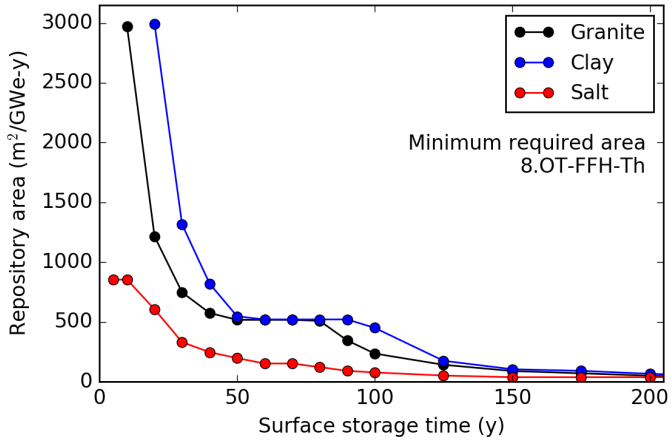

Figure D.7: Minimum required repository area (m^2/GWe-y) versus surface storage time for disposal of SNF generated from 8.OT—FFH—Th.

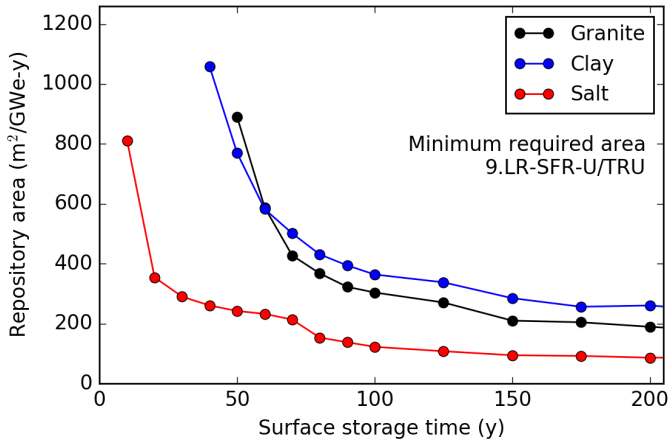

Figure D.8: Minimum required repository area (m^2/GWe-y) versus surface storage time for disposal of SNF and HLW generated from 9.LR—SFR—U/TRU.

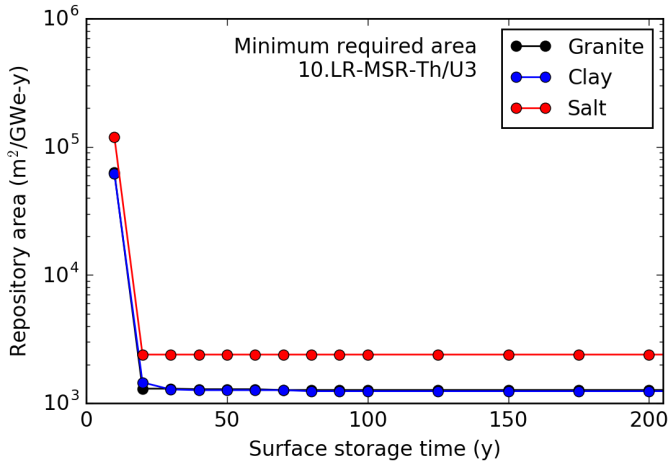

Figure D.9: Minimum required repository area (m^2/GWe-y) versus surface storage time for disposal of HLW generated from 10.LR—MSR—Th/U3.

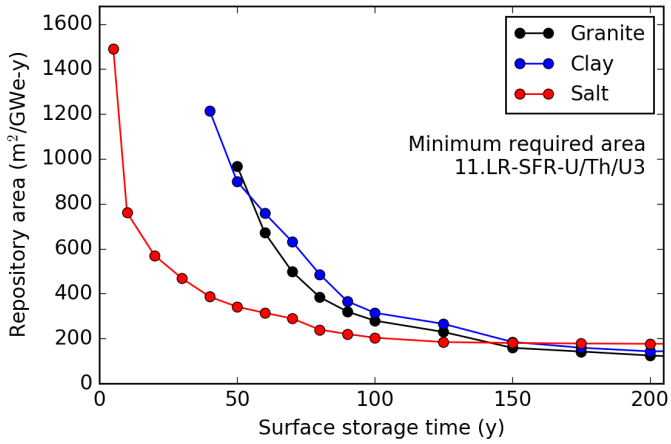

Figure D.10: Minimum required repository area (m^2/GWe-y) versus surface storage time for disposal of SNF and HLW generated from 11.LR—SFR—U/Th/U3.

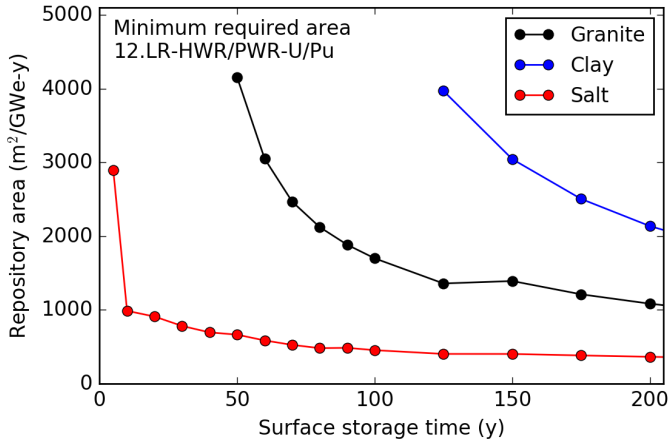

Figure D.11: Minimum required repository area (m^2/GWe-y) versus surface storage time for disposal of SNF and HLW generated from 12.LR—HWR/PWR—U/Pu.

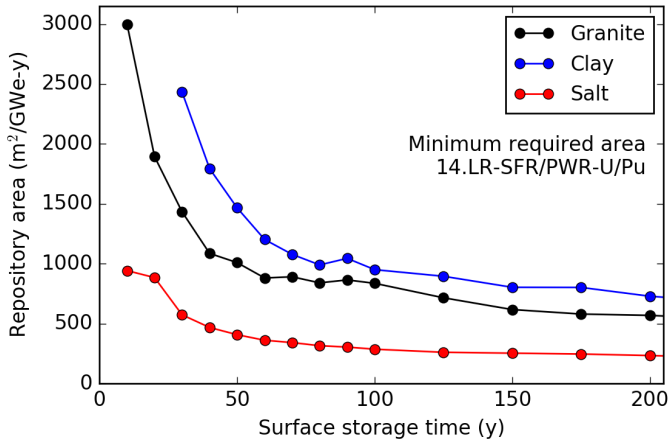

Figure D.12: Minimum required repository area (m^2/GWe-y) versus surface storage time for disposal of SNF and HLW generated from 14.LR—SFR/PWR—U/Pu.

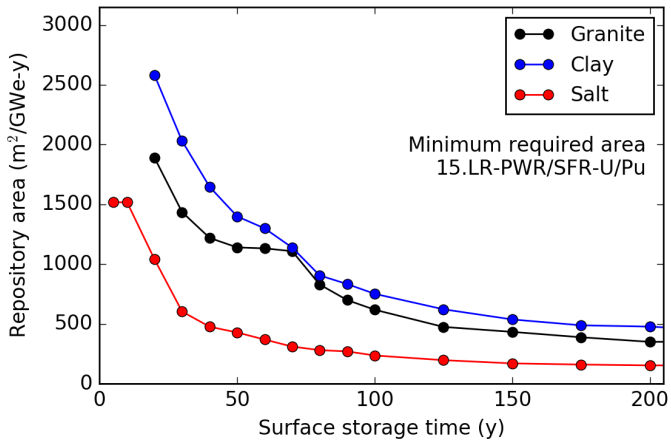

Figure D.13: Minimum required repository area (m^2/GWe-y) versus surface storage time for disposal of SNF and HLW generated from 15.LR—PWR/SFR—U/Pu.

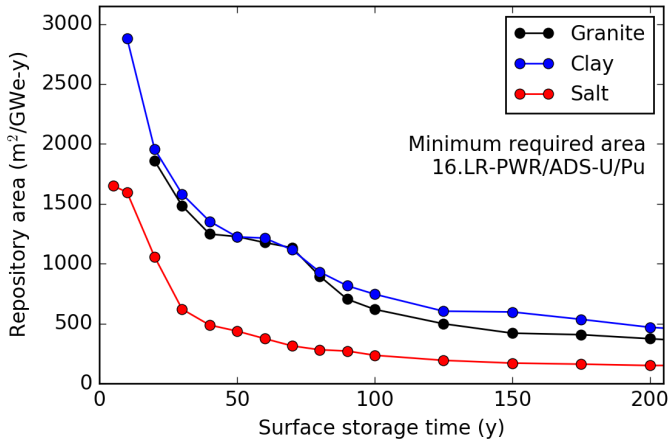

Figure D.14: Minimum required repository area (m^2/GWe-y) versus surface storage time for disposal of SNF and HLW generated from 16.LR—PWR/ADS—U/Pu.

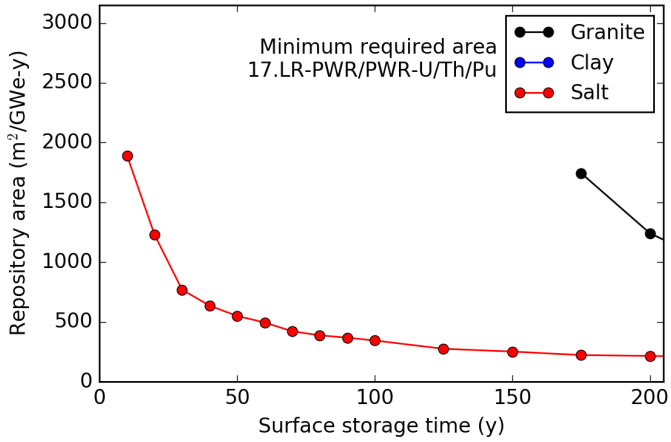

Figure D.15: Minimum required repository area (m^2/GWe-y) versus surface storage time for disposal of SNF and HLW generated from 17.LR—PWR/PWR—U/Th/Pu.

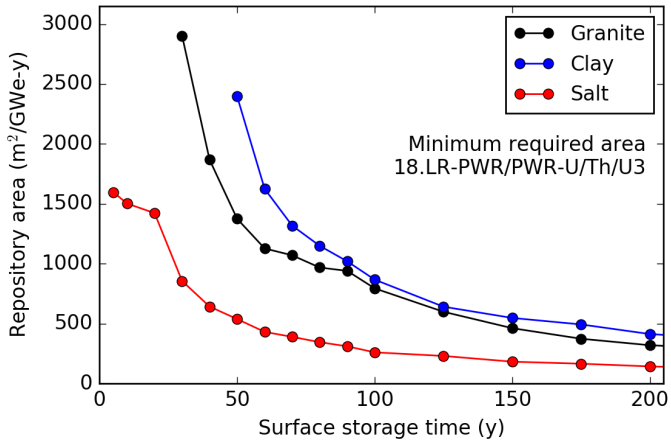

Figure D.16: Minimum required repository area (m^2/GWe-y) versus surface storage time for disposal of SNF and HLW generated from 18.LR—PWR/PWR—U/Th/U3.

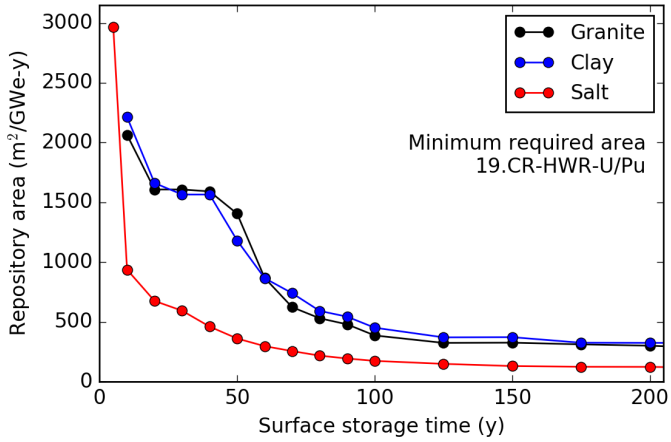

Figure D.17: Minimum required repository area (m^2/GWe-y) versus surface storage time for disposal of HLW generated from 19.CR—HWR—U/Pu.

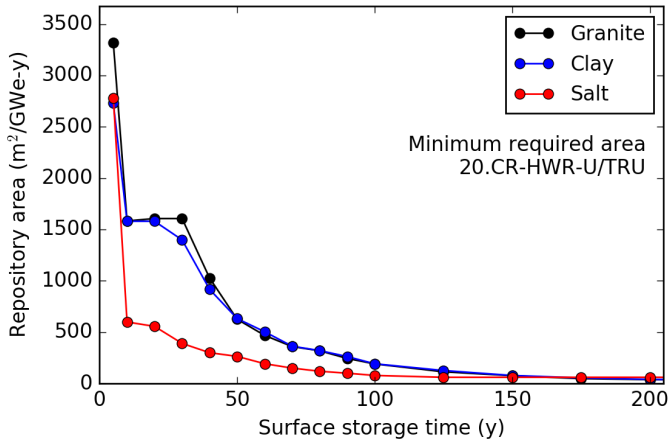

Figure D.18: Minimum required repository area (m^2/GWe-y) versus surface storage time for disposal of HLW generated from 20.CR—HWR—U/TRU.

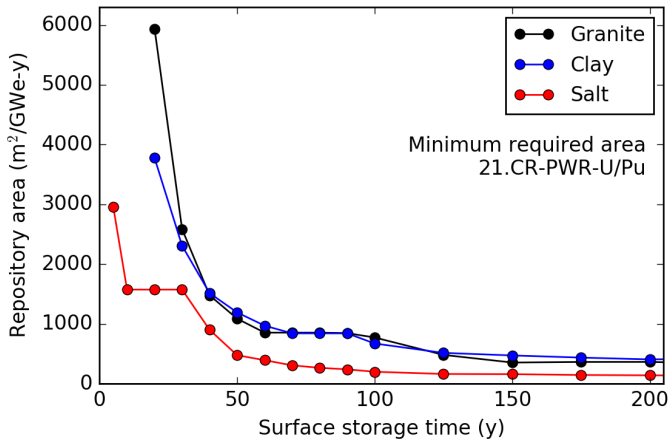

Figure D.19: Minimum required repository area (m^2/GWe-y) versus surface storage time for disposal of HLW generated from 21.CR—PWR—U/Pu.

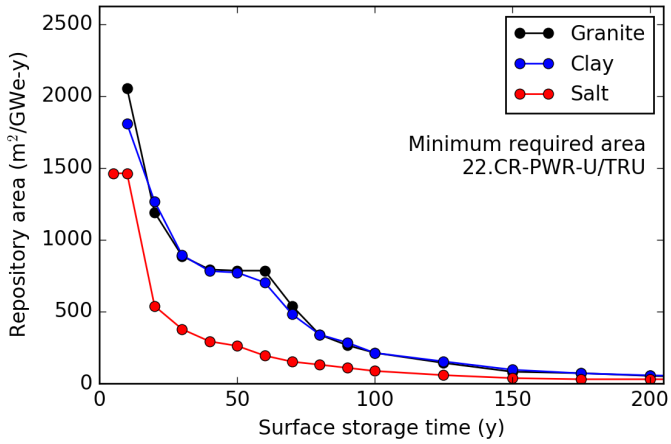

Figure D.20: Minimum required repository area (m^2/GWe-y) versus surface storage time for disposal of HLW generated from 22.CR—PWR—U/TRU.

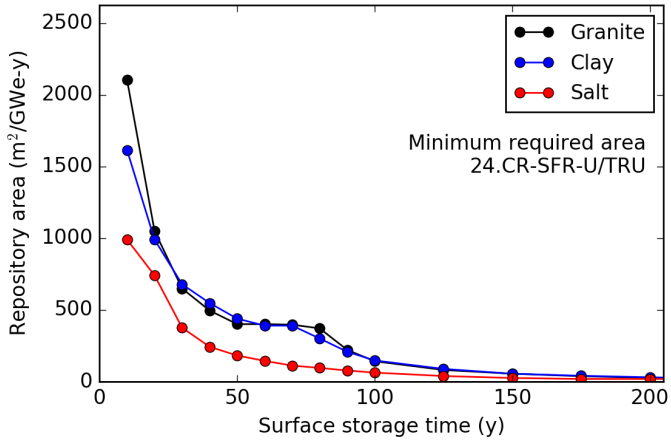

Figure D.21: Minimum required repository area (m^2/GWe-y) versus surface storage time for disposal of HLW generated from 24.CR—SFR—U/TRU.

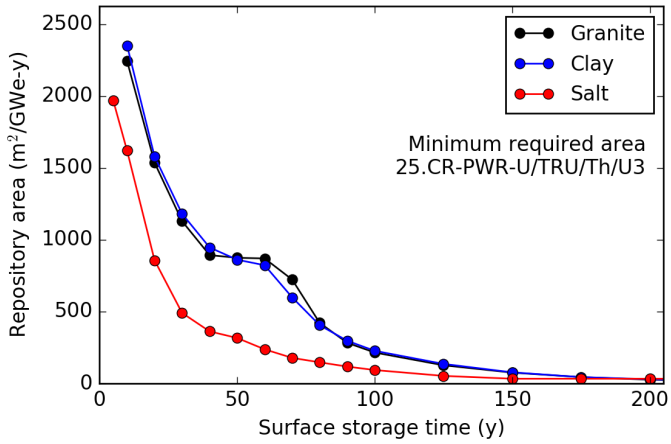

Figure D.22: Minimum required repository area (m^2/GWe-y) versus surface storage time for disposal of HLW generated from 25.CR—PWR—U/TRU/Th/U3.

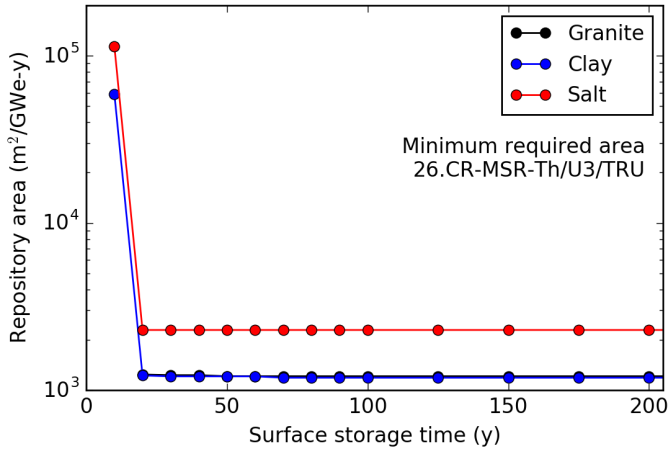

Figure D.23: Minimum required repository area (m^2/GWe-y) versus surface storage time for disposal of HLW generated from 26.CR—MSR—Th/U3/TRU.

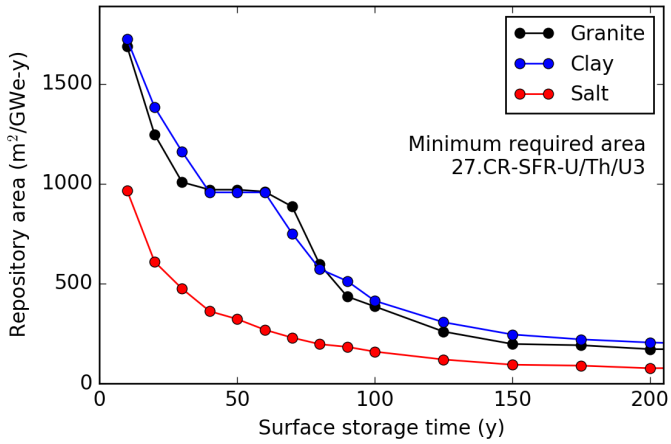

Figure D.24: Minimum required repository area (m^2/GWe-y) versus surface storage time for disposal of HLW generated from 27.CR—SFR—U/Th/U3.

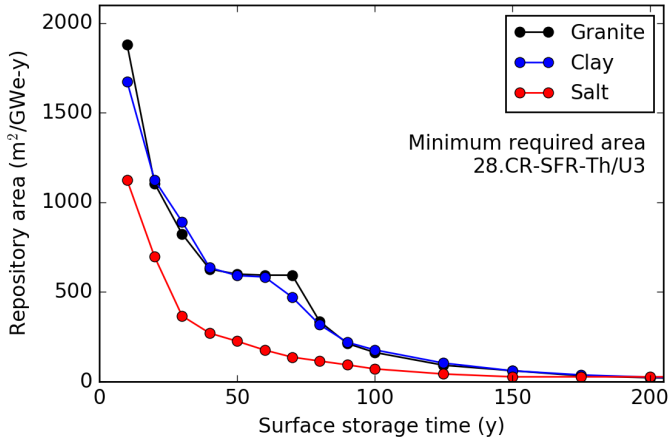

Figure D.25: Minimum required repository area (m^2/GWe-y) versus surface storage time for disposal of HLW generated from 28.CR—SFR—Th/U3.

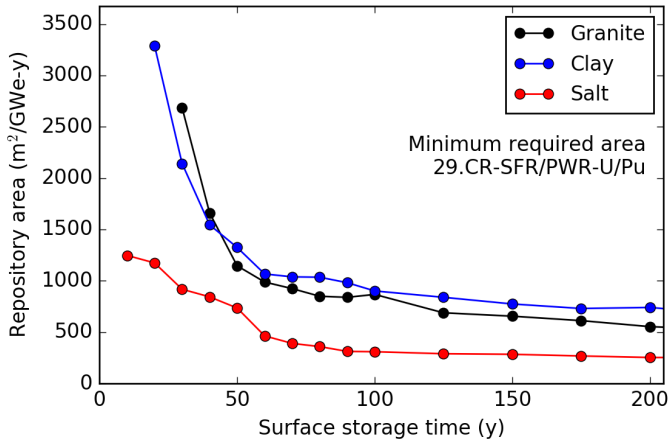

Figure D.26: Minimum required repository area (m^2/GWe-y) versus surface storage time for disposal of HLW generated from 29.CR—SFR/PWR—U/Pu.

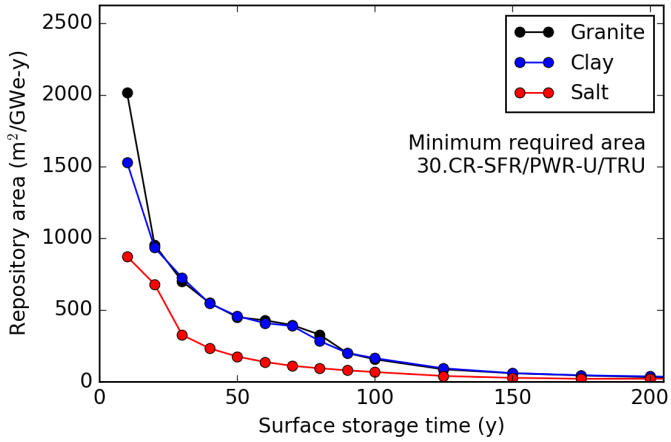

Figure D.27: Minimum required repository area (m^2/GWe-y) versus surface storage time for disposal of HLW generated from 30.CR—SFR/PWR—U/TRU.

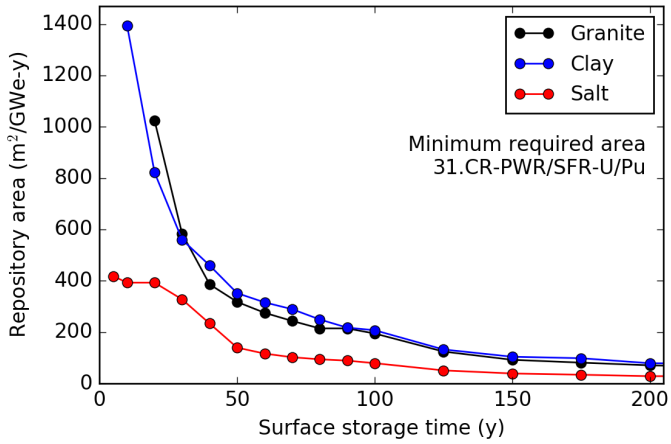

Figure D.28: Minimum required repository area (m^2/GWe-y) versus surface storage time for disposal of HLW generated from 31.CR—PWR/SFR—U/Pu.

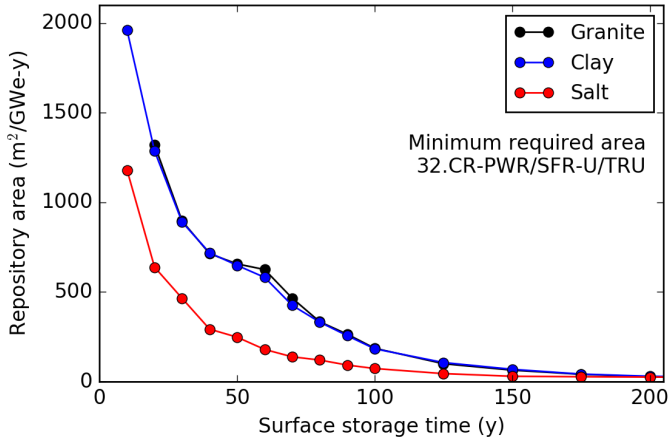

Figure D.29: Minimum required repository area (m^2/GWe-y) versus surface storage time for disposal of HLW generated from 32.CR—PWR/SFR—U/TRU.

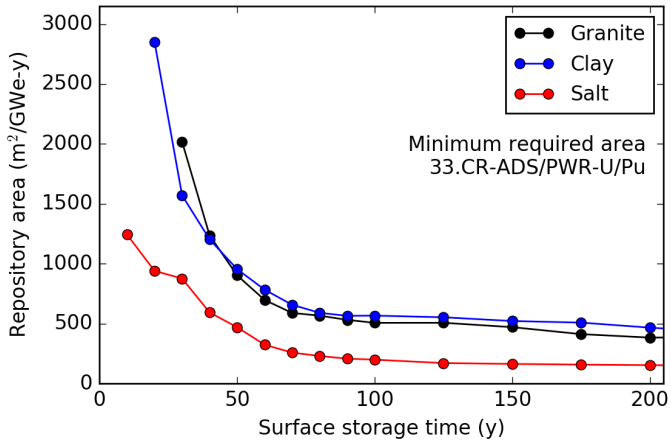

Figure D.30: Minimum required repository area (m^2/GWe-y) versus surface storage time for disposal of HLW generated from 33.CR—ADS/PWR—U/Pu.

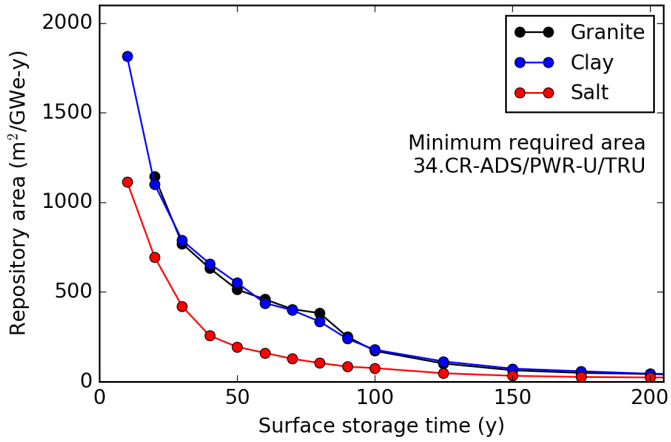

Figure D.31: Minimum required repository area (m^2/GWe-y) versus surface storage time for disposal of HLW generated from 34.CR—ADS/PWR—U/TRU.

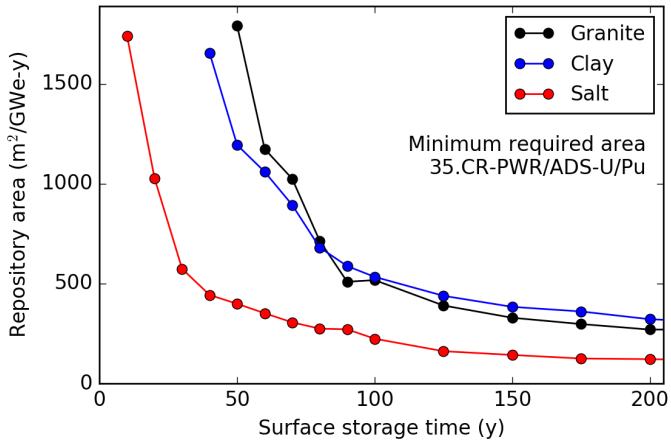

Figure D.32: Minimum required repository area (m^2/GWe-y) versus surface storage time for disposal of HLW generated from 35.CR—PWR/ADS—U/Pu.

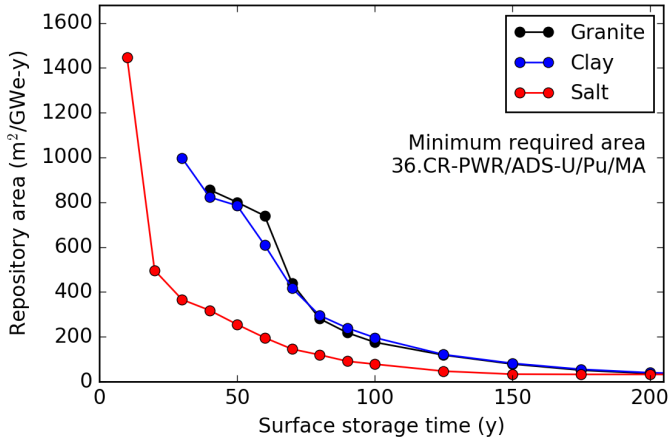

Figure D.33: Minimum required repository area (m^2/GWe-y) versus surface storage time for disposal of HLW generated from 36.CR—PWR/ADS—U/Pu/MA.

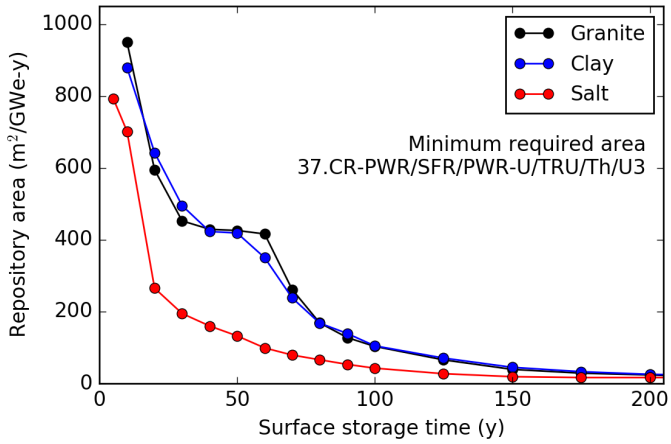

Figure D.34: Minimum required repository area (m^2/GWe-y) versus surface storage time for disposal of HLW generated from 37.CR—PWR/SFR/PWR—U/TRU/Th/U3.

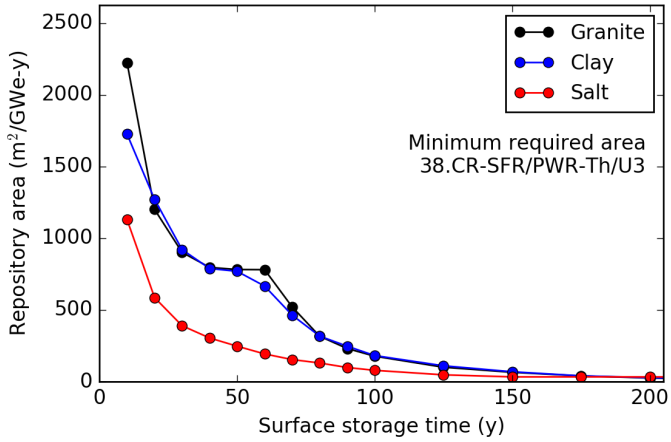

Figure D.35: Minimum required repository area (m^2/GWe-y) versus surface storage time for disposal of HLW generated from 38.CR—SFR/PWR—Th/U3.

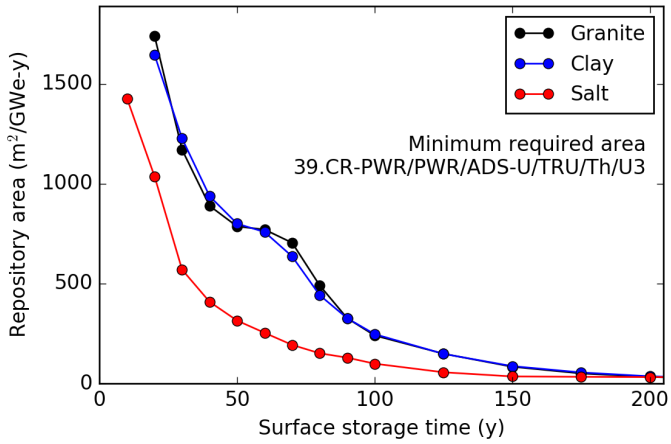

Figure D.36: Minimum required repository area (m^2/GWe-y) versus surface storage time for disposal of HLW generated from 39.CR—PWR/PWR/ADS—U/TRU/Th/U3.

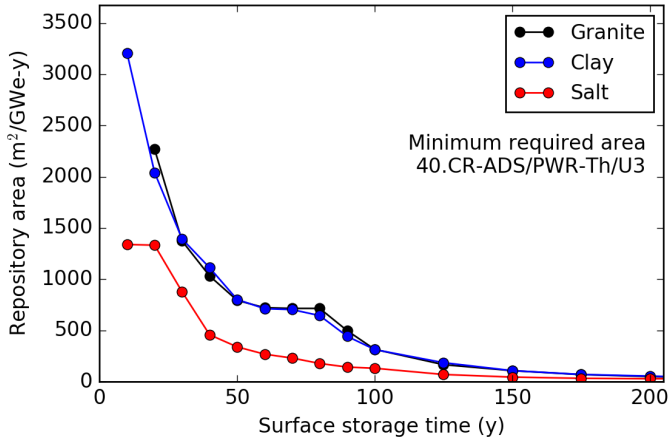

Figure D.37: Minimum required repository area (m^2/GWe-y) versus surface storage time for disposal of HLW generated from 40.CR—ADS/PWR—Th/U3.

Appendix E

Required surface storage time

This appendix presents the results for the surface storage time required before disposal is possible in each repository environment — granite, clay, and salt — for each waste stream from each fuel cycle case. The storage time is plotted against relevant values for waste package loading (for SNF) and waste form loading (for HLW). When the y-axis is plotted on a log-scale, horizontal grid lines are used to illustrate order of magnitude. Figures for 1.OT—PWR—U, 13.LR—PWR/PWR—U/Pu, and 23.CR—SFR—U/Pu are included in Chapter 4 Section 4.4.

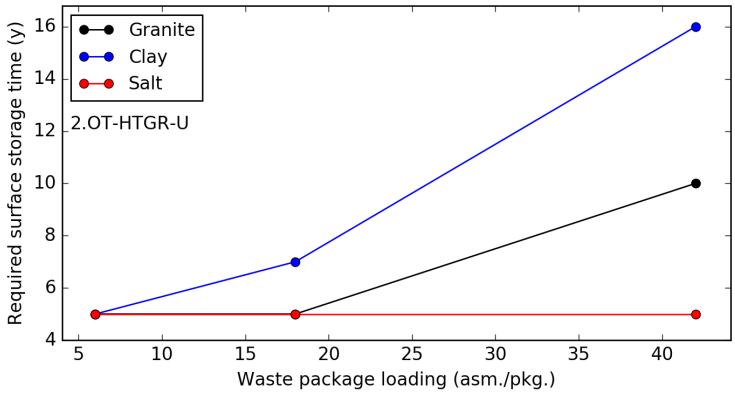

Figure E.1: Minimum required surface storage time (y) as a function of waste package loading for SNF generated from 2.OT—HTGR—U.

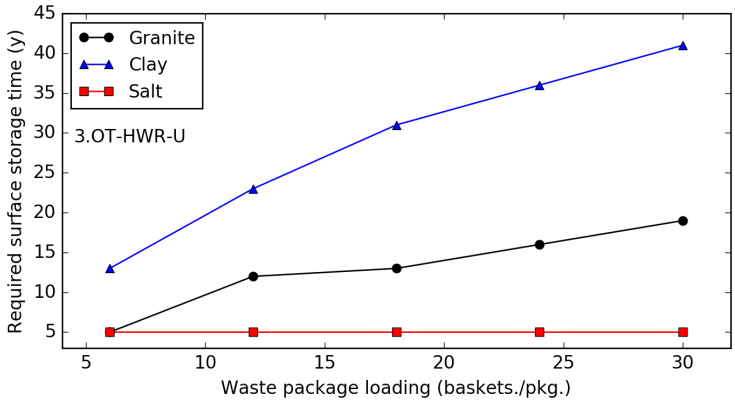

Figure E.2: Minimum required surface storage time (y) as a function of waste package loading for SNF generated from 3.OT—HWR—U.

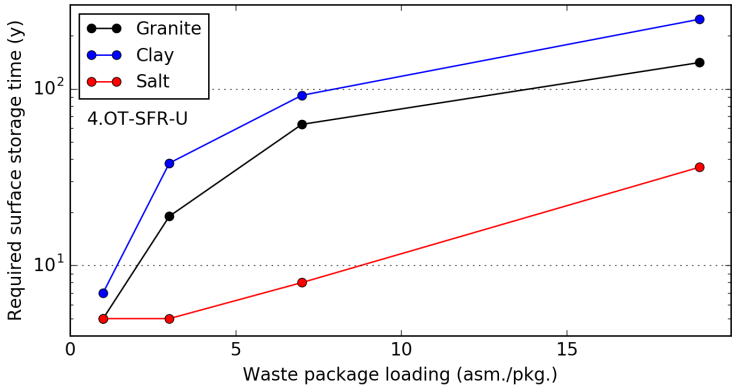

Figure E.3: Minimum required surface storage time (y) as a function of waste package loading for SNF generated from 4.OT—SFR—U.

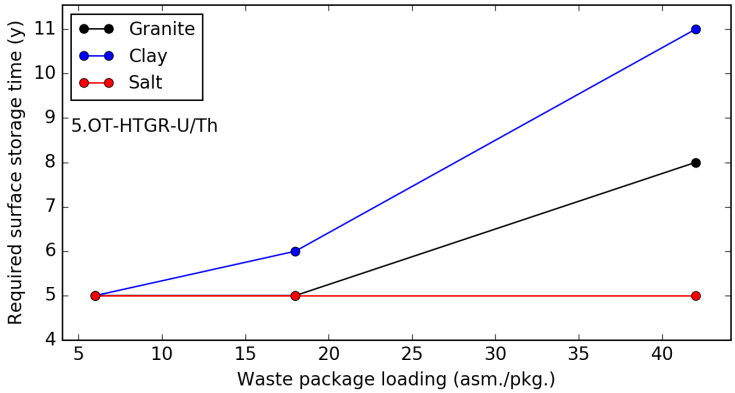

Figure E.4: Minimum required surface storage time (y) as a function of waste package loading for SNF generated from 5.OT—HTGR—U/Th.

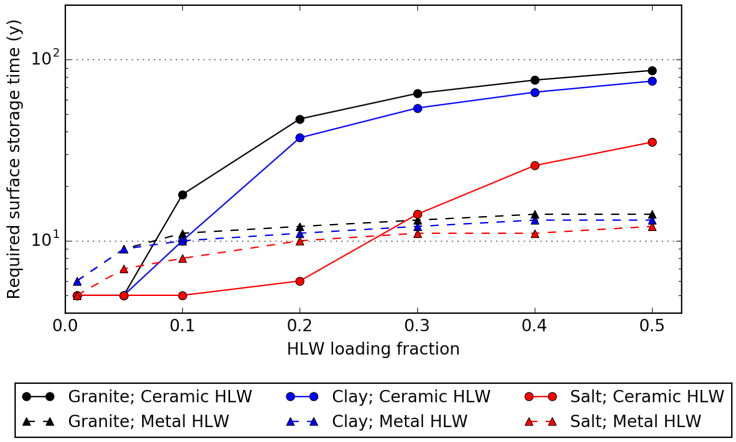

Figure E.5: Minimum required surface storage time (y) as a function of waste form loading for HLW generated from 6.OT—FFH—Th.

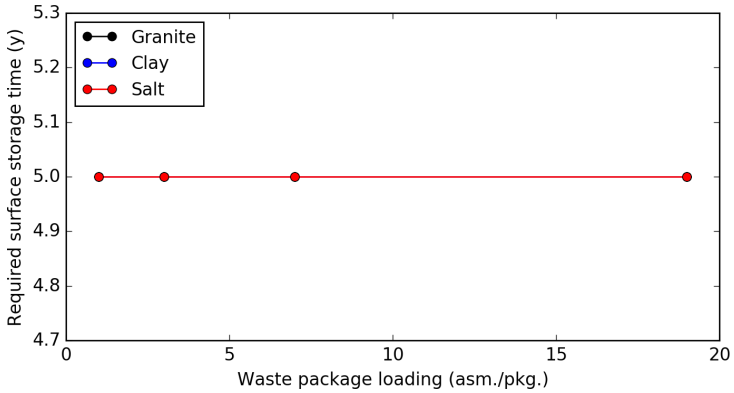

Figure E.6: Minimum required surface storage time (y) as a function of waste package loading for SNF generated from 7.OT—ADS—U.

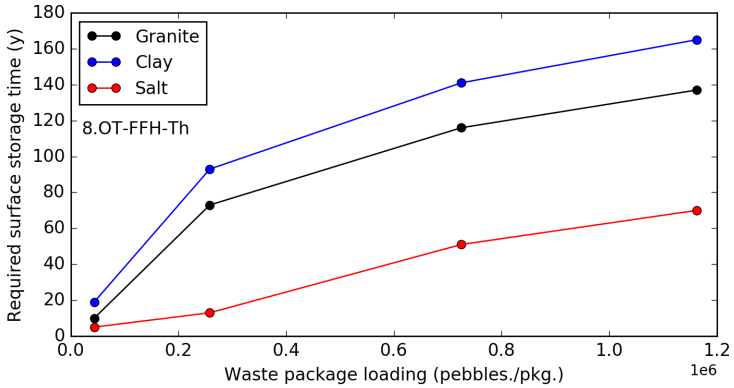

Figure E.7: Minimum required surface storage time (y) as a function of waste package loading for SNF generated from 8.OT—FFH—Th.

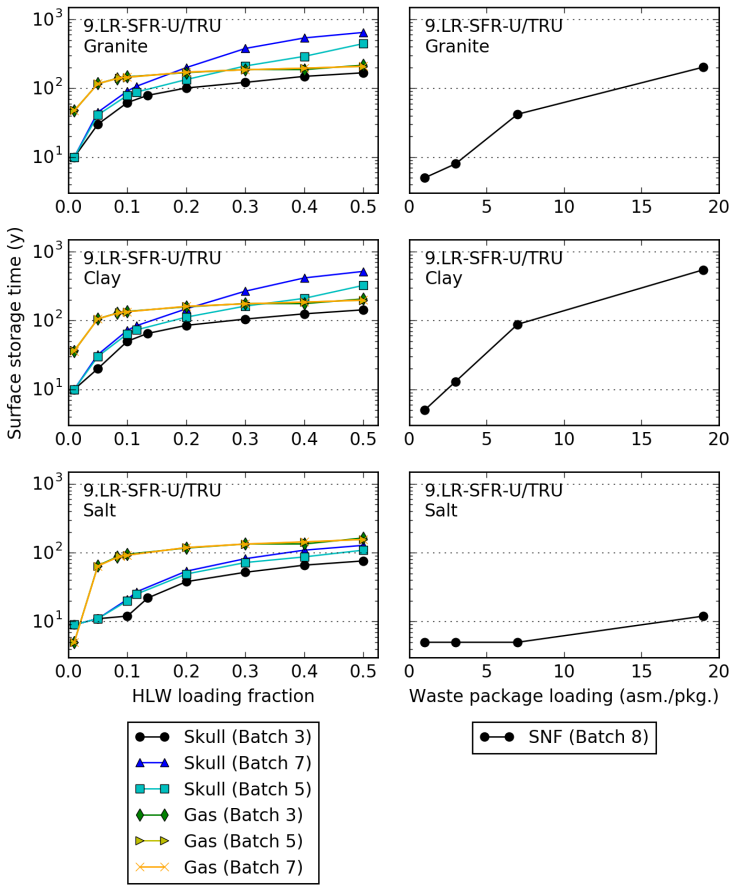

Figure E.8: Minimum required surface storage time (y) as a function of waste package (SNF) and waste form (HLW) loading for 9.LR—SFR—U/TRU.

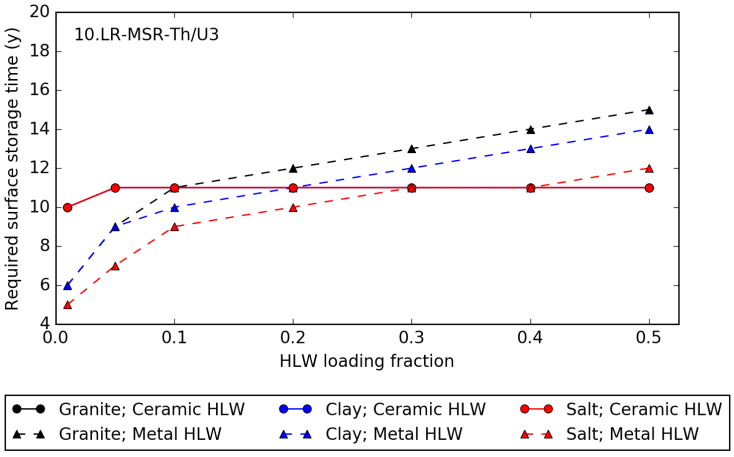

Figure E.9: Minimum required surface storage time (y) as a function of waste form loading for HLW generated from 10.LR—MSR—Th/U3.

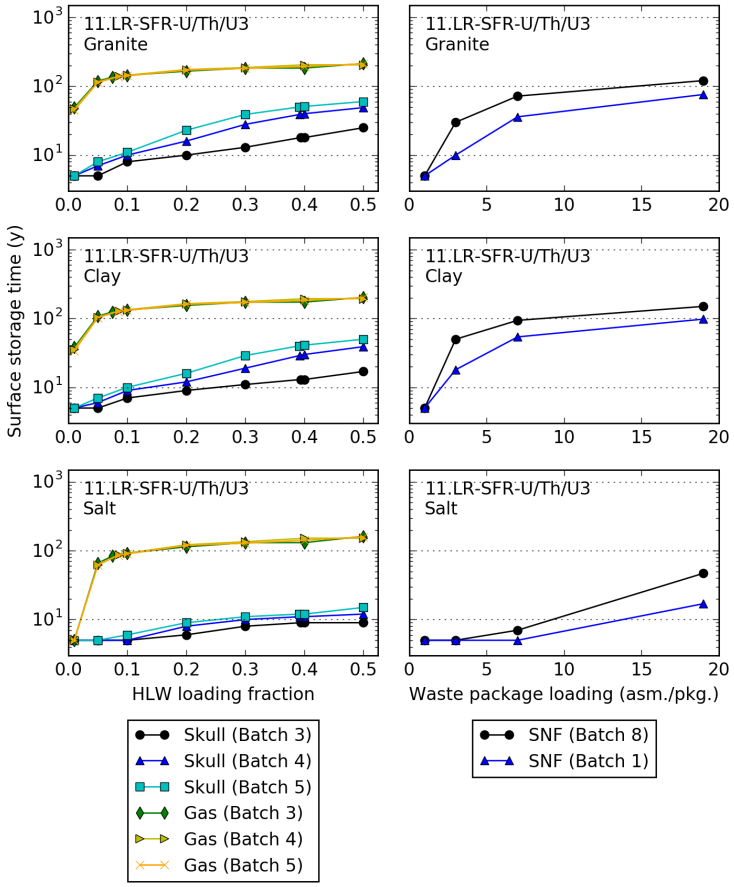

Figure E.10: Minimum required surface storage time (y) as a function of waste package (SNF) and waste form (HLW) loading for 11.LR—SFR—U/Th/U3.

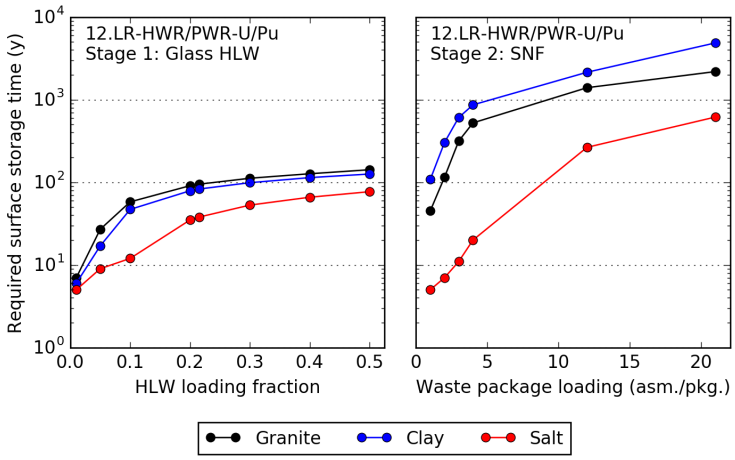

Figure E.11: Minimum required surface storage time (y) as a function of waste package (SNF) and waste form (HLW) loading for 12.LR—HWR/PWR—U/Pu.

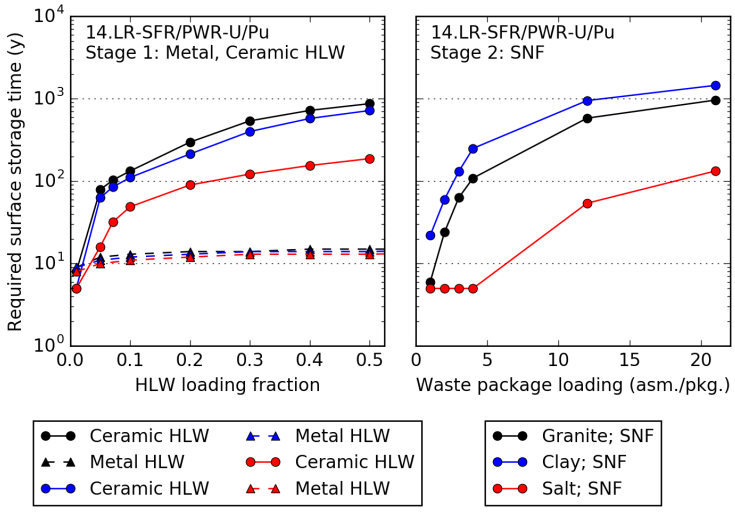

Figure E.12: Minimum required surface storage time (y) as a function of waste package (SNF) and waste form (HLW) loading for 14.LR—SFR/PWR—U/Pu.

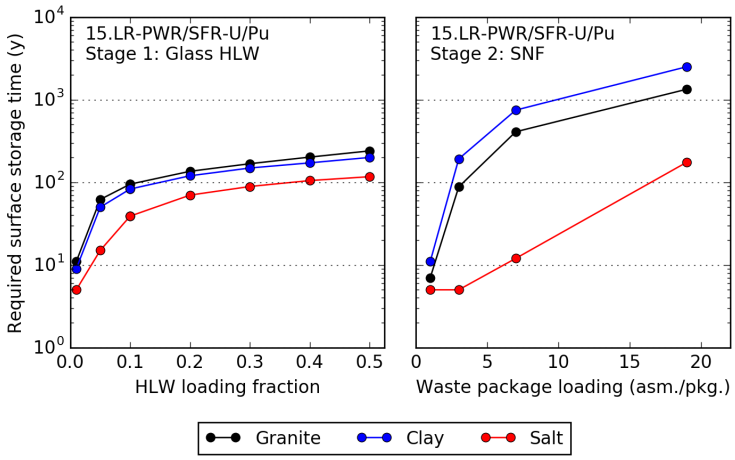

Figure E.13: Minimum required surface storage time (y) as a function of waste package (SNF) and waste form (HLW) loading for 15.LR—PWR/SFR—U/Pu.

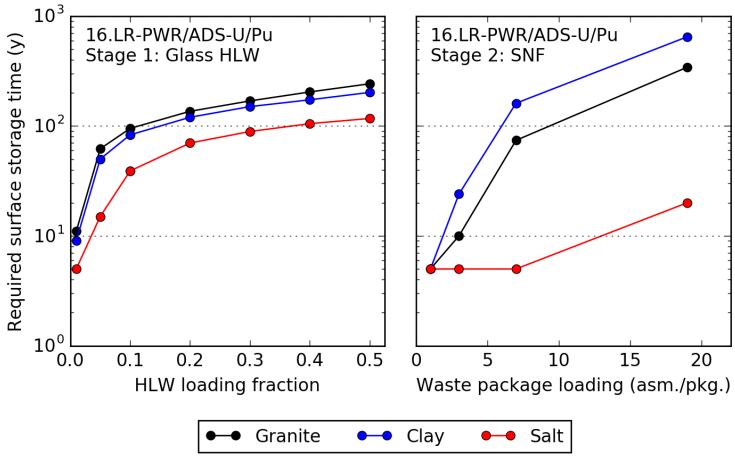

Figure E.14: Minimum required surface storage time (y) as a function of waste package (SNF) and waste form (HLW) loading for 16.LR—PWR/ADS—U/Pu.

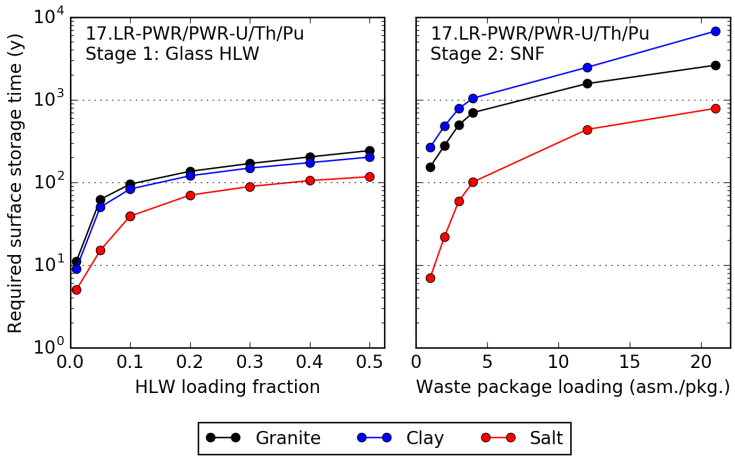

Figure E.15: Minimum required surface storage time (y) as a function of waste package (SNF) and waste form (HLW) loading for 17.LR—PWR/PWR—U/Th/Pu.

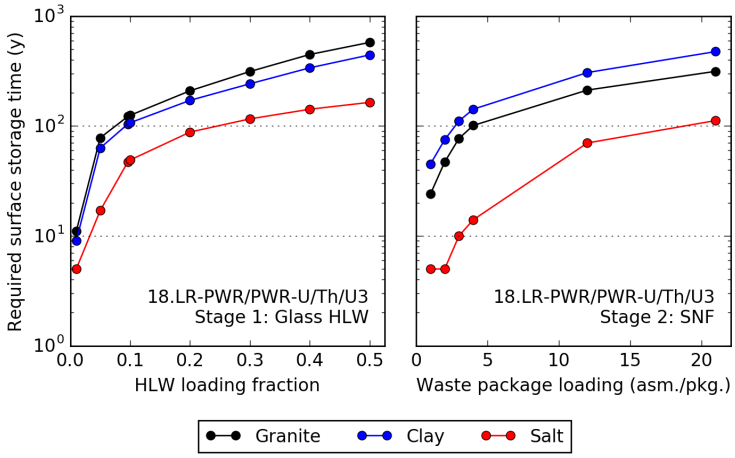

Figure E.16: Minimum required surface storage time (y) as a function of waste package (SNF) and waste form (HLW) loading for 18.LR—PWR/PWR—U/Th/U3.

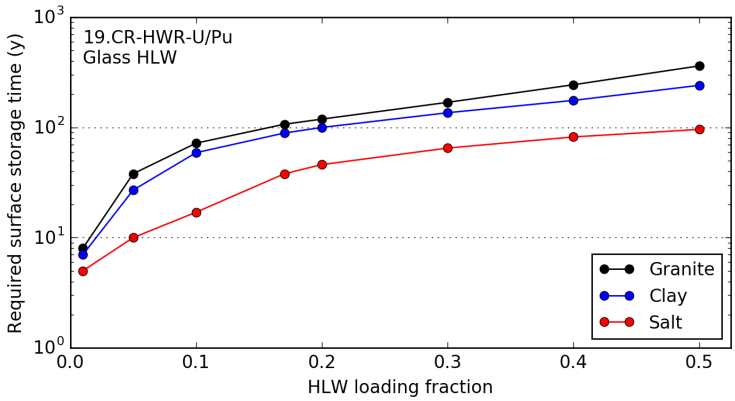

Figure E.17: Minimum required surface storage time (y) as a function of waste form loading for HLW generated from 19.CR—HWR—U/Pu.

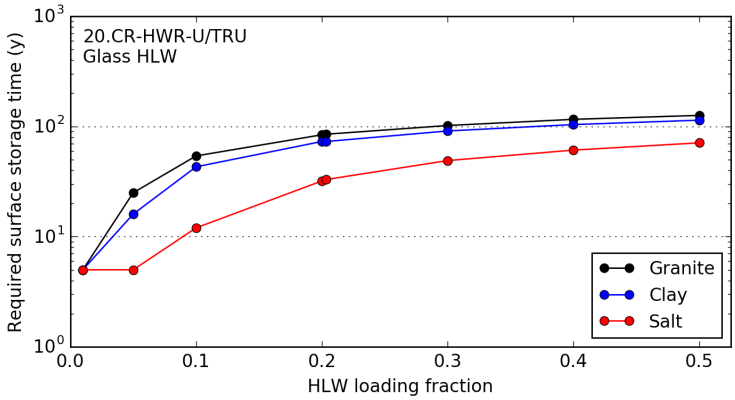

Figure E.18: Minimum required surface storage time (y) as a function of waste form loading for HLW generated from 20.CR—HWR—U/TRU.

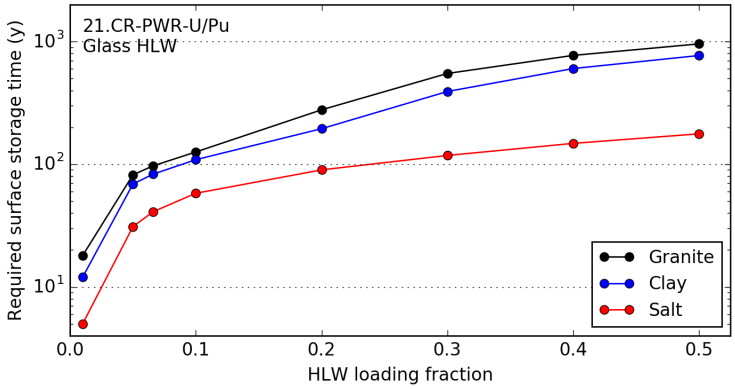

Figure E.19: Minimum required surface storage time (y) as a function of waste form loading for HLW generated from 21.CR—PWR—U/Pu.

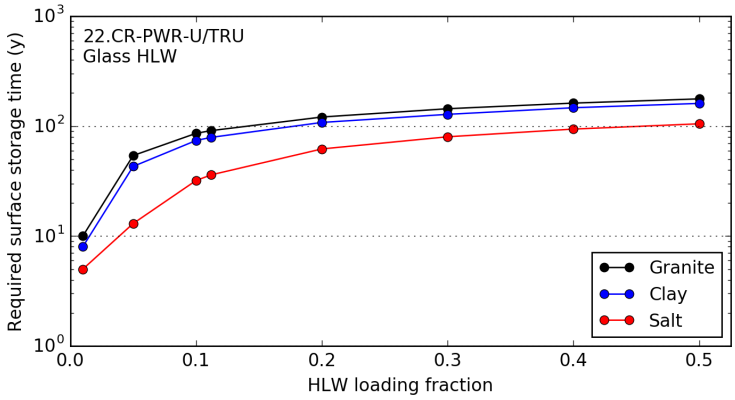

Figure E.20: Minimum required surface storage time (y) as a function of waste form loading for HLW generated from 22.CR—PWR—U/TRU.

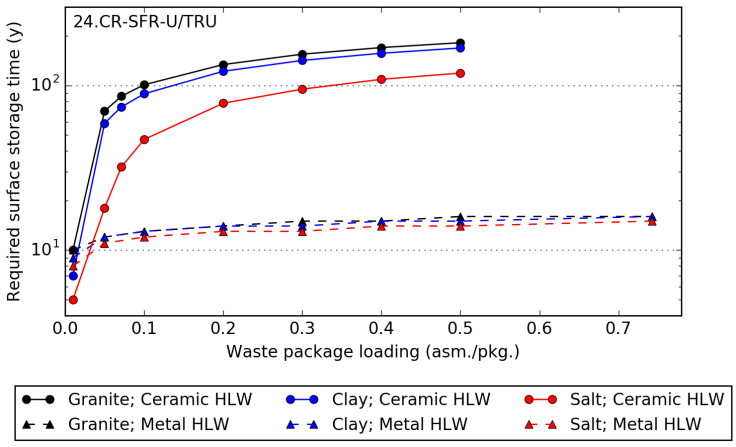

Figure E.21: Minimum required surface storage time (y) as a function of waste form loading for HLW generated from 24.CR—SFR—U/TRU.

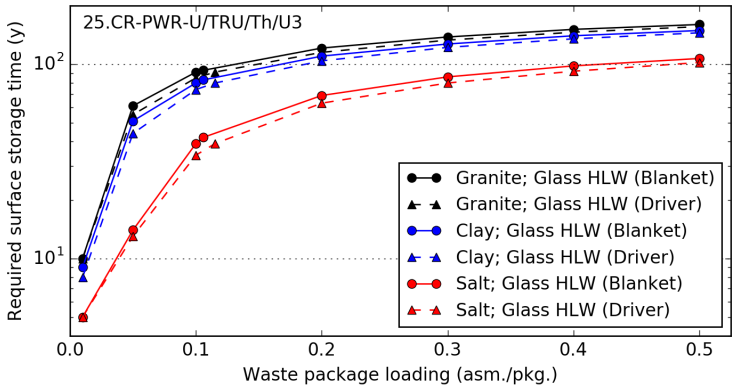

Figure E.22: Minimum required surface storage time (y) as a function of waste form loading for HLW generated from 25.CR—PWR—U/TRU/Th/U3.

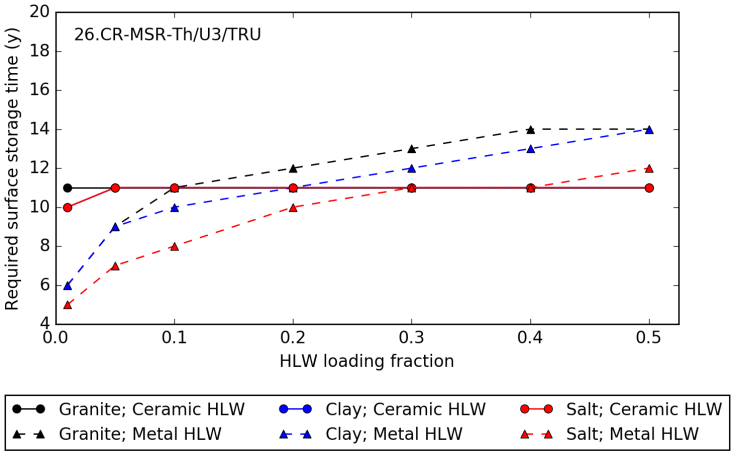

Figure E.23: Minimum required surface storage time (y) as a function of waste form loading for HLW generated from 26.CR—MSR—Th/U3/TRU.

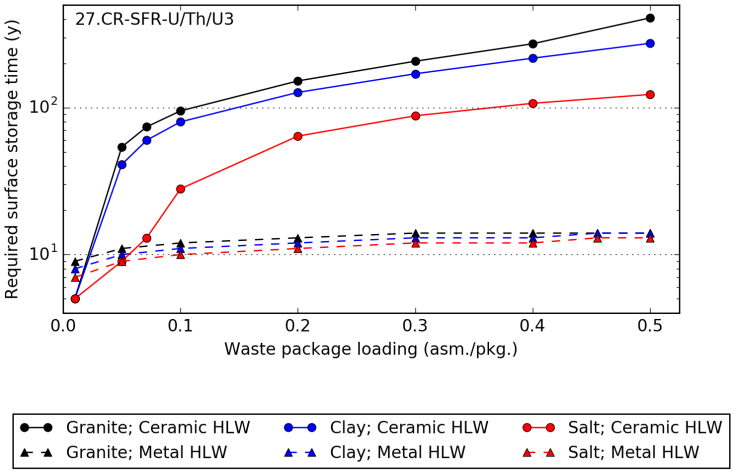

Figure E.24: Minimum required surface storage time (y) as a function of waste form loading for HLW generated from 27.CR—SFR—U/Th/U3.

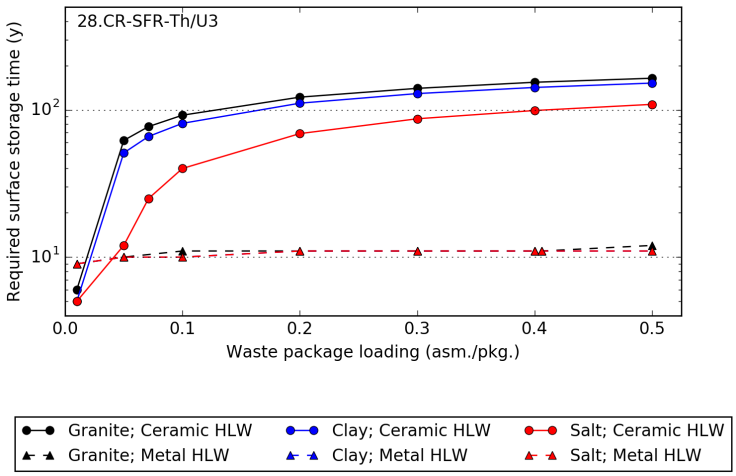

Figure E.25: Minimum required surface storage time (y) as a function of waste form loading for HLW generated from 28.CR—SFR—Th/U3.

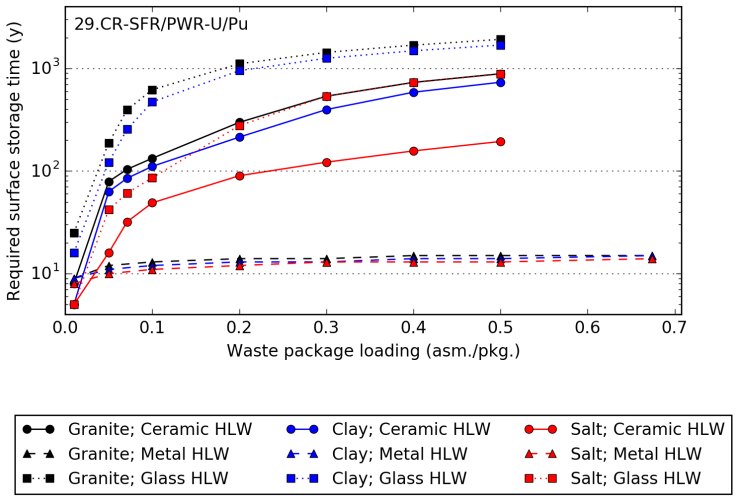

Figure E.26: Minimum required surface storage time (y) as a function of waste form loading for HLW generated from 29.CR—SFR/PWR—U/Pu.

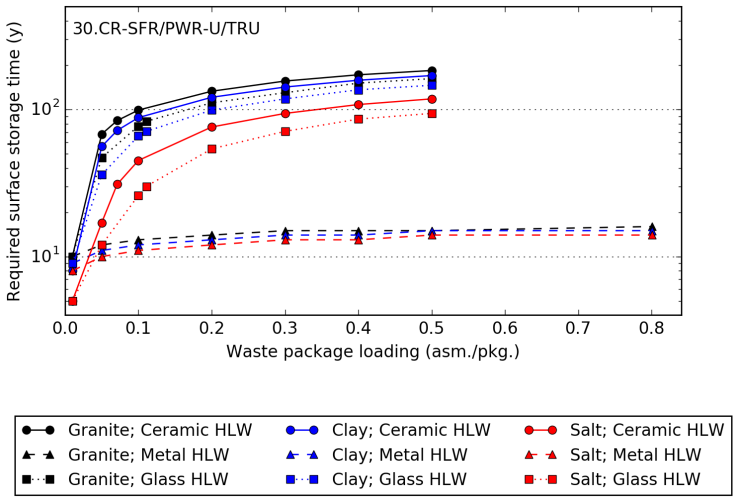

Figure E.27: Minimum required surface storage time (y) as a function of waste form loading for HLW generated from 30.CR—SFR/PWR—U/TRU.

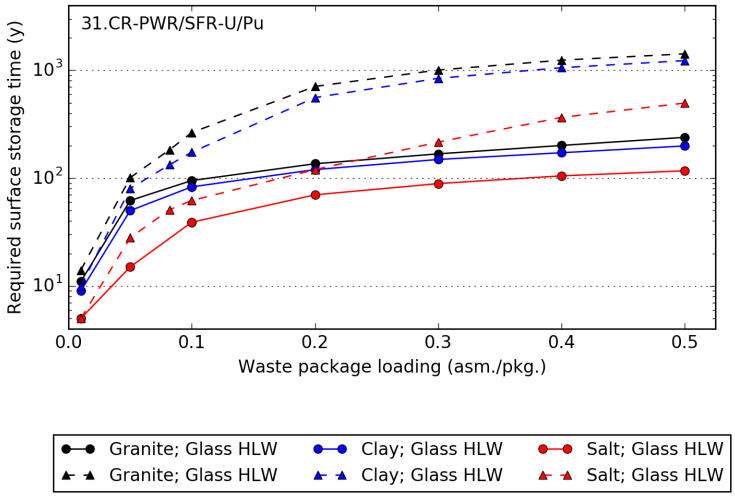

Figure E.28: Minimum required surface storage time (y) as a function of waste form loading for HLW generated from 31.CR—PWR/SFR—U/Pu.

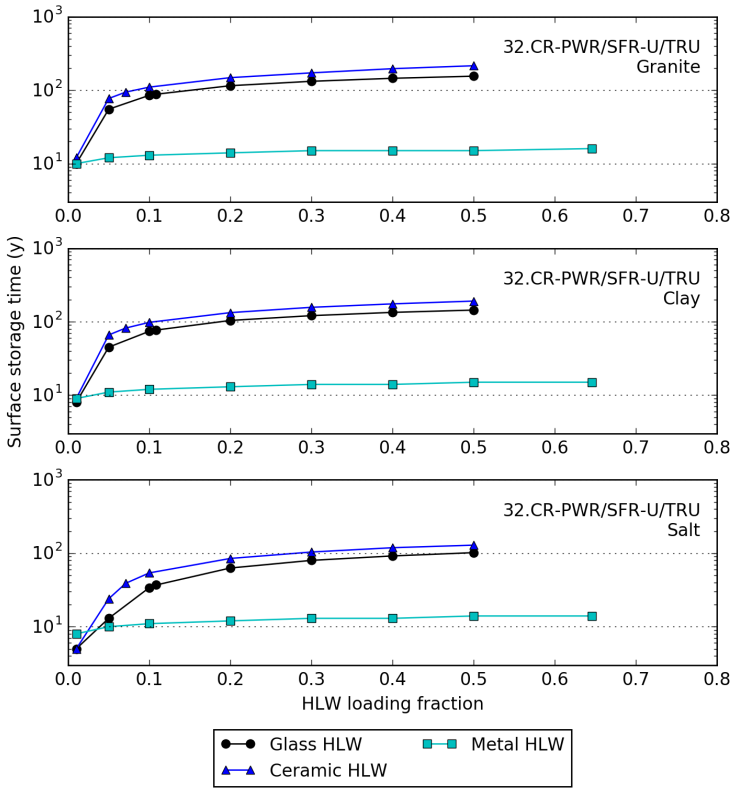

Figure E.29: Minimum required surface storage time (y) as a function of waste form loading for HLW generated from 32.CR—PWR/SFR—U/TRU.

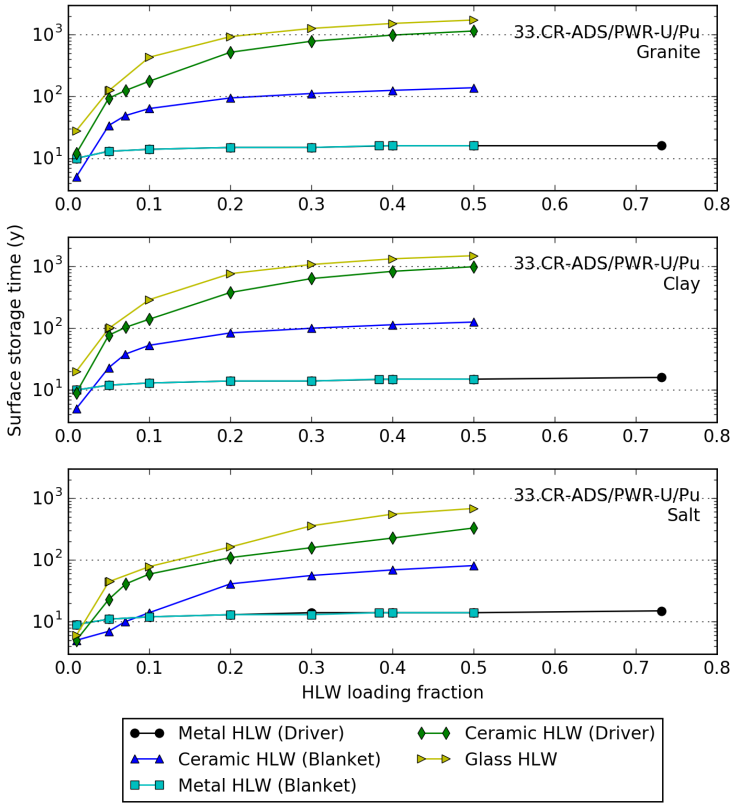

Figure E.30: Minimum required surface storage time (y) as a function of waste form loading for HLW generated from 33.CR—ADS/PWR—U/Pu.

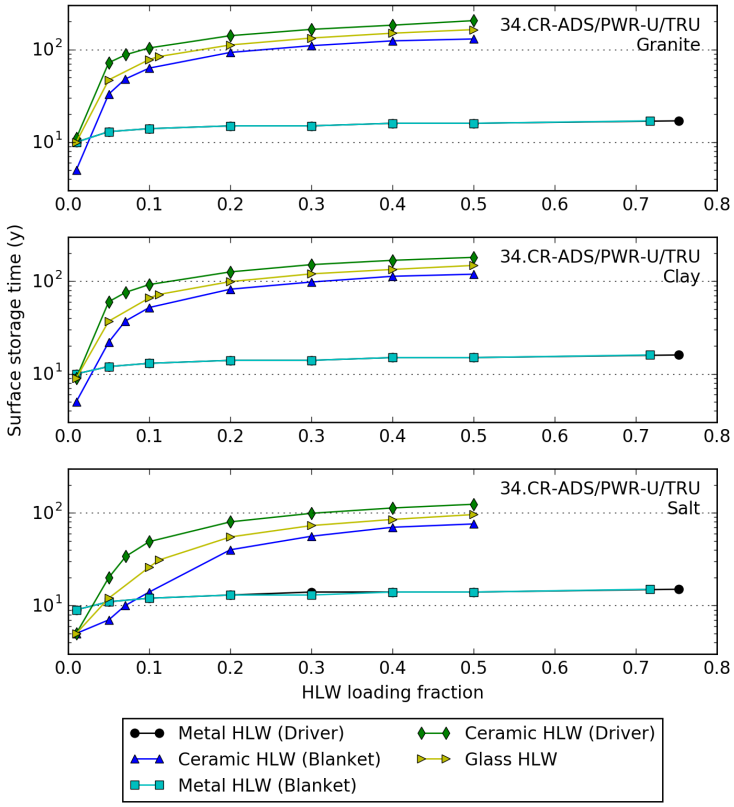

Figure E.31: Minimum required surface storage time (y) as a function of waste form loading for HLW generated from 34.CR—ADS/PWR—U/TRU.

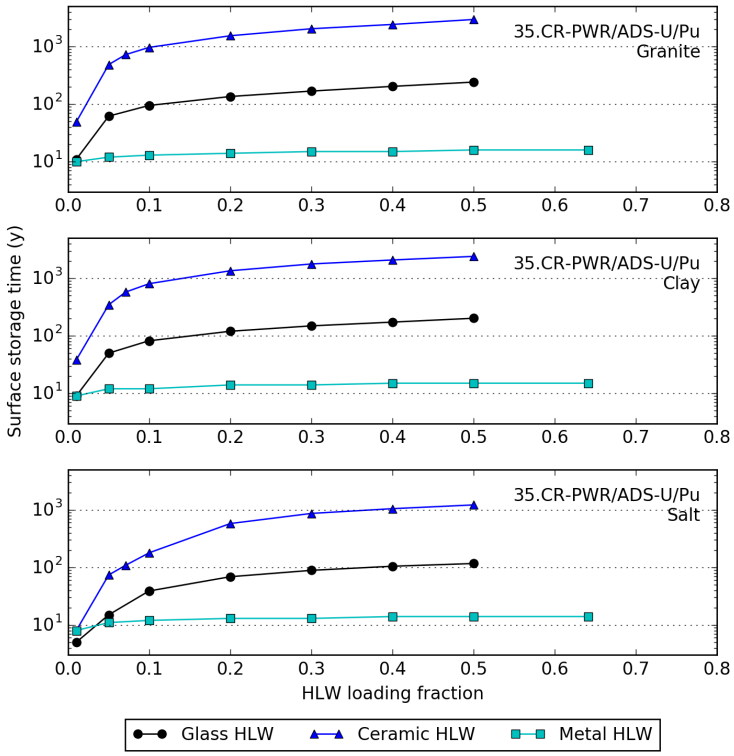

Figure E.32: Minimum required surface storage time (y) as a function of waste form loading for HLW generated from 35.CR—PWR/ADS—U/Pu.

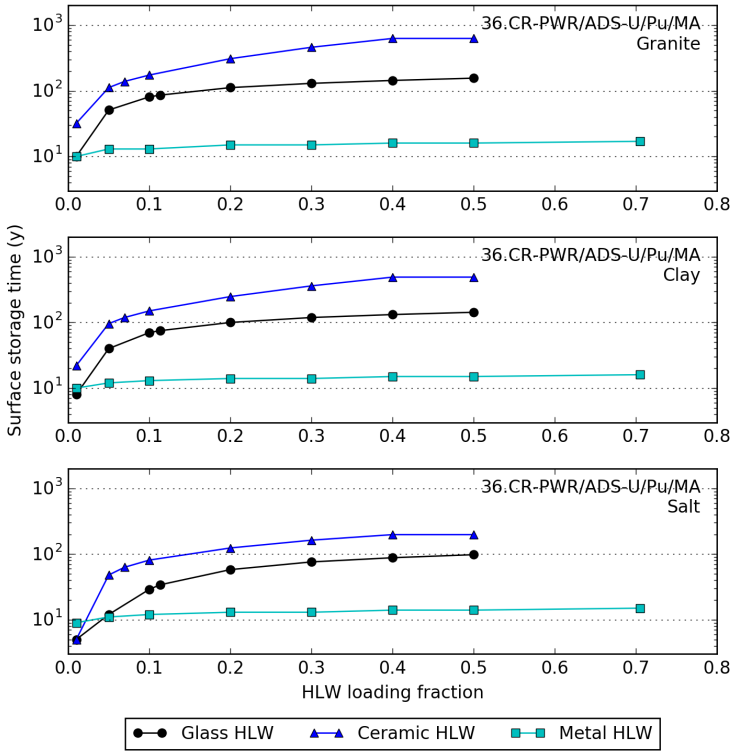

Figure E.33: Minimum required surface storage time (y) as a function of waste form loading for HLW generated from 36.CR—PWR/ADS—U/Pu/MA.

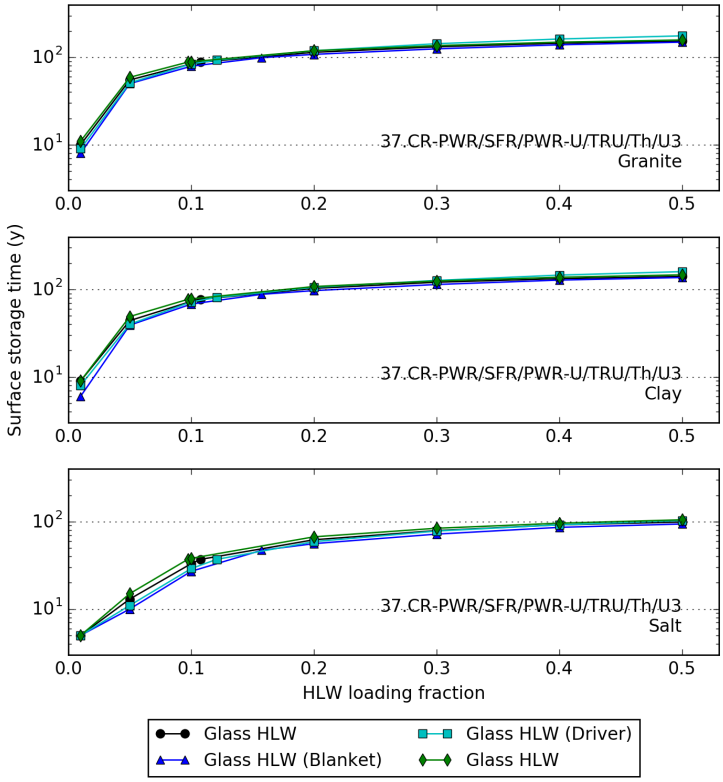

Figure E.34: Minimum required surface storage time (y) as a function of waste form loading for HLW generated from 37.CR—PWR/SFR/PWR—U/TRU/Th/U3.

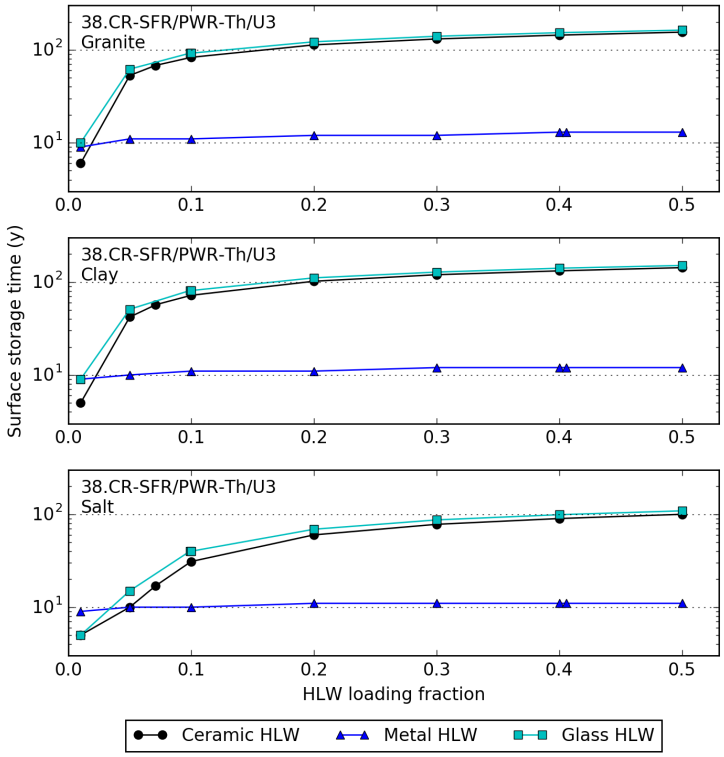

Figure E.35: Minimum required surface storage time (y) as a function of waste form loading for HLW generated from 38.CR—SFR/PWR—Th/U3.

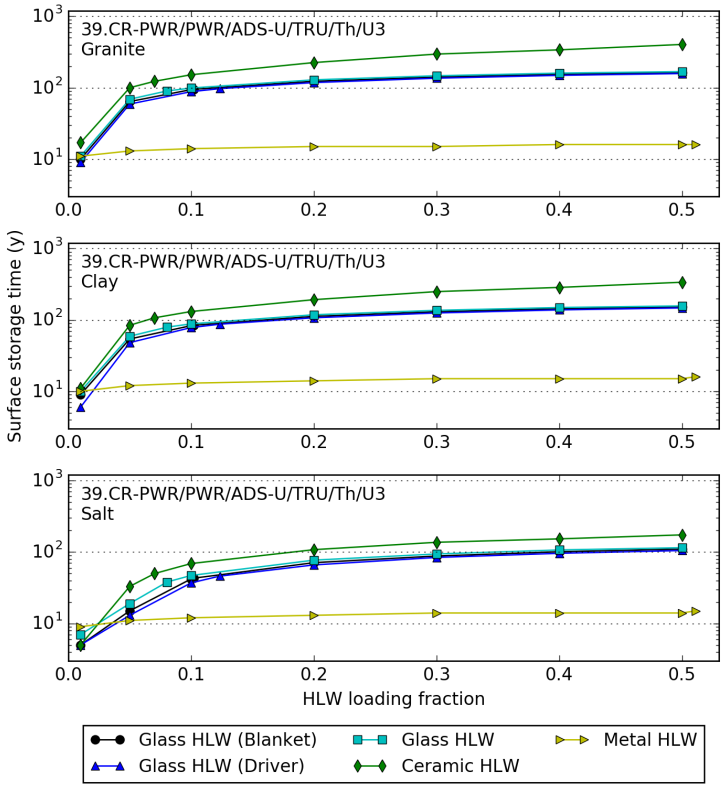

Figure E.36: Minimum required surface storage time (y) as a function of waste form loading for HLW generated from 39.CR—PWR/PWR/ADS—U/TRU/Th/U3.

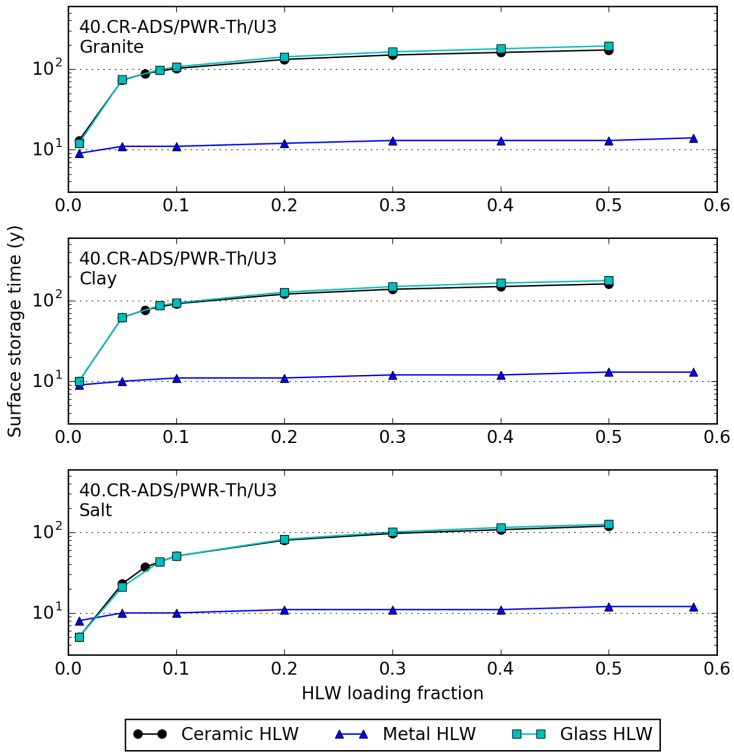

Figure E.37: Minimum required surface storage time (y) as a function of waste form loading for HLW generated from 40.CR—ADS/PWR—Th/U3.